Hydrodynamic and Sediment Transport Numerical Modelling and Applications at Tairua Estuary, New Zealand

A thesis

submitted in fulfilment

of the requirements for the degree

of

Doctor of Philosophy in Earth and Ocean Sciences

at

The University of Waikato

by

ZHI (CATHY) LIU

THE UNIVERSITY OF
WAIKATO
Te Whare Wānanga o Waikato

May 2014

Abstract

Tairua Estuary is a partially mixed estuary located on the east coast of the Coromandel Peninsula, North Island, New Zealand. Like many estuaries worldwide, Tairua Estuary is experiencing rapid sedimentation, which is causing a range of environmental and management issues. This study was undertaken to develop a combined hydrodynamic and sediment transport numerical model as a tool for improving management of sedimentation issues within Tairua Estuary.

Two field campaigns were undertaken in July 2010 and June 2011 to obtain calibration and verification datasets for two suites of numerical models – DHI MIKE and ASR 3DD – that were both used for hydrodynamic and sediment transport simulations to allow comparisons of the model suites. Additional models were used to simulate additional processes such as oil dispersal.

Observations and numerical modelling showed the tidal wave was distorted as it propagated into the Tairua Estuary, becoming increasingly asymmetrical with distance from the entrance. The tidal wave underwent more distortion during spring tides than during neap tides, resulting in the influx of more oceanic water in the upper Tairua Estuary during a spring tidal cycle, causing a greater increase of salinity.

The changing tidal distortion with tidal range also resulted in spring tides being flood dominated and neap tides being ebb dominated. The fate of fine sediments introduced into the lower estuary was, therefore, dependant on the state of the spring-neap cycle, with spring tides favouring deposition in the upper estuary, and neap tides favouring export to the continental shelf.

The effects of tidal behaviour in the estuary were modified by river discharge, with increasing discharge resulting in increased ebb dominance and export of sediment from the estuary. Further, as river discharge increased, the estuary became more stratified, particularly during periods of low tidal velocities. However, areas of Tairua Estuary with tidal current velocities higher than 0.5 m s-1, mostly around the tidal inlet, remained partially mixed, even when the river discharge reached a peak value of 200 m3 s-1.

During flood events, the upper part of estuary becomes highly stratified due to the large increase in freshwater discharge. Observations and numerical modelling showed that instabilities can develop in the resulting pycnocline in response to wind forcing and fluctuations in flood discharge, and these propagate as forced seiches within the estuary. The seiches interact with the turbid floodwaters and the

underlying salt wedge to influence the locations where fine sediment is deposited within the estuary, with enhanced deposition at the nodes of the seiches.

Sediment transport modelling indicated that suspended sediment from the river and sediment eroded from the estuary bed, primarily is transported seaward along the main channel of the estuary and through the northern side of the tidal inlet. Subsequently, coarser suspended sediment tends to deposit on the terminal lobe of the ebb tidal delta due to lower current speeds. Meanwhile, sediment suspended along Pauanui Beach by wave action enters the estuary along the southern side of the tidal inlet, and this sediment is mostly deposited on the flood tidal delta. The interaction of the sediment transport entering the estuary and exiting the estuary forms a large eddy over the ebb tidal delta, which acts as a sediment deposition-centre. The model results were consistent with the field observations.

The numerical models were calibrated against one field dataset and verified against the second using a variety of statistical measures for the goodness of fit. The results were characterised as excellent for elevation changes over most of the estuary, apart from the elevation for the Tairua River channel around the limit of tidal influence. The calibration and verification of current velocities resulted in a range of results from reasonable to excellent, depending on the numerical grid resolution and the complexity of the local bathymetry. The finest 20 m grids produced the best results, with some minor problems with the current velocity directions along the seaward boundary of the models. Overall the MIKE software suite was easier to use and ran faster, but the 3DD suite produced better results for shallow areas with narrow channels in the upper estuary.

Once calibrated and verified, the models were used to simulate a range of scenarios requested by the Waikato Regional Council. These included assessing the impact of potential sea level rise, development including channel realignment and marina construction, and the effects of oil spills within the estuary.

As sea level rises, the estuary is predicted to become increasingly flood dominated, which would result in greater sediment transport into the estuary from the Pauanui Beach system, and hence, subsequent deposition on the intertidal flats. Effectively, sea level rise would reverse the normal sequence of estuarine evolution, turning the clock back towards a more youthful estuary. It is also likely that saltwater intrusion was more frequent with increased sea level. However, the influx of sediment would also compensate for some of the sea level rise, and reduce the tendency for flood dominance.

Acknowledgement

'Cathy, you will find this research interesting and I am very sure that you could do it very well. Please remember what I have told you whenever you meet difficulties and feel hard during this study…'

Terry Healy on 30 May, 2010

Thank you, Terry Healy and Vernon Pickett. I could not forget any words from both of you. You are always in my heart and encourage me to go forward. I could see your smile on the day of my graduation ceremony.

To my chief supervisor, Dr. Willem de Lange, thank you for your advice and guidance throughout the project. I am also very appreciated for your friendship. No matter what difficulties I met, you were always the first person to encourage me and help me.

Thanks to Dr. Karin Bryan from the Waikato University, Dr. Christian Winter from the Bremen University, for your invaluable input and comments. From you, I not only learnt much knowledge, but also the way to be a scientist.

Thanks to the Waikato University and the Waikato Regional Council for the scholarship and funding to make the research possible. Thanks to DHI for supplying me three years free access to MIKE software and technical support. Thanks also to Waikato Regional Council and NIWA for supplying me with the data and information related to my research.

Thanks to Rob Bell, Nigel Goodhue, Nicole Hancock, and Margaret Bellingham from NIWA to supply me the data and information I needed for the research.

Thanks to Benjamin Tuckey from DHI and Dougal Greer from ASR for the technical support on numerical modelling.

Thanks to Dirk Immenga, Craig Hosking, Warrick Powrie and Brendan Cappely for the field assistance and much appreciated input into this study.

Thanks to Dan Borman, without his magic GIS skill and enough patience to help me develop the bathymetry files for modelling, a good numerical model would not be developed.

Thanks to Sydney Wright for behaving like my mum and being my best friend during my study.

Thanks to Janine Ryburn for assisting and guiding my lab work as much as you could.

Thanks to Liz Brodie, my software master, for coming downstairs many times to help me install the software I needed.

Thanks to Dr. Bryna Flaim, my office buddy, for conversation, encouragement and help.

Thanks to Dr. Rafael Guedes, my first MatLAB teacher.

Thanks to Daniel Tait to give me so much help with English and proof reading.

I want to give thanks to my friends that I met in New Zealand, John and Philippa, Malcolm and Mary, Sione and Janice, Mindy Sun and so on. Thank you for your love, hugs and big family you gave to me.

I would give my thanks to my dear husband Dr. Hong ZHOU, daughter Diny ZHOU and Coco ZHOU. Thank you for always picking me up from the office at midnight.

Mum, thank you for coming to New Zealand to help me take care of our new born baby Coco and cook for my family, even though you are already 73 years old. Thank you for the great love you give to me.

I am very lucky to meet all of you in New Zealand. My life is brilliant because of you and this thesis belongs to every one of you.

Zhi (Cathy) LIU

Hamilton, New Zealand

01 May., 2014

Table of Contents

PART II. DATA AND METHODS

CHAPTER THREE DATA RESOURCES

CHAPTER FOUR NUMERICAL MODELLING

PART III. RESULTS AND DISCUSSIONS

CHAPTER FIVE HYDRODYANMICS AND SEDIMENT TRANSPORT FEATURES OF TAIRUA ESTUARY

CHAPTER SIX SALINITY AND TEMPERATURE STRUCTURE

List of Tables

CHAPTER TWO

CHAPTER THREE

CHAPTER FOUR

CHAPTER FIVE

CHAPTER SEVEN

CHAPTER EIGHT

CHAPTER NINE

CHAPTER TEN

List of Figures

CHAPTER TWO

CHAPTER THREE

CHAPTER FOUR

CHAPTER FIVE

CHAPTER SIX

CHAPTER SEVEN

CHAPTER EIGHT

CHAPTER NINE

CHAPTER TEN

PART I: INTRODUCTION

CHAPTER ONE
OVERVIEW

This chapter introduces the research background, highlights the research objectives and the questions that needed to be answered, summarizes the methodologies used in this research, and outlines the structure of the thesis.

1.1 INTRODUCTION

Estuaries are complex environments in the coastal zone. They varies considerably in terms of geomorphology, tides, drainage basin and fluvial processes, water chemistry, wave characteristics, sediment provenance, land use and land cover, biodiversity, and degree of human modification (Jackson, 2013). Although estuaries constitute a significant portion of the world's coast, the published research focused largely on only a small subset of systems in Africa (e.g., Mgent), Asia (e.g., Pearl and Yangtzee), Australia (e.g., Batesman, Murray, and Swan), Europe (e.g., Chesapeake, Columbia River, Delaware, Narragansett, Puget Sound, San Francisco, and St. Lawrence), and South America (e.g., Bahia Blance and Rio de la Plata). Much of the research was based on empirical studies of individual estuaries (Jackson, 2013). Recent advances in instrumentation had led to better quantification and modelling of these systems (Fitzgerald & Knight, 2005).

New Zealand has as broad a range of estuaries and tidal inlets as any country in the world. There are some 300 estuarine systems spread around the 11,000 km of coast (McLay, 1976). The Tairua Estuary is located on the east coast of the Coromandel Peninsula, North Island New Zealand. Since Polynesian colonization ~800 BP, there have been significant land use changes, which have accelerated with the arrival of Europeans. Under the Resource Management Act 1991, and the associated New Zealand Coastal Policy Statement 2010, there is a requirement to avoid or mitigate the impacts of land use on the estuary. In practice, this requires methods for quantifying the impacts and effects of management strategies.

Tairua Estuary is infilling now. The hydrodynamics and sediment transport within Tairua Estuary are complicated because of the complex interplay between tidal currents and wave action at the inlet driving sediment transport, and the variable amount of fresh water inflow from the Tairua River. This is occurring at a time of intensified subdivision development and increasing demand for recreational use of

the harbour and inlets. Potentially such developments can accelerate deleterious environmental effects within the estuary, including nutrient enrichment.

Site-specific data are difficult and expensive to obtain. The method of numerical modeling is widely used more and more because it provides an invaluable aid to better understand estuarine hydrodynamic and sediment transport processes by supplementing the available observations, and also as environmental management tools to assess future impacts. Models provide an assimilation of knowledge as well an integration of the effects of interactions between many processes in time and space. In addition, their results can be used to predict the likely consequences of future events such as harbour development. However, prior to this study, the Tairua Estuary had not been modeled with a well-calibrated hydrodynamic and sediment transport model, and in general, there was a paucity of hard field data for Tairua Estuary.

Hence, the study was needed to investigate the hydrodynamic, sediment transport and stratification characteristics of the Tairua Estuary using the method of numerical modelling to better understand how the estuarine physical processes depend on the combination of external forcing of tides, river discharge and environmental conditions. The forcing mechanisms of seiche at the lower Tairua Estuary and the impacts on the hydrodynamic and sediment transport within the estuary were discussed after receiving the meteorological data and calibrated and validated numerical model results. Further, these models could be used to assess the impacts of relative sea level rise, marina development, channel dredging/realignment on estuarine physical process and sediment transport. Oil spill dispersal pathways with different environmental conditions including wind speed, wind direction, oil spill locations, oil properties and tidal flows were also benefit to the management strategies.

This research gives the recommendation from numerical modelling to better understand the estuarine processes of the Tairua kind of estuaries and is helpful for coastal geological research and management.

1.2 MAIN QUESTIONS

Sedimentation within Tairua Estuary has long been a concern. Even though it is clear that Tairua Estuary is infilling, it is uncertain whether the estuary is supplying sand to Pauanui Ocean Beach or vice-versa. The flood and ebb tidal delta indicate "the presence of two-way sand transport through the inlet where reversing tidal flows are dominant" (Kirk, 1991). Healy et al. (1981) proposed that Pauanui Beach was in a long-term state of slow erosion with sediment being removed from the beach and deposited inside the estuary. However, Carryer (1982) showed that Pauanui Spit has been under a state of long term net accretion with

sand taken out with the ebb flows from Tairua Estuary.

Q1： What are the dominant mechanisms of Tairua Estuary sediment infilling? What is the likely effect of relative sea level rise?

The relative sea level rise (SLR) resulting from climate change and flood discharged from Tairua River mouth have been suggested as two of the factors contributing to the high sedimentation rates within the estuary (Healy et al. 1981).

Q2: How the the hydrodynamics of estuaries change in response to relative sea level rise (SLR) and river flood?

During the field work in 2010, a seiche was observed in the lower Tairua Estuary. This event was associated with strong stratification and high suspended sediment concentrations due to a freshwater flood.

Q3: What are the forcing mechanisms of seiche? And what impacts could seiche have on sediment transport within the estuary?

Various oil spill models have been developed by the other scientists. However, the factors influencing oil spill distribution, especially the relationship between the oil spill distribution pathway and estuarine physical process had not been studies so much.

Q4: Are there other factors influence the oil spill trajectory? What is the relationship between estuarine process and the oil spill spreading pathway?

The Paku Marina project includes the construction of Paku Marina, dredging the access channel, and realigning channel. Even though Reeve et al (2009) suggested that the moderate human interference in the form of dredging and structural construction does not have a significant impact on the overall geomorphology of estuaries in the long-term. The impacts of the dredging and structural construction within an estuary on the estuarine process are also important for the coastal management. An important purpose of this research is to apply hydrodynamic and sediment transport models to address these questions and the potential impacts of the harbour/catchment developments and natural hazards. Specific issues of interest identified by the Waikato Regional Council (WRC) were:

Q5: What are the potential impacts on the estuarine flood/ebb delta because of the channel dredging through tidal inlet?

1.3 METHODOLOGIES

The method of numerical modelling was used in this study. The free MIKE and 3DD modules were supplied by the DHI and ASR ltd. Co to support this research. 2-dimensional and 3-dimensional hydrodynamic, sediment transport and oil spill models were set up based on the field data and station data from Waikato Regional Council and The National Institute of Water and Atmospheric Research (NIWA). The numerical models were calibrated by the data collected in the first field campaign during August 2010, and validated by the second field campaign during June 2011, which as a result were helpful for theoretical analyses and case studies.

- Field Deployments

  Two field deployments were carried out during August 2010 and July 2011, to collect the data of water surface elevation, current speed & direction, water temperature, salinity and turbidity data for numerical model calibrations and validation, also for determining the characteristics of hydrodynamic, sediment transport, water stratification and their interactions with the external forcing such as wind, river flow and seasons.

- Numerical Modelling

  Three different resolutions (50 m, 20 m and 10 m grid size) of two-dimensional hydrodynamic models were developed and calibrated with field observations of surface elevation and current speed data. In addition, a three-dimensional hydrodynamic flexible mesh (FM) model and two-dimensional non-cohesive sediment (sand) transport model were developed to extend the calibrated hydrodynamic model. The MIKE 21 suite, MIKE 3 Flow Model FM from the DHI, and the 3DD suite, POL3DD suites from the ASR were selected to set up these models.

- Theoretical Calculation

  Theoretical equations were used to evaluate key aspects of hydrodynamic and sediment transport behaviours based on the field data, station data and numerical model simulation results.

1.4 THESIS OUTLINE

Part I. INTRODUCTION

Chapter 1 Overview

This chapter supplied the background information of this research, stated the

research aims, main questions, methodologies driving the research and the thesis outline.

Chapter 2 Literature Review of the Study Area

This chapter reviews the background literatures about Tairua Estuary including its history and development, location and geography, oceanography, sediment, water salinity and temperature of Tairua Estuary. All these supplied the background information and boundary data for numerical modelling.

Part II. DATA RESOURCES AND METHODS

Chapter 3 Data Resources

This chapter summarises the principal of the field experimental design, the instrument used for the two field deployment, and associated lab analyses for instrument calibration.

Chapter 4 Numerical Modelling

This chapter discusses the numerical modeling process using the MIKE 21 HD and 3DD Flow modules. It includes the procedure of bathymetries development, boundary files generating, and key parameters selecting, the calibration and validation process of the MIKE 21 and 3DD Flow models with 50 m and 20 m resolution, and finally, the models with same resolution developed by different modules and the models with different resolution but developed using same modules were compared.

Part III. THEORITICAL RESEARCH

Chapter 5 Hydrodynamics and Sediment Transport Features

This chapter updated the physical parameters of Tairua Estuary through comparing with the data from the other scientists' research. And the general hydrodynamic and sediment transport characteristics within Tairua Estuary based on the field observations, the calibrated hydrodynamic models and the results of harmonic analyses of tidal elevation and current speed were discussed.

Chapter 6 Salinity and Temperature Structure

This chapter investigates the vertical and horizontal salinity/temperature distribution features and using the simulation results of a three-dimensional

MIKE 3 FM Flow Model and the field observations. And the impacts of tidal flow and river discharge on estuarine hydrodynamics and sediment transport features were also discussed.

Chapter 7 Forcing Mechanisms of Seiche Hazard and Impacts on Sedimentation

In this chapter, the forcing mechanisms of the seiche event are investigated using meteorological data, field data and numerical models. The impacts of the event on the sedimentation were also discussed.

Chapter 8 Effects of Relative Sea Level Rise on Estuarine Physical Process

Thirteen scenarios were set up with selected river discharge and projected sea level elevations over the next 120 years to study the impacts of potential sea level rise on estuarine process, taking into account of river freshwater discharges, the tidal range, water depth, water surface area, residual current and mean sediment flow rates.

Part IV. MODEL APPLICATION

Chapter 9 Impacts of Marina Construction, Channel Realignment and Dredging on Estuarine Process

This study assessed the potential impacts of a proposed marina construction project (including channel realignment and dredging) on hydrodynamics and sedimentation within Paku Bay and the tidal inlet.

Chapter 10 Continuous Oil Spill Trajectory within Tairua Estuary

Five model scenarios were run to track a continuous oil spill, and investigate the variation in the shape and size of the oil slicks and the evaporation rate, under the impacts of the tidal flow, air/water surface temperature, oil type and wind conditions.

Part V. SUMMARY AND FUTURE WORK

This chapter summarised the answers of the main questions by this study and identifies possible future directions for further research.

CHAPTER TWO
LITERATURE REVIEW OF STUDY AREA

This chapter reviews the background literatures about Tairua Estuary including its history and development, location and geography, oceanography, sediment, water salinity and temperature of Tairua Estuary..All these supplied the background information and boundary data for numerical modelling.

2.1 ESTUARY DEFINITION

The most widely accepted definition of the estuary is that of Pritchard (1967).

> *'…an estuary is a semi-enclosed coastal body of water which has a free connection with the open sea and within which seawater is measurably diluted with freshwater derived from land drainage.'*

However the estuary definition of Day (1981) is suggested by Hume and Herdendorf (1988) as an attentive because it includes the coastal lagoons temporarily cut off from the sea by barrier formation and hypersaline coastal bodies of water in which evaporation exceeds freshwater inflow.

> *'…a partially enclosed coastal body of water which is either permanently or periodically open to the sea and within which there is a measurable variation of salinity due to the mixture of seawater and freshwater derived from land drainage.'*

Prandle (2009) defined estuaries are where 'fresh' river water and saline seawater mix. They act as sinks and sources for pollutants, the biological and chemical nature and with temporal variations in tidal amplitude, river flow, seasons, winds and waves.

2.2 HISTORY AND DEVELOPMENT

Tairua was a small fishing village whose name translates to "two tides" (Wises New Zealand Guide, 1979). Early European settlement of the area in the late 19th century was based around sawmilling (predominantly Kauri) and gold prospecting. Tairua became a popular holiday destination in the late 1960s (Tairua History, 2012). The permanent population was 1,296 recorded residents in the 2006 census. Basing on the forecast resident population from census figures, there will be 1900

dwellings in Tairua by 2016, an increase of over 500 dwellings on the 2001 total of 1370 dwellings (Statistics New Zealand, 2007).

2.3 LOCATION AND GEOGRAPHY

Tairua Estuary is located on the Coromandel Peninsula of New Zealand's North Island (Figure 2-1). It is 6 km^2 in area, 51 per cent of which is intertidal, separated from the open ocean to the east by the 2.65 km long Pauanui Sand Spit and the 1.2 km long Ocean Beach Tombolo to the north (Hume and Gibb, 1987). Paku hill occurs in the central embayment at the entrance to a tidal inlet. The Tairua catchments are steep and rugged, rising to a maximum height of 830 m above sea level at the river's headwaters. The total catchments area is 282 km^2, almost half of which is indigenous forest (Waikato Regional Council Report, 2008). Tairua Estuary is typical of the estuaries on the north-eastern side of the North Island as it is barrier enclosed (Hume and Herdendorf, 1993). Geomorphic changes in this part of the estuary are common, even over a single tidal cycle. However, the inlet is stable with regards to its position, remaining flush against the headland of Paku (Hume and Herdendorf, 1988).

An investigation by EarthTech Consulting Ltd (1991) showed that the low lying flats of Tairua Estuary are floored by a 30 m thick sedimentary deposit. The estuary’s seafloor comprises of medium sands to 10 m depth, with silty sands to 0.2-1.5 m thick. The Tairua tidal inlet comprises of a main channel that is 130 m wide with a mean depth of 2.79 m at mid-tide and a maximum channel depth of 4 m (Hume and Herdendorf, 1992). The lower 1.5 km of the estuary comprises of extensive tidal sand flats which occur on both sides of the estuary. The sand flats display some two-dimensional bed forms and the occasional three-dimensional bed forms. The tidal flats are regarded as relatively stable with few large scale bed forms present, indicating only moderate sediment transport at that area (Hume and Gibb, 1987).

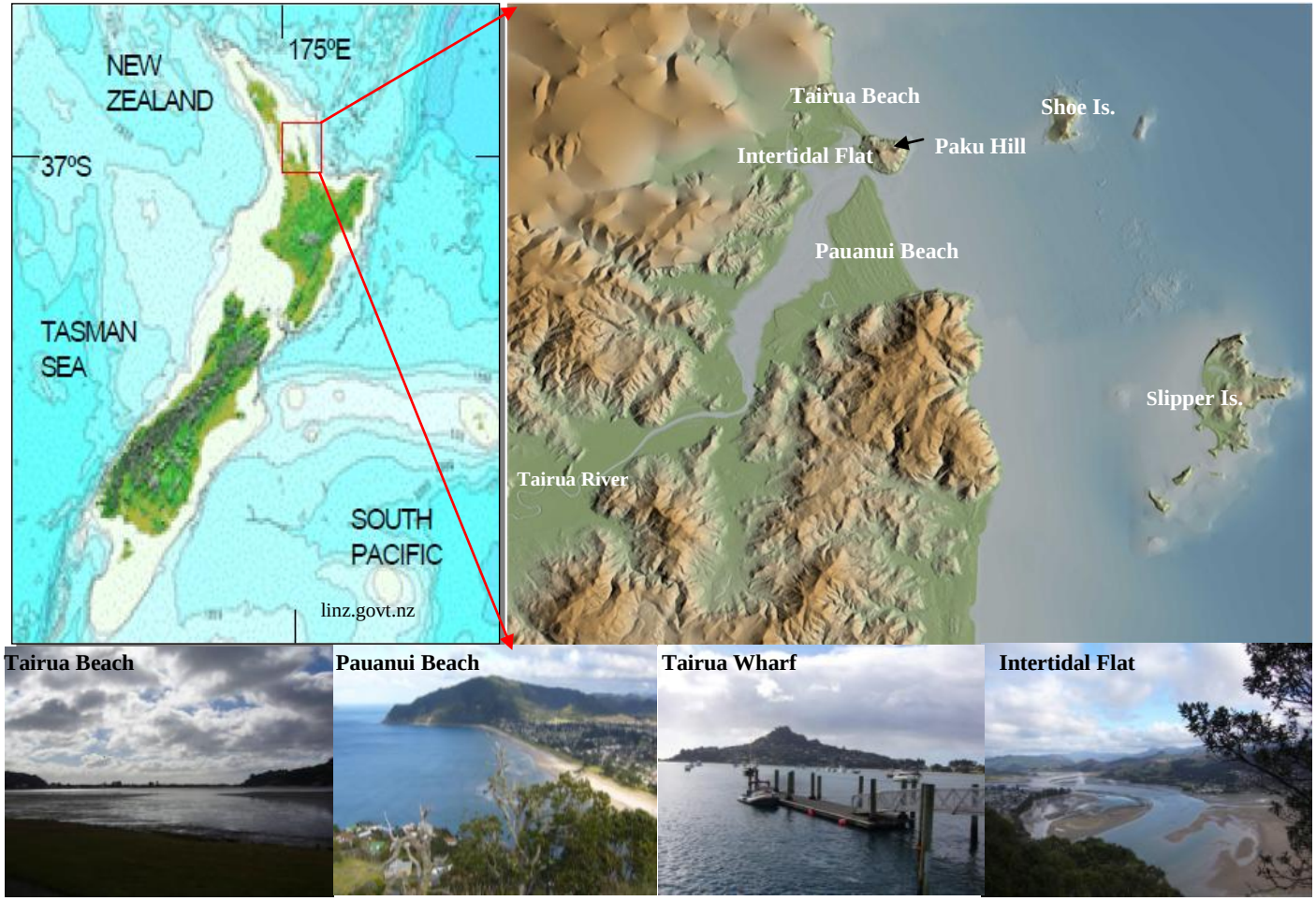

Figure 2-1 Tairua Estuary is located on the Coromandel Peninsula of the North Island, New Zealand.

2.4 WATER SALINITY

Salinity is the saltiness or dissolved salt content of a body of water in the open ocean the range of salinity is generally from about 34 ‰ (grams of salt per litre of solution) to 38 ‰, with an average of about 35 ‰ (Hardisty, 2007), river water can be assumed to be fresh, so that the salinity decreases in the upstream direction. A study of saline mixing by Bell in 1994 identified that 82% of incoming water was new ocean water and that harbour flushing took 1.3 tidal cycles to replace the entire tidal prism volume and 2.3 tidal cycles to replace the mean annual freshwater discharge. Habib et al. (2007) collected the surface salinities data on the shelf during summer of 1978-1979 (Figure 2-2 and Figure 2-3). Six lines of stations (three in each line between 100 and 500 m) from off Slipper Island outside of Tairua Estuary to Cape Brett were sampled. The surface salinity contours shows that the surface salinity is about 35.1‰ during summer and is about 33.7‰ during winter. Ridgway (1968) generated a vertical profile of salinity for the east of New Zealand in Figure 2-4. It shows that the salinity offshore is ranged from an average of 34.5‰ on the water surface to an average 34.7‰ at the water bottom.

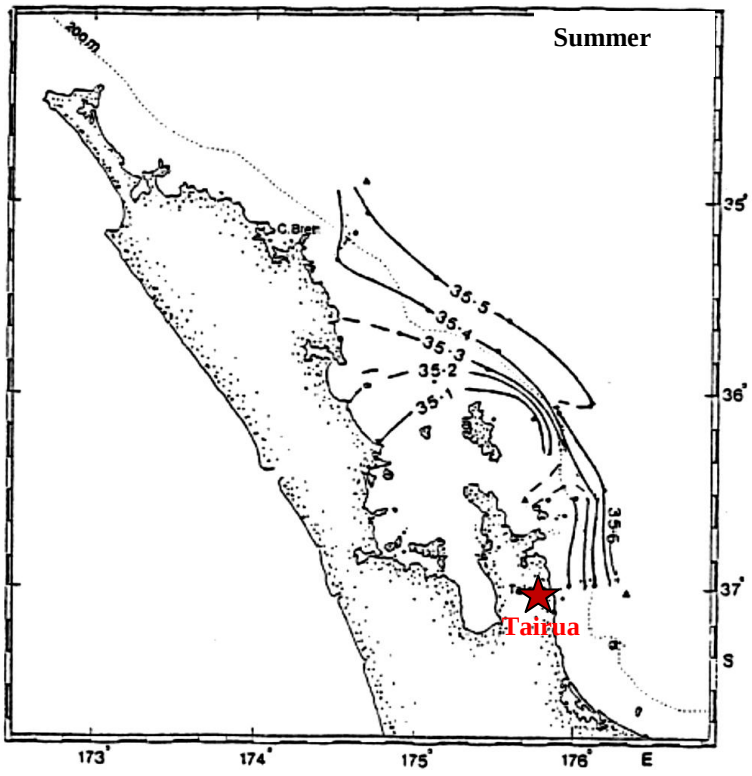

Figure 2-2 Surface salinities (‰) along the shelf break for December 1978 (Habib et al. 2007).

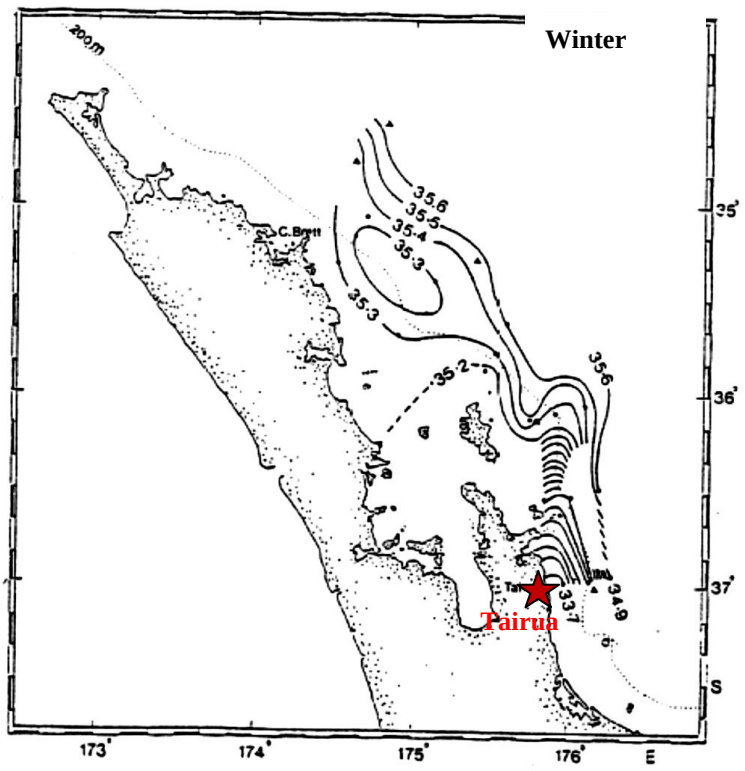

Figure 2-3b Surface salinities (‰) along the shelf break for March/April 1979 (Habib et al. 2007).

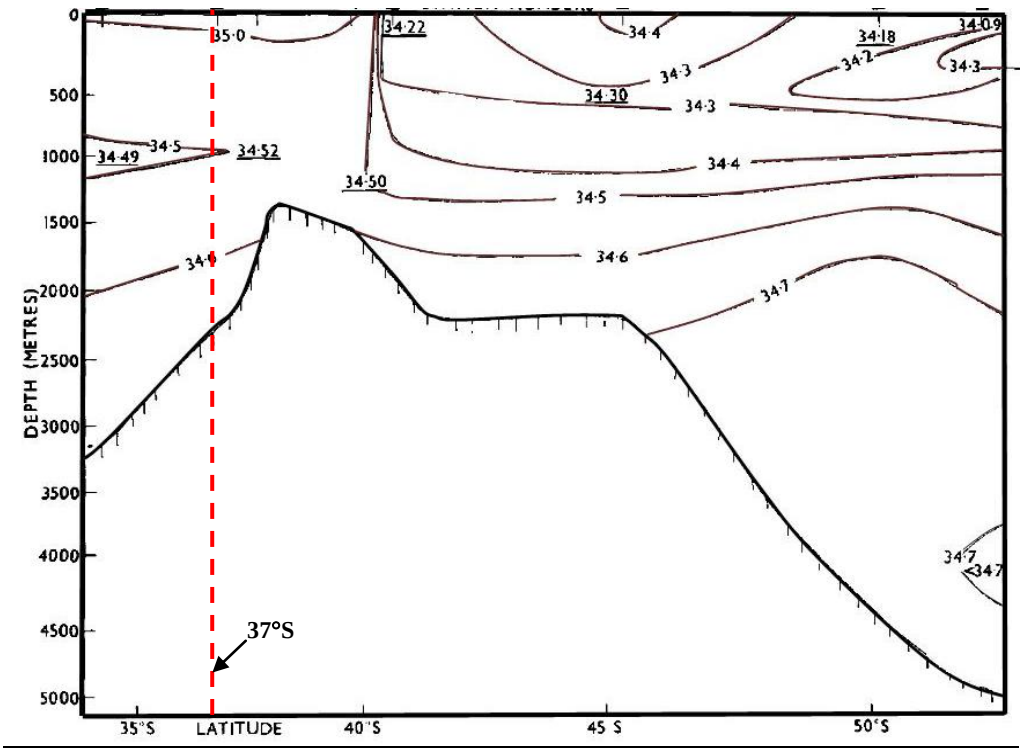

Figure 2-4 Vertical salinity profiles for the east of New Zealand (Ridgway, 1968). Tairua Estuary is located at about Lat. 37°S as shown in red dotted line.

2.5 WATER TEMPERATURE

Sea surface temperature (SST) is the water temperature close to the ocean's surface. New Zealand water tends to be colder in the south and warmer in the north. As spring arrives, the water gradually warms and reaches its highest temperature in late summer. The average seawater surface temperature (SST) is 15 °C in winter and 21°C in summer (Walrond, 2013).

The peak seawater temperature close to the Pauanui Spit and the Tairua Beach was in the range of 20 to 23°C (68 to 73°F) on 8 February, and was at its lowest on 20 August with a range of 13 to 16°C (55 to 61°F). This data was derived from the analysis of oceanographic satellite measurements of nearby open water by the AMS (American Meteorological Society) over two decades.

The vertical profile of water temperature for the east of New Zealand was made by Ridgway (1968) and shown in Figure 2-5. It presents that the water temperature outside of Tairua Estuary (175ºE, 37ºS) is ranged from about 1°C 4000 m below the water surface to about 15°C at the water surface in an average.

These data will be used to estimate the range of the water temperature for numerical modelling and case studies in the following chapters.

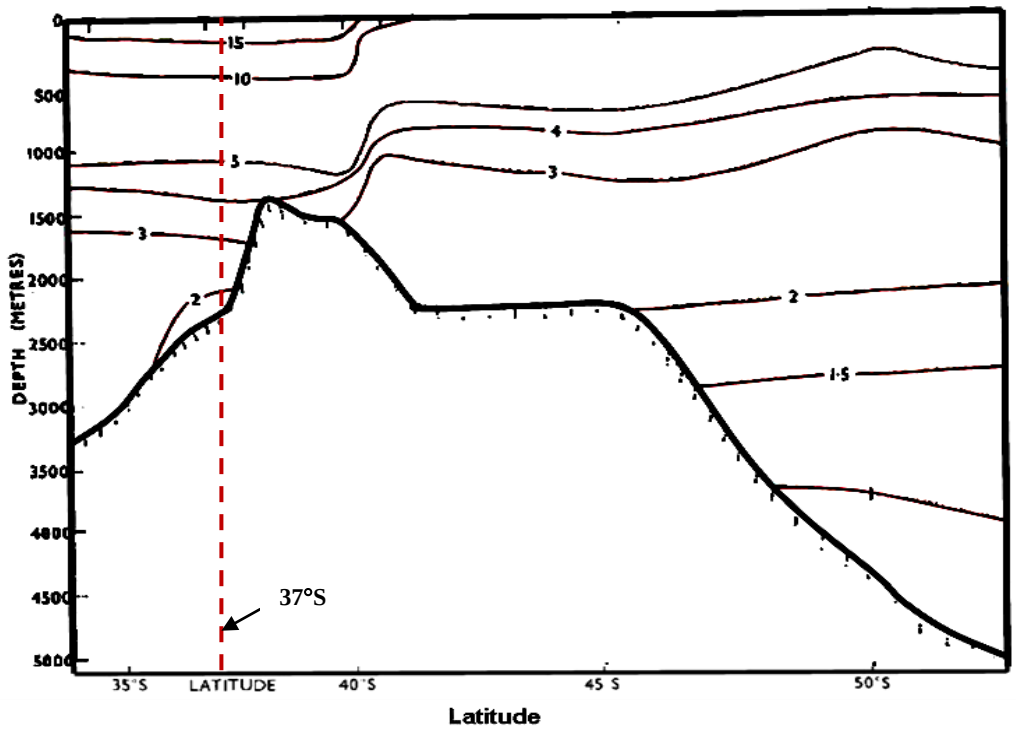

Figure 2-5 Vertical temperature profiles at the east of New Zealand (Ridgway, 1968). Tairua Estuary is located at about Lat. 37°S as shown in red dotted line.

2.6 SEDIMENT COMPONENT AND PROPERTY

The sediments of the estuary enclosed beaches in Tairua Estuary are moderately well-sorted and mostly medium-grained sands comprised of predominantly plagioclase feldspar and volcanic glass (Gibb, 1983). Hume and Gibb (1987) found that the sediments of the lower 1 km of Tairua Estuary are comprised of medium to fine grained sand which is well to very well-sorted and commonly contains shell fragments and small gravel-sized particles within the sand-sized sediment. These sediments are supplied from the Tairua River, Pere Stream, Graham's Creek and the ebb tidal delta. The shell fragments are generated locally and make up to 10% of the sediment volume. The extensive tidal flats of the lower Tairua Estuary are comprised of predominantly plagioclase feldspar and volcanic glass (>50%) with minor amounts of quartz (<5%), cristobalite, opaque, pyroxene and hornblende. Tairua Beach is steep and reflective, and is comprised of shelly 0.4 mm medium sand (Gibb, 1983). GNS Science Report (2007) recorded that the seabed offshore from the beaches is very fine sand with coarse-grained rippled sands in patches to 50-60 m depth.

Sediment samplings at 275 sites within Tairua Estuary were carried out and the sediment grain size of the 111 samples were analysed between November 2009 and March 2010 by Robertson & Peters (2006). The sediment grain size analysis results shown in Figure 2-6 and Figure 2-7 indicated that the sediments are dominated by both fine sand (63-250 μm) and medium sand (250-500 μm) within Tairua Estuary. The majority (55%) of these samples contained 40% or more fine sand, and 24% of sites contained 50% or more fine sand. Similarly, 50% of samples contained 40% or more medium sand, and 14% of samples contained 50% or more medium sand. Mud (grain size <63 μm) was found in 60% of the samples, with the majority (70% of those which contained mud) containing less than 10% mud. The highest proportion of mud found was 85%, and only one other sample contained 50% or more mud. The main body of the estuary should be sandy with muddies areas in the remote areas furthest from the tidal inlet (as is evident in Figure 2-7).

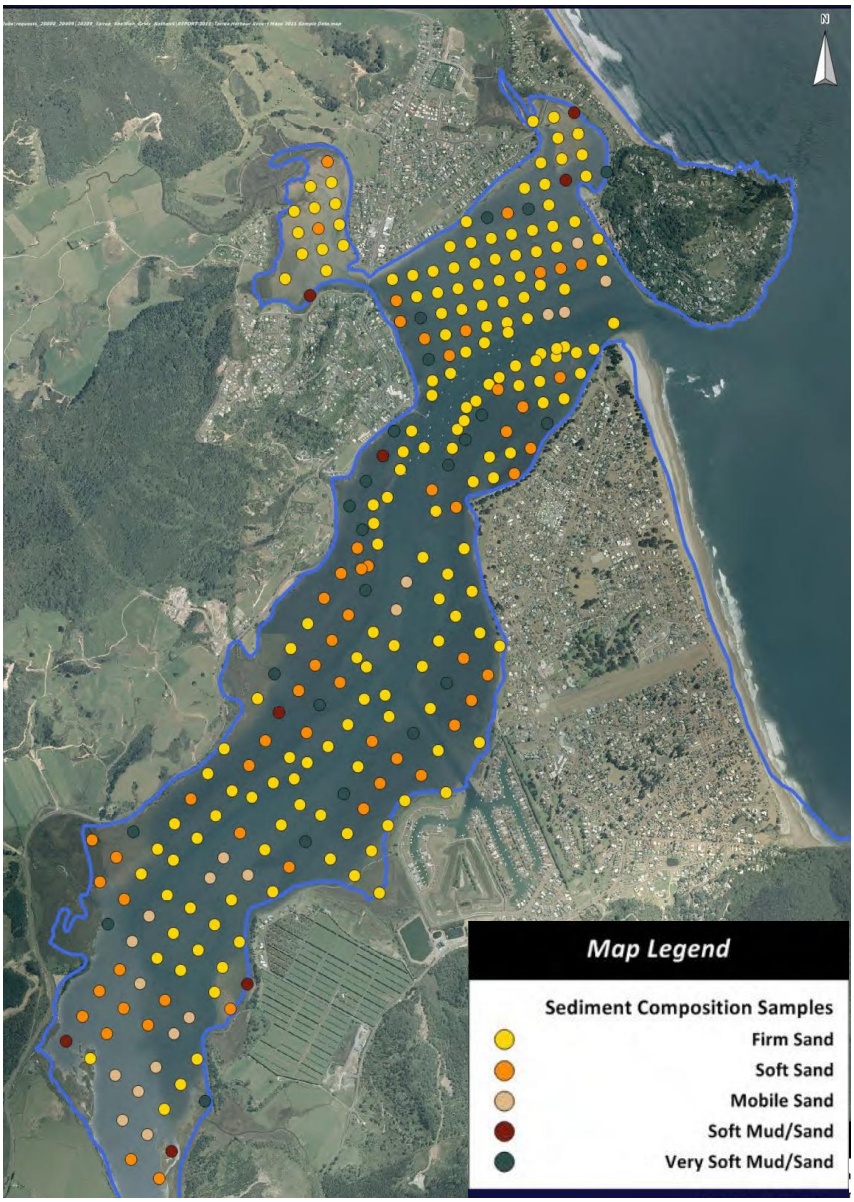

Figure 2-6 Locations of sediment composition samples within Tairua Estuary where sediment samples were collected (Robertson & Peters, 2006).

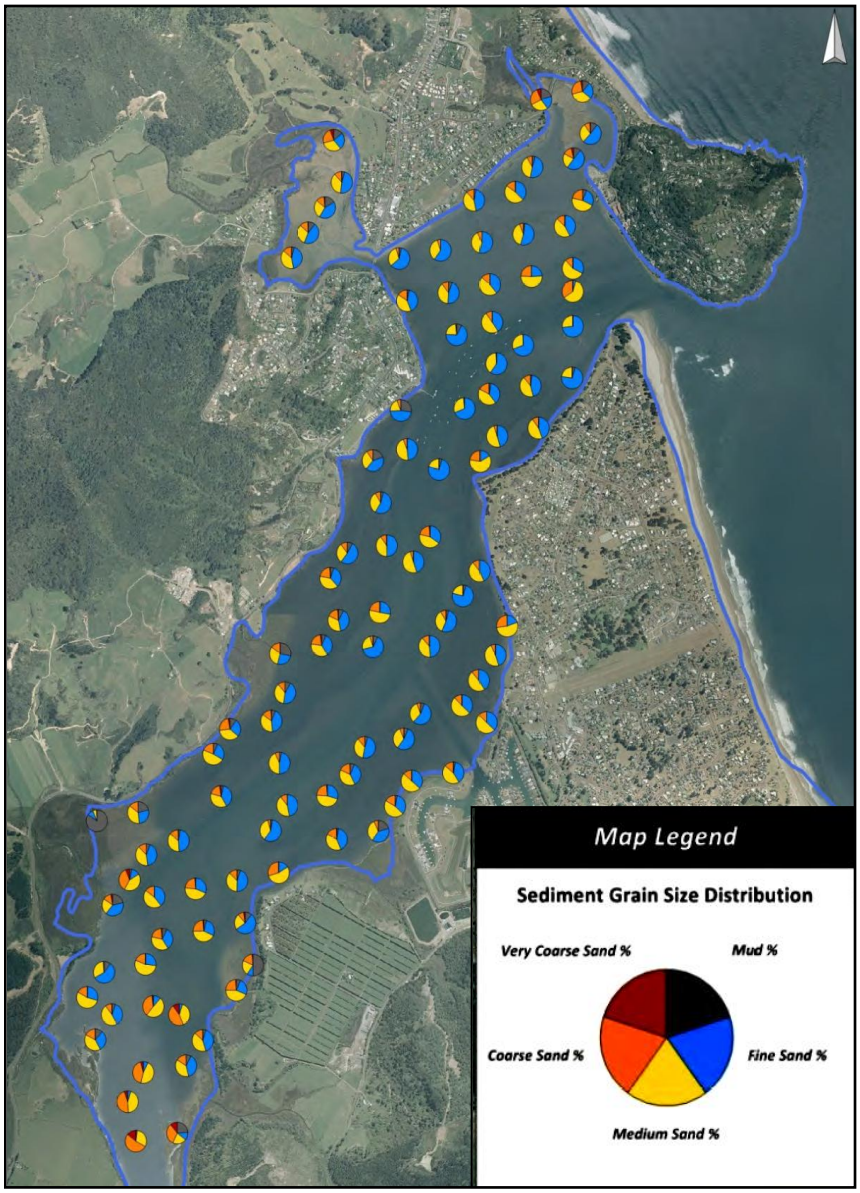

Figure 2-7 Sediment grain size distribution within Tairua Estuary where sediment samples were collected (Robertson & Peters, 2006).

2.7 PHISICAL PROPERTY

Tides refer to a periodic vertical or horizontal water movement, which has coherent amplitude and phase relationship to some periodic geophysical movement (Pugh 2004).

The tidal range (the difference between the high and low waters) varies around New Zealand, reaching 3.5-4 m on the west coast but only 1-2 m on the east coast. Tairua Estuary is a micro-tidal estuary with a spring tidal range of 1.63 m

observed at the Tairua Wharf and a neap tidal range of 1.22 m at the Paku jetty (Barnett Consultants, 1991). The estuarine area covers 6.1 km^2 at high tide, the intertidal area is 77% of the high tide area (Hume and Herdendorf, 1992). The spring tidal prism of the estuary is 5.02 million m^3 flowing through a tidal inlet with 430 m^2 cross area. The peak spring tide discharge through the inlet is 436 $m^3 s^{-1}$ and a mean velocity of 0.66 m s^{-1} tidal currents speed through the tidal inlet (Hume and Herdendorf, 1993). The tidal exchange of estuarine water with coastal water is quite high, approximately 82% of the incoming flood tide comprising 'new' ocean water (Bell, 1994).

The related oceanographic data for Tairua Estuary are listed in Table 2-1. The mean high water level for spring tides (MHWS), the mean high water on neap tides (MHWN), the mean low water for spring tides (MLWS), the mean low water on neap tides (MLWN) and the mean sea level are presented in Table 2-2.

Table 2-1 Oceanography value relating to the Tairua tidal inlet

Description	Value*	Value^
Catchment area	280 km^2	
Surface area at MHWS	6.12 km^2	
Spring tidal range	1.6 m	
Spring tidal prism	5.02×10^6 m^3	
Peak Springs discharge	436 m^3/s	
Mean throat velocity	0.66 m s^{-1}	
Peak throat velocity	1.01 m s^{-1}	1.6 m s^{-1}
Throat width	130 m	
Mean depth	2.8 m	
Throat area (measured)	430 m^2	

*Hume & Herdendorf, 1988; ^ Joynes and Barnett, 1991

Table 2-2 Tides for Tairua Estuary (Green, 1994)

Lat. Lon.	Sea Level Heights (m)				
	MHWS	MHWN	MLWN	MLWS	MSL
37°00´ **S,** 175°51´**E**	1.9	1.6	0.4	0.1	1.0

2.8 SEDIMENT TRANSPORT RATE

The dominant variables controlling the processes and rates of tidal inlet sediment transportation include tidal prism, inlet geometry, wave and tidal energy, sediment supply, spatial distribution of the back barrier channels, regional stratigraphy, near shore slope and the engineering modifications (FitzGerald, 2000). Hume and Gibb (1987) calculated sedimentation rates of 6 mm per year over the Tairua tidal flats. The rate was as high as 10-19 mm yr^{-1} at the tidal inlet and up to 22 mm per year at the estuary entrance. This high rate of sedimentation is attributed to the estuary's large size, steep catchments and the vulnerability of the land to erosion. In addition, the large scale clearance of kauri from intensive milling over the last century has most likely contributed to the high sedimentation rates (Hume and Gibb 1987). The sediment transport for Tairua Estuary is about 80.7 ton per square kilometer per year estimated from the NIWA's suspended-sediment yield estimator model by Hicks and Shankar in 2006. A marker bed study has estimated the sedimentation rate in the lower estuary, between 1933 and 1984, to have ranged between 2 mm and 22 mm per year and to have averaged 6 mm per year, much greater than the pre-European settlement sedimentation rates.

2.9 SEDIMENT INFILLING

Estuaries with relatively smaller tidal prisms and large catchments are potentially more vulnerable to sediment infilling (Jones & Preston, 2008). Tairua Estuary has a small spring tidal prism of 5.02 million m^3 comparing with the large tidal prism of 47.8 million m^3 at the Coromandel Harbour, which has a similar catchments area of 271 million m^2 (Hume and Herdendorf, 1992). Hence, the Tairua Harbour is at most risk of infilling, followed by Whitianga, Wharekawa, Whangamata and Whangapoua (Jones et al, 2008).

2.10 CLASSIFICATIONS AND FEATURES OF TAIRUA ESTUARY

Dyer (1979) classified estuaries into four types including salt-wedge estuaries, partially-mixed estuaries, well-mixed estuaries and fjords. Dyer (1973) classified Tairua Estuary as a partially-mixed estuary where the whole mass of water in the estuary moves backwards and forwards with a tidal periodicity of about 12.5 hours, and there is considerable friction between the water and the estuary bed creating the turbulence. Turbulence tends to mix the water column more effectively than entrainment, causing the salinity to decrease to the head of the estuary in the lower layer and to increase progressively towards the sea in the surface layer; though there is no water movement there is a salt exchange

vertically; the landward flow at the bottom can be of order 0.05 m s^{-1} with tidal oscillations of 0.5 m s^{-1}.

Hume & Herdendorf (1988) classified Tairua Estuary as a fluvial eroded barrier-enclosed single-spit (type 4) and Tombolo (type 5) compound estuary, with the features of a barrier enclosed estuary where waves mix river and shelf-derived sands in the littoral system; a mixed estuary with high tidal prism; with high susceptibility to sediment infilling and resulted in channel infilling, expansion of tidal flats, tidal arm siltation and tidal prism reduction; and with low channel/shoal, inlet and barrier stability.

Hume et al. (2003) developed an Estuary Environment Classification (EEC) system to classify New Zealand estuaries on the basis of factors such as climate, the catchments characteristics, oceanic and riverine conditions. Tairua Estuary is classified as Category G: a tidal lagoon. It has the features of shallow basin of various shapes with extensive intertidal area; narrow entrance to the sea, ebb and flood tidal deltas at mouth; tidally dominated circulation and mixing; small river influence compared to the tides; good flushing because much of the water leaves the estuary on the outgoing tide; mixes well because strong tides and shallowness prohibit density stratification; and wind generated 2-D circulation, mixing and wave re-suspension is important in larger systems where fetch is great and wind is strong.

According to Hume's NZ estuary classification (Coastal Xplore Webtool, 2007), Tairua Estuary belongs to the Category F: barrier enclosed lagoons or drowned valleys with the features of shallow basins and narrow mouths, usually formed by a Spit or sand barrier; complex shorelines with numerous arms leading off a main basin; extensive intertidal area cut by deal deep channels; sand bodies (ebb and flood tidal deltas) occur at the mouth on littoral drift shores; tidal prism makes up a large proportion of the tidal volume; river inputs over the tidal cycle small compared to the total volume of the estuary; hydrodynamic processes dominated by the tides; little wind generated circulation, mixing and wave re-suspension of the substrate because of restricted fetch; substrate sandy in main body and muddy in the arms.

Although different classifications have been proposed over time, it is suggested that Tairua Estuary is expected to be well mixed, tidally dominated, with extensive intertidal areas. The main body of the estuary should be sandy with muddies areas in the remote areas furthest from the tidal inlet (as is evident in Figure 2-7). This study will assess if this basic classification is appropriate for Tairua Estuary.

2.11 ESTURINE PROCESS

2.11.1 Hydrodynamics of Vertical Processes

Simpson & Souza (1995) observed in the Rhine region of the North Sea and showed large semidiurnal oscillations in water-column stratification at times of reduced mixing. The amplitude of these semidiurnal variations resulted primarily from the interaction of cross-shore tidal-current straining with the density gradient. In the Hudson River estuary, and also in the upper reaches of the Tamar, tidal straining maintained stratification during the ebb, while it promoted the growth of a uniform, near-bed mixed layer during the flood (Nepf & Geyer, 1996). In general, maximum and minimum near-bed stratification occurred during late ebb and late flood, which reflected the dominant role played by tidal straining in determining intertidal variations. Stacey et al. (2001) discussed that the estuarine circulation might be partially caused by barotropic (water level driven) forcing in this flood-ebb stratification asymmetry.

Sharples et al. (1994) observed vertical density structure in the Upper York River estuary, the results showed periods of mixed and stratified conditions in which reduced stratification, or complete mixing, occurred during strong spring tidal currents and significant stability during weaker currents. In strongly stratified estuaries, tidal variations in stratification are reflected in the depth and thickness of the density interface between surface and bed layers (Cudaback & Jay, 2000).They also found that bottom friction increased vertical shear on the ebb and decreased it on the flood, so that the pycnocline grew thicker on the ebb and thinner on the flood.

The onset and variability of estuarine density stratification has many consequences for water and sediment transport and ecology (Joordens et al., 2001; Boicourt, 1992). Thermohaline stratification may influence the near-bed velocity profile in low to medium energy estuaries and other systems influenced by buoyancy. Even without the influence of buoyancy, a pronounced tidal current asymmetry, in which flood speeds significantly exceed ebb speeds, is a common feature in the upper reaches of many strongly tidal estuaries. In a study of South San Francisco Bay, faster current speeds led to a reduction of roughness length, which is hypothesized to be due to sediment erosion. Within energetic estuaries, suspended particulate matter (SPM) eroded from the bed sediments by strong currents may cause density stratification and influence the stability of the water column (Cheng et al., 1999). Alvarez et al. (1999) demonstrated that sediment-load effects on the depth averaged tidal dynamics of a bay system were likely to be small, but the consequences for mean circulation in highly turbid, stratified estuaries may be much more significant.

Pattiaratchi et al. (1997) have shown that locally generated wind waves, particularly those associated with strong sea-breeze activity play a dominant role in controlling near shore and foreshore processes. Waves will also play a role in estuarine plume regions and in large estuaries, where they may influence sediment and mixing processes in shallow subtidal and intertidal areas (Green & MacDonald, 2001; Ruhl et al., 2001; Christie et al., 1999; Green et al., 1997). In very shallow areas, such as over intertidal mudflats and within coral reef lagoons, even small breaking waves appear to be capable of enhancing local turbidity.

2.11.2 Hydrodynamics of Transverse Processes

The effects of channel shape on cross-estuary (transverse or lateral) spatial variations in the along channel (longitudinal or axial) velocity are known to be significant in partially mixed estuaries (Friedrichs & Hamrick, 1996).

Valle-Levinson et al. (2000a) used a towed ADCP over approximately 4 km-wide sections (which featured a channel flanked by shoals) to investigate this aspect of the transverse momentum balance. They showed that transverse baroclinic pressure gradients were larger during neap than spring tides and that, during springs, advective accelerations were predominantly greater than Coriolis accelerations, especially over the edges of the channel.

Valle-Levinson and Atkinson (1999) have shown that similarly strong spatial gradients can occur even in the flow through very wide estuaries. They utilized ADCP data from the lower Chesapeake Bay to illustrate bathymetrically induced spatial gradients in the currents. The greatest transverse shears and convergence zones were found on the shoulders of the channel, where bathymetric changes were sharpest.

Longitudinal tidal currents can also generate transverse circulation patterns as they respond to the curvature of a meandering channel. These secondary flows are particularly persistent in the presence of stable density stratification when the effects of vertical mixing and friction are greatly reduced (Lacy & Monismith, 2001).

Valle-Levinson et al. (1998) found that most of the subtidal volume exchange took place in the main channels. Gravitational circulation and wind forcing produced the mean flow patterns in the channels, regardless of wind direction, whereas the flow over shoals was caused by tidal rectification (Li & O'Donnell, 1997) and wind forcing, with the dominating influence determined by wind direction. Subtidal currents over the shoals were driven in the same direction as the wind stress, whereas a return flow occurred in the deep channel, as would be anticipated for a system dominated by barotropic forcing and bed friction (Geyer, 1997).

2.11.3 Tidal Asymmetry and Sediment Transport

Estuarine morphology is to a large extent determined by the residual sediment transport pattern. However, residual sediment transport depends on differences in magnitude and duration between ebb and flood tidal currents (Dronkers, 1986).

The evolution of an estuary depends essentially on two processes: the long-term averaged sediment supply from inland or coastal origin, and the direction and magnitude of the long-term averaged sediment transport; abrupt changes in the estuarine morphology caused by storm surges or by engineering works (Dronkers, 1986). In the final stage of evolution, river water is discharged directly on the coastal shelf (Schubel & Meade, 1977).

The main factors deciding the sediment supply and sediment transport pattern (Dronkers, 1986) include:

-The river inflow related to an input of sediment and a cross-sectional flow structure affected by density differences. The density differences tend to increase flood currents in the deepest parts of the channel, especially in the lower half of the vertical profile, and tend to decrease flood currents near the surface and in the shallow parts of the cross-section. The inverse holds for the ebb currents. This flow structure has an important impact on the sediment transport (Postma, 1967; Festa & Hansen, 1978).

-The sediment characteristics. The influence of tidal asymmetry on the residual fluxes of coarse and fine sediment is different. The suspension load of coarse sediment is strongly limited by the current speed and it adapts to changes in the current speed rapidly in comparison with the tidal time scale. For fine sediment, saturation of the suspended load seldom occurs. Most fine sediment settles only at very low current speed and the settling time delay is important.

-Wind waves, swell. The purely wave-induced sediment transport is relatively less important in estuaries than on the coastal shelf. However, the influence of wind waves, in tidal flat areas at high water, on the re-suspension of sediment is a significant phenomenon (Anderson, 1972; McDowell & O'Connor, 1977). In combination with subsequent tidal transport, it can cause a substantial seaward sediment flux.

-The current velocity distribution and variation during a tidal cycle. Two elements are mainly responsible for residual sediment fluxes. The tidal variation at the tidal inlet, which bears the characteristics of tidal wave propagation on the coastal shelf (amplification, distortion); the tidal propagation inside the tidal basin, generally consisting of a complex geometrical system formed by meandering and braiding channels and tidal flats.

Globally speaking the following features of tidal wave deformation is relevant for residual sediment transport (Uncles, 2001): difference between the maximum tidal currents during ebb and flood, which in particular affects the residual flux of the coarse suspended fraction; and difference between the slack water periods preceding ebb and flood, which particularly influences the residual flux of the fine suspended fraction.

2.12 CONCLUSION

This literature reviewed the information of the Tairua Estuary for the numerical modelling and updating. It also supplied the main results of the hydrodynamic and sediment transport researches on Tairua Estuary by other scientists, for comparing with the results done by this research.

The literature review of the classification of Tairua Estuary by other scientists basing on different factors helps to summary the features of Hydrodynamic and sediment transport of Tairua Estuary.

PART II. DATA AND METHODS

CHAPTER THREE
DATA RESOURCES

The data supporting this research were obtained from field instruments, laboratory work and other data sources. This chapter introduces the field instruments and provides detailed information about the observed data, the lab methodology for instruments calibration and the environmental data recorded at the stations belonging to the Waikato Regional Council and NIWA.

3.1 FIELD WORK

This research involved two field instruments deployments during August 2010 and June 2011, for collecting data on waves, tidal currents, river discharge and suspended sediment concentrations for calibrating and verifying hydrodynamic and sediment transport numerical models of Tairua Estuary.

3.1.1 Field Instruments Deployment in July 2010

3.1.1.1 *Principal of the Experimental Design*

The first field instruments were deployed mainly at the lower reach of the Tairua Estuary for 40 days covering the neap and spring tides during high Tairua River discharge season in August, 2013. The instruments collected data on water levels tidal currents, and Tairua River flow for calibrating the numerical models and also the study of flow constrictions; suspended sediment concentrations for sediment transport study; two S4s were used to collect the tidal flow data and compare with the tidal data from NIWA's model results for the model boundary files.

3.1.1.2 *Deployed Instruments*

The first field deployment was undertaken from 27 July, 2010 to 4 September, 2010. The deployed instruments include two InterOcean S4ADWs (electromagnetic current meter), three Argonaut ADVs (Acoustic Doppler

Velocity meter), one Argonaut ADP (Argonaut Acoustic Doppler Profiler), one DOBIE tide gauge installed with OBS (Optical Backscatter Sensor), one SCUFA Fluorometer, and one RBR Tide Gauge (Table 3-1 and Figure 3-1).

3.1.2 Field Instruments Deployment in June 2011

3.1.2.1 *Principals of the Experimental Design*

The second field deployment to provide additional data for verifying the hydrodynamic and sediment transport numerical models. During the initial model setup and calibration process, a few issues were identified related to a lack of available data from the upper estuary. Therefore, the same instruments were deployed at the same locations during this field deployment. There appeared to be stratification in the upper estuary resulting in the formation of a salt wedge under the layer of the freshwater discharge from the Tairua River, contrary to expectations based on the classification of the estuary by previous studies. Two CTD and four DataFlows were used to collect salinity and temperature data for the water stratification research.

3.1.2.2 *Deployed Instruments*

The second field deployment was undertaken from 8 June 2011 to 12 July 2011. The deployed instruments included two InterOcean S4ADWs, three Argonaut ADVs, one Argonaut ADP, one DOBIE tide gauge installed with a D&A Instruments OBS, one RBR Tide Gauge at the same sites as the first field deployment. Extra instruments included one ADCP, two CTDs and four DataFlows deployed this place. And a wind station was set up within the main channel (Figure 3-2 and Table 3-2).

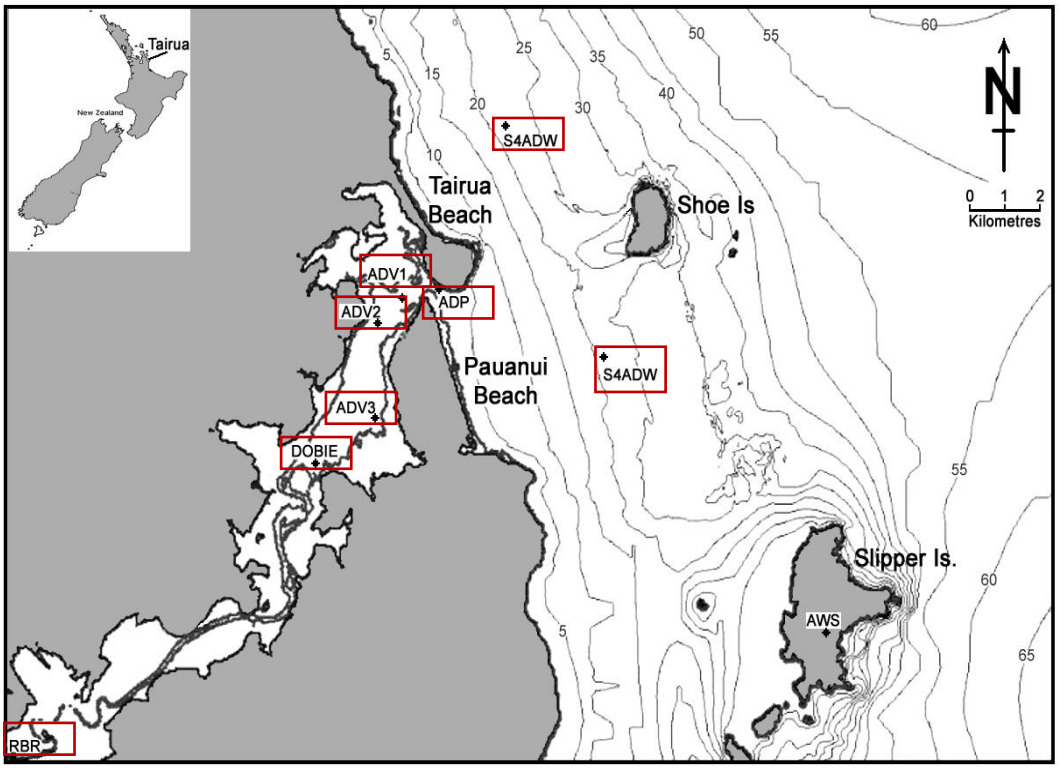

Figure 3-1 Locations of the deployed instruments in Tairua Estuary from 26 July, 2010 to 13 September, 2010. They include two S4ADW, one ADP, three ADVs, one DOBIE, and one RBR.

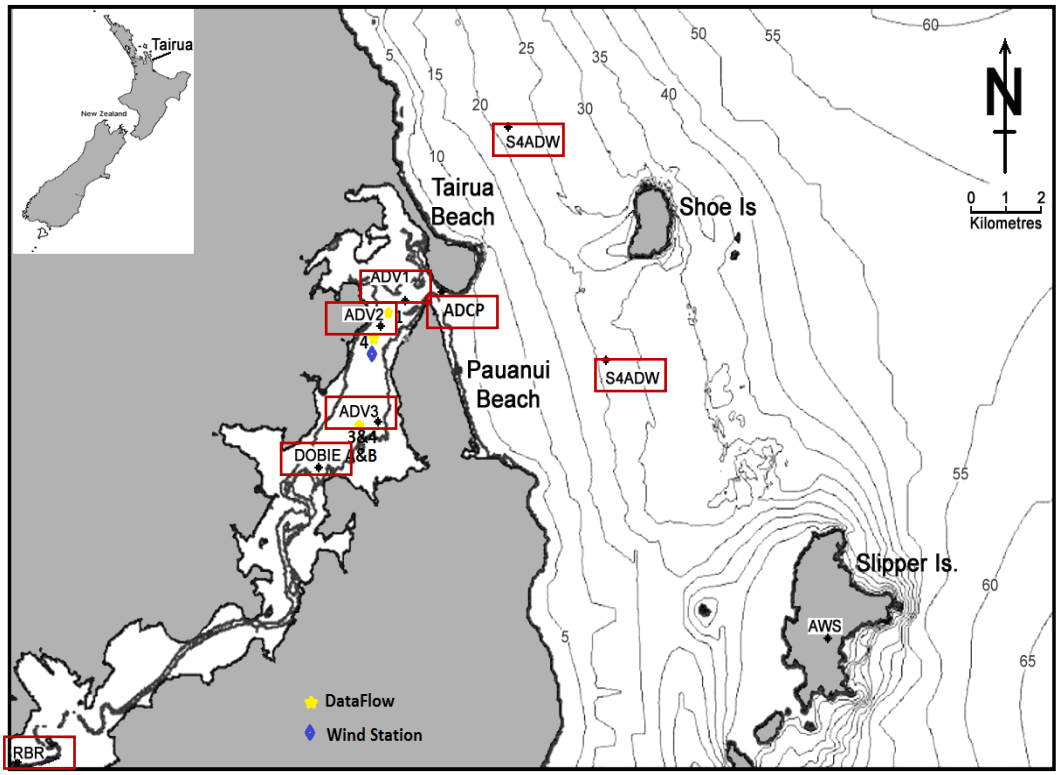

Figure 3-2 Locations of the deployed instruments in Tairua Estuary during the second field campaign from 8 June to 12 July, 2011. They include four Dataflow, one wind station, and all the other instruments deployed during the 1st field work at the same locations.

Table 3-1 Information of the deployed instruments (from 28 July to 14 Sept., 2010)

Name	Period	Site	Time Step
S4 North	27/07/2010 00.00 28/08/2010 00.00	Tairua Beach 36° 59.00´ S, 175° 52.60´ E	0.5 s Burst 18 min per hour
S4 South	27/07/2010 00.00 28/08/2010 00.00	Pauanui Beach 37° 01.00´ S, 175° 54.00´ E	
ADCP	27/07/2010 12.00 08/09/2010 10.30	Estuary entrance 37° 00.28´ S, 175° 51.91´ E	10 min
ADV1	27/07/2010 12.00 07/09/2010 18.10	Mooring Place 37° 00.38´ S, 175° 51.44´E	5 min
ADV2	27/07/2010 12.00 07/09/2010 17.55	Wharf 37° 00.58´ S, 175° 51.10´E	5 min
ADV3	27/07/2010 12.00 07/09/2010 18.25	Pauanui Waterway 37° 01.30´ S, 175° 51.07´E	5 min
DOBIE	27/07/2010 06.30 08/09/2010 05.00	Pauanui Waterway 37° 02.22´ S, 175° 50.37´E	30 min
SCUFA	26/07/2010 11.12 13/09/2010 09.30	Pauanui Waterway 37° 02.22´ S, 175° 50.37´E	30 min
RBR	28/07/2010 09.00 04/09/2010 17.00	Tairua River mouth 37° 04.47´ S, 175° 46.96´E	10 min

Table 3-2 Information of the deployed instruments (from 6 June to 14 July, 2011)

Name	Period	Site	Time Step
S4 North	08/06/2011 10.30 11/07/2011 12.30	Tairua Beach 36° 59.00´ S, 175° 52.60´ E	0.5 s Burst 18 min per hour
S4 South	08/06/2011 10.00 12/07/2011 12.00	Pauanui Beach 37° 00.52'S, 175° 52.46'E	
ADCP	09/06/2011 06.52 09/06/2011 18.04	Estuary entrance 37° 00.32'S, 175° 52.03'E	30 min
ADV1	09/06/2011 11.50 12/07/2011 10.25	Mooring 37° 00.38' S, 175° 51.44'E	5 min
ADV2	09/06/2011 12.00 12/07/2011 10.35	Wharf 37° 00.58'S, 175° 51.10'E	5 min
ADV3	09/06/2011 13.10 12/07/2011 10.05	Pauanui Waterway 37° 01.30' S, 175° 51.07'E	5 min
DOBIE A	08/06/2011 10.00 26/06/2011 10.30	Pauanui Waterway 37° 02.19'S, 175° 50.39'E	30 min
DOBIE B	08/06/2011 10.30 08/07/2011 09.30	Power pole 37° 01.30' S, 175° 51.07'E	30 min
Dataflow 4054	08/06/2011 12.15 12/07/2011 10.30	Wharf (with ADV2) 37° 00.576'S, 175° 51.103'E	15 min
Dataflow 4055	08/06/2011 12.54 12/07/2011 10.45	Power pole (vertical, with ADV3) 37° 01.30' S, 175° 51.07'E	15 min
Dataflow 4056	08/06/2011 12.54 12/07/2011 10.45	Power pole (horizontal, on ADV3) 37° 01.30' S, 175° 51.07'E	15min
Dataflow 4053	08/06/2011 12.45 12/07/2011 09.20	Wharf (on buoy) 37° 00.58'S, 175° 51.10'E	15 min
Wind Station	08/06/2011 14.30 12/07/2011 09.00	37° 00.64'S, 175° 51.13'E	30 min

3.1.3 Instruments, Principles and Setting-up

3.1.3.1 *InterOcean S4ADW*

The S4 Electromagnetic Current Meter measures the voltage resulting from the motion of a conductor (water flow velocity) through a magnetic field according to Faraday's law of electromagnetic induction. An alternating magnetic field and synchronous detection techniques are used to measure the voltage at the sensing electrodes. Two orthogonal pairs of electrodes and an internal flux gate compass provide the current vector (user manuals).

Two S4ADWs are mounted 0.93 m above the seabed in a fixed frame (Figure 3-3a) to collect the data of the surface elevations, current speed and waves at 2 Hz (0.5s) for 18 minute bursts every one hour. They were located outside of the estuary offshore from the Tairua and Pauanui Beaches (Figure 3-1 and Figure 3-2).

3.1.3.2 *SonTek ADP*

The SonTek ADP (Argonaut Acoustic Doppler Profiler) uses digital incoherent processing for the measurement of velocity profiles (manual). Although this technique works well for measuring mean currents, it cannot produce velocity data with the sufficient accuracy and time resolution required for directional wave analyses (Kraus, 1994).

One Argonaut ADP (Figure 3-3b) was deployed at the Tairua tidal inlet to record the velocity data at a critical calibration point for the hydrodynamic model. The ADCP recorded the water temperature (°C), water pressure (dbar), current speed (cms^{-1}) and current direction referred to the true north (degree) every 10 minutes.

3.1.3.3 *Argonaut ADV*

The Triton ADV (Acoustic Doppler Velocity meter) uses the pulse-to-pulse coherent Doppler technique. This principle consists of transmitting a pair of pulses separated by a lag, and computing the phase difference between the two pulses (user manuals).

Three Argonaut ADVs (Figure 3-3c) were distributed along the main channel of the lower Tairua Estuary. They recorded one-minute-averaged water pressure (dbar), current speed ($cm\ s^{-1}$) and current direction relative to true north in bursts for 5 minutes every 20 minutes. The default water temperature was 20°C. The default salinity was 34.5 ppt. And the default sound speed was 1520.9 $m\ s^{-1}$. No wave spectra were measured by the ADVs. The reference water depth was -0.20m. The coordinate system was East, North and Up coordinates, a local Earth based coordinate system (ENU).

3.1.3.4 *RBR Tide Gauge*

The TWR-2050P RBR (Figure 3-3d) is a self-contained submersible tide and wave logger, designed for unattended measurement of tides and waves. Tidal averaging time is user-selectable to remove the effect of wave activity. The temperature channel of the TWR-2050P is calibrated to an accuracy of ±0.002°C (ITS-90), with typical annual drift of better than 0.002°C (user manuals).

The RBR tide gauge was used to record a one-minute-averaged water depth and water temperature at the river mouth (under the Tairua Bridge). It was a key location as it is one of the open boundaries in the model. The RBR recorded the temperature in °C, air pressure in dbar and water depth in metre every 10 minutes at a rate of 1 Hz. It is necessary to determine the elevation of the bridge deck relative to mean sea level to provide a suitable datum for the RBR data. Fortunately, there was a stainless steel pin located on the upstream side of the bridge at 1847378.18E 58932209N representing 7.60 m water level (NZTM2000), which provided a suitable datum.

3.1.3.5 *SCUFA Fluorometer*

The fluorescence channel of the SCUFA Fluorometer was configured to detect chlorophyll α and Cyanobacteria using Rhodamine WT tracer dye. Turbidity data was recorded simultaneously with the fluorescence data, allowing for meaningful comparisons between the fluorescence and turbidity data (user manuals).

The SCUFA (Figure 3-3e) was used to record the turbidity data simultaneously at the same site with the DOBIE every 10 seconds; it's used to calibrate the DOBIE data and to ensure the turbidity data could be recorded in case one of the instruments stopped working.

3.1.3.6 *ADCP*

The ADCP (Acoustic Doppler Current Profiler) is a sound navigation and ranging system (SONAR) that attempts to produce a record of current velocities for a range of depths. The SONAR is used for the measurement of oceanography, estuary, river, stream flow, and weather forecasting. Depending on the field application, an ADCP may use one or more ceramics as transducers. These transducers are aimed such that the sound pulse travels through the water in different, but known directions. As the sound energy leaves and arrives at the transducer face it is shifted in frequency, known as the Doppler Effect, by the relative velocity of the water. By repetitive sampling of the return echo, and by 'gating' the return data in time, the ADCP can produce a 'profile' of water currents over a range of depths (user manuals).

To collect the data of the current speed and direction throughout the water column, an RD 1200 kHz broadband ADCP was boom-mounted on the boat (Figure 3-3f) and towed across the water surface from the Tairua tidal inlet to the Pauanui Waterway at a speed of approximately 4 knots. The ship position and flow velocity were calculated from Differential Global Positioning System (DGPS) and bottom tracking.

3.1.3.7 *DOBIE equipped with OBS*

The DOBIE is a pressure recorder that was installed with a D&A OBS-3s as an external sensor (Figure 3-3g) and deployed on the river floor to record the water levels and water turbidity between the upper and lower estuaries every 0.5 hours (user manuals).

The OBS is an optical sensor for measuring the turbidity and suspended sediment concentration by detecting infra-red light scattered from suspended matter. The response of the OBS sensors strongly depends on the size, composition and shape of the suspended particles. The measurement range for sand particles (in water free of silt and mud) is set to about 1 to 100 kg m^{-3}. The sampling frequency is 2 Hz.

3.1.3.8 *SEACAT Profiler CTD*

The SBE 19plus V2 (Version 2) SEACAT Profiler (Conductivity, Temperature and Depth) (Figure 3-3h) was used to measure the conductivity, temperature, pressure (depth) and salinity. Salinity is measured in psu (practical salinity units). The 19plus V2 samples continuously at up to 4 scans per second (4 Hz) (2 Hz with Digit-quartz), recording up to 1000 individual profiles. The 19plus V2 can supply power to 7 external sensors and log their outputs with each CTD scan. Nine D-size alkaline batteries provide up to 60 hours of continuous operation when logging C, T, and P at 4 Hz (user manuals).

To measure the salinity and temperature profile during a complete tidal cycle on 8 June, 2011, one CTD was dropped down and brought up every 30 minutes at the Tairua Wharf, and another was carried by a boat (Taitimu of Waikato University) across the lower estuary and cast into the water, at the two ends of the lower reach of Tairua Estuary (Tairua tidal inlet and the Pauanui Waterway) every hour. At each site they were continuously lowered at a constant speed of approximately 1.5 metre per minute.

3.1.3.9 *DataFlow*

Dataflow is a water level, temperature and salinity recorder. Four DataFlows were deployed from 9.00 am 8 June, 2011 to 10.30 am 12 July, 2011 to collect temperature and salinity data every 15 minutes. The temperature and conductivity

of four DataFlows were calibrated before deployment commenced. Two DataFlows (Figure 3-3j) were deployed at the same location as the ADV3 close to the Pauanui Waterway and tied to the power pole. Since the DataFlows have a limited operational range, they need to be deployed in an area of reduced tidal amplitude. Another two Dataflow temperature and salinity recorders were deployed at the same site as the ADV2 at the Tairua Wharf to record the conditions near the bed and close to the surface. The near surface recorder was mounted on a buoy to maintain a constant depth below the water surface.

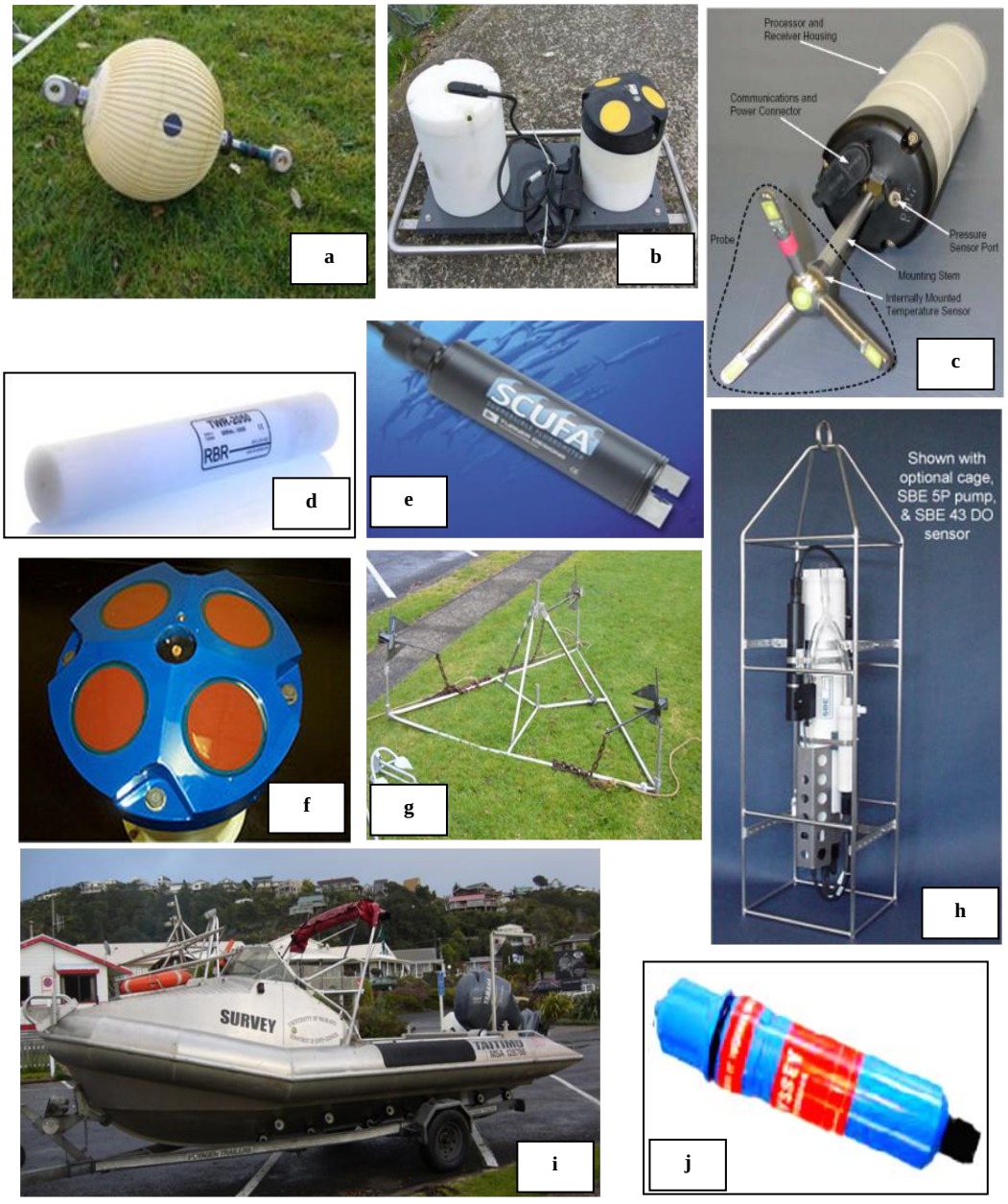

Figure 3-3 Field instruments include (a) the electromagnetic current meter S4 ADW, (b) the SonTek ADP, (c) the ADV Triton with strain-gage pressure sensor (Mudge, 2003), (d) the RBR tide gauge, (e) the SCUFA Fluorometer, (f) the head of an ADCP with the four transducers, (g) the steel structure for mounting the instruments on the bottom, (h) the SEACAT Profiler CTD, (i) the Taitimu survey boat for instruments deployment, (j) and the Dataflow.

3.2 LAB ANALYSES

3.2.1 OBS Calibration

3.2.1.1 *Preparation of the Stock Solution (4000 NTU)*

Reagent grade hydrazine sulphate ($N_2H_4.H_2SO_4$) 5g was dissolved in 400 ml of distilled water and 50 g of pure hexamethylenetetramine was dissolved in 400 ml of distilled water. The two solutions were combined in a 1000 ml flask and diluted to the 1000 ml mark with distilled water. The solution was left to stand for 48 hours at 25°C (77°F) in order to allow time for a suspension to develop. This was the 4000 NTU stock solution used to prepare the 'formazin standards'. And the 'standard solution' was prepared using the prepared 'formazin standard'. The procedure was summarised in Table 3-3 and Table 3-4.

Table 3-3 The procedure preparing for the formazin standard

No	Formazin Standard (NTU)	Methods	DI water (ml)
1	100	550 ml 4000 NTU--> 22000 ml 100 NTU	21450
2	80	17600 ml 100 NTU--> 22000 ml 80 NTU	4400
3	50	13750 ml 80 NTU--> 22000 ml 50 NTU	8250
4	40	17600 ml 50 NTU--> 22000 ml 40 NTU	4400
5	30	16500 ml 40 NTU--> 22000 ml 30 NTU	5500
6	15	11000 ml 30 NTU--> 22000 ml 15 NTU	11000
7	10	5500 ml 40 NTU--> 22000 ml 10 NTU	16500
8	8	17600 ml 10 NTU--> 22000 ml 8 NTU	4400
9	5	13750 ml 8 NTU--> 22000 ml 5 NTU	8250
10	2.5	11000 ml 5 NTU--> 22000 ml 2.5 NTU	11000
11	1	8800 ml 2.5 NTU--> 22000 ml 1 NTU	13200
		Total	108350

Table 3-4 The procedure preparing standard solution (total volume is 22 litre)

No.	Solution (NTU)	Solution Take out	Formazin Input	Note
1	0	0	water	22000 ml DI water
2	2.5	13.75 ml	13.75 ml 4000 NTU	
3	5	13.75 ml	13.76 ml 4000 NTU	
4	8	16.52 ml	16.52 ml 4000 NTU	Pour out
5	10	0	55 ml 4000 NTU	22000 ml DI water
6	15	27.57 ml	27.57 ml 4000 NTU	
7	30	82.81 ml	82.81 ml 4000 NTU	
8	40	55.42 ml	55.42 ml 4000 NTU	Pour out
9	50		275 ml 4000 NTU	22000 ml DI water
10	80	167.09 ml	167.09 ml 4000 NTU	
11	100	112.24 ml	112.24 ml 4000 NTU	
12	110	55.14 ml	55.14 ml 4000 NTU	

3.2.1.2 *The Calibration Tank Preparation*

A 22 L tank with a lid was used to house the OBS sensor and blender. A hole was made in the lid for inserting the OBS sensor and blender inside. The calibration tank was cleaned with distilled water and kept at room temperature for one day. The calibration tank ensures that the OBS sensor is kept in a clean and dark environment. The OBS sensor was fixed on a tank mounting plate and put inside the black tank.

The OBS was connected to its cable with two sensors (A & B) being calibrated one by one using the same formazin solution. The two OBS's were to the tank mounting plate. The OBS was left to equilibrate to the tank water temperature. Normally an OBS requires 6 minutes before the output stabilizes after being exposed to a 25ºC change in temperature.

3.2.1.3 *Calibration*

The data were assumed to fit a linear equation y=a*x + c, where y is the turbidity (NTU) and x is voltage (V). The relationship between the raw data recorded by the OBS_A and OBS_B (Volt) and the formazin (NTU) are presented in Figure 3-4. They show that both the OBS_A and OBS_B fit their linear equations well. Then these two equations could be used to convert the OBS observed data to the turbidity value in NTU.

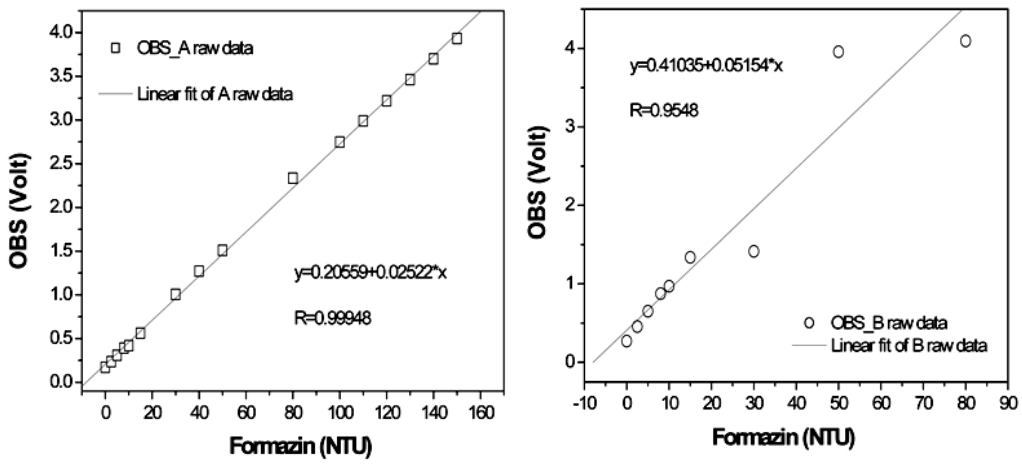

Figure 3-4 Calibration results of the two OBS sensors

3.2.2 Suspended Sediment Concentration

Water samples were collected from the estuary bottom together with the CTD casts at the estuary tidal inlet, the Tairua Wharf and the Pauanui Waterway on 8 June, 2011. The suspended sediment concentration was measured by drying and weighing the residual sediment after sample filtering.

3.2.2.1 *Filter Preparation*

Filters (GF/C) were pre-washed with 500 ml DI water to remove residual contaminants from the manufacturing process. Then the pre-washed filters were dried in an oven at 80 ºC temperature for one day. Once the filters were dried they were transferred to desiccators to cool and stabilize overnight. The clean, dry and stabilized filters were stored in a sealed box after weighing.

3.2.2.2 *Sample Filtering*

Water samples were stored in a freezer after being collected from the field. They were taken from the freezer and stored in a refrigerator (4°C) overnight one day before the sample was to be filtered. The water sample was poured out into a graduated cylinder after shaking the container to make it homogenous. A measured volume filters with samples were placed in the 80ºC drying oven and allowed to evaporate for five days to constant weight. Finally, the dried filters with sediment samples were weighed after transferring dried filters to desiccators and allow stabilising overnight.

3.2.2.3 *Data Processing*

The difference between the final filter weight and the initial weight equals the weight of the suspended solids per volume of sample (Equation 3-1). The results are plotted in Figure 3-5.

$$\mathrm{SSED} = {}^{(\mathrm{B}-\mathrm{A})\times 1000}/_{\mathrm{V}} \qquad (3\text{-}1)$$

Where, A is the filter weight, g; B is the filter weight plus sediment weight, g; V is the volume of the sample filtered in litres.

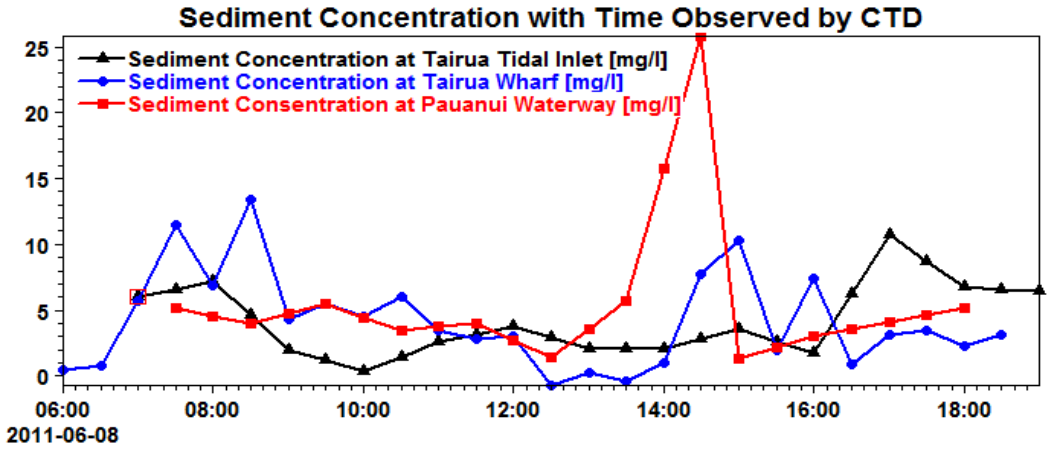

Figure 3-5 Suspended sediment concentration (mg/l) with different time on 8 June, 2011 at Tairua Tidal Inlet, Tairua Wharf and Pauanui Waterway respectively. Water samples were taken beside the three ADVs after being put down on water bottom.

3.3 STATION DATA

3.3.1 Rainfall

The Tairua weather station recorded an average annual precipitation of 1,800 mm, over the 10 year period of records, with a maximum annual rainfall of 2,326 mm and a minimum of 1,280 mm. The average annual rainfall for the Tairua catchments is high when compared to the average annual rainfall in the North Island. The average monthly rainfalls over the ten year period from 1984 to 1994 in Table 3-5 (Waikato Regional Council report, 1994) shows a lack of any strong seasonal variation in rainfall as there is no distinct wet or dry season over the year. High intensity localized rainfall events occur relatively frequently and often trigger landslides.

Additional rainfall data were obtained from the Waikato Regional Council station (site number. 234.9, Map reference: 1840723-5897068), located at an altitude of 625 m above mean sea level at the Pinnacles between the Kauaeranga and Tairua catchments. The wind speed and direction data were recorded from the Automatic Weather Station (AWS) on Slipper Island offshore from Tairua Estuary. Atmospheric pressure and daily air temperature data were obtained from the Whitianga Airport AWS located 23 km NNW of Tairua. Additional water level data were also obtained from the tide gauges of the Waikato Regional Council deployed at the Whitianga Harbour, Coromandel Peninsula and the Firth of Thames.

The time series of the monthly average rainfall and number of rain days during 2010 and 2011 recorded at the Whitianga Aero AWS is shown in Figure 3-6. The Whitianga Aero AWS (station number: 1520, network number: B65862) is located 24 km north-west of the Tairua tidal inlet (-36.834°S, 175.677°E). It indicates that there is more rainfall from May to September (NZ winter) with a maximum of 458.2 mm in May and less rainfall from October to April (NZ summer) with a minimum of 23 mm in March. The very high rainfall (about 410 mm) during November and December in 2011 is abnormal compared the average monthly rainfall distributions over ten years in Table 3-5.

Table 3-5 The mean monthly rainfall (mm) over ten years at Tairua catchments from 1984

Jan	Feb	Mar	April	May	June	July	Aug	Sept	Oct	Nov	Dec
128	135	211	136	123	180	188	161	125	134	137	122

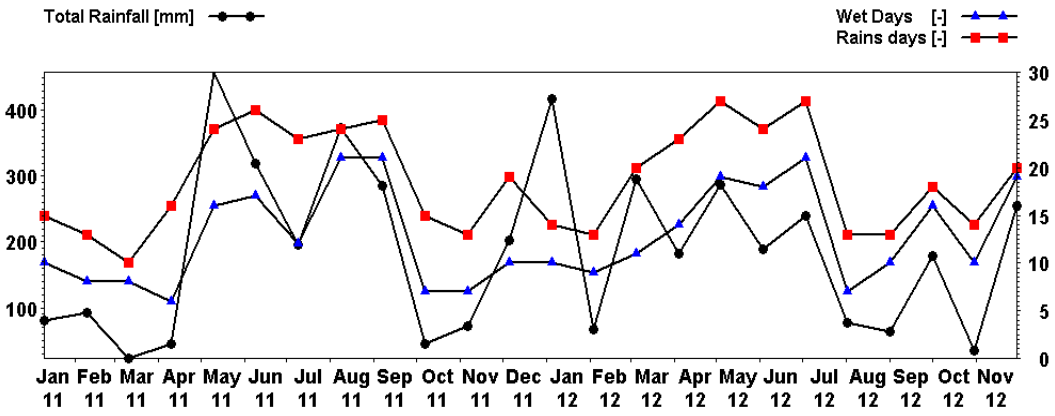

Figure 3-6 Monthly mean rainfall and the wet, rain days during 2010 and 2011 based on the observed rainfall data at the Whitianga Aero Aws. station.

3.3.2 Wind

Wind data were downloaded from the climate data website (Cliflo) of the National Institute of Water and Atmospheric Research (NIWA). The wind data were recorded hourly from Slipper Island AWS station (Latitude: -37.052, Longitude: 175.943. Height above MSL: 103 m) from 5 October, 2005 to 6 June, 2010 (Figure 3-7). The wind rose in Figure 3-8a shows that the prevailing winds on Slipper Island outside of Tairua Estuary is mainly from the north, west and south-west direction. Of these, the south-westerly wind is dominant, occurring 22% of

the time, wind from north-eastern direction is also very frequent and accounts for 19% of the time and it is much stronger than the wind from other directions. Wind from other direction each account for approximate 7-8 % of the wind direction. The max wind strength is 14.4 m s^{-1}, with an average value of 4.8-7.2 m s^{-1} from any other direction.

On the 8th of June, 2011, a weather station was set up 6.89 m above the river bed within Tairua Estuary Channel (Figure 3-7) and collected data for one month. The wind rose measured is plotted in Figure 3-8b and the wind time series recorded within Tairua Estuary (black line) and on Slipper Island (blue line) outside of the estuary from 8 June, 2011 to 20 June, 2011 are shown in Figure 3-9. The plots indicate that the wind magnitude outside of the estuary (with 19.05% calm wind) is higher than the wind within the Estuary (with 63.79% calm wind). It is because of the screening effect of the surrounding mountainous terrain. Wind from the north and the south direction was filtered more and wind from the north-east and south-west is screened less because of the higher mountains located along the channel. And wind from north-east to south-west within the estuary (with the maximum wind speed 9.6 m s^{-1}) is similar to the data recorded on Slipper Island (with the maximum wind speed 14.4 m s^{-1}).

Figure 3-7 A weather station was set up along the main channel of the Tairua Estuary during the second phase of field work to supplement NIWA's Wind Station on Slipper Island from June 8 to June 12, 2011 (Google Earth).

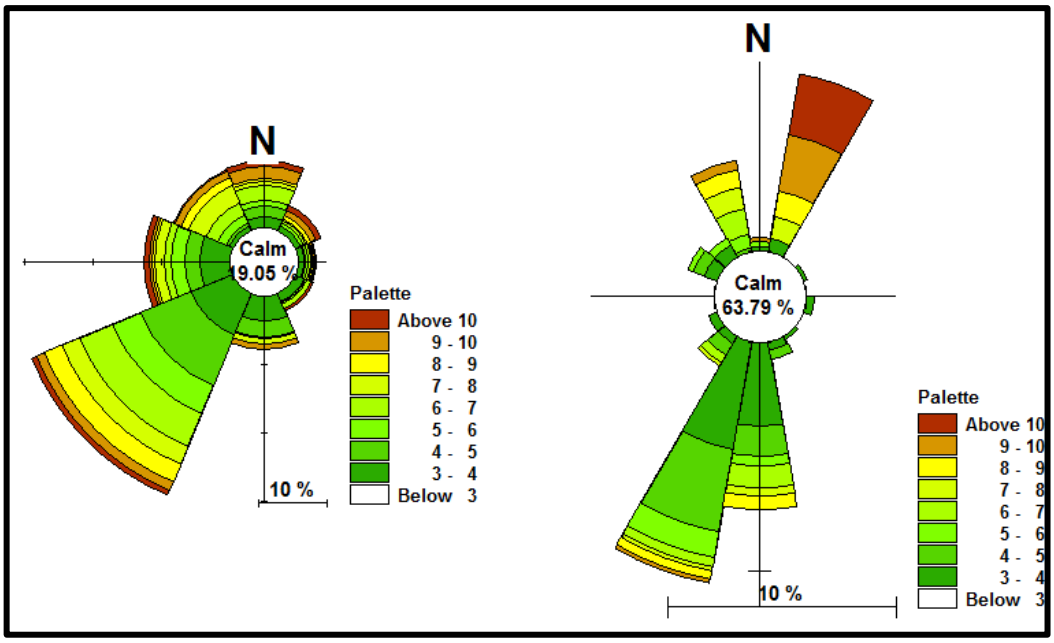

Figure 3-8 Wind rose map recorded on Slipper Island (left) and along the main channel within Tairua Estuary (right) from 8 June, 2011 to 14 July 2011.

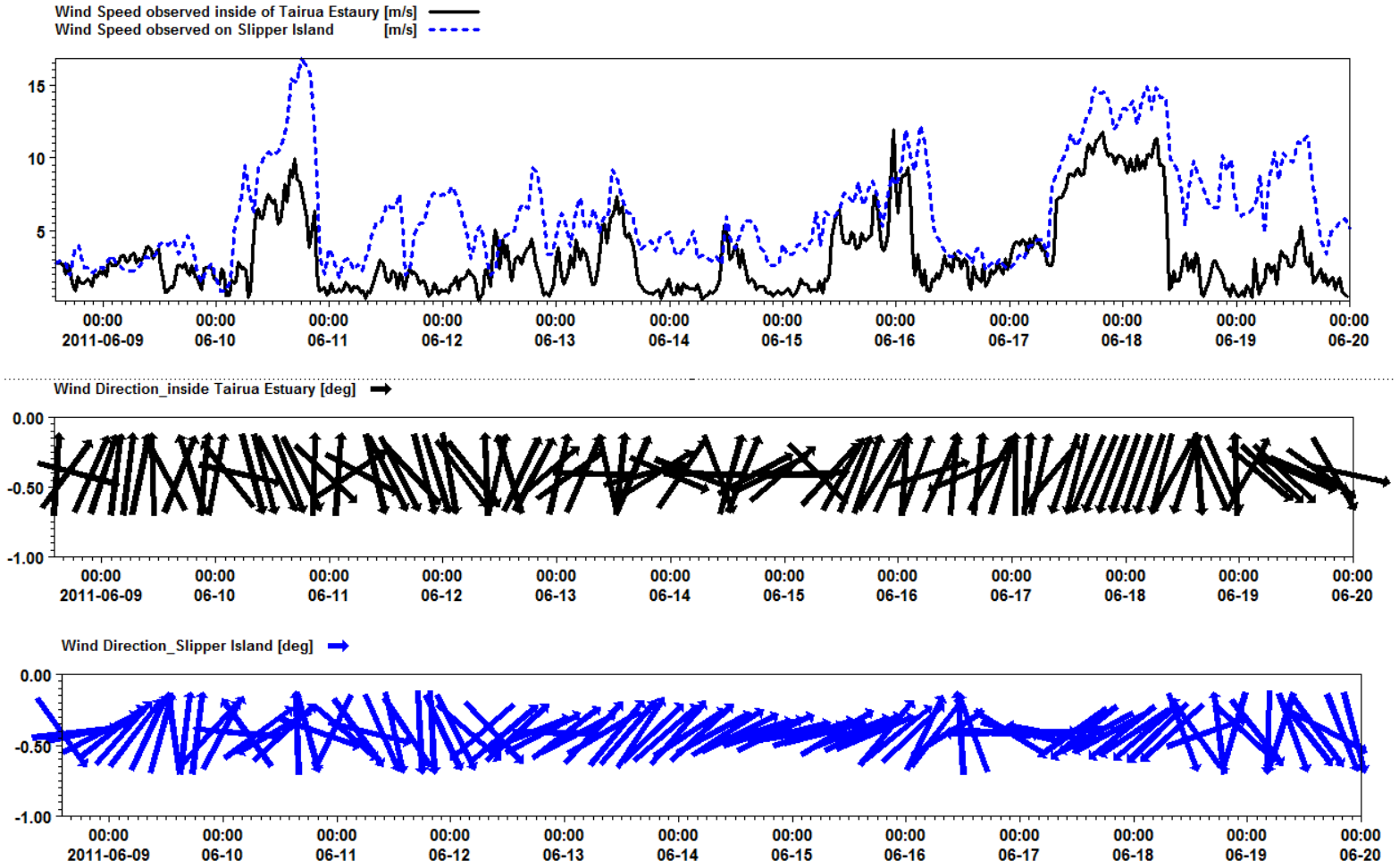

Figure 3-9 Comparison of the wind speed and directions recorded on Slipper Island (blue line) and along the main channel of the Tairua Estuary (black line).

3.3.3 Air Temperature

The hourly air temperature data over 20 years was downloaded from NIWA's website. The data were recorded at the Auckland Ardmore weather station (Agent number: 1965. Latitude: -37.03, Longitude: 174.96, 23 m above MSL) from 7 June, 1990 to 6 July, 2012. The average air temperature and the relative humidity from 1 January, 1991 to 31 December, 2011 were calculated and plotted in Figure 3-10. The results indicate that the minimum air temperature is -3.2 °C, the maximum value is 26.1°C and the mean value is 14.14 °C. The maximum air temperature dry bulb is 18.49°C in January and the lowest is 9.47°C in July. Both of the air temperature wet bulb and the air temperature dew point is lower than the air temperature dry bulb.

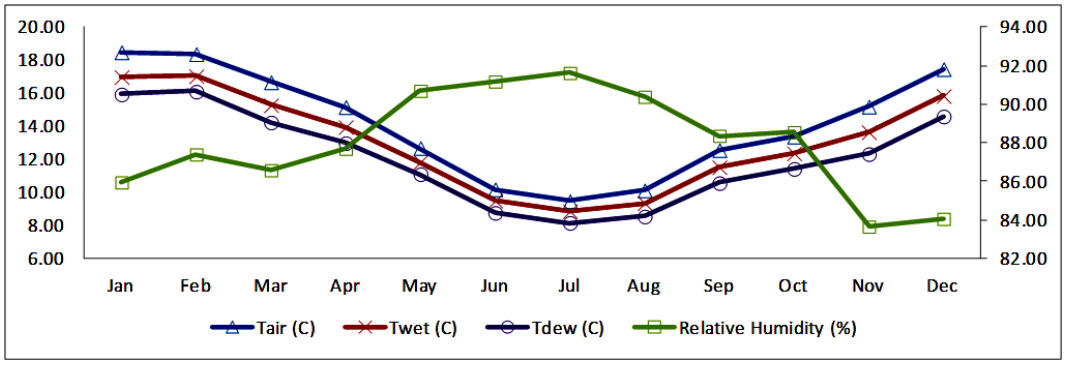

Figure 3-10 The mean air temperature and relative humidity observed at the Auckland Ardmore station from 1 January, 1991 to 31 December, 2011.

The hourly mean air temperature at the Whitianga Aero AWS station during June, 2011 (winter) and December, 2010 (summer) were downloaded from NIWA's station and plotted in Figure 3-11 respectively. These plots indicate that the average air temperature is about 10 °C during the winter in 2010 and is about 20°C during the summer in 2010 which is the same year of the field instruments deployment. Thus, these two time series were input into the model for the winter case and summer case.

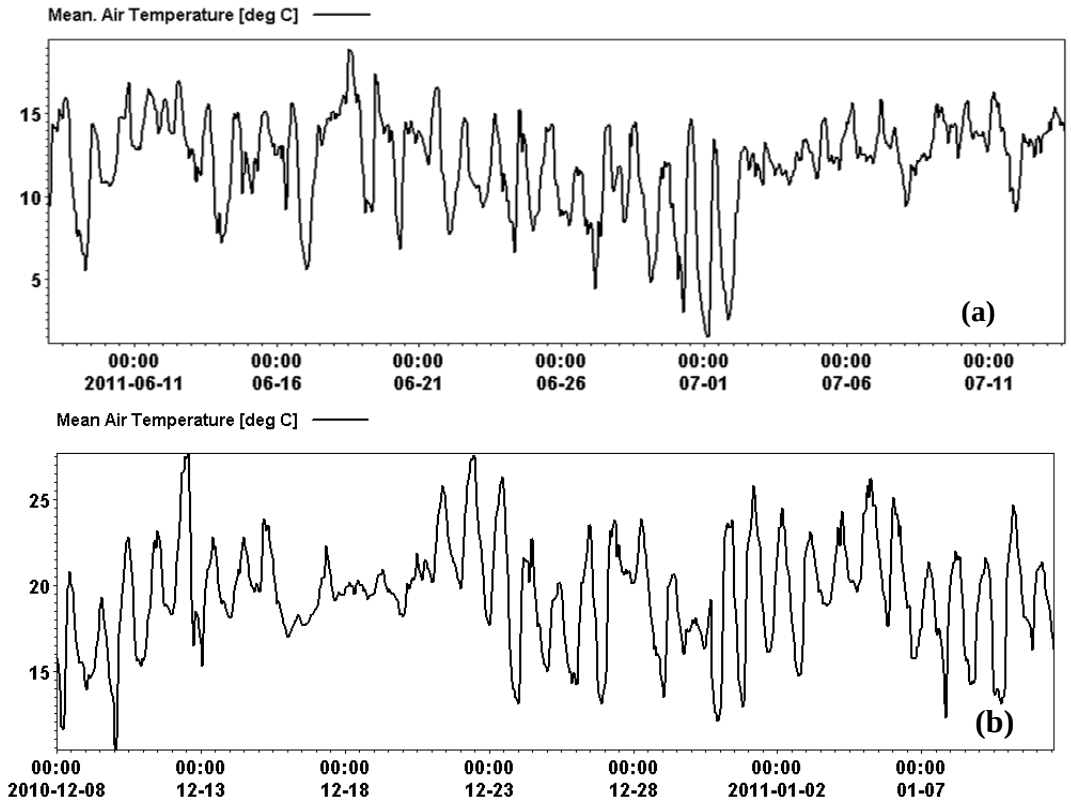

Figure 3-11 Mean hourly air temperature recorded at the station of the Whitianga Aero Aws. during (a) winter and (b) summer. The time series are applied in MIKE 3 FM flow model as a case for the salinity and temperature research.

3.3.4 Freshwater Discharge from the Tairua River

The fresh river water discharge was recorded every 5 minutes on the Broken Hills Station at the Tairua River. This station is approximately 11 km upstream of the Tairua River mouth. The data show that no tidal flow reaches the station. These data were used to specify the river boundary for the numerical models

The measurement of the river discharge at the river gauging site plays a vital role in the comprehensive and coordinated planning required for the utilisation of local water resources. However, continuous measurement of stream discharge is difficult to obtain and direct discharge measurement is a time consuming and costly procedure. Therefore in practice, a two-step procedure is followed. First, the discharge in a given stream is related to the corresponding elevation of the water surface (gauge). Secondly, the gauge of the stream is observed routinely, and the discharge is estimated by using the previously determined stage-discharge relationship, or alternatively, known as the rating curve (Perumal, 2007). The relationship between the fields observed Tairua River discharge and the water

elevation (the rating curve) are calculated and plotted in Figure 3-12. This curve can be used to calculate the water elevations based on the river discharge.

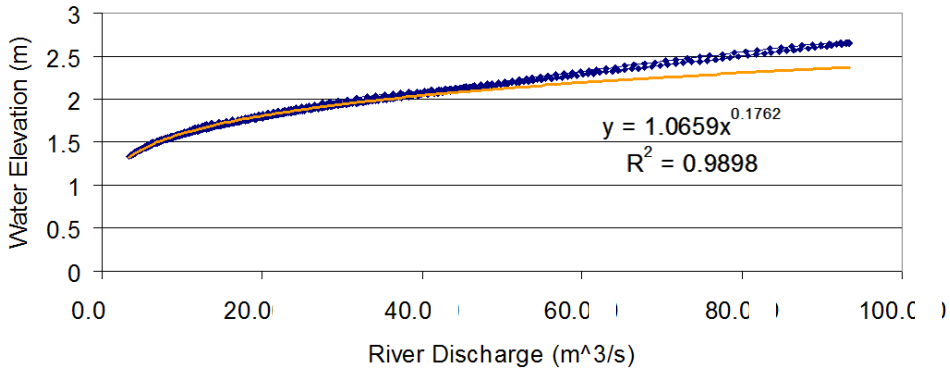

Figure 3-12 The relationship between Tairua River discharge and the rating curve of water elevation. The river discharge was observed at the Broken Hills station on the Tairua River shown as blue star line (Waikato Regional Council, August, 2010).

The New Zealand Transverse Mercator (NZTM) projection was used for this study. All the surface elevation and water depth data refers to mean sea level (MSL). All time refers to New Zealand Standard Time (NZST), which is twelve hours in advance of Coordinated Universal Time (UTC).

3.4 CONCLUSION

The two field campaigns collected data together with station data and the data suggested by the other scientists (introduced in Chapter 2) supplied the data for:

- The boundary time series for setting up the numerical models.
- Calibrating and validating for numerical models.

CHAPTER FOUR
NUMERICAL MODELLING

This chapter outlines the process of the numerical modelling of Tairua Estuary using both of the MIKE 21HD and 3DD Flow modules. The models were developed using a two-phase nesting procedure, producing a series of depth-averaged models forced by tides, winds and river discharge. Two bathymetry grids developed include the 'whole_50m' grid has cells 50 m by 50 m covering 275.25 km^2 area from Slipper Island to Tairua River; the 'estuary_20m' grid has 20 m by 20 m cell size covering an area of 93.39 km^2 from the Tairua ebb tidal delta to the Tairua River mouth. The models have been calibrated against the observed field data using van Rijn's statistic criteria. The hydrodynamic models agree well with the instruments data and are suitable for the depth-averaged sediment transport modelling and oil spill modelling.

4.1 INTRODUCTION

The ability to numerically simulate estuarine hydrodynamics has large economic and ecological importance for the management and development of estuaries (Whitehouse et al, 2000). Numerical simulation has proven to be the best method for understanding sediment transport and hydrodynamics over large spatial areas (Toorman, 2002). To date the Tairua tidal inlet and estuary has not been modelled with a well calibrated hydrodynamic and sediment transport model, and there is generally a paucity of field data for the estuary.

Two software packages were used to develop numerical models in this research because

- DHI software including the MIKE 21 and MIKE 3 modules is used by many regional councils and consultant companies in New Zealand;
- 3DD software including the 3DD Flow and POL 3DD is used by Waikato Regional Council in New Zealand;
- Using both of the two software packages makes it possible to compare the simulation results and find the advantages/disadvantages of the software.

In this chapter, two-dimensional hydrodynamic models are set up both in MIKE 21 HD module and 3DD module covering a month long period starting at 12.00 am 28 July, 2010. It includes two-phase modelling: the 'whole_50 m' model covers the estuary, river and offshore island area with 50×50 m cell size and the 'estuary_20 m' model covers the estuary and the river part with 20×20 m cell size.

The model calculated surface elevation and current speed from the tidal inlet to the river mouth are analysed, compared and statistics qualified.

The calibrated Mike 21 and 3DD hydrodynamic models contribute to a series of models for the case studies in Part IV. The MIKE 21 ST (depth-averaged sediment transport) model, MIKE 3 FM HD (three-dimensional flexible mesh hydrodynamic) model for the salinity and temperature regimes study and the POL 3DD Oil Spill model for the oil spill trajectory forecasting with different tides, river flow and wind conditions.

4.2 MIKE 21 HD MODEL DEVELOPMENT

4.2.1 Module and Main Equations

The MIKE 21 HD, release 2011, Service Pack 6 was used to set up the hydrodynamic model of Tairua Estuary. It uses an Alternating Direction Implicit (ADI) technique to integrate the equations for mass and momentum conservation in the space-time domain. The equation matrices for each direction and each individual grid line are resolved by a Double Sweep (DS) algorithm.

The MIKE 21 HD module is a general numerical modelling system for the simulation of water levels and flows in estuaries, bays and coastal areas. It simulates unsteady two dimensional fluid flows in one layer (vertically homogeneous).

The following equations, the conservation of mass and momentum integrated over the vertical, describe the flow and water level variations (MIKE 21 HD manual).

$$\frac{\partial \delta}{\partial t} + \frac{\partial p}{\partial x} + \frac{\partial q}{\partial y} = \frac{\partial d}{\partial t} \tag{4-1}$$

$$\frac{\partial p}{\partial t} + \frac{\partial}{\partial x}\left(\frac{p^2}{h}\right) + \frac{\partial}{\partial y}\left(\frac{pq}{h}\right) + gh\frac{\partial \delta}{\partial x} + \frac{gp\sqrt{p^2+q^2}}{c^2h^2} - \frac{1}{\rho_w}\left[\frac{\partial}{\partial x}(h\tau_{xx}) + \frac{\partial}{\partial y}(h\tau_{xy})\right] - \Omega_q - fVV_x + \frac{h}{\rho_w}\frac{\partial}{\partial x}(p_a) = 0 \tag{4-2}$$

$$\frac{\partial q}{\partial t} + \frac{\partial}{\partial y}\left(\frac{q^2}{h}\right) + \frac{\partial}{\partial x}\left(\frac{pq}{h}\right) + gh\frac{\partial \delta}{\partial y} + \frac{gp\sqrt{p^2+q^2}}{c^2h^2} - \frac{1}{\rho_w}\left[\frac{\partial}{\partial y}(h\tau_{yy}) + \frac{\partial}{\partial x}(h\tau_{xy})\right] - \Omega_p - fVV_y + \frac{h}{\rho_w}\frac{\partial}{\partial y}(p_a) = 0 \tag{4-3}$$

In the equations, $h(x,y,t) = \delta - d$ is water depth (m); $d(x,y,t)$ is the time varying water depth (m); $\delta(x,y,t)$ is surface elevation (m); $p,q(x,y,t)$ is flux densities in x- and y-directions ($m^3\ s^{-1}\ m^{-1}$) ; u,v is depth-averaged velocities in x-

and y-direction; $C(x,y)$ is the Chezy resistance ($m^{1/2}$ s^{-1}); g is the acceleration due to gravity (m s^{-2}); $f(V)$is wind friction factor; $V, V_x, V_y(x,y,t)$ is wind speed and components in x- and y- directions (m s^{-1}); $\Omega(x,y)$ is the Coriolis parameter, latitude dependent (s^{-1}); $p_a(x,y,t)$ is atmospheric pressure (kg m^{-1} s^{-2}); ρ_w is density of water (kg m^{-3}); x,y is space coordinates (m); t is time (s); $\tau_{xx}, \tau_{yy}, \tau_{xy}$ is the components of effective shear stress.

4.2.2 Bathymetry Development

The bathymetry, including the Shoe Island and the Slipper Island, is shown in Figure 4-1. The area within the blue solid line is derived from LiDAR, multi-beam echo-soundings, and single beam echo-soundings by the University of Waikato. The other area is interpolated based on the points produced by NIWA and digitizing of hydrographic maps. The datasets have been archived in an ArcGIS v9.2 file (Geodatabase format), consistent with the current Coastal Marine Group hydrographic GIS database schema (Scarfe, 2009). The datasets are reduced to Moturiki Vertical datum 1953, consistent with DML survey data available for this area.

The Manifold software was used to interpolate the points for generating the bathymetry grid map. The grid size was 5×5 m and the interpolating method used was ‘ordinary kriging’. Falcão et al. (2013) carried out a validation tests at the Lima River Estuary, North-western Portugal for commonly available spatial interpolators and indicated that the ordinary ‘kriging method’ is the most adequate interpolator. The default land value for the bathymetry used in MIKE is an elevation of 10 m and in 3DD it is a depth of -9 m. The elevations higher than 2 m in MIKE and less than -2 m in 3DD were set as land to reduce the model running time. All the depths were adjusted to mean sea level (MSL). The MIKE modules use the American language system, that is, the plots output by MIKE using the unit of ‘kilometer’ instead of ‘kilometre’, the unit of ‘meter’ instead of ‘metre’ and so on. The MIKE plots have not been edited to change the units to the New Zealand spelling.

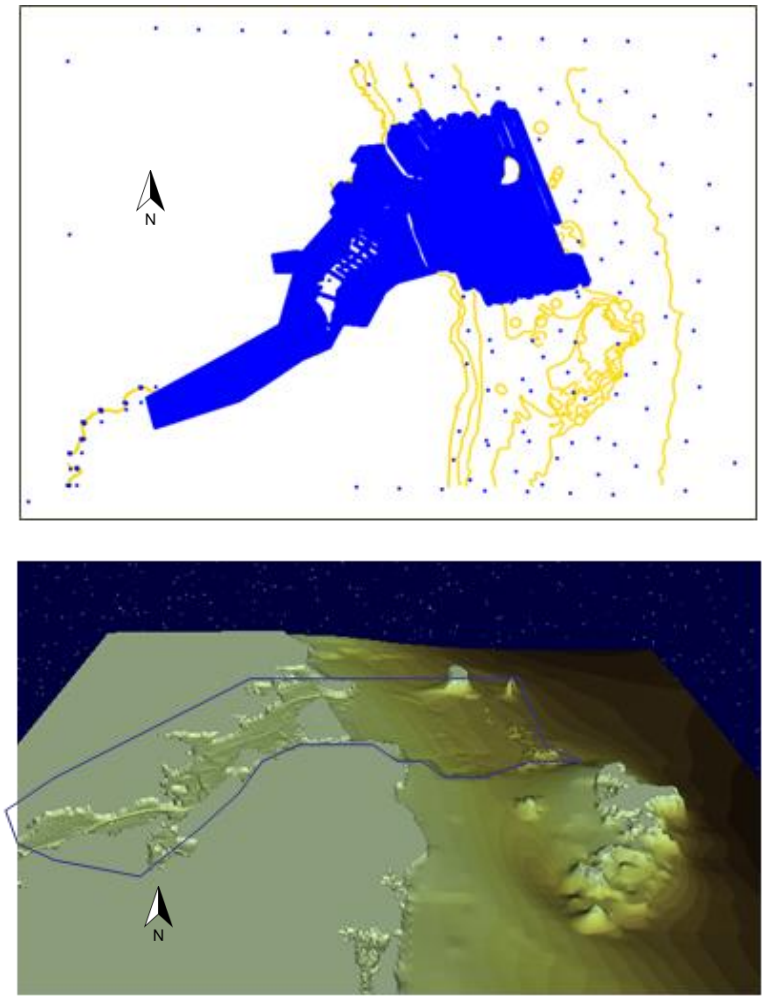

Figure 4-1 Multi-beam, single-beam and LiDAR surveyed data by the University of Waikato in June, 2009 (blue area) and NIWA (Koordinates.com) before interpolating (top), and the developed 3D bathymetry of Tairua Estuary covering the Shoe Island and Slipper Island (bottom).

During the process of the modelling, three different grid extents were developed based on the model calibration results. The first bathymetry covers only the multi-beam surveyed area, but the northern and southern offshore boundaries were closed (Figure 4-2a). The calibration results showed that there was a phase difference of both the water surface elevation and current speed compared to the field data; the second bathymetry was extended to cover the Shoe Island and the Slipper Island, however the southern boundary cut through the Slipper Island and resulted in a big eddy on the southern offshore boundary (Figure 4-2b); the third bathymetry was finally developed by extending the southern boundary (Figure 4-2c). This grid produced offshore tidal behaviour consistent with observations. However, to provide useful run time, the grid resolution had to be relatively coarse at 50 m by 50 m.

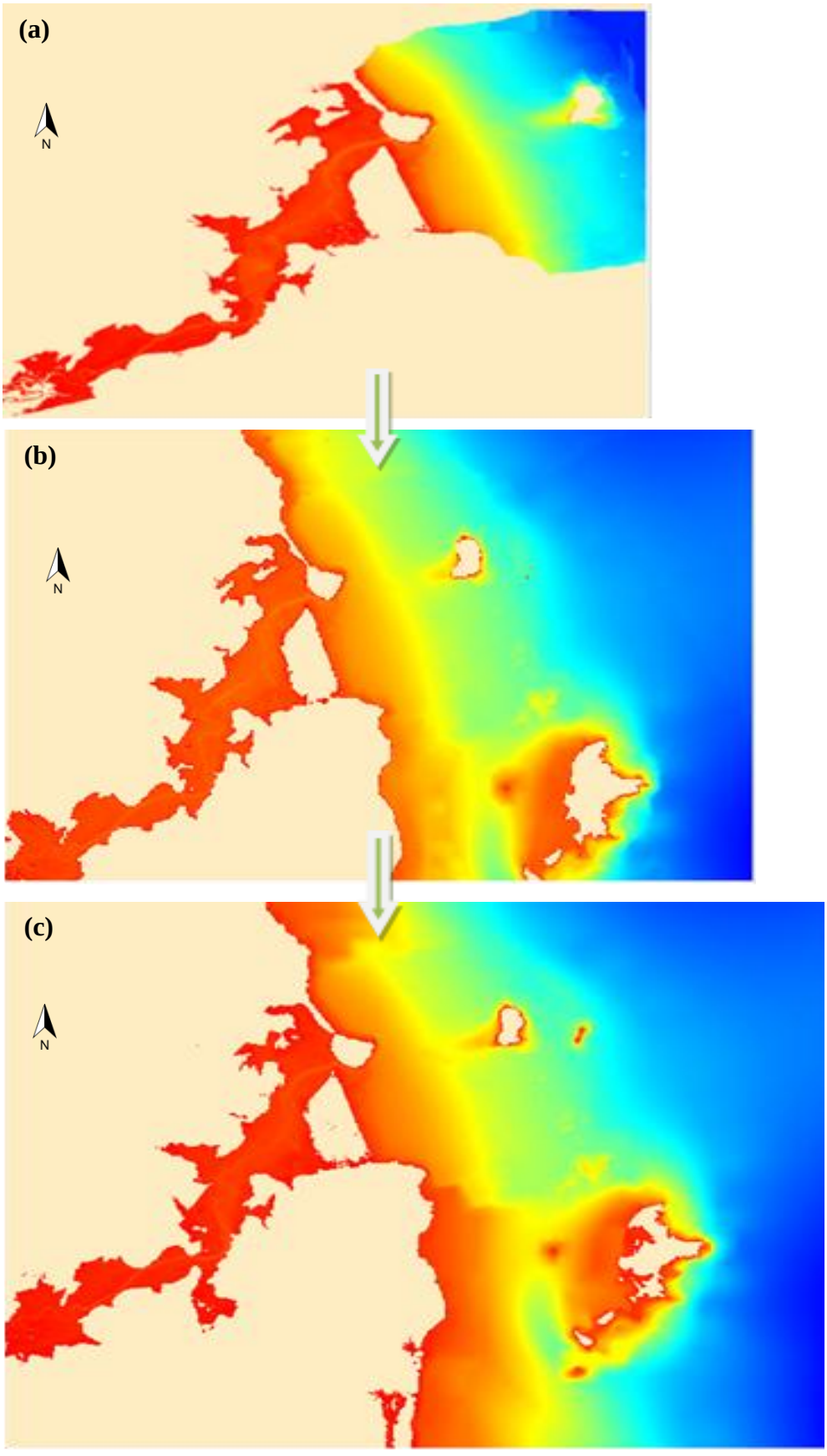

Figure 4-2 Process of the bathymetry development

To reduce the running time, the depth higher than 3 m was set as 10 m for Mike models because the software considers the 10 m depth as land and not taken into calculation, and the depth less than -3 m was set as -9 m because the 3DD software considers the -9 m depth as land and not taken into calculation. Depth is positive upwards in MIKE and positive downwards in 3DD.

Therefore, two different nested resolution grids were used for the two-phase models in this research include the 'whole-50m' model with 367 × 300 cell numbers and 50 m × 50 m cell size; the 'estuary-20m' model with 466 × 501 cell numbers and 20 m × 20 cell size (Figure 4-3).

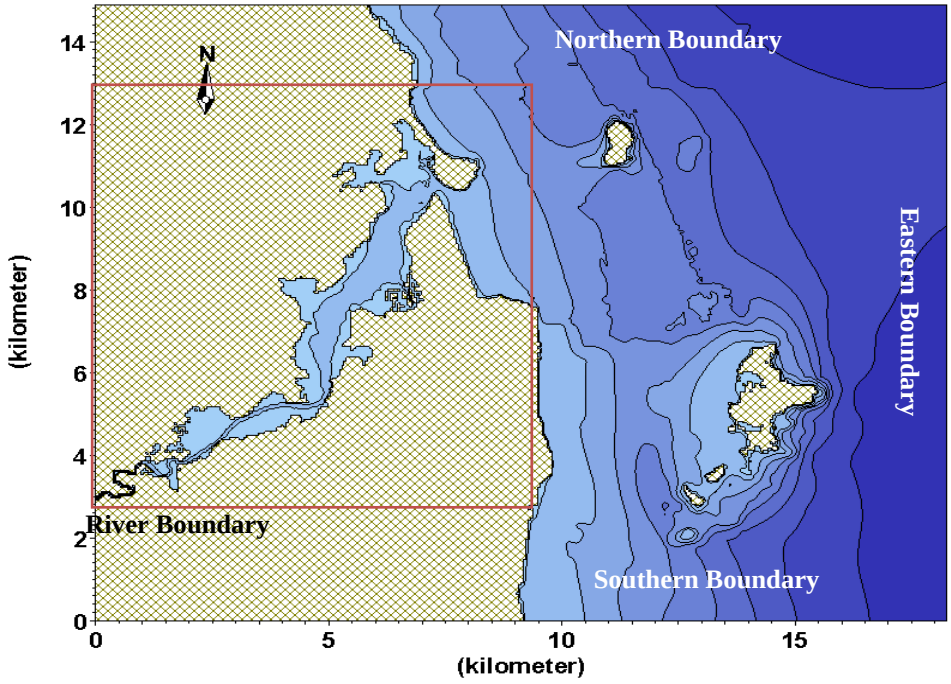

Figure 4-3 The 'whole-50m' bathymetry (black frame) and the 'estuary-20m' bathymetry (red frame). Plot was generated using the MIKE 21 plot composer.

4.2.3 Boundaries

If the description of the bathymetry is the most important task in the modelling process, then the description of the water levels and river flows at the open boundaries is the second most important task. Better boundary conditions lead to better output and fewer instability problems (MIKE 21 HD manual, 2012).

4.2.3.1 *Offshore Tidal Boundaries*

Four boundary conditions including three offshore tidal boundaries and one river discharge boundary were prescribed to force the 'whole_50 m' hydrodynamic model (Figure 4-3). And the tidal boundaries of the 'estuary_20m' model were nested from the 'whole_50m' model results.

Each tidal boundary was interpolated from the tidal surface elevations that were extracted from the output of NIWA's regional RiCOM (River and Coastal Ocean Model) model at every 20 grids along the boundaries as a time series file (Figure 4-4). The RiCOM numerical model is general-purpose hydrodynamics and transport modelling by Waters and Casulli (1998), Walters (2005) and Walters et al. (2006). The locations of the points are attached in Appendix I. All the tides refer to mean sea level (MSL). Time interval is 1 minute. Time zone is NZST. The latitude and longitude are in NZTM GD2000. Time starts from 12.00am on 27 July, 2010, and runs to 12.00am on 4 September, 2010. The default flow direction is perpendicular to the tidal boundaries.

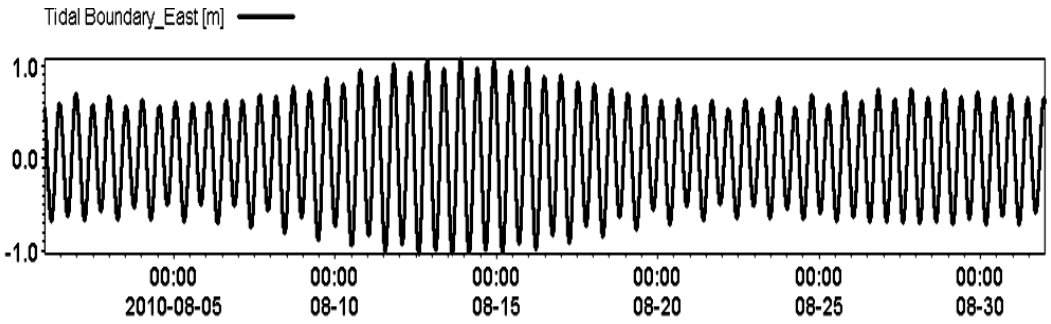

Figure 4-4 Time series of offshore tidal elevation boundary used to force the numerical models during the first field campaign in 2010.

4.2.3.2 *River Boundary*

Figure 4-5a is the water depth recorded by the RBR tide gauge under the Tairua Bridge, the western river boundary of the model. This plot demonstrates that tides could reach the Tairua River mouth under the Tairua Bridge. The estimated river flow in m^3 s^{-1}, determined from the RBR elevation could be input into the boundary only if there is no tidal influence. Therefore, it could not be used as the river flow boundary.

The Broken Hills station on the Tairua River is maintained by the WRC. It is about 11.6 km upstream of the Tairua River mouth. Analyses of the data shows that there are no tides reaching there (Figure 4-5b) and therefore the time series of the river discharge with 5 minutes time interval observed there was used as the river flow boundary.

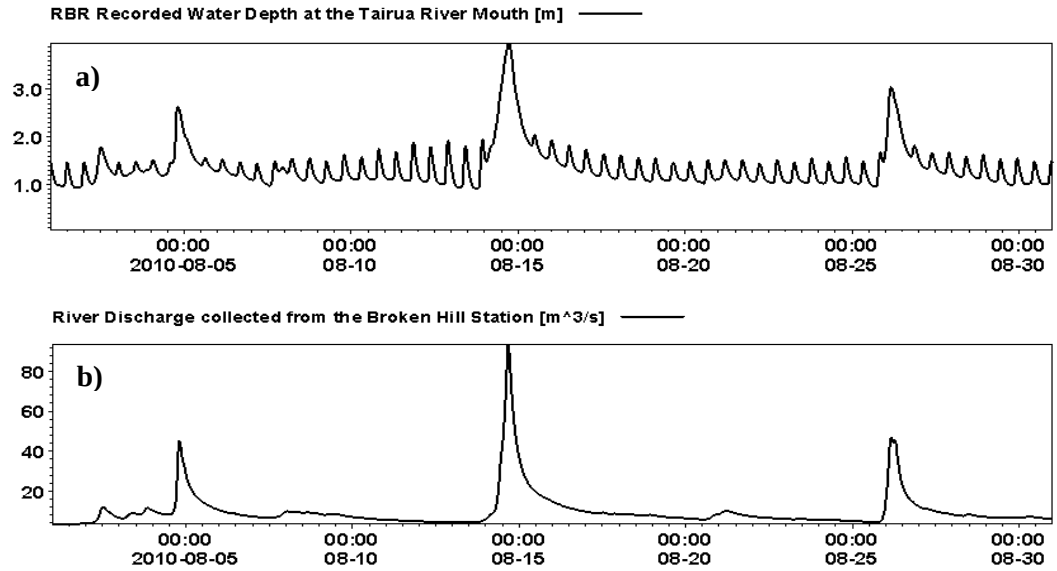

Figure 4-5 Time series of a) water depth recorded by RBR current meter and b) the Tairua River discharge (m3 s^{-1}) observed at the Broken Hill Station, 11.6 km upstream of the Tairua River mouth.

4.2.4 Wind

The wind data (discussed in section 3.3.2) were recorded at Slipper Island Wind Station (AWS 31827 B75091, 37.052S 175.943E) of NIWA (Figure 4-6), and were applied 10 m above the water surface in the models.

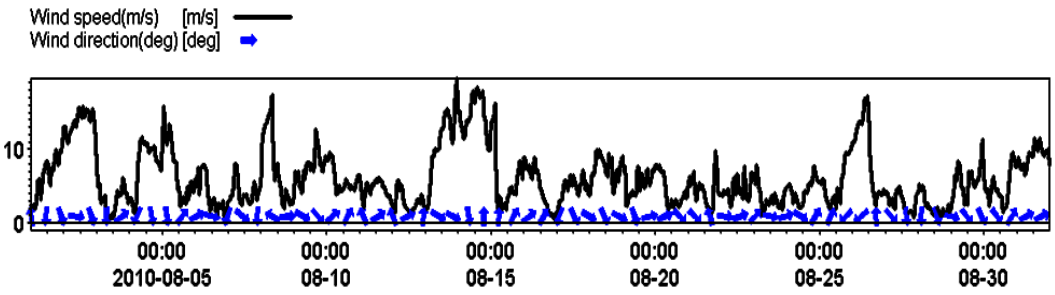

Figure 4-6 Wind speed and direction observed at Slipper Island (NIWA's station) from 28 July to 3 September, 2010

The drag coefficient of the wind stress could be calculated in the model as

$$C_D = (0.9 + 0.08W_S) \times 10^{-3} \quad (4\text{-}4)$$

Where, W_S is the wind speed in m s^{-1} and applied 10 m above water surface. The direction of the wind was given in degrees relative to true north.

4.2.5 Eddy Viscosity

The effective shear stresses in the momentum equations contain momentum fluxes due to turbulence, vertical integration and sub grid scale fluctuations (Madsen et al., 1988; Wang, 1990). The terms are included using an eddy viscosity formulation to provide damping of short wave-length oscillations and to represent sub grid scale effects (MIKE 21 HD Manual, 2012).

A time-varying function of the local gradients in the velocity field for the eddy viscosity is based on the so called Smagorinsky concept (Smagorinsky, 1963), which yields

$$E = C_S^2 \Delta^2 \sqrt{\left(\frac{\partial U}{\partial x}\right)^2 + \frac{1}{2}\left(\frac{\partial U}{\partial y} + \frac{\partial V}{\partial x}\right) + \frac{\partial V}{\partial y}} \quad (4\text{-}5)$$

Where, U and V are depth-averaged velocity components in x and y direction, Δ is the grid and C_s is a constant to be chosen in the interval of 0.25 to 1.0 (MIKE 21 HD manual, 2012). A uniform velocity-based Smagorinsky factor 0.5 was used for the whole model.

When calibrating the models, stability problems (blow-ups) always occurred at the boundary corners close to the beach. To solve this problem, the bathymetry along the tidal boundaries was smoothed over 200 m distance, and a very high resistance with the Manning numbers in the range of 5~20 m^3 s^{-1} was specified close to the land.

4.2.6 Bottom Roughness Length

As introduced in Chapter 2, Robertson and Peters (2006) collected 111 bed sediment samples for Tairua harbour, and mapped the sediment grain size distribution (Figure 2-5 and Figure 2-6). The median grain size was interpolated into a 2 × 2 m grid using Golden Surfer software (Figure 4-7). The d_{50} map shows that the sediment particle size ranges mainly from 0.36 mm to 0.49 mm. Thus, according to the Udden-Wentworth Scheme of grain size classification standard, it is medium sand.

Soulsby (1997) suggested all flows over sands as hydro-dynamical rough flow ($\frac{u_* k_S}{\nu} > 70$). Therefore the bed roughness length is given by

$$z_0 = \frac{k_S}{30} \quad (4\text{-}6)$$

The bed roughness length z_0 for a flat, non-rippled, bed of sand is expressed in terms of the Nikuradse roughness k_s. The most used relationships between k_s and the median grain size d_{50} is

$$k_s = 2.5 d_{50} \quad (4\text{-}7)$$

Combining Equations (4-6) and (4-7), the bed roughness length z_0 is directly related to grain size for hydro-dynamical rough flows as

$$z_0 = \frac{d_{50}}{12} \quad (4\text{-}8)$$

The bed roughness length is calculated according to the Equation 4-8 and plotted in Figure 4-8. It was applied in the model as a cell-by-cell file.

4.2.7 Courant Number

The Courant number is defined as

$$C_R = c\frac{\Delta t}{\Delta x} \quad (4\text{-}9)$$

Where, c is the celerity ($c = \sqrt{gh}$), Δt is the time step and Δx is the grid spacing, g is gravity and h is water depth. The time interval 8 seconds is selected to make the Courant Number between 1 and 5 as suggested by the MIKE manual (2012). The 30-days model results were saved every 75 time steps (10 minutes).

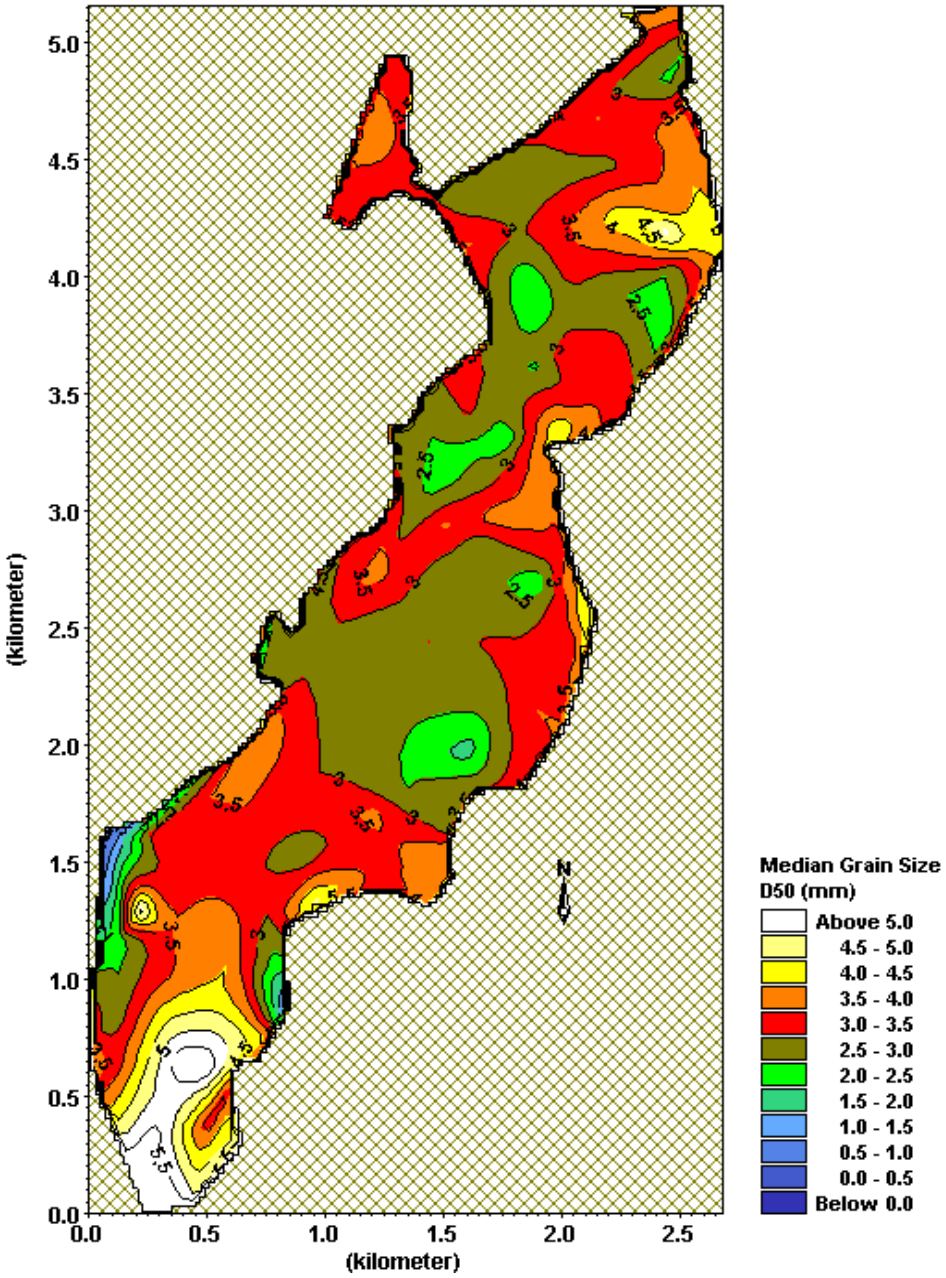

Figure 4-7 Map of median grain size (d50) interpolated on sediment samples which were discussed in section 2.6 and shown in Figure 2-5.

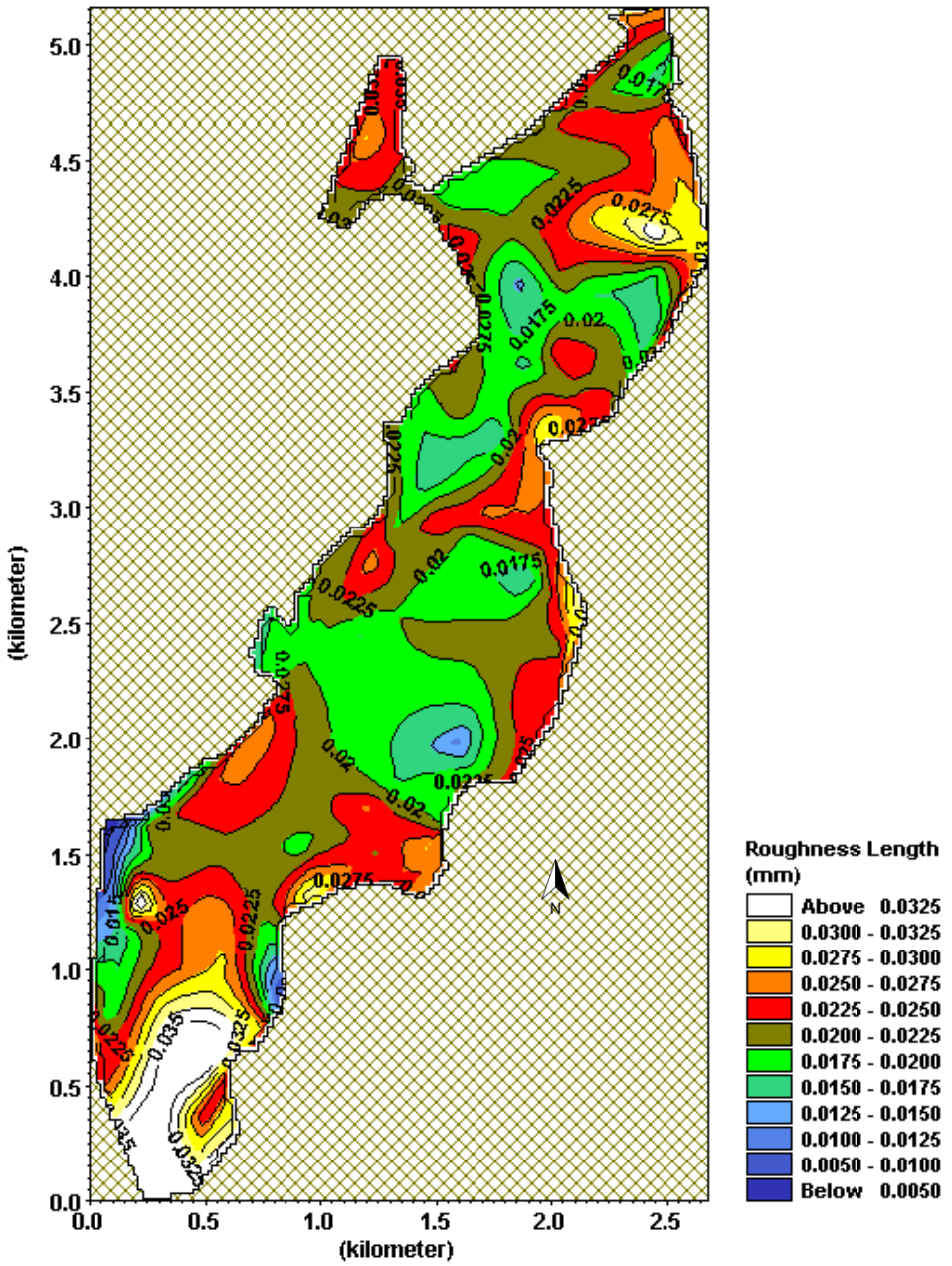

Figure 4-8 Bed roughness length computed on the d50 map shown in Figure 4-7.

4.2.8 Model Parameters

Table 4-1 Parameters for the 'whole-50m' MIKE 21 HD model

Module	Hydrodynamics only	
Bathymetry File	Bathy_Whole50m _edge_g2.dfs2	apply Coriolis forcing, no landslides
MIKE21 HD Set-up	HD_Whole50m_30d_g2.m21	
MIKE21 HD Result	HD_Whole50m_30d_g2.dfs2	
Grid Size	50m Y, 50m X	
Grid Numbers	Imax = 366, Jmax = 299	distance X = 18300 m, distance Y = 14950 m
Coordinates Origin	X origin = 1847382.5 m, Y origin = 5890322.5 m	
Orientation	0	
Time Step	8 seconds	Max. Courant Number: 4.1
No. of Time Steps	318600 (30days)	28/07/2010 12:00-27/08/2010 00:00
Enable Flood and Dry	drying depth = 0.2 m, flooding depth = 0.3 m	
Initial Surface Level	0 m	
Northern Boundary	118, 298 – 365, 298	offshore tidal boundary
Eastern Boundary	365, 0 – 365, 298	offshore tidal boundary
Southern Boundary	185, 0 – 365, 0	offshore tidal boundary
Western Boundary	0, 3	river discharge boundary (Broken Hill station)
Eddy Viscosity	0.5	Smagorinsky formulation, velocity based.
Resistance	32	
Wind	TS_wind_one month_1minute.dfs0	time Series File (recorded on the Slipper Island)

Table 4-2 Parameters of the 'estuary-20m' MIKE 21 HD model

Module	hydrodynamics only	
Bathymetry File	Bathy_Estuary_river_20m_v2.dfs2	apply Coriolis Forcing, no landslides
MIKE21 HD Set-up	HD_estuary_river_20m_30d.m21	
MIKE21 HD Result	HD_estuary_river_20m_30d.dfs2	
Grid Size	20m Y, 20m X	
Grid Numbers	Imax = 465, Jmax = 500	distance X = 9300 m, distance Y = 10000 m
Coordinates Origin	X origin = 1847382.5 m, Y origin = 5890322.5 m	
Orientation	0	
Time Step	5 seconds	Max. Courant Number is 3.91
No. of Time Steps	501120	30 days: 29/07/2010 00:00-27/08/2010 00:00
Enable Flood and Dry	drying depth = 0.2, Flooding Depth = 0.3	
Initial Surface Level	0 m	
Northern Boundary	339, 499 – 464, 499	profile file: North_tides_new.dfs1
Eastern Boundary	464, 237 – 464, 499	profile file: East_tides_new.dfs1
Western Boundary	0, 59	BrokenHills_discharge_boundary_5min.dfs0
Eddy Viscosity	0.5	Smagorinsky formulation, velocity based.
Resistance	bed roughness length file	grids file (Figure 4-8)
Wind	TS_wind_one month_1minute.dfs0	time Series File

4.3 3DD HYDRODYNAMIC MODEL DEVELOPMENT

Some of the model setting-up and calibrating procedures are similar between the MIKE 21 HD model and the 3DD Flow model. Here only the steps which are different between the two modules are discussed in this section.

4.3.1 3DD Module

The 3DD (Window Version 5.03) is a computational marine and freshwater laboratory coupled suite of dynamics and process numerical models written by ASR Ltd. The 3DD suite provides state-of-the-art hydrodynamic and dispersal simulations based on highly accurate mixed Eulerian/Lagrangian mathematical techniques. The model solves the momentum and continuity equations for estuarine circulation on an Eulerian grid. The conservation equations for temperature and salinity are solved using either an Eulerian scheme or a Lagrangian particle technique. Shallow water wave simulations can also be undertaken using the Boussinesq approximation (3DD user manual, 2011).

4.3.2 Time Steps

The time step in the 3DD model is also limited by the Courant Number. In 3DD, it is recommended that the Courant number should be less than 0.7. The number is expressed as

$$C_r = \frac{\Delta x}{\Delta t (2 g d_m)^{\frac{1}{2}}} \quad (4\text{-}10)$$

Where, Δx is the model grid size; Δt is time step; and d_m is the maximum depth in the grid. The initial time step is relative to time zero in the boundary and environmental file.

In the 'whole-50m' model, the maximum feasible time step is 0.95 s, so a 0.8 s time step was used. The output file was saved every 750 steps (10 minutes), and total number of steps was 3186000 (29.5 days).

4.3.3 Bottom Roughness

The sea bed friction is obtained from the Chezy's C formula given by,

$$C = 18 \log_{10}(0.37 d / z_0) \quad (4\text{-}11)$$

The roughness length z_0 is defined in the Karman Prandtl (1930) vertical velocity profile.

$$u = 5.75u_* \log_{10}(z/z_0) \quad (4\text{-}12)$$

Where, d is the water depth, m; z_0 is the roughness length, m; u is the velocity at z meters above the sea bed, m s^{-1}; and u_* is friction velocity, m s^{-1}.

The roughness length is the parameter needed by the model and typical values for z_0 are suggested by ASR.

-order 0.001 m in estuaries;

-order 0.01 m over rough irregular beds;

-and order 0.08 m over very rough beds like coral.

Constant value of 0.001 was input as the bottom roughness into both the 'whole-50m' and the 'estuary-20m' models.

4.3.4 Eddy Viscosity

Typical values for the eddy viscosity coefficient are in the range of 0.1~5 $m^2 s^{-1}$. The higher end of the range is normally reserved for coarser grids. A constant 1 $m^2 s^{-1}$ horizontal eddy viscosity was input into both the 'whole-50m' and the 'estuary-20m' models.

4.3.5 Nesting

The 3DD Flow module provides support for nesting the boundaries from a coarse grid for a large area to one or more finer grids for smaller areas. The coarse grid computation is executed first and the finer grid computations use these results to determine their boundary conditions. Nesting can be repeated at ever decreasing scales.

After the 'whole-50m' 3DD Flow model was calibrated, the 3DD Flow nest module is applied to extract the boundaries for the 'estuary-20m' model from the 'whole-50m' model output.

This process of boundary nesting is different between the MIKE 21 HD and 3DD Flow modules. In MIKE 21 HD module, the time series of the boundary data are extracted at the points along the tidal boundaries from the master model output, and the boundary file can be generated by interpolating the extracted data at each point in the profile series file. In 3DD Flow module, the boundary tidal time series of the estuary-20m model can be nested from the whole-50m model directly.

4.3.6 Vertical Velocity

The surface elevation and current speed observed by the ADP at the tidal inlet, ADV1 at the moorings, ADV2 at the Tairua Wharf and ADV3 at the Pauanui Waterway were used to compare with the model computed depth-average results for calibrating the models. The instruments were deployed 0.95 m above the water bottom, therefore, the Law of the Wall from von Kármán (1930) described in Equation 4-13 was used to convert the model calculated current velocity from the average water depth to 0.95 m above the water bottom for the comparison.

$$u_z = \frac{u_*}{k}\ln\left(\frac{z}{z_0}\right) = \frac{\sqrt{C_d}}{0.4}u_{100}\ln\left(\frac{z}{z_0}\right) \quad (4\text{-}13)$$

Where, u_* is friction velocity; k is von Karman's constant (equals to 0.4), z is elevation above sea bed and z_0 is the hydraulic bed roughness length; C_d is the fluid drag coefficient; and u_{100} is the mean horizontal velocity at 100 cm above the water bed.

4.3.7 Model Parameters

The 'whole-50m' and the 'estuary-20m' 3DD Flow model parameters are presented in Table 4-4 and Table 4-5 respectively.

Table 4-3 Parameters for the 'whole-50m' 3DD Flow model

Module	Hydrodynamics only
Grid Size	50 m Y, 50 m X
Grid Numbers	Imax = 366 Distance X = 18300 m Jmax = 299 Distance Y = 14950 m
Coordinates Origin	X origin = 1847382.5 m Y origin = 5890322.5 m
Time Step	0.8 s Save the result file every 10 minutes
No. of Time Steps	3186000 = 29.5 days 28/07/2010 11.00am-26/08/2010 10.30pm
Enable Flood and Dry	Effective depth = 0.3 Drying height = 0.05
Initial Surface Level	0 m
Northern Boundary	119, 299 – 366, 299 north tidal (elevation) boundary
Eastern Boundary	366, 1 – 366, 299 east tidal (elevation)_boundary
Southern Boundary	186, 1 – 366, 1 south tidal (elevation) boundary
Western Boundary	1, 601 river discharge boundary
Eddy Viscosity	1
Roughness Length	0.001
Wind	recorded on the Slipper Island every 1 minute

Table 4-4 Parameters for the 'estuary-20m' 3DD Flow model

Module	Hydrodynamics only	
Grid Size	20m Y, 20m X	
Grid Numbers	Imax = 465	Distance X = 18300 m
	Jmax = 500	Distance Y = 14950 m
Coordinates Origin	X origin = 1847382.5 m	Y origin = 5890322.5 m
Time Step	0.6 s	Results file saved every 10 minutes.
No. of Time Steps	4248000 29.5 days	
	28/07/2010 11.00am-26/08/2010 11.00pm	
Enable Flood and Dry	Effective depth = 0.3	Drying height = 0.05
Initial Surface Level	0 m	
Northern Boundary	340, 500 – 465, 500	nested tidal boundary
Eastern Boundary	465, 238 – 465, 500	nested tidal boundary
Western Boundary	1, 4	river discharge boundary
Eddy Viscosity	1	
Roughness Length	0.001	
Wind	recorded on the Slipper Island every 1 minute	

4.4 MODEL CALIBRATION

4.4.1 Model and Instrument Results in Figures

To compare the instruments measured data with the model calculated results, the model results were extracted at the grid cells that corresponded to the instruments locations (Table 4-5) using the MIKE Zero Toolbox.

Table 4-5 Locations of the deployed instruments in model cells

Instrument	Locations	Whole-50m	Estuary-20m
ADP	Lat. 37°0'19" S, Lon.175°52'1.5" E	(155, 207)	(386, 373)
ADV1	Lat. 37°0'22.8" S, Lon.175°51'26.1" E	(137, 206)	(343, 369)
ADV2	Lat. 37°0'34.6" S, Lon.175°51'6.18" E	(127, 199)	(318, 352)
ADV3	Lat. 37°1'18.2" S, Lon.175°51'4.2" E	(125, 172)	(312, 284)
RBR	Lat. 37°4'27.3" S, Lon.175°46'57.66" E	(0, 59)	(0, 3)

4.4.2 Statistics Qualification

The evaluation of model performance aims to express the goodness of fit between field data and model results by simple and objective measures.

The mean error (ME) is the mean of the differences between predicted Y and observed X value. It is a measure of the overall forecast bias. A positive ME indicates that the model results on average overestimate the measured data.

$$\mathrm{ME} = \frac{1}{\mathrm{N}}\sum_{\mathrm{i}=1}^{\mathrm{N}}(\mathrm{y_i} - \mathrm{x_i}) \tag{4-14}$$

To avoid the neutralization of positive by negative errors, the discrepancy is squared, thereby forming the mean square error (MSE).

$$\mathrm{MSE} = \frac{1}{\mathrm{N}}\sum_{\mathrm{i}=1}^{\mathrm{N}}(\mathrm{y_i} - \mathrm{x_i})^2 \tag{4-15}$$

The root mean-squared error ($RMSE$) is the most commonly used measure of numeric prediction quality, as it contains the same scale and unit as the variables X and Y.

$$\mathrm{RMSE} = \sqrt{\frac{1}{\mathrm{N}}\sum_{\mathrm{i}=1}^{\mathrm{N}}(\mathrm{y_i} - \mathrm{x_i})^2} \tag{4-16}$$

Being less influenced by outliers than is the case for MSE and RMSE, a more robust measure of accuracy is the mean absolute error (MAE).

$$\mathrm{MAE} = \frac{1}{\mathrm{N}}\sum_{\mathrm{i}=1}^{\mathrm{N}}|\mathrm{y_i} - \mathrm{x_i}| \tag{4-17}$$

The MAE can be made dimensionless by dividing it by the mean of the observations to give the relative mean absolute error ($RMAE$). It deviates from zero according to the scale of incongruity between observed and simulated values.

$$\mathrm{RMAE} = \frac{1}{\mathrm{N}}\sum_{\mathrm{i}=1}^{\mathrm{N}}|\mathrm{y_i} - \mathrm{x_i}| \,/\, \frac{1}{\mathrm{N}}\sum_{\mathrm{i}=1}^{\mathrm{N}}|\mathrm{x_i}| \tag{4-18}$$

All model error estimates so far assume that the observed data (measured) is free of errors, which in practice cannot be achieved due to unavoidable systematic and random measurement errors. Van Rijn et al. (2002) propose an additional term to reduce the absolute error by the accuracy of the measured data Δ. This forms the adjusted mean absolute error ($AMAE$) and adjusted relative mean absolute error ($ARMAE$), in which the term is set zero if the absolute error is smaller than the accuracy of the measurements.

$$\mathrm{AMAE} = \frac{1}{\mathrm{N}}\sum_{\mathrm{i}=1}^{\mathrm{N}}(|\mathrm{y_i} - \mathrm{x_i}| - \Delta) \tag{4-19}$$

$$\mathrm{ARMAE} = \frac{1}{\mathrm{N}}\sum_{\mathrm{i}=1}^{\mathrm{N}}(|\mathrm{y_i} - \mathrm{x_i}| - \Delta) / \frac{1}{\mathrm{N}}\sum_{\mathrm{i}=1}^{\mathrm{N}}|\mathrm{x_i}| \tag{4-20}$$

A common method to determine the linear relation between two series of X and Y is the linear correlation coefficient r, given by the covariance of X with Y, divided by the product of the standard deviation of X and the standard deviation of Y.

$$\mathrm{r} = {\sigma_{\mathrm{xy}}}/{\sigma_{\mathrm{x}}\sigma_{\mathrm{y}}} \tag{4-21}$$

The covariance is the mean value of all the pairs of differences from the mean for X multiplied by the differences from the mean for Y.

$$\sigma_{xy} = \frac{1}{N-1}\sum_{i-1}^{N}(x_i - \bar{x})(y_i - \bar{y}) \quad (4\text{-}22)$$

The standard deviations of X and Y are

$$\sigma_x = \sqrt{\frac{1}{N-1}\sum_{i-1}^{N}(x_i - \bar{x})^2} \quad (4\text{-}23)$$

$$\sigma_y = \sqrt{\frac{1}{N-1}\sum_{i-1}^{N}(y_i - \bar{y})^2} \quad (4\text{-}24)$$

The linear correlation coefficient indicates the extent to which the pairs of two variables converge to a straight line, its value ranging from −1 (complete negative correlation) to 0 (no correlation) to 1 (perfect correlation). The statistical measure r^2 (or explained variance) is derived by squaring the correlation coefficient, which can be understood as the percentage of variance that the two series have in common (Winter, 2007).

Van Rijn also defined the model statistics method in 2003. He proposed to evaluate the performance of the models on the basis of the Relative Mean Absolute Error (RMAE) formulae as

Wave height $$RMAE = \langle |H_c| - |H_m| - \Delta H_m \rangle / \langle H_m \rangle \quad (4\text{-}25)$$

Velocity $$RMAE = \langle |V_c| - |V_m| - \Delta V_m \rangle / \langle V_m \rangle \quad (4\text{-}26)$$

Where, H is wave height, ΔH_m is the error of measured wave height, V is velocity ('+' is north going, '-' means south going), ΔV_m is the error of measured velocity. c means computed. $\langle ... \rangle$ means averaging procedure over time series. The absolute difference of the computed and measured values minus the measurement error cannot be smaller than zero (e.g. $|H_c| - |H_m| - \Delta H_m$ is zero, if < 0). Basically, it means that the computed value is within the error band range of the measured value. The statistics qualification of error ranges based on the method of Van Rijn (2002) is listed in Table 4-6.

Table 4-6 Qualification standards of error ranges according to Van Rijn (2002)

Qualification	Wave Height RMAE	Velocity RMAE	Morphology BSS
Excellent	<0.05	<0.1	1.0-0.8
Good	0.05-0.1	0.1-0.3	0.8-0.6
Reasonable/fair	0.1-0.2	0.3-0.5	0.6-0.3
Poor	0.2-0.3	0.5-0.7	0.3-0
Bad	>0.3	>0.7	<0

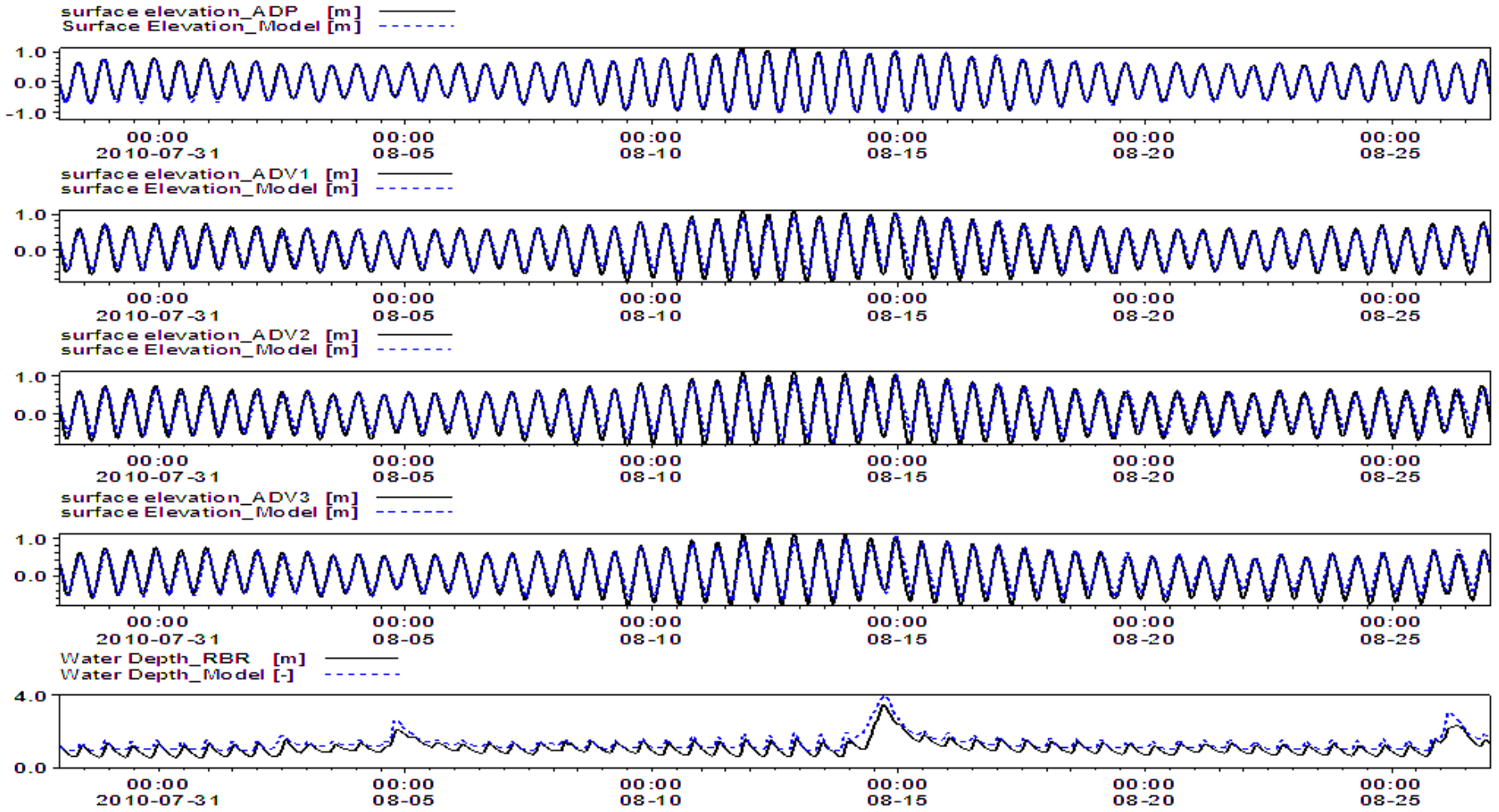

Figure 4-9 Comparison between the 'whole-50m' MIKE 21 HD model calculated (blue dot) and instruments recorded (black solid) surface elevations during the field campaign in 2010 for calibration.

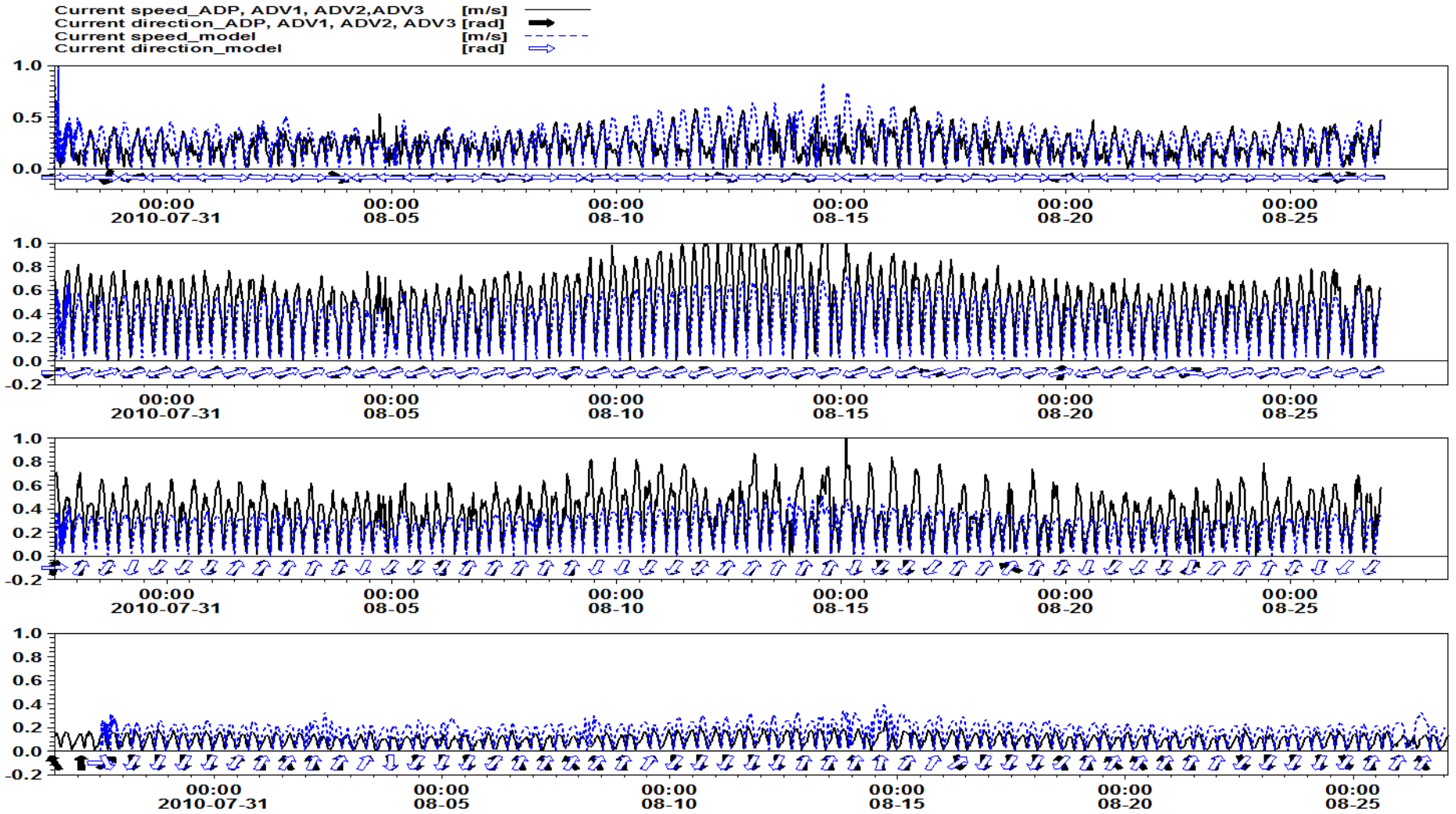

Figure 4-10 Comparison between the 'whole-50m' MIKE 21 HD model calculated (blue dot) and instruments recorded (black solid) tidal currents during the field campaign in 2010 for calibration.

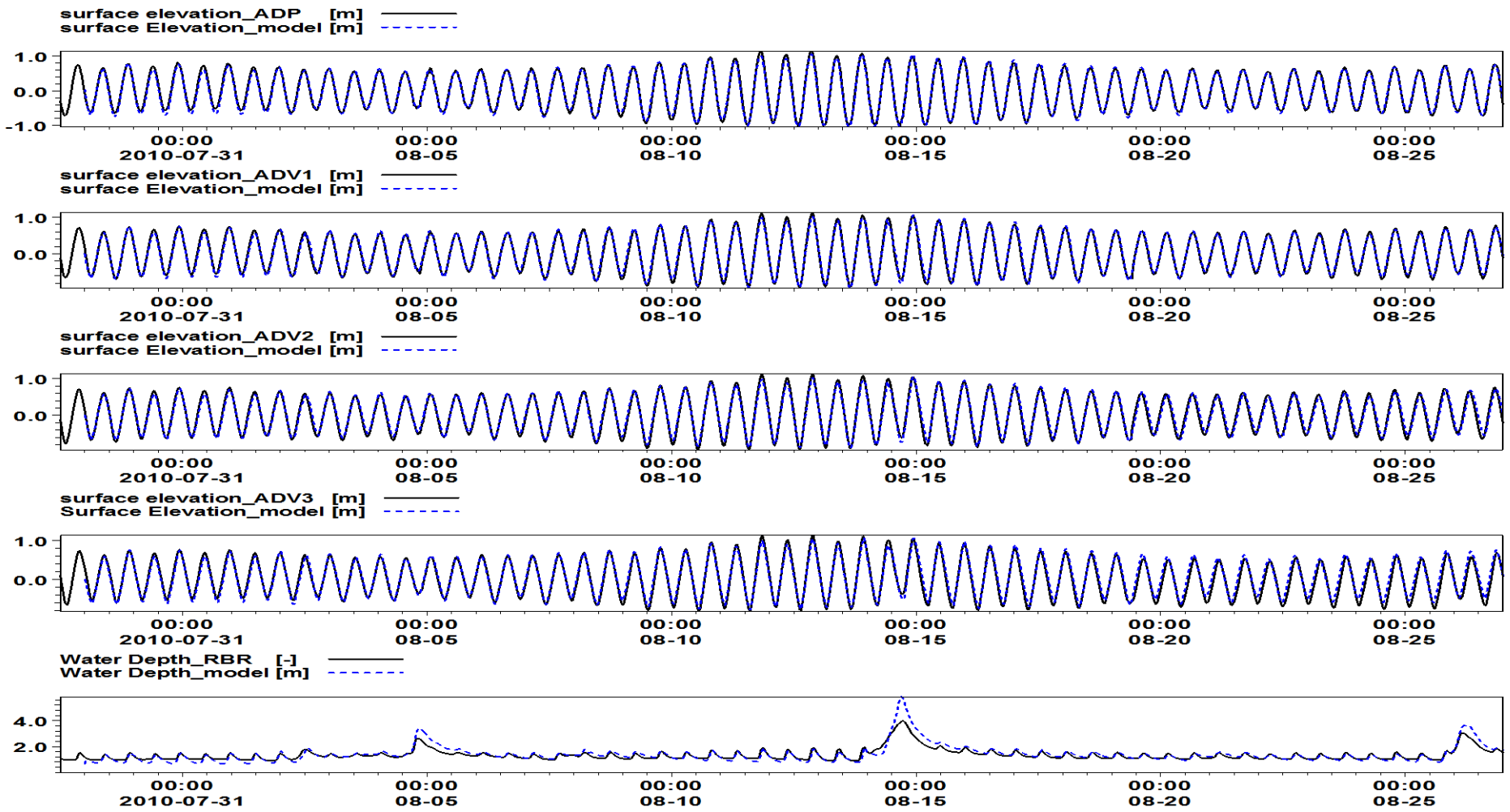

Figure 4-11 Comparison between the 'estuary_20m' MIKE 21 HD model calculated (blue dot) and instruments recorded (black solid) surface elevations during the field campaign in 2010 for calibration.

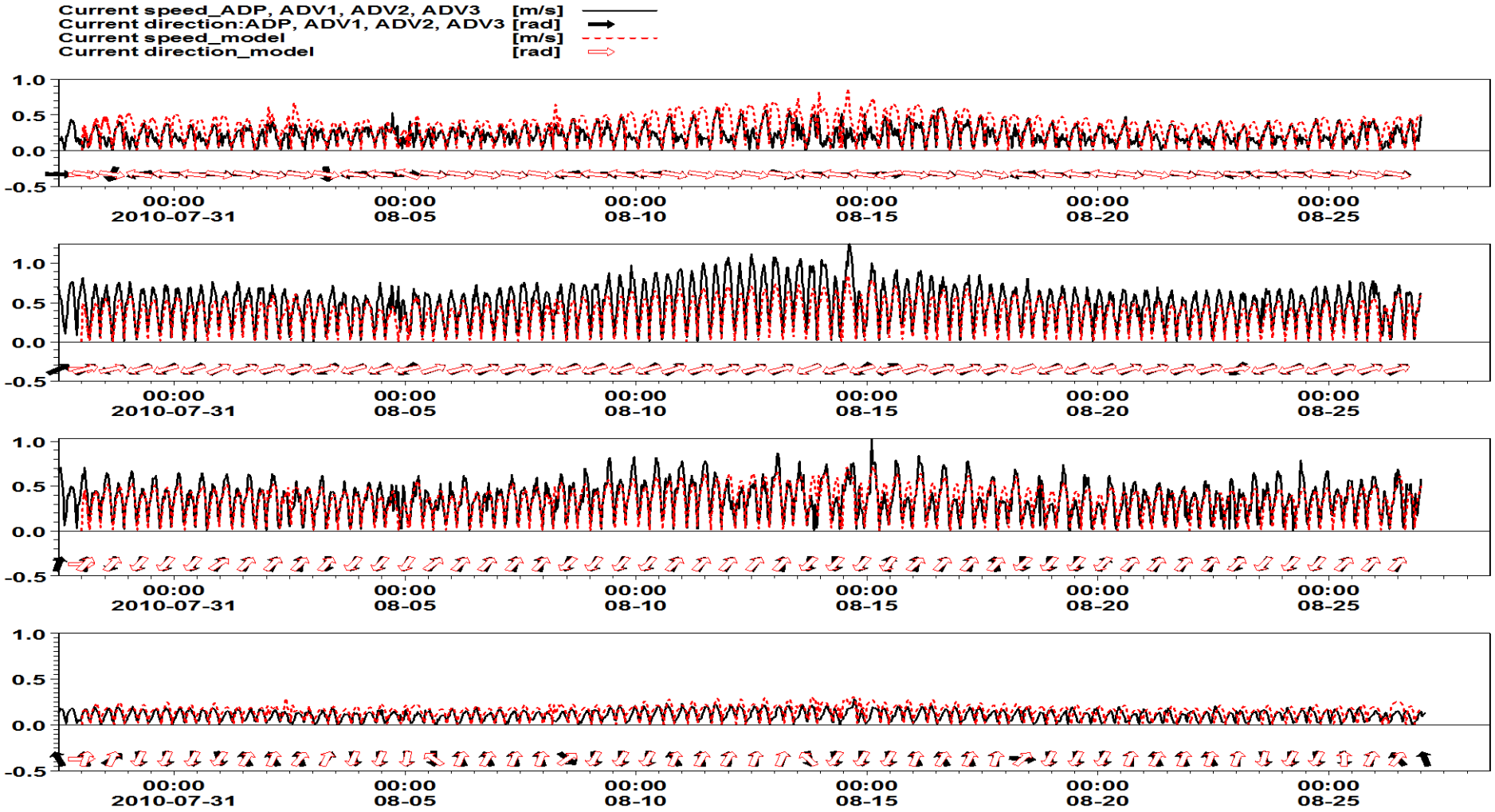

Figure 4-12 Comparison between the 'estuary_20m' MIKE 21 HD model calculated (red dot) and instruments recorded (black solid) tidal currents during the field campaign in 2010 for calibration.

Table 4-7 Statistics qualification results of the 'whole_50m' MIKE 21 HD model

Items	ME	MSE	RMSE	MAE	RMAE	γ	RMAE (Van Rijn)	Qualification
ADP water level	-0.008	0.003	0.058	0.046	0.100	0.994	0.165	**Reasonable**
ADV1 water level	0.041	0.020	0.141	0.162	0.260	0.964	-2.37 => 0	**Excellent**
ADV2 water level	0.041	0.028	0.166	0.135	0.313	0.948	-2.009 =>0	**Excellent**
ADV3 water level	0.047	0.017	0.129	0.103	0.255	0.965	-1.12 => 0	**Excellent**
RBR water depth	-0.258	0.098	0.313	0.259	0.191	0.990	-0.18 => 0	**Excellent**
ADP current speed	0.064	0.023	0.151	0.115	0.514	0.882	0.286	**Good**
ADV1 current speed	-0.109	0.035	0.188	0.155	0.318	0.959	-0.22 => 0	**Excellent**
ADV2 current speed	-0.106	0.030	0.174	0.145	0.400	0.940	-0.29 => 0	**Excellent**
ADV3 current speed	0.076	0.009	0.093	0.082	0.856	0.940	-0.48 => 0	**Excellent**
ADP current direction_rad	0.005	0.020	0.143	0.062	0.129	0.965		
ADV1 current direction_rad	0.057	0.023	0.151	0.084	0.230	0.951		
ADV2 current direction_rad	-0.008	0.050	0.224	0.105	0.347	0.844		
ADV3 current direction_rad	-0.288	0.306	0.553	0.391	0.683	0.555		

Table 4-8 Statistics qualification results of the 'estuary-20m' MIKE 21 HD model

Items	ME	MSE	RMSE	MAE	RMAE	γ	RMAE (Van Rijn)	Qualification
ADP water level	-0.009	0.003	0.057	0.046	0.100	0.994	-0.38 => 0	**Excellent**
ADV1 water level	0.007	0.003	0.057	0.044	0.103	0.994	-0.57 => 0	**Excellent**
ADV2 water level	0.011	0.007	0.086	0.069	0.160	0.986	-0.79 => 0	**Excellent**
ADV3 water level	0.030	0.010	0.098	0.074	0.182	0.978	-0.45 => 0	**Excellent**
RBR water depth	0.058	0.068	0.260	0.163	0.120	0.988	0.042	**Excellent**
ADP current speed	0.110	0.031	0.176	0.131	0.588	0.907	0.496	**Reasonable**
ADV1 current speed	-0.111	0.028	0.167	0.132	0.272	0.974	-0.23 => 0	**Excellent**
ADV2 current speed	-0.009	0.013	0.113	0.088	0.244	0.960	-0.03=> 0	**Excellent**
ADV3 current speed	0.057	0.005	0.073	0.063	0.657	0.943	-0.5331	**Excellent**
ADP current direction	0.038	0.014	0.118	0.059	0.123	0.980		
ADV1 current direction	0.050	0.012	0.111	0.066	0.179	0.975		
ADV2 current direction	0.111	0.056	0.236	0.186	0.608	0.874		
ADV3 current direction	0.269	0.202	0.450	0.271	0.476	0.864		

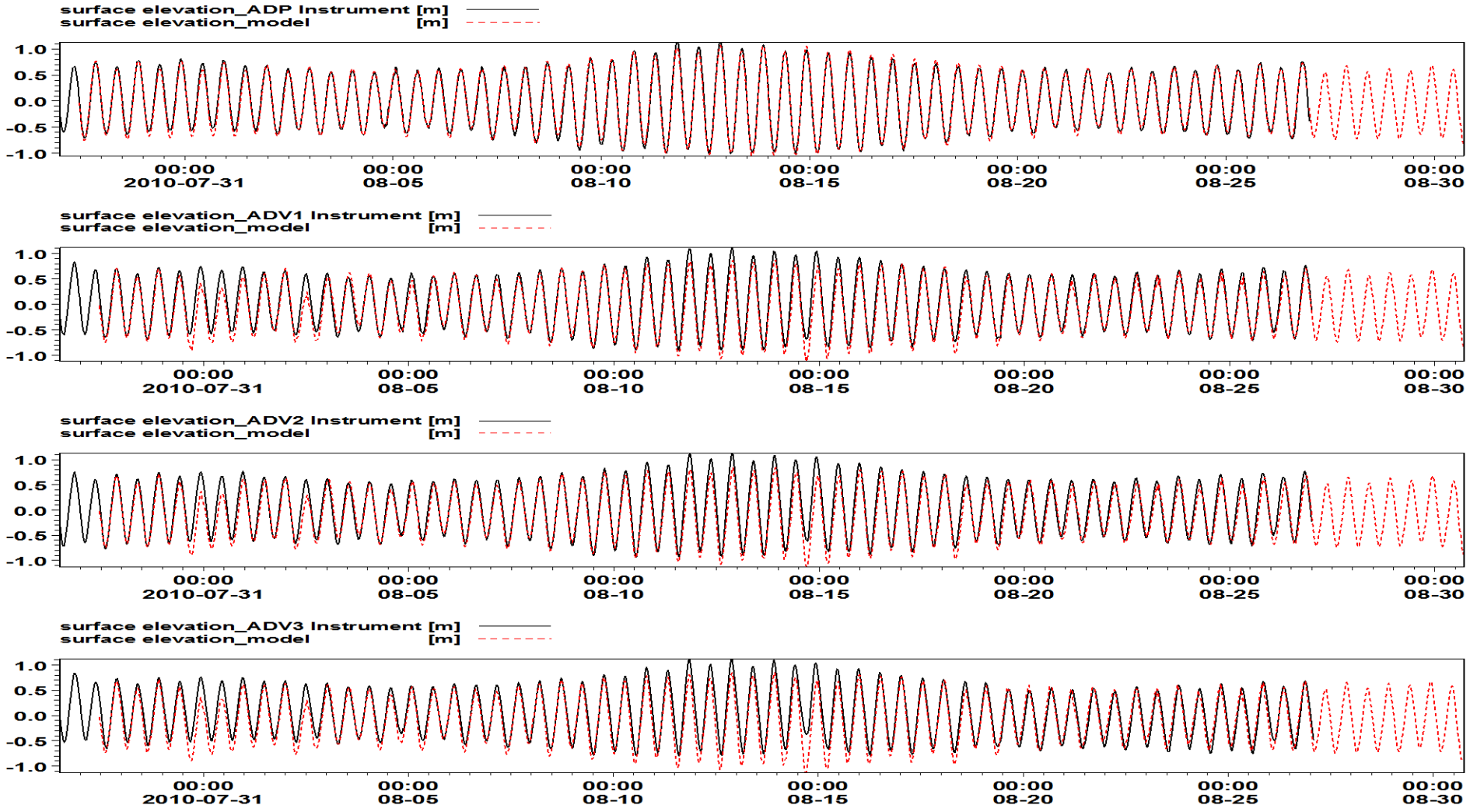

Figure 4-13 Comparison between the 'whole_50m' 3DD Flow model calculated (red dot) and instruments recorded (black solid) surface elevations during the field campaign in 2010 for calibration.

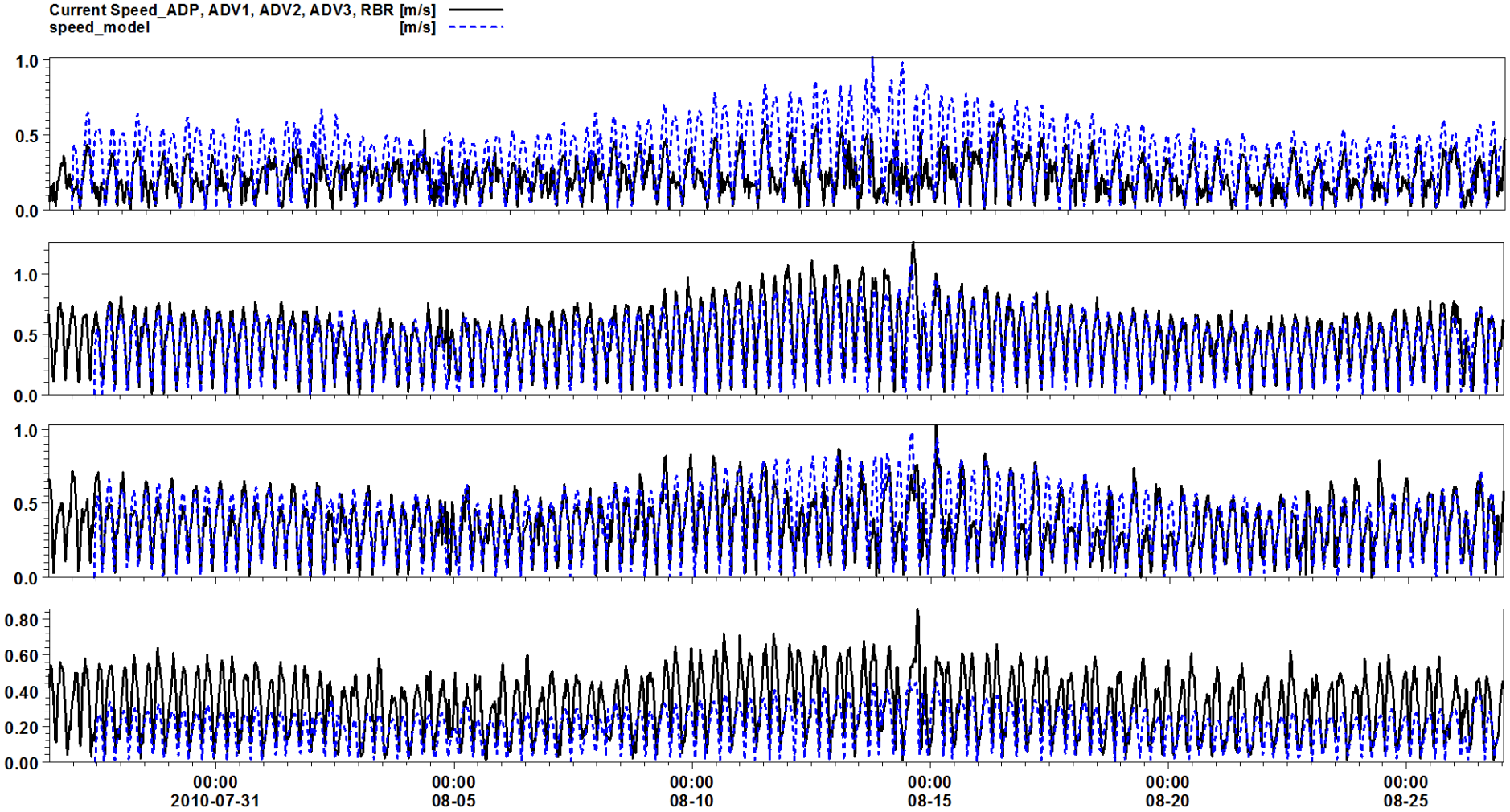

Figure 4-14 Comparison between the 'whole_50m' 3DD Flow model calculated (blue dot) and instruments recorded (black solid) tidal currents during the field campaign in 2010 for calibration.

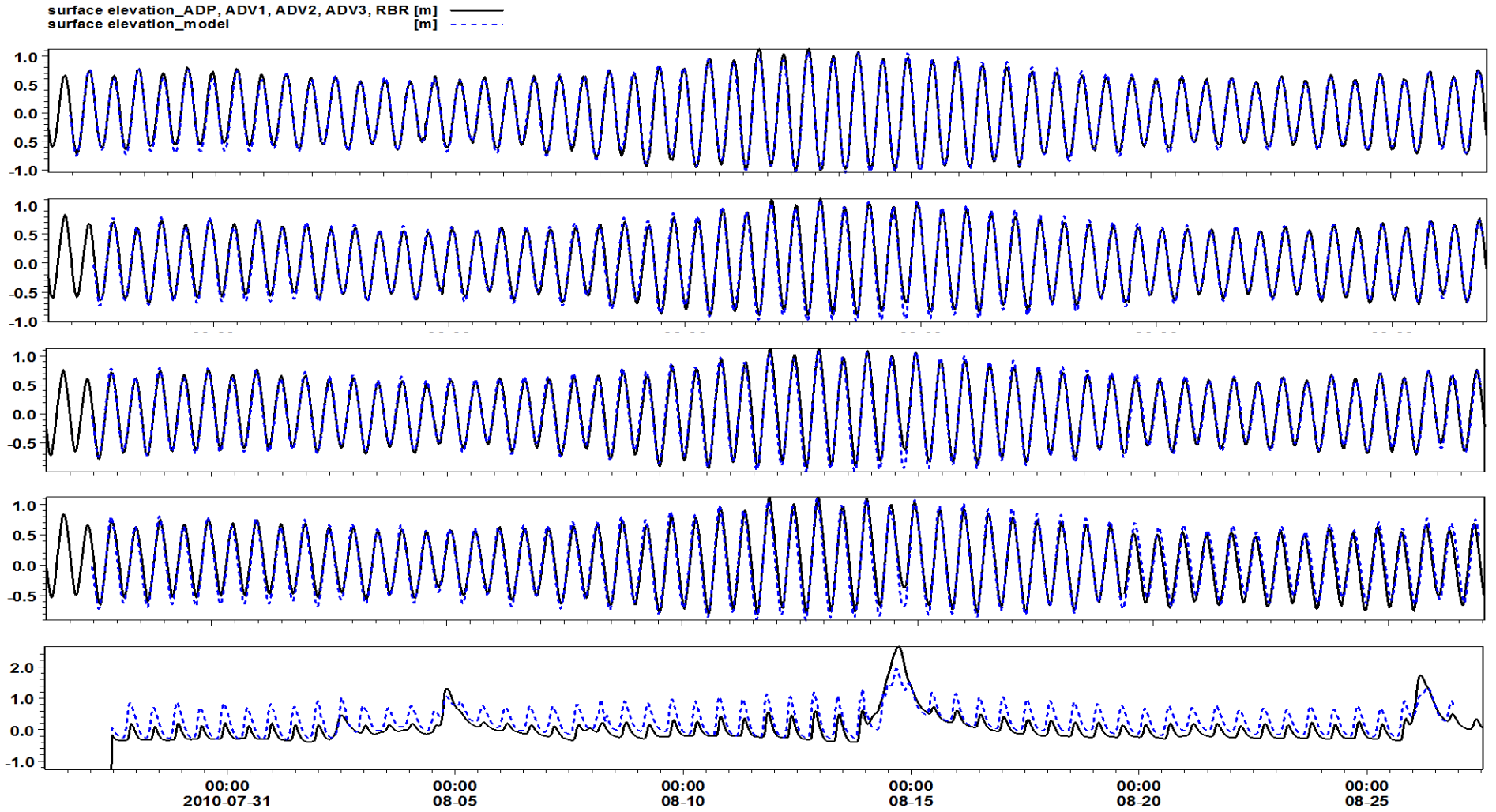

Figure 4-15 Comparison between the 'estuary_20m' 3DD Flow model calculated (blue dot) and instruments recorded (black solid) surface elevations during the field campaign in 2010 for calibration.

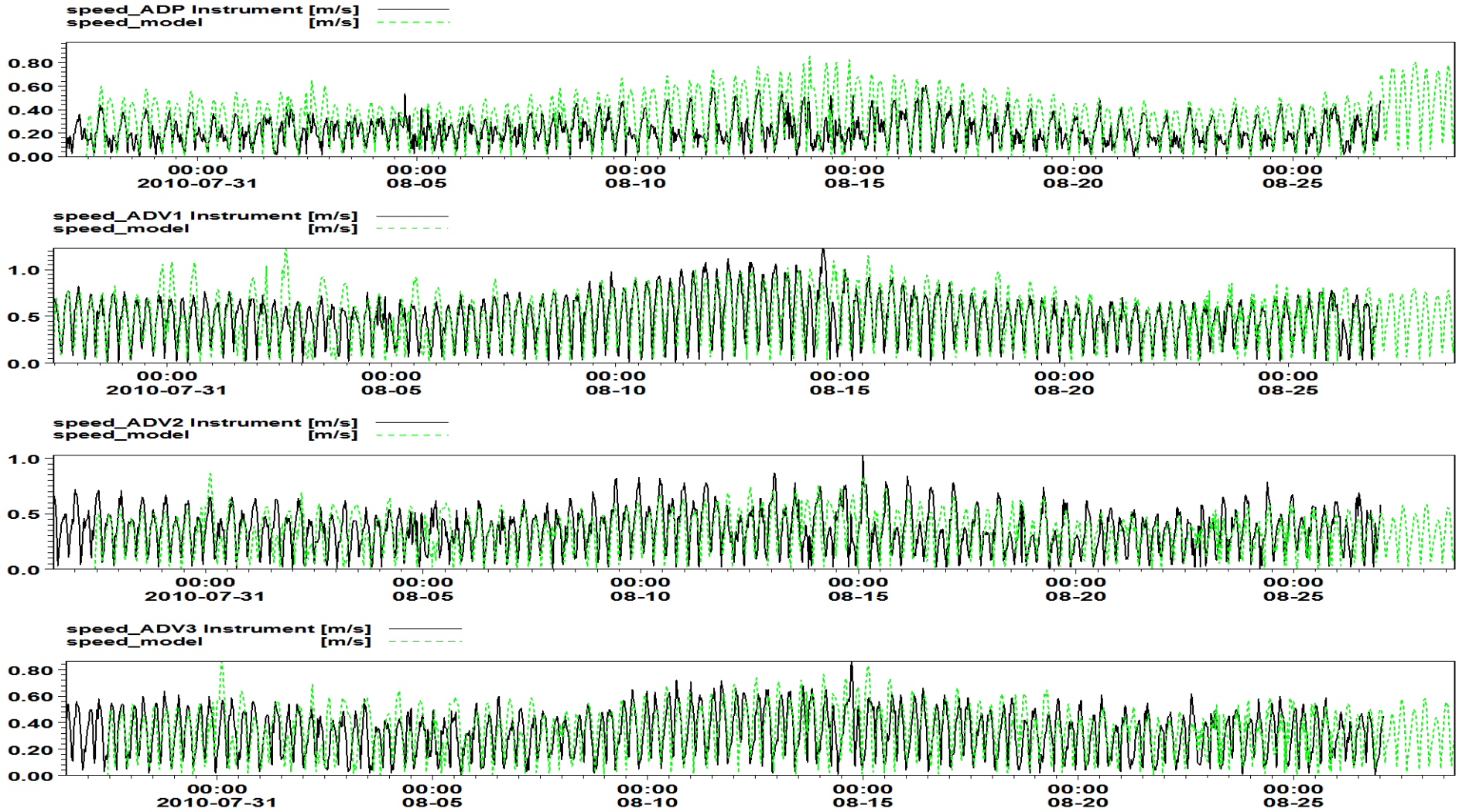

Figure 4-16 Comparison between the 'estuary_20m' 3DD Flow model calculated (green dot) and instruments recorded (black solid) tidal currents during the field campaign in 2010 for calibration.

Table 4-9 Statistics qualification results of 'whole-50m' 3DD Flow model

Items	ME	MSE	RMSE	MAE	RMAE	*r*	RMAE (Van Rijn)	Qualification (Van Rijn)
ADP water level	-0.004	0.003	0.057	0.046	0.099	0.994	0.007	**Excellent**
ADV1 water level	-0.009	0.005	0.069	0.054	0.127	0.991	0.036	**Excellent**
ADV2 water level	-0.012	0.007	0.081	0.064	0.148	0.987	0.014	**Excellent**
ADV3 water level	-0.008	0.016	0.128	0.101	0.249	0.965	0.050	**Excellent**
RBR water depth	0.198	0.142	0.377	0.295	1.071	0.649	0.166	**Reasonable**
ADP current speed	0.119	0.034	0.185	0.143	0.647	0.911	0.439	**Reasonable**
ADV1 current speed	0.011	0.012	0.110	0.084	0.172	0.980	0.022	**Excellent**
ADV2 current speed	0.024	0.015	0.124	0.093	0.362	0.957	0.067	**Excellent**
ADV3 current speed	-0.100	0.024	0.156	0.133	0.407	0.941	0.300	**Good**

Table 4-10 Statistics qualification results of 'estuary-20m' 3DD Flow model

Items	ME	MSE	RMSE	MAE	RMAE	*r*	RMAE (Van Rijn)	Qualification (Van Rijn)
ADP water level	-0.004	0.003	0.057	0.046	0.099	0.994	0.007	**Excellent**
ADV1 water level	-0.013	0.006	0.077	0.060	0.140	0.989	0.045	**Excellent**
ADV2 water level	-0.018	0.008	0.088	0.069	0.158	0.985	0.027	**Excellent**
ADV3 water level	-0.018	0.019	0.137	0.110	0.273	0.961	0.072	**Excellent**
RBR water level	0.058	0.068	0.260	0.163	0.120	0.988	0.042	**Excellent**
ADP current speed	0.159	0.051	0.225	0.180	0.812	0.906	0.495	**Reasonable**
ADV1 current speed	-0.05	0.016	0.128	0.097	0.199	0.974	-0.103 => 0	**Excellent**
ADV2 current speed	0.035	0.019	0.138	0.104	0.287	0.951	0.097	**Excellent**
ADV3 current speed	-0.129	0.031	0.176	0.147	0.451	0.940	-0.394	**Good**

4.5 MODEL VALIDATION

4.5.1 Methods

The calibrated 3DD hydrodynamic models were validated using the 2nd field work campaign in June 2011. All the model parameters were kept same as the calibrated models.

4.5.2 Results

The validation results of the 'whole-50m' model calculated surface elevation were presented in Figure 4-17 and Figure 4-18; and the 'estuary-20m' model calculated current speed were validated in Figure 4-19 and Figure 4-20 from the tidal inlet to the Tairua River mouth through the moorings, the Tairua Estuary and the Pauanui Waterway stations.

According to both of the 'whole_50m' and 'estuary_20m' 3DD Flow models which were calibrated using the instruments data observed during the 1st field work in July 2010 can be used to calculate the water elevation and current speed during the 2nd field work in June 2011. The models were validated, too.

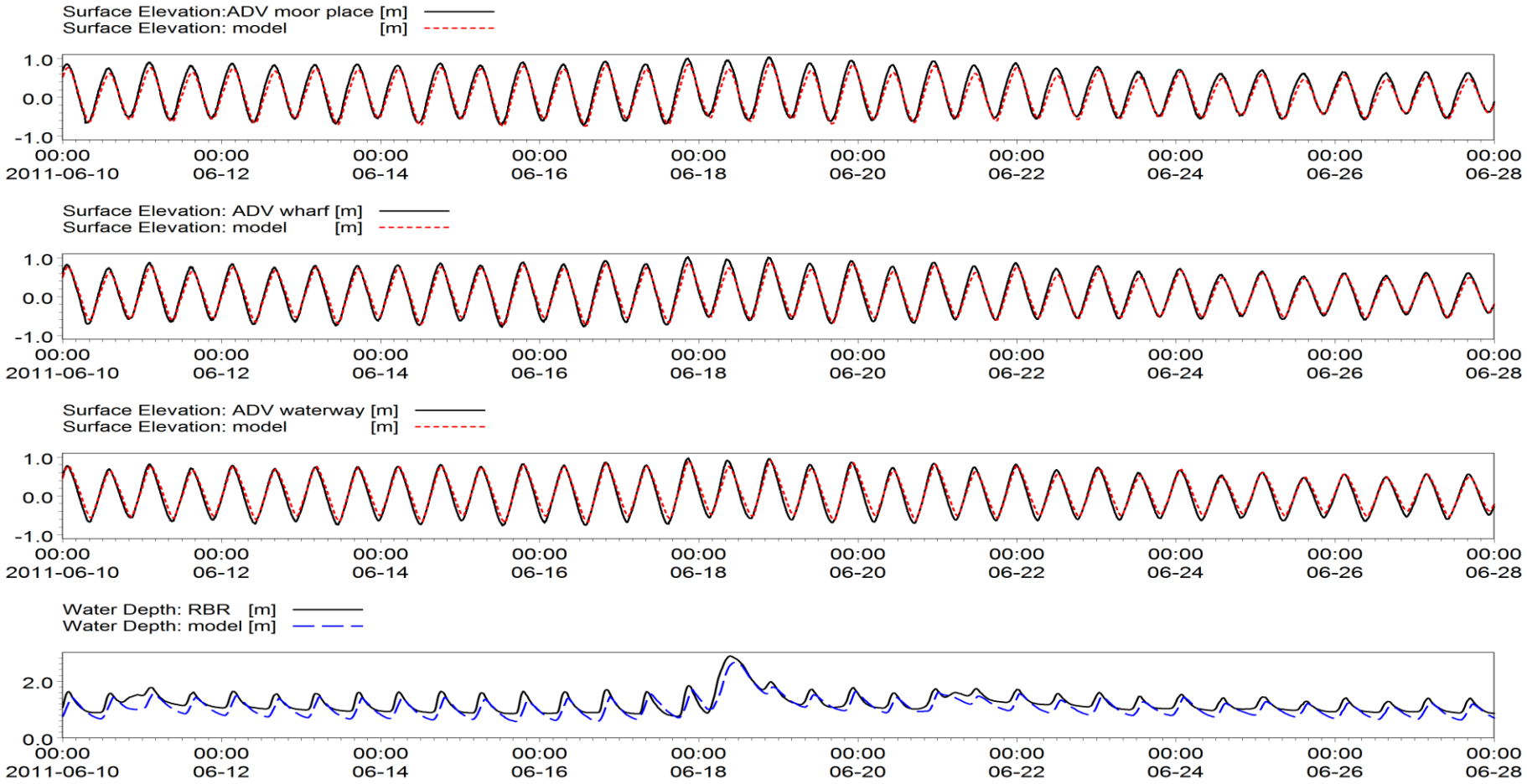

Figure 4-17 Comparison between the calculated (red dot) and observed (black solid) surface elevation and river depth (blue dot) of the 'whole_50m' 3DD model during the 2nd field campaign in 2011 for validation.

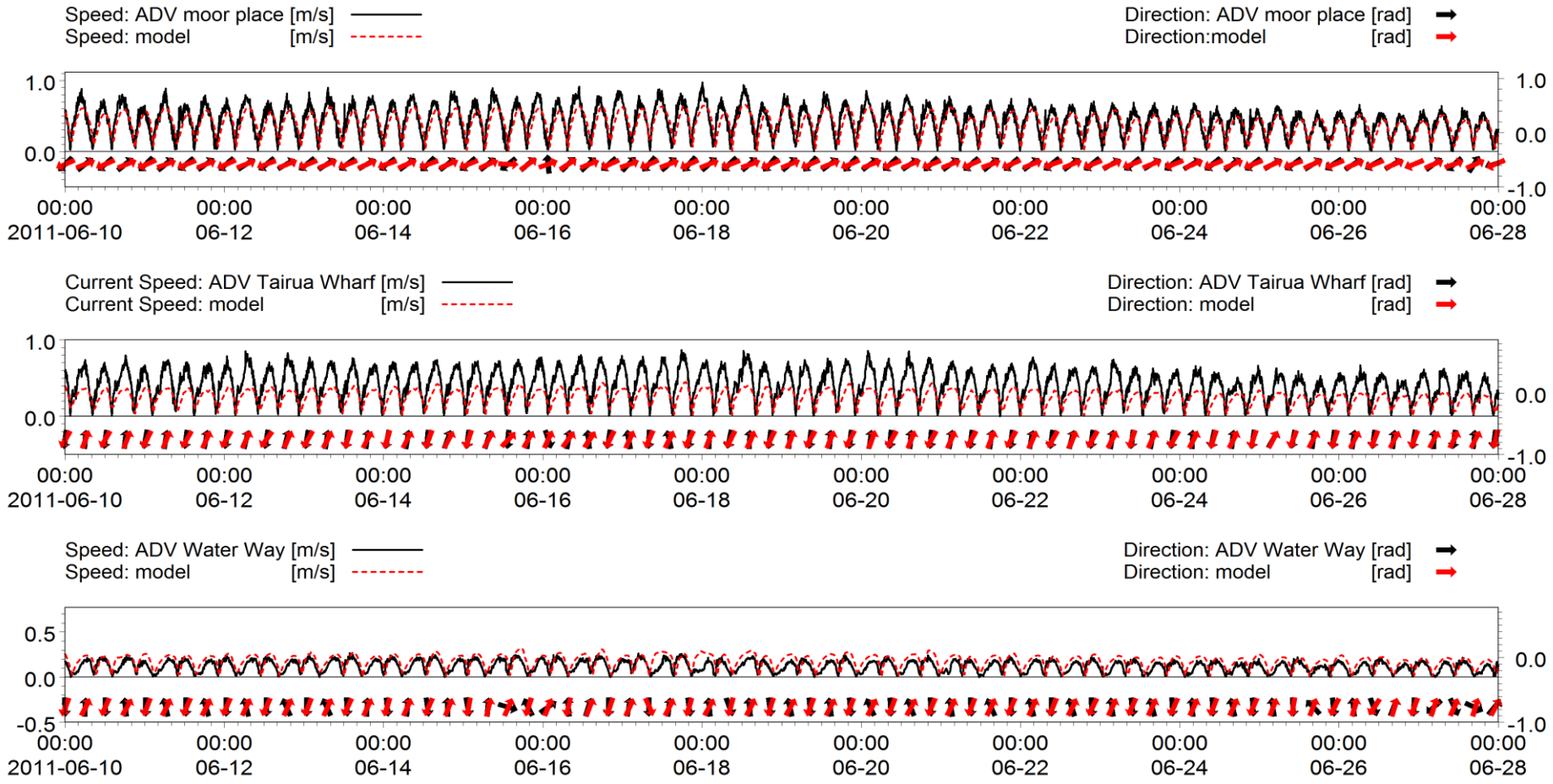

Figure 4-18 Comparison between the calculated (red dot) and observed (black solid) current speed of the 'whole_50m' MIKE 21 HD model during the 2nd field campaign in 2011 for validation.

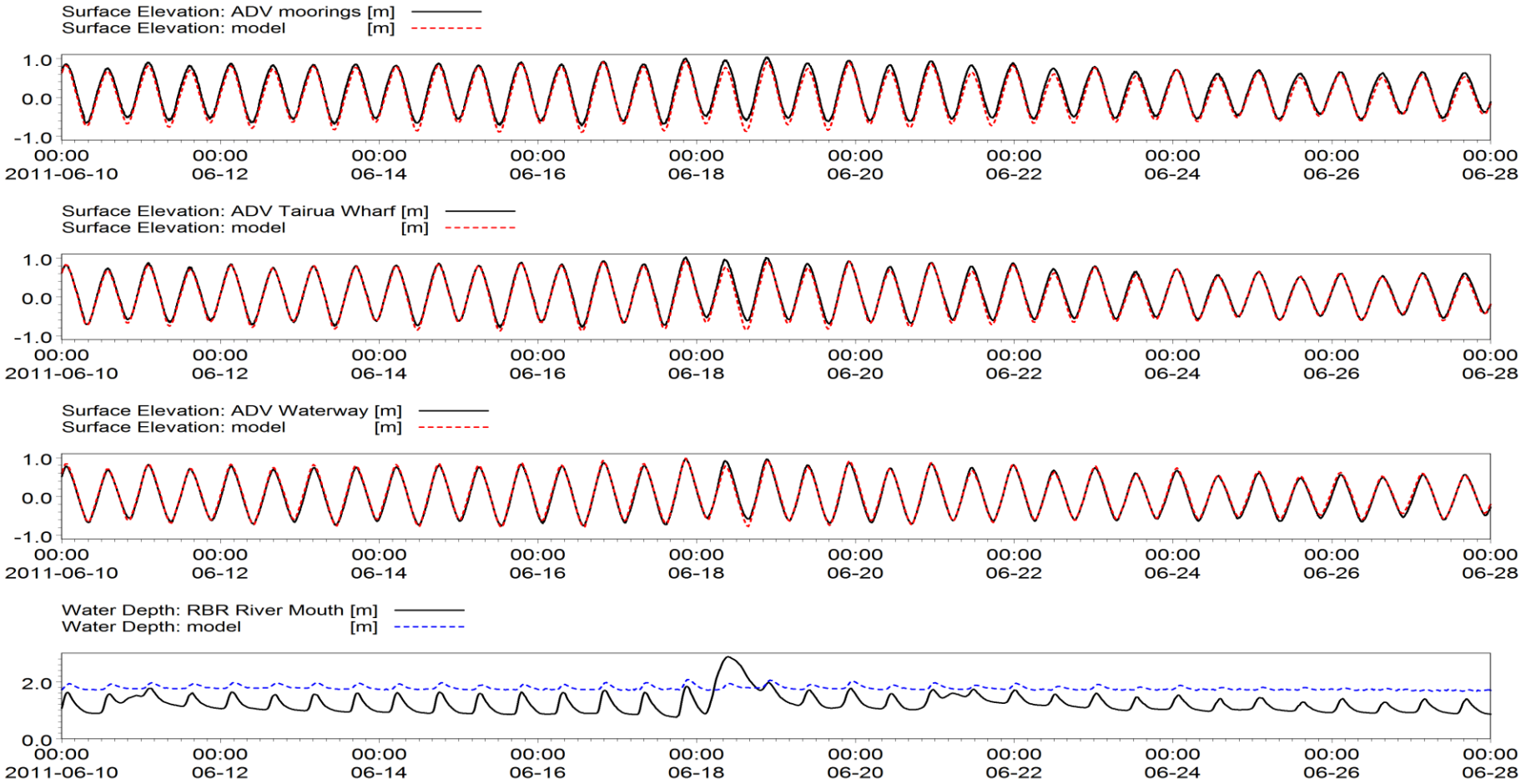

Figure 4-19 Comparison between the calculated (red dot) and observed (black solid) surface elevation and river depth (blue dot) of 'estuary_20m' MIKE 21 HD model during the 2nd field campaign in 2011 for validation.

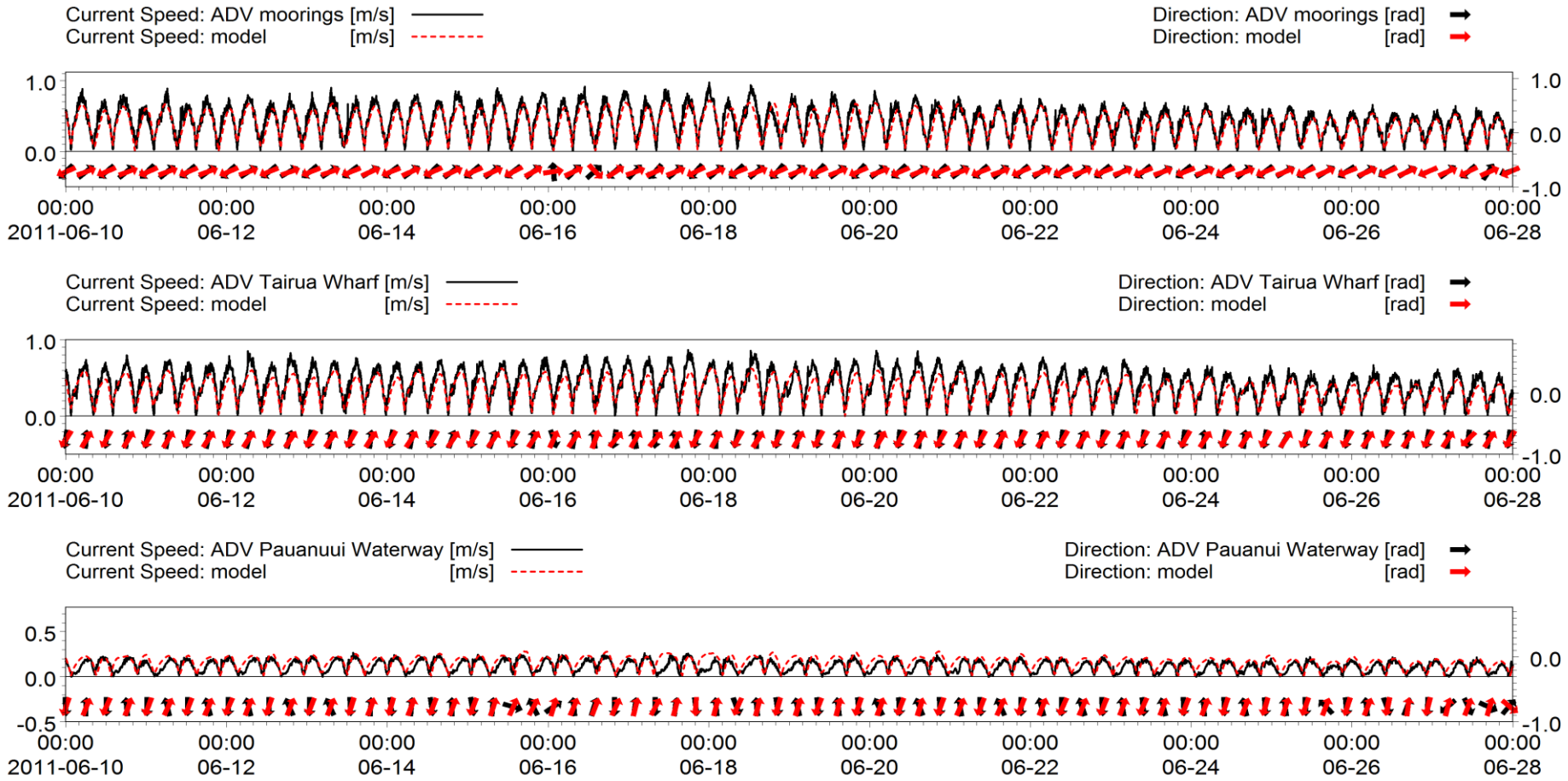

Figure 4-20 Comparison between the calculated (red dot) and observed (black dot) current speed of 'estuary_20m' MIKE 21 HD model during the 2nd field campaign in 2011 for validation.

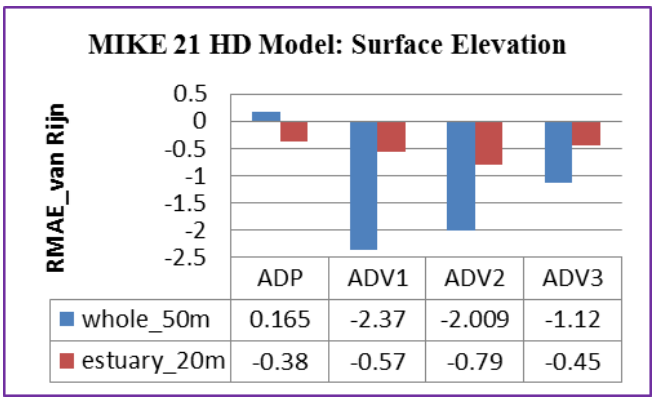

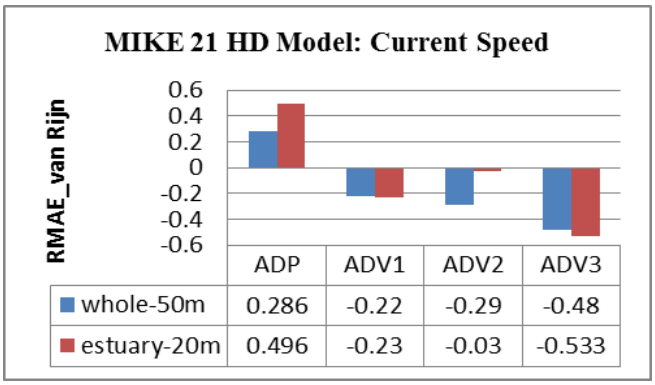

Figure 4-21 Comparison of the statistics qualification of the calculated surface elevation and the current speed between the 'estuary-20m' and 'whole-50m' MIKE 21 HD models.

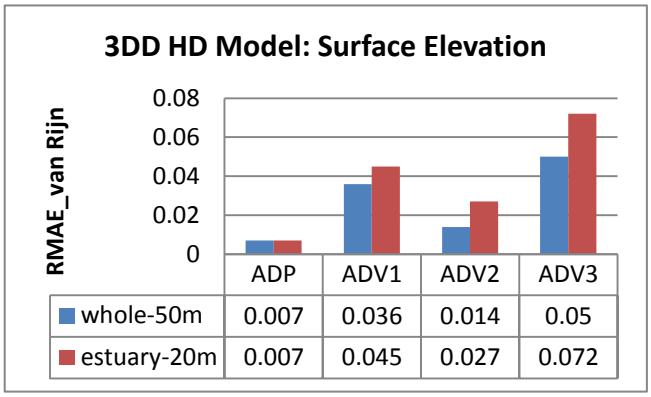

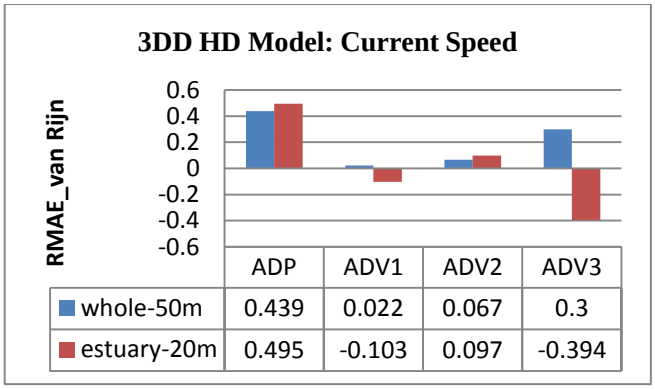

Figure 4-22 Comparison of statistics qualification of the calculated surface elevation and the current speed between the 'estuary-20m' and 'whole-50m' 3DD models.

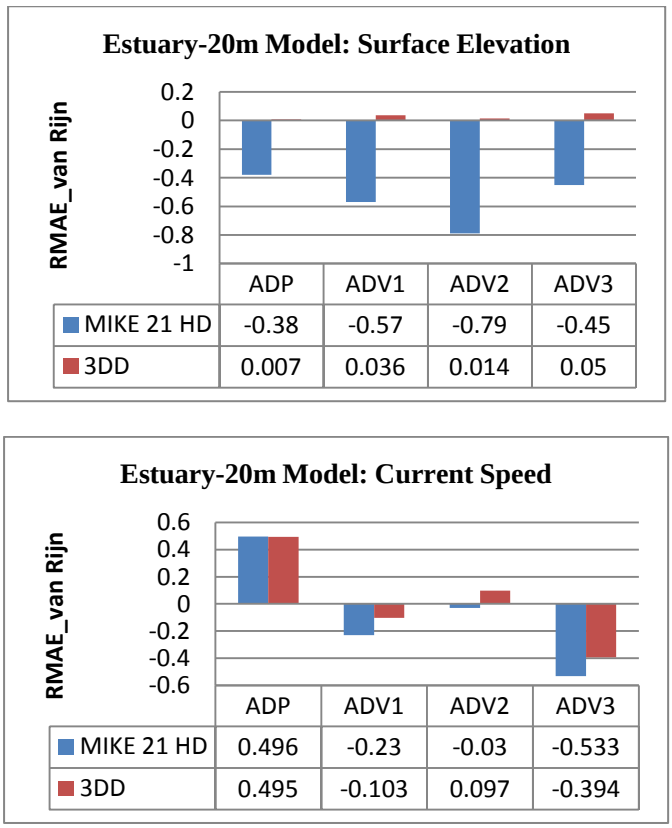

Figure 4-23 The Van Rijn's RMAE values of the calculated surface elevation and current speed between the 'estuary-20m' MIKE 21 HD model and 3DD Flow model.

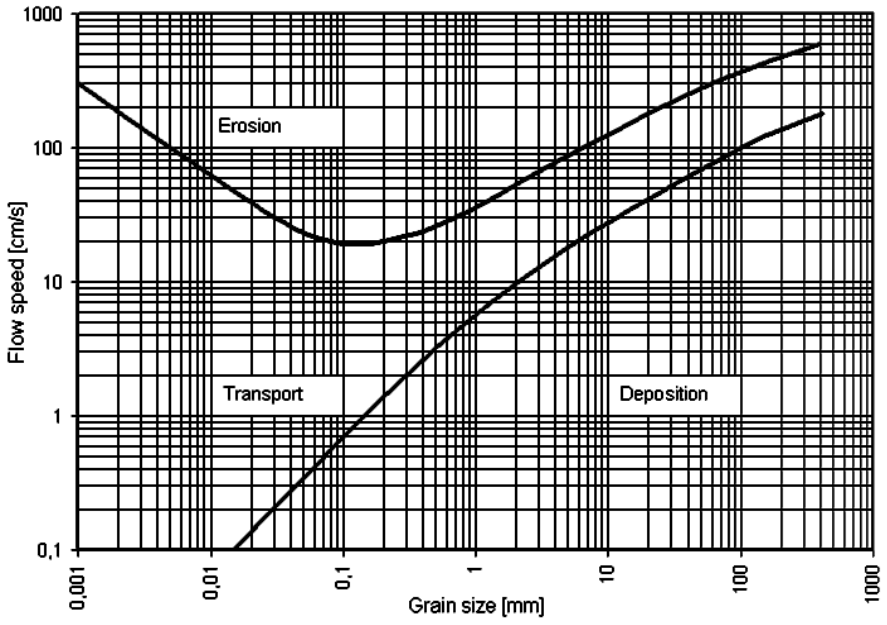

Figure 4-24 The Logarithmic HjulstrÖms diagram shows the relationship between the grain size, flow speed and sediment transportation (HjulstrÖms, 1935).

4.6 DISCUSSION AND CONCLUSIONS

Tairua Estuary hydrodynamic numerical models with 50 m and 20 m grid size were developed. According to the statistics qualification results based on Winter and Van Rijn's theory, the 'whole-50m' and the 'estuary-20m' MIKE 21 HD/ 3DD Flow models are all feasible for simulating the hydrodynamic behaviours at the Tairua estuary. The model with finer grids was more accurate than the coarser grid models because less information was lost. And also the grids used to extract the model results were closer to the coordinates the instrument deployed. The current speed at the location of the tidal inlet is not as good as the others. This might be because the model was run on a fixed bed, however, the hydrodynamics of the estuary will change the sediment layer thickness in reality, especially at the tidal inlet, it will result in a less accurate current speed. Both of the MIKE 21 HD and the 3DD flow modules are suitable for hydrodynamic modelling of Tairua Estuary.

The results of the 'whole-50m' and the 'estuary-20m' MIKE 21 HD model output and the 3DD Flow model output were extracted and displayed using the MIKE Zero Plot Composer toolbox. These model calculated surface elevation (Figure 4-9, 4-11, 4-13 and 4-15) and current speed (Figure 4-10, 4-12, 4-14 and 4-16) were presented and compared with the instruments data at the locations of the ADP (tidal inlet), ADV1 (the moorings), ADV2 (Tairua Wharf), ADV3 (Pauanui Waterway) and RBR (Tairua River mouth) every half hour from 27 July to 4 September, 2010 for calibrating qualitatively. Model statistics qualification results are presented in Table 4-7 to Table 4-10.

The 'whole-50m' and the 'estuary-20m' MIKE 21 HD and 3DD Flow models calculated the surface elevations from the tidal inlet to the Pauanui Waterway coincide well with the instruments data. The model calculated surface elevation at the Tairua River mouth (the RBR tide gauge) is smaller than the instruments data because river discharge recorded at the Broken Hill station which was without tidal influence was input as the western boundary in the models. The Broken Hill station is located approximately 11 km upstream of the model river boundary. In reality, the tributary streams and groundwater flowing into the river system between the Broken Hills and the Tairua Bridge likely result in higher river discharge at the Tairua River mouth in models.

Comparing the 'whole-50m' and the 'estuary-20m' tidal currents, the current speeds computed by the models are lower than the instruments data at the locations of the moorings and Tairua Wharf close to the intertidal flat and the tidal inlet at the lower Tairua Estuary. This is possibly caused by the higher friction parameters in the model used to improve model stability. However, the current speeds and directions computed by the 'estuary-20m' model with finer grid size coincide better with the instruments data than the 'whole-50m' model. The

statistics qualification results of the 'whole-50m' model and the 'estuary-20m' model also indicates that both of the 50 m and 20 m models are well-calibrated. However, the 'estuary-20m' model with finer grids is better than the 'whole-50m' coarser model because the coarser grids in the 'whole-50m' model lose some of the topography details when compared to the 'estuary-20m' model. It might be the case that the bathymetry is one of the most important factors influencing the hydrodynamics of the estuarine area.

Meanwhile, it also presents that the current speed at the location of ADP (tidal inlet) is not as good as the other sites according to the statistics qualification results. The maximum current speed is about 0.4-0.5 m s^{-1} and the minimum current speed is 0.1-0.2 m s^{-1} at the tidal inlet recorded by the ADP current meter. The mean size of the sediment at the tidal inlet is about 0.5-0.6 mm (Figure 2-5 and Figure 2-6). According to the HjulstrÖms curve (1935) which shows the relationship between the medium grain size of sediment and the critical velocity of sediment erosion, transportation or deposition (Figure 4-20), sediment at the bottom of the tidal inlet erodes with the maximum current speed and transported with the minimum current speed back and forth with the flood and ebb flow. However, the bathymetry does not change in the hydrodynamic modelling. This could be a reason of the current velocity difference between the model results and the instruments data.

Figure 4-21 shows the calculated RMAE value of the two models with different resolutions (50 m and 20 m) using the same software (MIKE) according to Van Rijn's theory, the lower the RMAE value, the better the model; and the computed value is within the error range of the measured value (RMAE=>0) if RMAE<0. It means the 'whole-50m' and the 'estuary-20m' MIKE 21 HD models are both 'excellent' from the mooring place through the Tairua Wharf to the Pauanui Waterway. According to Table 4-9 and 4-10, the RMAE values are less than 0.08; it means that the two models are 'excellent' in calculating the surface elevation. These results present that the 'estuary-20m' model is more accurate than the 'whole-50m' model possibly because the coarser grids lose more bathymetry information during calculations. The RMAE results of the models with same resolution (20 m) but different software modules (MIKE 21 HD and 3DD Flow) were compared in Figure 4-23. The surface elevations calculated by the two modules both coincide well with the instruments data. The current speed computed by the 3DD Flow model is better than the MIKE 21 HD model. Their similar results indicated that both of the MIKE 21 HD module and the 3DD flow module were feasible and trustable for calculating the surface elevation and current speed.

The finer the grid resolution, the longer time the model will run, and the higher risk of model crash. Therefore, the grid resolution was selected as 50 m for the study area including the outside ocean and estuary itself, 20 m for the area within

estuary and 10 m for the Paku Marina construction at the Paku Bay. As both of the MIKE and 3DD models with 50 m and 20 m grid resolutions were calibrated, the models calculated results were compared and the results indicated there is not very much difference between the models, which support my idea that the relative finer grids will not change the model results, therefore, the conclusions in this thesis.

The software of MIKE and 3DD also has their own abilities. Both of MIKE and 3DD modules calculated the depth averaged results, however, MIKE takes less calculating time than 3DD; MIKE is less accurate in calculating along the curved river than 3DD; it is more feasible to nest boundaries from coarse model to fine model using 3DD than MIKE; some of the modules of 3DD have not been well calibrated; MIKE supplies a better and logical man-machine communication frontend. Therefore, both of the MIKE and 3DD were used for this study for their different abilities.

PART III. RESULTS AND DISCUSSIONS

CHAPTER FIVE
HYDRODYANMICS AND SEDIMENT TRANSPORT FEATURES OF TAIRUA ESTUARY

This chapter discusses the hydrodynamics and sediment transport patterns within Tairua Estuary based on both field observations and calibrated hydrodynamic model results. The tides (dominance, tidal asymmetry and propagations) and the tidal currents (max./min. current speed, residual currents) were studied using the method of harmonic analysis. The results updated the physical parameters of Tairua Estuary. The critical sediment movement and settling velocities were calculated and mapped within Tairua Estuary and compared with the maximum and minimum current speed to investigate the sediment erosion, deposition and transportation patterns. The study found that the main factors influencing the estuarine sediment transport pattern include the river flow, sediment characteristics, current velocity distribution and variation during tidal cycle, wind waves and swell. The simulation results of the residual current speed and residual circulation pattern revealed that Tairua Estuary is dominated by ebb tides, sediment is being transported out of the estuary at present situation, portions of it deposits at the ebb delta, and portions of sediment is taken back into the estuary together with eroded sediment from the Pauanui Beach.

5.1 INTRODUCTION

Estuaries are governed by tidal flow from the sea and river discharge from rivers. Estuaries cannot be considered in isolation. The entire estuarine system has many inter-dependent parts such as the movement of water under the action of tides and river discharge entering an estuary. River discharge is closely inter-related with the movement of sediment within an estuary. Both the water and sediment movements are affected by wave action and tidal currents occurring in the outside ocean (McDowell and O´Connor, 1977).

Hydrodynamic analysis of an estuarine system helps better understand the factors that influence estuarine circulation. The estuarine circulation pattern is important in determining sediment movement. Fine grained materials move in suspension and tend to follow residual water flows. Deposition and re-erosion can occur around the time of slack water. Coarser grained material tends to travel along the sea bed where it is affected by high velocities and moves in the direction of the maximum current (Postma, 1967).

Knowledge of sediment transport is most often used to predict when and where erosion or deposition will occur, the likely magnitude of erosion or deposition, and the time and distance over which it will occur. Understanding the hydrodynamics and transport process in coastal water bodies is very important in the design, construction and maintenance of various structures such as ports, harbours, jetties etc. and the protection of these water bodies against environmental degradation (Rldho et al., 2005).

This chapter discussed the characteristics of tidal flows, river discharge, residual circulations and sediment transport using the methods of harmonic analyses, theoretical calculation and numerical modelling, for better understand the hydrodynamic and sediment transport features of Tairua estuary, which are the basis for the discussion about the impacts of relative sea level rise (SLR), seiche and marina construction on hydrodynamic and sediment transport characteristics, and also the oil spill trajectory.

5.2 METHODS

5.2.1 Harmonic Analyses

The tide-generated force can be expressed as a series of harmonic components. The tide harmonic analyses are the transformation of the observed tides from the time domain to the frequency domain.

The amplitude and the phase of the principal harmonic components M2, S2, N2, K1, O1 and M4 tidal elevations and tidal currents at the Tairua Estuary were calculated on the basis of the model outputs, using the tides analyses tool on Foreman (1977) IOS method in the MIKE 21 Toolbox.

The calculated results were plotted and attached in Appendix VI. The magnitude of the harmonic components was extracted at the locations of the field deployed instruments including the ADP at the tidal inlet, ADV1 at the moorings close to the tidal inlet, ADV2 in front of the Tairua Wharf, ADV3 at the entrance of the Pauanui Waterway and the RBR at the Tairua River mouth (Table 5-1 and Table 5-2).

Table 5-1 Principal harmonic components of tidal level at Tairua Estuary

Components	Darwin Symbol	Amplitude (m)				
		ADP	ADV1	ADV2	ADV3	RBR
Principal Lunar	M2	0.723	0.656	0.641	0.602	0.191
Principal Solar	S2	0.087	0.070	0.067	0.060	0.030
Larger lunar elliptic	N2	0.175	0.148	0.142	0.127	0.033
Luni-solar diurnal	K1	0.075	0.068	0.068	0.062	0.067
Principal lunar diurnal	O1	0.022	0.018	0.018	0.018	0.095
Shallow water overtides of principal lunar	M4	0.004	0.015	0.014	0.017	0.083

Table 5-2 Principal harmonic components of tidal currents at Tairua Estuary

Components	Darwin Symbol	Major currents (m s^{-1})				
		ADP	ADV1	ADV2	ADV3	RBR
Principal Lunar	M2	0.484	0.554	0.513	0.216	0.048
Principal Solar	S2	0.055	0.053	0.048	0.018	0.007
Larger lunar elliptic	N2	0.106	0.114	0.104	0.043	0.004
Luni-solar diurnal	K1	0.023	0.025	0.024	0.011	0.008
Principal lunar diurnal	O1	0.004	0.007	0.009	0.005	0.015
Shallow water overtides of principal lunar	M4	0.093	0.064	0.045	0.047	0.013

5.2.2 Theoretical Calculations for Sediment Transport

The threshold current speed of sand bed motions and critical settling velocity of suspended sediment was calculated using the tools of MATLAB based on the theory of Soulsby (1997).

5.2.2.1 *Threshold Current Speed of Sand Bed Motions*

For very slow flow over a sand bed, the sand remains immobile. The threshold (or initiation) of motion or incipient motion is defined as a velocity at which a few grains begin to move (Soulsby, 1997).

Van Rijn (1984) gives the formulae of the threshold depth-averaged speed $\overline{U}_{cr}$ required to move a grain of diameter d on a flat, horizontal, un-rippled bed in

water of depth h for a steady current. These formulae are valid for fresh water at 15℃, ρ_s=2650 kg m^{-3} and g=9.81 m s^{-2}.

$$\overline{U}_{cr} = 0.19(d_{50})^{0.1}\log_{10}(4h/d_{90}) \quad \text{for } 100 \leq d_{50} \leq 500\ \mu m \tag{5-1}$$

$$\overline{U}_{cr} = 8.5(d_{50})^{0.6}\log_{10}(4h/d_{90}) \quad \text{for } 500 \leq d_{50} \leq 2000\ \mu m \tag{5-2}$$

Soulsby (1997) combined the threshold bed shear-stress formula Whitehouse (1997) with the bed friction law by Soulsby (1997) to get the threshold current speed equation 5-3, with any non-cohesive sediment and water conditions for which D_*>0.1 and is valid in any units.

$$\overline{U}_{cr} = 7(\frac{h}{d_{50}})^{1/7}[g(s-1)d_{50}f(D_*)]^{1/2} \tag{5-3}$$

With

$$f(D_*) = \frac{0.3}{1+1.2D_*} + 0.055[1 - \exp(-0.020D_*)] \tag{5-4}$$

$$D_* = [\frac{g(s-1)}{v^2}]^{1/3}d_{50} \tag{5-5}$$

Where, d_{50} is median grain size; h is water depth; d_{90} is grain diameter for which 90% of the grains by mass is finer; D_* is dimensionless grain size; $s = \rho_s/\rho$ is the ratio of densities of grain and water (grain density ρ_s=2650 kg m^{-3} and water density ρ=1027 kg m^{-3}; v is kinematic viscosity, $v = 1.36 \times 10^{-6}$ m^2 s^{-1} for fresh water at 15℃.

5.2.2.2 *Critical Settling Velocity of Suspended Sediment*

For current speeds or wave conditions significantly above the threshold of motion, sand is entrained off the sea bed and into suspension, where it is carried at the same speed as the current. Their settling velocity of the suspended sediment must be smaller than the upward turbulent component of current velocity to remain grains in suspension, which is related to bed friction velocity. The settling velocity of sand in water is determined by its diameter, density and the water viscosity (Soulsby, 1997). There are a number of scientists who contributed to the formulae to calculate the sand settling velocity in water, e.g., Gibbs et al. (1971) for spherical sand, Hallermeier (1981) and Van Rijn (1984) for natural sand.

Soulsby (1997) derived the formula for natural sands, based on optimizing two coefficients in a combined viscous plus bluff-body drag law against data for irregular grains.

$$w_s = \frac{v}{d}[(10.36^2 + 1.049D_*^3)^{\frac{1}{2}} - 10.36] \tag{5-6}$$

Soulsby (1997) compared the five formulae using Hallermeier collated and tabulated data. The results show that the Soulsby formula (Equation 5-6) gave the best results, and is also the simplest. In this research, the sand settling velocities were calculated and mapped using Soulsby formula.

5.2.3 Numerical Modelling

Three different grid resolution (50 m, 20 m and 10 m grid size) depth-averaged hydrodynamic models were developed with tidal/non-tidal boundaries (Chapter Four). These well-calibrated models were used to investigate the hydrodynamics of Tairua Estuary together with the field observed data.

5.3 RESULTS AND DISCUSSION

5.3.1 Tides

5.3.1.1 *Tidal Elevations*

Tides are the rise and fall of sea level caused by the gravitational forces exerted by the moon and sun combined with the rotation of the Earth. The time and amplitude of the tides are influenced by the position of the sun and moon relative to the earth, by the amphidromic systems of the oceans, and by the shape of the coastline and near-shore bathymetry. Tairua Estuary experiences two high and two uneven low tides every day. This is referred to as a semi-diurnal tide (Figure 5-1).

Figure 5-1 shows the tidal elevation (black) and tidal currents (blue) during spring and neap tides recorded by the ADP current meter deployed at the tidal inlet in August, 2010. For spring tides (Figure 5-1a), the min. surface elevation is -1.018 m (lowest low water) and the maximum surface elevation is 1.132 m (highest high water), the mean surface elevation is 0.020 m. On neap tides (Figure 5-1b), the min. surface elevation is -0.588 m (lowest low water) and the maximum surface elevation is 0.649 m (highest high water), the mean surface elevation is -0.013 m. The data are not corrected for atmospheric pressure, which contribute to the changes in mean sea level.

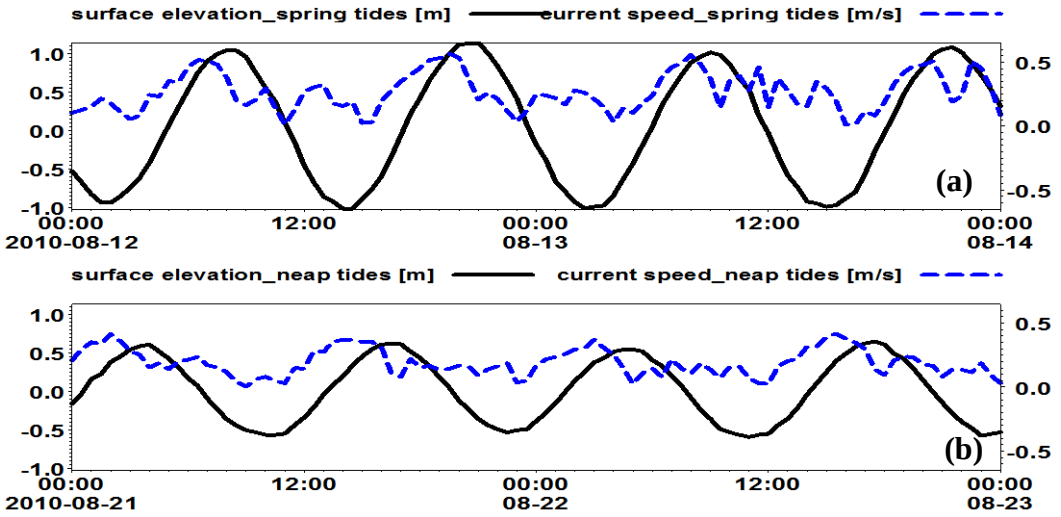

Figure 5-1 Observed surface elevations (black solid) and current speed (blue dot) during spring and neap tides in August, 2010.

5.3.1.2 *Tidal Range*

Tidal range is the difference between consecutive high and low water in a tidal cycle. It is called macro-tidal when the tidal range is greater than 4 m, and micro-tidal when it is less than 2 m. Intermediate ranges are termed meso-tidal (Masselink and Short, 1993). The height of the tides for the High Water Spring (HWS), Low Water Spring (LWS), High Water Neap (HWN), and Low Water Neap (LWN) were extracted at the instrument locations at the lower Tairua Estuary based on the calibrated 'estuary_20m' hydrodynamic model (Table 5-3). During spring tides, the maximum tidal range is approximately 2.02 m at the tidal inlet. It decreases from the tidal inlet to 1.68 m at the Pauanui Waterway. During neap tides, the maximum tidal range is 1.17 m at the tidal inlet and decreases to 1.08 m at the Pauanui Waterway. The tidal ranges are all equal to or less than 2 m. Therefore, Tairua Estuary is a micro-tidal estuary.

As a result of the relatively small variation in the water depth, the tidal wave undergoes more distortion during the spring tides (Figure 5-2a) than during the neap tides (Figure 5-2b).

Table 5-3 Average tidal magnitude on spring and neap tides

	Tide Magnitude (m)			
	HWS	**LWS**	**HWN**	**LWN**
Tidal Inlet (ADP)	1.00	-1.02	0.60	-0.57
Moorings (ADV1)	1.00	-0.8	0.60	-0.54
Tairua Wharf (ADV2)	1.00	-0.76	0.61	-0.52
Pauanui Waterway (ADV3)	0.98	-0.70	0.59	-0.49

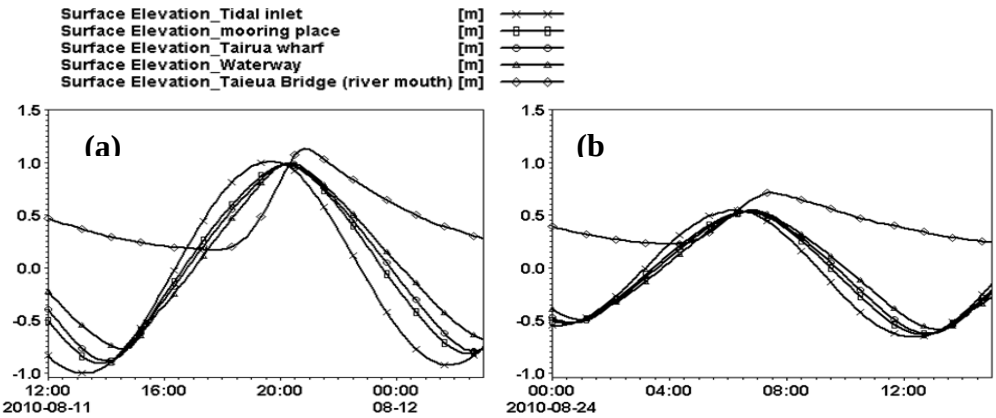

Figure 5-2 Observed surface elevations from the tidal inlet to the river mouth in Tairua Estuary during the (a) spring tides and (b) neap tides.

5.3.1.3 *Semi-diurnal/Diurnal Tides Dominance*

Figure 5-1 shows the tidal elevation (black) and tidal currents (blue) during spring and neap tides recorded by the ADP current meter deployed at the tidal inlet in August, 2010. For spring tides (Figure 5-2a), the min. surface elevation is -1.018 m (lowest low water) and the maximum surface elevation is 1.132 m (highest high water), the mean surface elevation is 0.020 m. On neap tides (Figure 5-2b), the min. surface elevation is -0.588 m (lowest low water) and the maximum surface elevation is 0.649 m (highest high water), the mean surface elevation is -0.013 m. The data are not corrected for atmospheric pressure which contribute to the changes in mean sea level.

Tairua Estuary experiences two high and two uneven low tides every day (Figure 5-1). Therefore, Tairua Estuary is an estuary with semi-diurnal tides.

The dominance of the semi-diurnal or the diurnal tides at any locality can be estimated from the ratio (equation 5-7) of the major local constituents (K_1, O_1, M_2, S_2) without considering the effects of the shallow water (Macmillan, 1966; Neuman and Pierson, 1966; Defant, 1961).

$$F = \frac{K_1 + O_1}{M_2 + S_2} \qquad (5\text{-}7)$$

According to the equation 5-7, the semi-diurnal influences increase as this ratio decreases, and are dominant when it is less than unity. The ratio F is calculated as 0.58 at the tidal inlet, 0.57 at the moorings, 0.50 at the Tairua Wharf, 0.89 at the Pauanui Waterway, and 2.64 at the mouth of the Tairua River using the data listed in the Table 5-1. The results indicate that Tairua Estuary is dominated by semi-diurnal tides in the lower reaches of the estuary with a significant diurnal effect at the river mouth.

Figure 5-3a shows the instruments ADP observed surface elevations at the tidal inlet of Tairua Estuary during the August, 2010. It presents two high tides and two low tides in one day, two spring tides and two neap tides in one month. The tidal ranges are different with spring flood tides, spring ebb tides, neap flood tides and neap ebb tides. Figure 5-3b is the daily observed tides at NIWA's station during the whole year of 2010. It shows that the height of the two spring tides each month is different. During the whole year, it also has one maximum spring tide and one minimum neap tide as a result of the inclination of the plane of rotation of the moon round the earth. Therefore, tides at the coastal area of Tairua Estuary are mixed semi-diurnal tides.

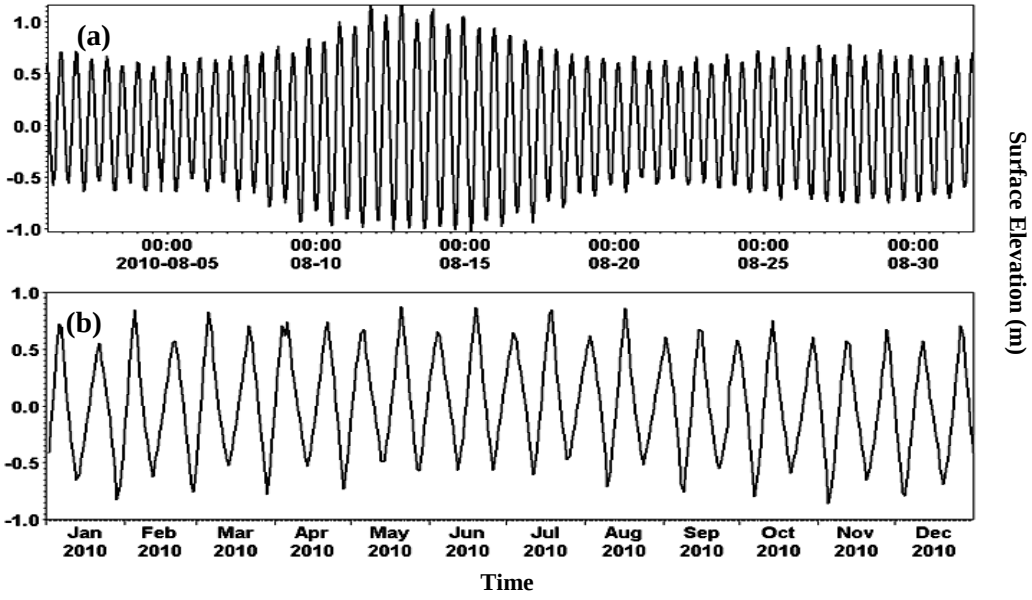

Figure 5-3 Tides at the Tairua tidal inlet observed by (a) ADP every 0.5 hr. from 1 August, 2010 to 1 September, 2010; (b) from NIWA's station daily during 2010.

5.3.1.4 *Flood/Ebb Tide Dominance*

The mutual interference of different tidal constituents can give rise to tidal asymmetry. The case where the time to high water is advanced and the time to low water is delayed, is referred to as 'flood dominant' because the maximum velocity is greater during the flood tide than in the ebbing tide. The opposite of this is referred to as being ebb dominant. The flood/ebb tidal dominance plays a pivotal role in estuarine sediment transport (Aubrey & Speer, 1985; Brown and Davies, 2010) because when the bed shear stress for mobility is exceeded, the dimensionless transport of sand is a function of current speed or shear velocity (Ackers and White, 1973). Thus, the long-term estuaries stability depends on the small differences in the ebb and flood current speeds which can result in significant implications for the net transport of sand (Kang and Jun, 2003). M_2 and M_4 tides at the lower reach of estuary are the main constituents determining the flood/ebb tidal dominance. The amplitudes of M_2 and M_4 tides are influenced

by the physical properties of the estuary such as width, depth, roughness and the extent of tidal flats (Kang and Jun, 2003). The relative phase of a semi-diurnal tide such as M_2 and S_2 and a shallow water tide such as M_4 and MS_4 determines flood/ebb tidal dominance. The M_2-M_4 tidal interactions could possibly determine the tidal dominance (Boon and Byrne, 1981; Speer and Aubrey, 1985).

Kang and Jun (2003) developed the ebbing time equation as

$$t_l - t_h = \frac{\pi - 2\varphi'}{\omega_2} = (\pi + 4\varepsilon \cdot sin\sigma')\omega_2 \quad (5\text{-}8)$$

Where, t_l is the time to low water; t_h is the time to high water; φ is the ellipse phase; σ' is the relative phase, $\sigma' = 2\varphi_2 - \varphi_4$; ε is the amplitude ratio between semi-diurnal and quarter-diurnal constituents, $\varepsilon = A_4/A_2$, A is the semi-major magnitude; ω_2 is the frequency of semi-diurnal tidal constituent; therefore the flood/ebb dominance depends on the sign of $\sin\sigma'$ in case of tidal water level and $\cos\sigma'$ in case of tidal current.

The ebbing time at the locations from the Tairua tidal inlet to the Tairua River mouth was calculated based on the field data collected 1 m above the water bed using Equation 5-8. The results were listed in Table 5-4, which present a decreasing trend of M2 amplitude landward. However, the M4 amplitude increases at the river mouth. Tairua Estuary is ebb dominated with ebbing time more than 6.21 hr except for the location in front of the Pauanui Waterway channel (ADV3). The residual currents were calculated over 28 days from the depth-averaged, tides, river and wind forced 'estuary_20m' HD model and plotted in Figure 5-7, which also indicates that Tairua Estuary is dominated by ebb tides.

Table 5-4 Computed ebbing time at the locations of the deployed instruments

Station	A_2	A_4	Amp. Ratio	φ_2	φ_4	Relative Phases (°)	Ebbing Time (hr)
ADP	0.723	0.004	0.006	187.55	77.02	298.08	6.23
ADV1	0.656	0.015	0.023	200.52	198.22	202.82	6.39
ADV2	0.641	0.014	0.022	205.13	232.43	177.83	6.37
ADV3	0.602	0.017	0.028	212.27	331.54	93.00	6.00
RBR	0.191	0.083	0.435	259.40	101.08	57.72	9.38

5.3.1.5 *Tidal Propagations*

The phase of M_2 and K_1 tidal currents compared with the phase of tidal elevations at the stations from the tidal inlet to the river mouth are listed in Table 5-5. At the tidal inlet (ADP), the phase differences are 62° and 70° for M_2 and K_1 constituents, respectively, with the tides leading the tidal currents. At the moorings, the phase

differences are 110° and 110°. While the phase differences are 91° and 91° for M_2 and K_1 constituents at the Tairua River mouth, respectively.

Table 5-5 Phase difference of M2 and K1 tidal currents and tidal elevations

Stations	Tidal Elevation		Tidal currents Speed	
	M2 Phase	K1 phase	M2 Phase	K1 phase
Tidal Inlet (ADP)	187.54	191.81	125.87	121.97
Moorings (ADV1)	200.52	199.43	310.82	309.36
Tairua Wharf (ADV2)	205.13	201.85	314.35	313.93
Pauanui Waterway (ADV3)	212.27	205.61	322.72	326.79
River Mouth (RBR)	259.40	169.69	167.93	78.48

Figure 5-4 shows the tidal elevations at the locations of the tidal inlet, moorings, Tairua Wharf, Pauanui Waterway and Tairua River mouth on spring (Figure 5-4a) and neap tides (Figure 5-4b). The figures show that the mean value of the tidal elevation is about 0 m (MSL) at the tidal inlet. It is higher at the stations further inland within an estuary because the peak ebb elevation is smaller than the peak flood elevation (the rectangular area in Figure 5-4) and it results in the mean surface elevation higher than mean 0 m. This increase is higher during the spring tides than during the neap tides, especially at the Tairua River mouth (red dot line to blue dot line). Evidently, more water can accumulate in the upper part of Tairua Estuary during the spring tidal cycle. It causes an increase of salinity and net sediment movement landward during spring tides, and net seaward sediment movement during neap tides.

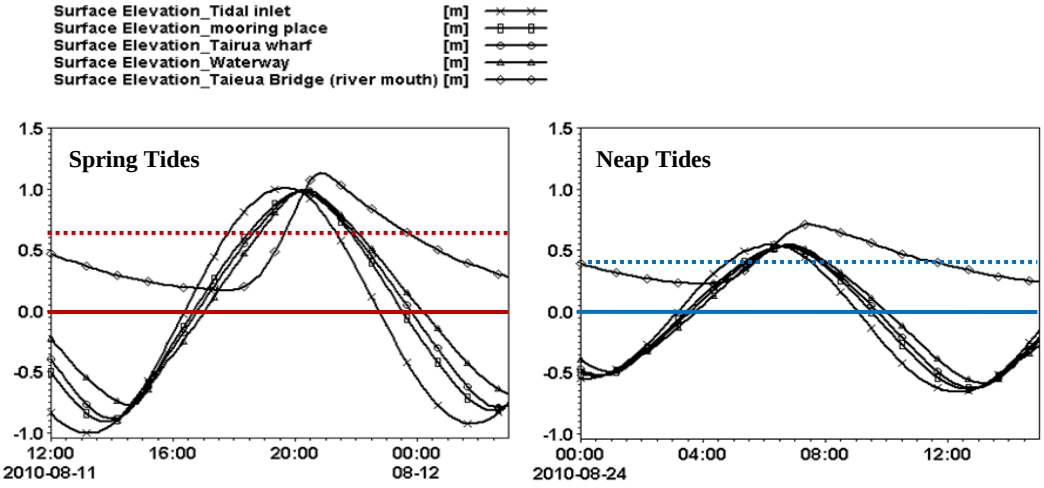

Figure 5-4 Mean tidal level at the tidal inlet (solid line) and Tairua River mouth (dot line) on a) spring tides, and b) neap tides. The results were calculated on the basis of the surface elevations from Tairua tidal inlet to the mouth of Tairua River (black solid curves with marks).

5.3.1.6 *Current Speed at the Tairua Tidal Inlet*

Figure 5-1 shows the current speed during spring and neap tides recorded by the ADP current meter deployed at the tidal inlet during August of 2010 for spring tides (Figure 5-1a), the minimum current speed is 0.011 m s^{-1} at the mid ebb flow and the maximum current speed is 0.568 m s^{-1} at the mid flood tides, the mean current velocity is 0.267 m s^{-1}. On neap tides (Figure 5-1b), the minimum current speed is 0.005 m s^{-1} at the mid ebb flow and the maximum current speed is 0.417 m s^{-1} at the mid flood tides, the mean current velocity is 0.192 m s^{-1}.

5.3.1.7 *Maximum and Minimum Current Speed*

The maximum current speed occurs halfway through the tidal cycle i.e. mid tide and the minimum current speed occurs at high and low water. The maximum current speed at spring tide can be estimated by $(M_2 + S_2) + (K_1 + O_1)$, where the four major harmonics are assumed to be in phase. The maximum current speed at neap tides is estimated to be not less than $(M_2 - S_2) + (O_1 - K_1)$ where the four major harmonics were assumed to be out of phase at the same time (Cheng and Gartner, 1985). The estimated and observed maximum current and minimum current at each of the stations along Tairua Estuary are listed in Table 5-6. The estimated maximum and minimum currents were calculated on the basis of the harmonic components of tidal current. The estimated and the observed current speed is close to each other.

Table 5-6 Estimated and observed tidal currents on spring and neap tides

Station	Estimated Current Speed		Observed Current Speed	
	Max. spring current (m s^{-1})	Min. neap current (m s^{-1})	Max. spring current (m s^{-1})	Min. neap current (m s^{-1})
Tidal Inlet	0.566	0.410	0.623	0.407
Moorings	0.639	0.483	0.716	0.428
Tairua Wharf	0.594	0.450	0.619	0.383
Pauanui Waterway	0.250	0.192	0.241	0.174

The maximum and minimum current speed for spring tides were calculated using the MIKE Zero toolbox ‘statistics’ for the ‘estuary_20m’ HD model output and are plotted in Figure 5-6. The maximum current speed occurs mainly along the main estuary channel during the ebb tide, and can reach 0.4-0.6 m s^{-1} at the tidal inlet, the Pepe Stream, the Grahams Stream entrance and the northern corner of Paku Hill close to Tairua Beach. The minimum current speed is approximately 0-0.1 m s^{-1} along the main channel during the flood tide.

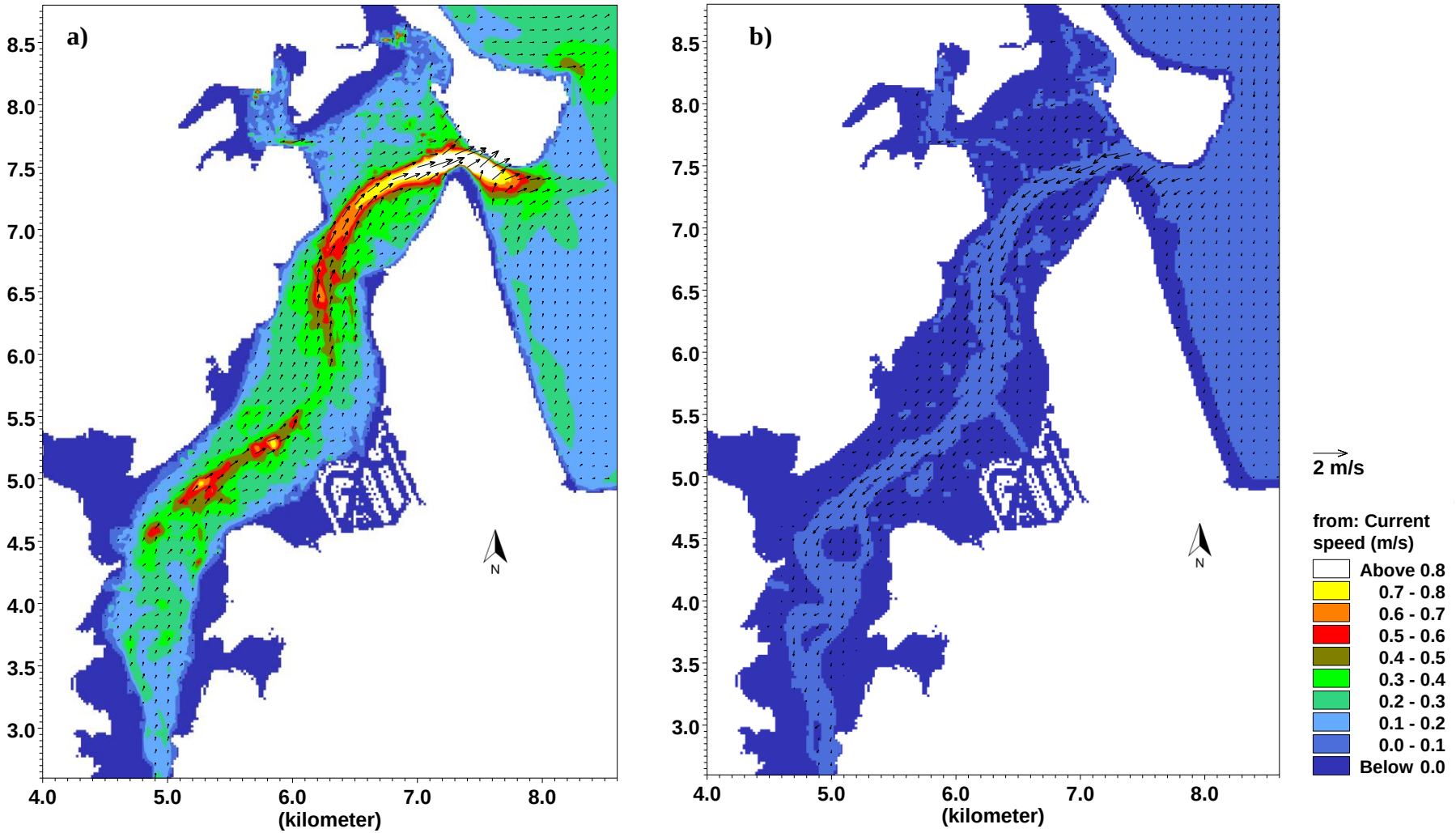

Figure 5-5 a) Maximum and b) minimum current speed for spring tides.

5.3.1.8 ***Residual Currents***

The tide-induced residual currents are defined as the flow that is caused by the non-linearity of tidal currents in relation to horizontal boundary geometry and bottom topography. Although the classical two-layered estuarine flow driven by the combination of the seaward sloping sea surface and the upstream or riverward longitudinal density gradient is the most frequent model of residual flow, other components primarily those driven by the near and far field winds are major contributors at times (Carter, 1988). For environmental management in coastal areas, the tidal residual currents are important because they are related to the long-term transport of sediment and nutrients in the water column and in the exchange of waters between different basins. The residual currents were calculated on the basis of the depth-averaged 'estuary_20m' HD model during the tidal cycles which occurred over 28 days (12.30am on 30 July, 2010 – 11.00am on 26 Aug. 2010) using the 'Statistics' method in the Mike Zero Toolbox.

The estuarine circulation pattern is important for determining sediment movement. Fine grained material moves in suspension and follows the residual water flow, though there may be deposition and re-erosion around about slack water. The coarser grained material travels along the bed and is affected most by high velocities and moves in the direction of the maximum current (Postma, 1967). The map of the residual currents at Tairua Estuary (Figure 5-6) shows that there is strong residual current flow along the main channel from the river mouth to the tidal inlet. To make the plot easier to be read, the residual currents at the zones of the lower estuary (Zone A), middle estuary (Zone B) and upper estuary (Zone C) were enlarged in Figures 5-7, 5-8 and 5-9. The strongest residual currents (0.6-0.65 m s^{-1}) could be found at the tidal inlet where the ebb jet forms the ebb tidal delta. A portion of the ebb flow returns between the Pauanui Beach and the ebb tidal delta, along with the Pauanui Beach flow into the tidal inlet and generate the shallow area shown in Figure 5-7. The photo of this shallow area between the head of the Pauanui spit and the ebb tidal delta was taken by Winter in 2013. A large eddy is also generated inside the estuary close to the tidal inlet where it forms the flood tidal delta. In the middle Tairua Estuary (Zone B), the residual currents are 0.2-0.25 m s^{-1} along the main channel. There is an eddy (0.1-0.2 m s^{-1}) close to Tairua Wharf and an eddy (0.2-0.4 m s^{-1}) close to the Pleasant Point resulted from the channel orientation change (About 40º). This result helps to explain the phenomena that more sediment deposits at this location. Zone C is located in the upper reach of Tairua Estuary. It connects the river mouth and the estuary's main channel. A relatively large amount of sediment from the river upstream tends to deposit in Zone C and results in comparatively shallow zone there. Zone C is also dominated by the ebb flow and has the highest residual currents of 0.1-0.15 m s^{-1}.

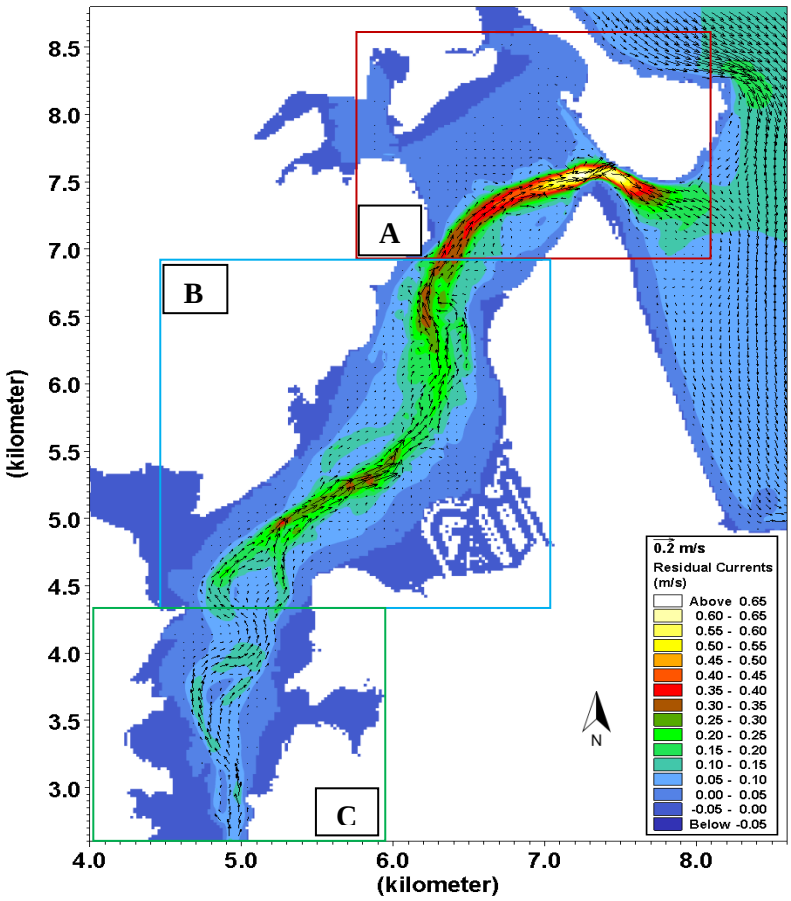

Figure 5-6 Residual currents calculated by 'estuary_20m' MIKE 21 HD model during 28 continuous days.

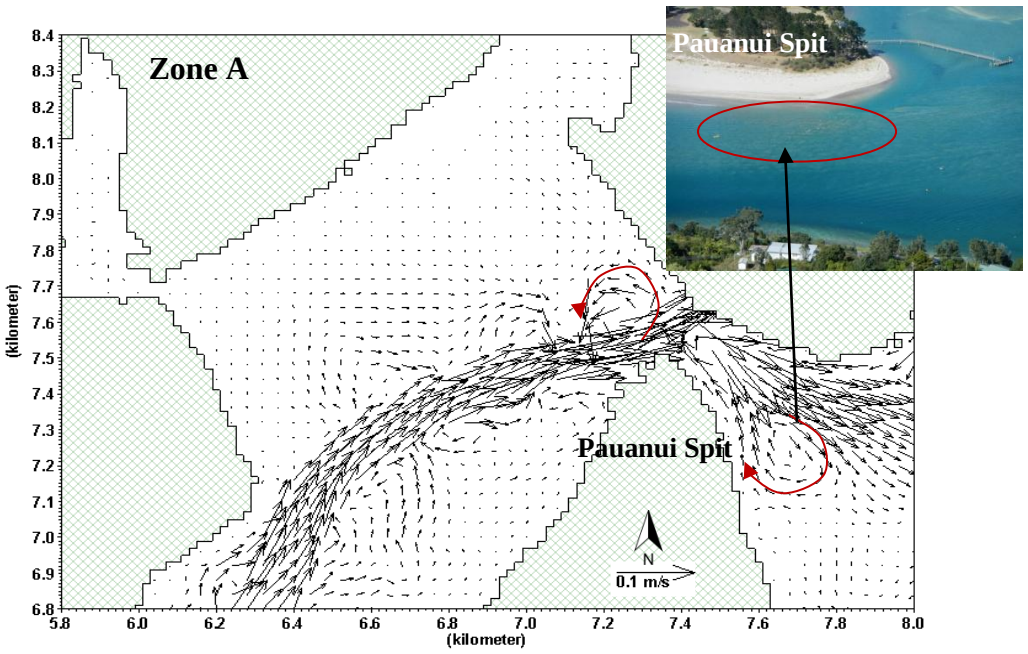

Figure 5-7 Residual currents calculated by 'estuary_20m' MIKE 21 HD model during 28 continuous days (Zone A in Figure 5-6). Red curve arrows showed the two eddies generated the flood delta and ebb delta. The colour picture was taken by Christian Winter in 2013.

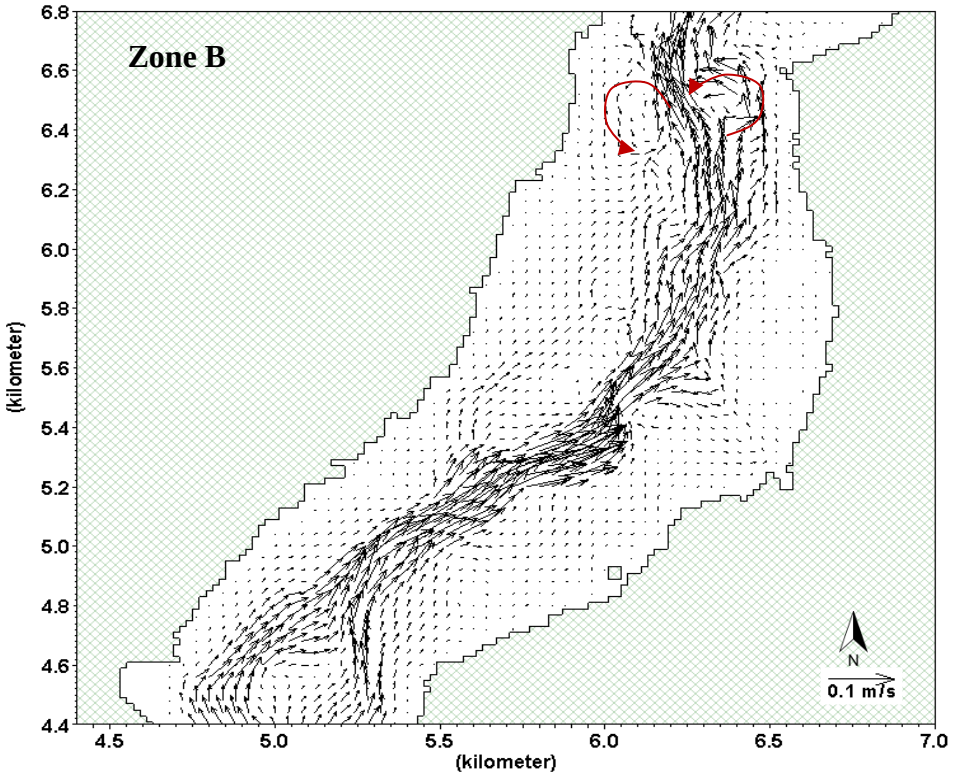

Figure 5-8 Residual currents calculated during 28 continuous days (Zone B in Figure 5-6). Red curve arrows showed the two eddies close to the Tairua Wharf resulting from the channel orientation change.

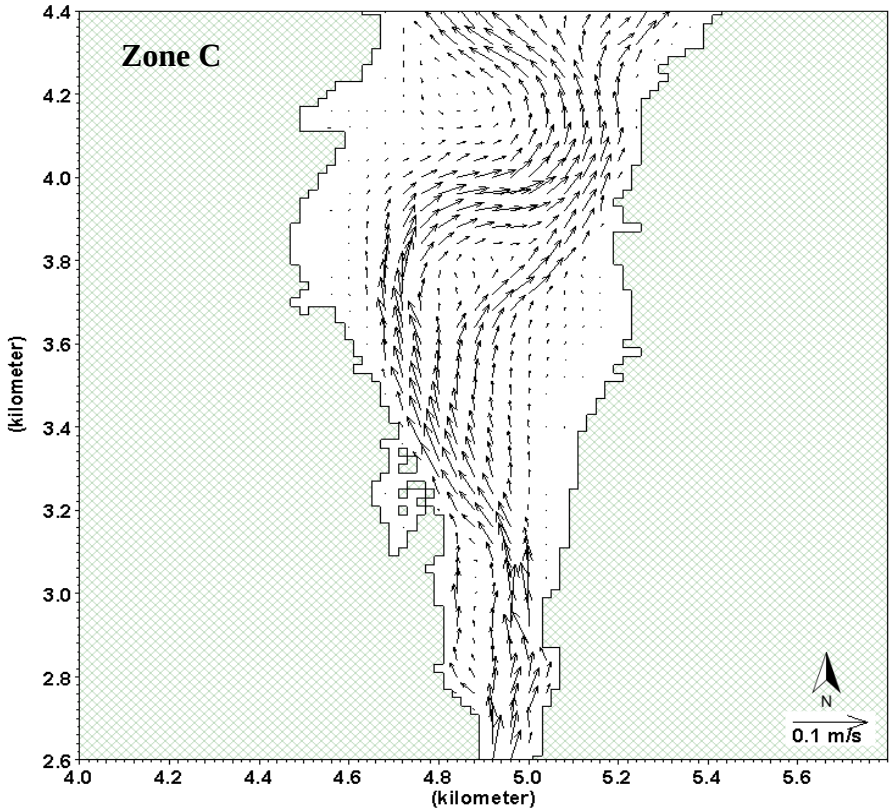

Figure 5-9 Residual currents calculated during 28 continuous days (Zone C in Figure 5-6).

5.3.2 River Freshwater Inflow

The Tairua River is located on the Coromandel Peninsula. It flows north and then northeast for a total of 35 km from its source in the Coromandel Range to the west of Whangamata, passing through the town of Kikuai before reaching the Pacific Ocean at Tairua on the Peninsula's east coast. Freshwater inflow enters Tairua Estuary mainly from the Tairua River, but additional inflow is provided by the tributary streams shown in Figure 5-10. Figure 5-11 is the time series and the annual mean river flow from the Tairua River, Pepe Stream and Graham Stream from 9.00am on 1 August, 1983 to 12.05pm on 1 March, 1985. The mean and maximum river level, flow of the three rivers and streams are listed in Table 5-7.

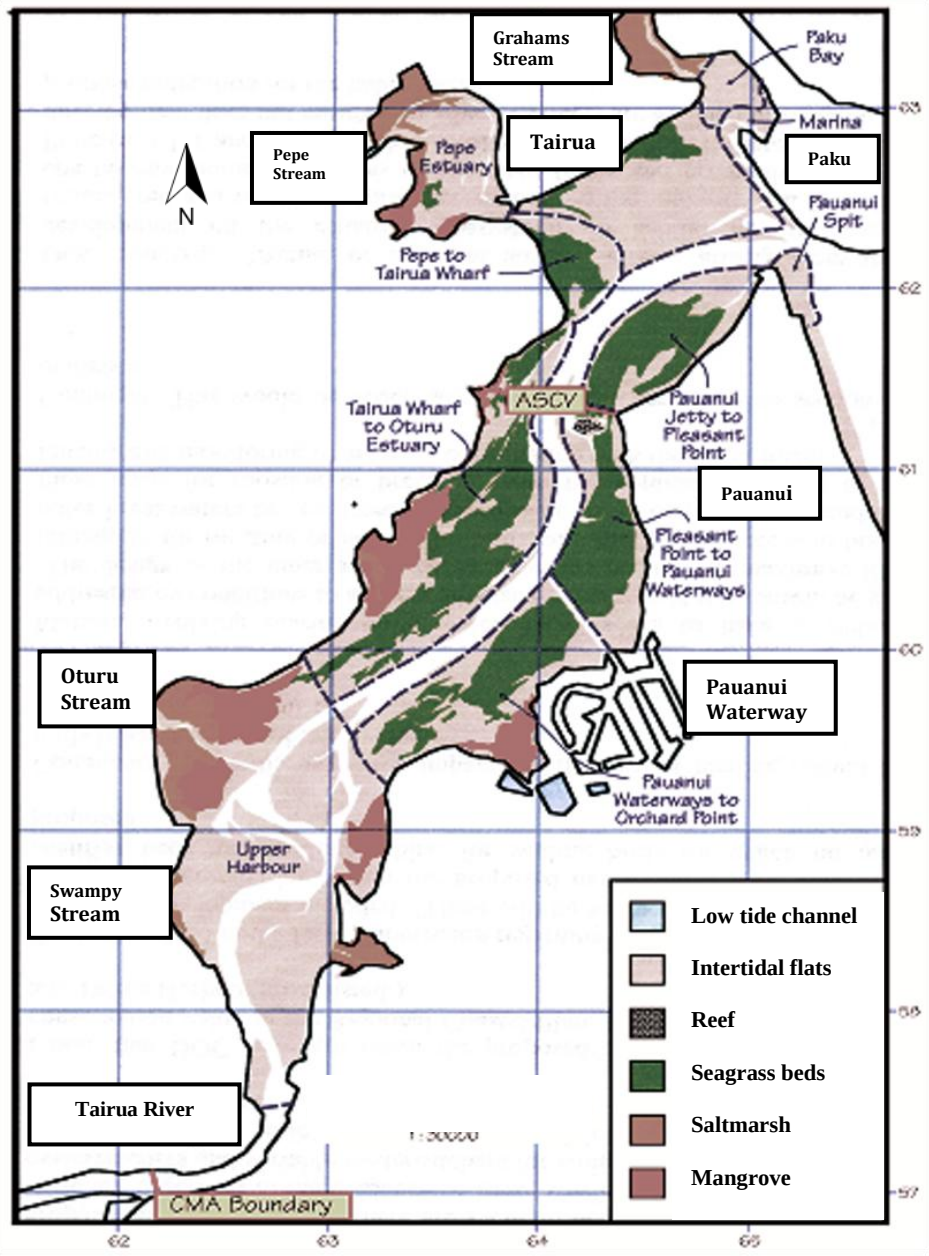

Figure 5-10 Tairua Estuary and the tributary streams that flow into the estuary (edited based on the plot from Waikato Regional Council).

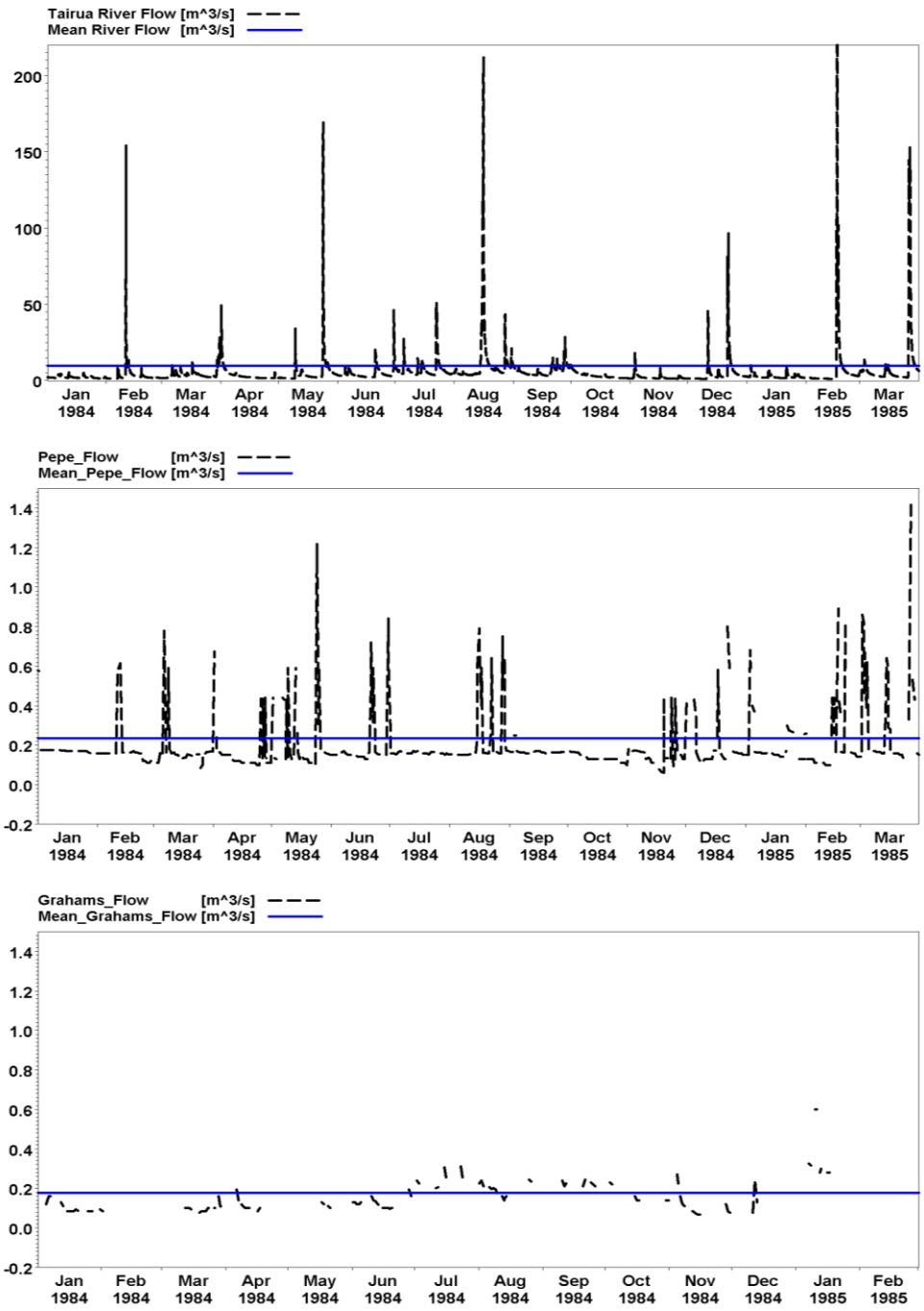

Figure 5-11 Time series (black dot line) and the annual mean value (blue solid line) of the river flow from the Tairua River, Pepe Stream and Graham River from 9.00am on 1 Aug., 1983 to 12.05pm on 1 March, 1985.

Table 5-7 Annual mean and maximum river level and discharge within Tairua Estuary

River	Mean Surface Elevation (m)	Max. Surface Elevation (m)	Mean River Flow (m^3/s)	Max. River Flow (m^3/s)
Tairua	-	-	9.7784	220
Pepe	0.52772	1.46	0.23346	1.46
Graham	0.25745	1.34	0.17698	0.75

Figure 5-12 is the river discharge (black solid line) recorded at the Broken Hills station operated by the Waikato Regional Council at the Tairua River mouth. There are no tides reaching the Broken Hills station. The annual average river discharge is 8 m^3 s^{-1} at Tairua Estuary (Hume and Gibb, 1987). During the first field campaign, three floods with heavy rainfall occurred at the Tairua River mouth. The flood, with about 42 m^3 s^{-1} freshwater flow, occurred on 4 August. The second flood occurred on 14 August, 2010 with a freshwater flow 86 m^3 s^{-1} and the third flood took place on 26 August, 2010 with a freshwater flow of 42 m^3 s^{-1}. The model calculated current speed at the river mouth is plotted as red dot in Figure 5-12. The plots indicate that the tides reach the Tairua River mouth where the RBR current meter deployed; the current speed at the Tairua River mouth increases with the floods. The current speed at the river mouth reaches 1 m s^{-1} with the large flood on 14 August, 2010.

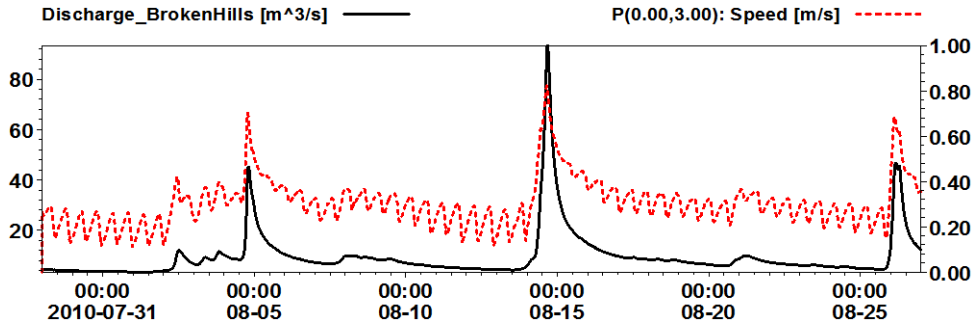

Figure 5-12 Freshwater discharged from the Broken Hill station (black solid) and the model calculated current speed at the Tairua River mouth (red dot).

The RBR current meter recorded water depth (black line) and the model calculated water depth (red line) are presented in Figure 5-13. The model calculated water depth is less than the instruments (RBR) recorded data. This might be due to the discharge from the tributaries between the Broken Hill station and the Tairua river mouth. The average tidal wave is 0.3 m at this location. The fluctuations during the ebb tides indicate the influence of the constriction caused by the river elbows and the shallow tidal flats within the estuary.

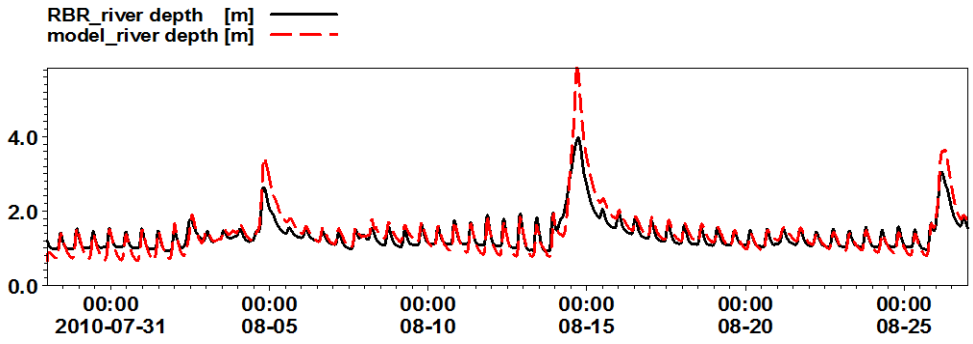

Figure 5-13 RBR recorded (black solid) and model calculated (red dot) water depth at the Tairua River Mouth (under the Tairua Bridge) during August 2010.

Major time delays of the tidal wave are evident at the river mouth region due to the propagation of the tide through the estuary. Figure 5-14 compares the surface elevation at the tidal inlet, Pauanui waterway and the river mouth. The peak of the tide has an average of 30 minutes delay and the trough of the tide has an average of 40 minutes delay between the tidal inlet and the Pauanui waterway in the lower reaches of Tairua Estuary. Further upstream the time delays increase relative to the ocean and the tidal asymmetry is also accentuated. The peak of the tide has an average 3 hours and 40 minutes delay and the trough of the tide has an average delay of 6 hours between the tidal inlet and the Tairua River mouth. This asymmetric tidal variation is typical of tidal estuaries (Aubrey and Speer, 1985), and may be due to the M_4 over tide. The higher the river discharge from the Tairua River mouth to the lower estuary, the smaller the tidal wave magnitude due to the higher energy of the freshwater input.

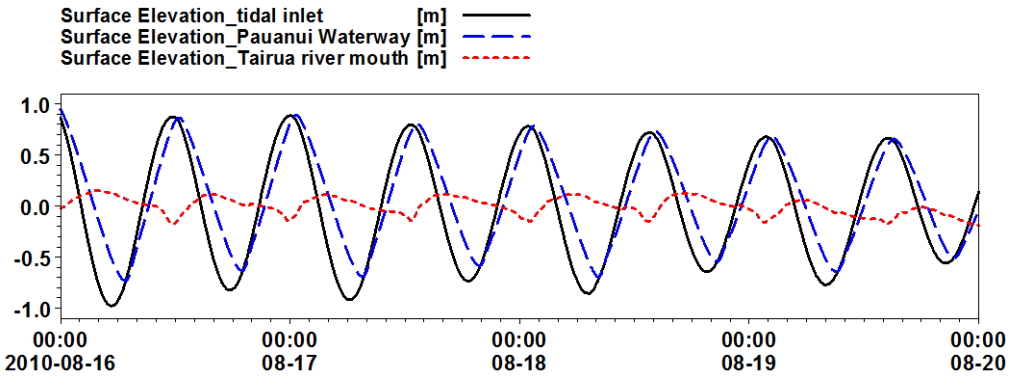

Figure 5-14 Surface elevations at the Tairua tidal inlet (black solid), Pauanui Waterway (blue dot) and the Tairua River mouth (red dot) of Tairua Estuary.

The RBR tide gauge recorded a heavy flood (86 m^3/s discharge) at the Tairua River mouth starting from 4.15pm on 14 August, 2010 (Figure 5-12 and Figure 5-13). Taking this heavy flood as the river boundary in modelling, the maximum current speed within Tairua Estuary was calculated and plotted in Figure 5-15. The results were compared with the maximum current speed for spring tides (Figure 5-5a). The maximum currents are lower with flood discharge (0.6-0.7 m s^{-1}) compared with the currents without a flood (more than 0.8 m s^{-1}). It is an evident that the tides spread from the ocean to the estuary inside and the high current speeds are along the main channel for spring tides (no floods). However, the tidal flow is pushed outside the estuary by the large discharge from the flood at the river mouth. This means that a freshwater flood from Tairua River mouth will reduce the energy of flooding tidal flow even for spring tides.

Figure 5-15 shows very high currents offshore Paku Hill. It is resulted from the model boundary limitation. However, this research is more focused on the inside estuary, and the model calculated current speed and tidal elevation coincide well

with the field collected data from tidal inlet to the river mouth, which support that the very high current speed shown in Figure 5-15 will not influence the research conclusions indeed.

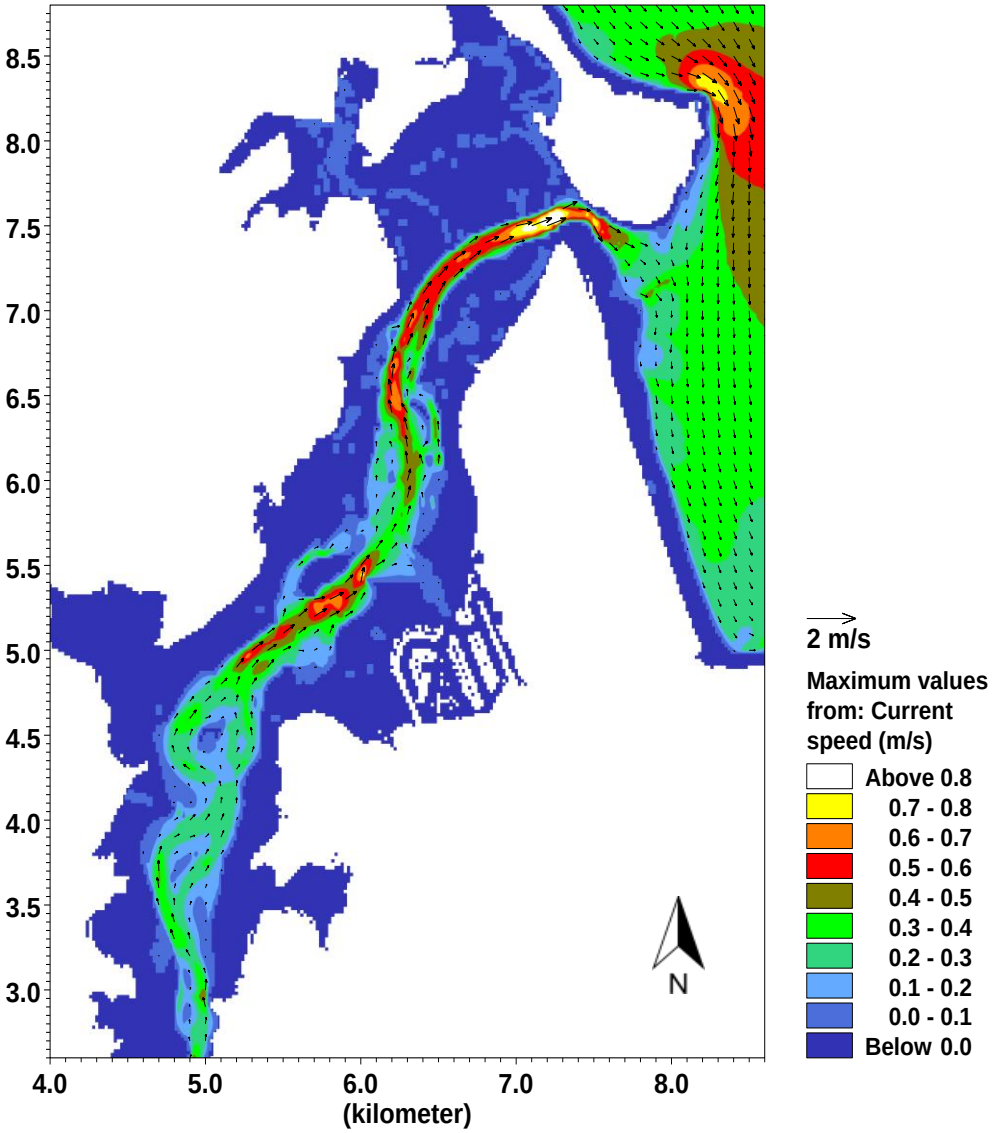

Figure 5-15 The maximum current speed during the large floods discharged from the Tairua River upstream at 4.15 pm on 14 August, 2010.

5.3.3 Sediment Transport

During the tidal cycle, the suspended sediment concentrations vary as erosion and deposition occur (Dyer, 1986). As introduced in Chapter 3, water samples were collected from the lower estuary, together with CTD casts at the estuary tidal inlet, the Tairua Wharf and the Pauanui Waterway on 8 June, 2011. The suspended sediment concentration (SSC) data were processed by drying and weighing the

samples. Figure 5-16 shows the suspended sediment concentration, tidal elevation and the current speed at the tidal inlet, the Tairua Wharf and the Pauanui Waterway at the lower reaches of Tairua Estuary on 8 June, 2011 (during the spring high river discharge period). The plots show that the SSC value increased with the current speed close to the estuary entrance. There is higher suspended sediment in front of the Tairua Wharf, than at the tidal inlet and the Pauanui Waterway. This means that the suspended sediment within Tairua Estuary close to the tidal inlet is mostly eroded from the water bottom rather than advection from the outside ocean. The high river discharge from the river mouth at approximately 2.00pm (Figure 5-16c) contributed fine sediment to the lower reach of the estuary, probably which was then distributed to the tidal inlet. The SSC value decreased from 27 mg l^{-1} at the Pauanui Waterway at 2.20pm (Figure 5-16c), to 11 mg l^{-1} in front of the Tairua Wharf (Figure 5-16b) at about 2.50pm, and 12 mg l^{-1} at the tidal inlet (Figure 5-16a) at about 3.00pm during the ebb tides.

As introduced in Chapter 2, the surficial sediment sampling was carried out between November 2009 and March 2010 by the Waikato Regional Council. In total 275 sites were sampled in Tairua Estuary, and sediment grain size analysis was carried out on 111 samples (Figure 2-5 and Figure 2-6). The median grain size (D50) in mm is mapped in Figure 5-17, and shows the median grain size distribution within Tairua Estuary as being mostly in the range of 0.2-0.4 mm. Therefore, according to the Wentworth scale, it is medium sand. However, the grain size is coarse sand (0.5-0.7 mm) for the area close to the tidal inlet and parts of the upper reach of the estuary.

The threshold current velocities for surficial sediment and the threshold settling velocities of suspended sediment were calculated from the median grain size and are mapped in Figure 5-18 and Figure 5-19, respectively.

- For suspended sediment transport, the deposition patterns are strongly influenced by the grain size. The coarser the grain size, the higher the critical sediment settling velocity. The critical settling velocity of suspended sediment is about 0.025-0.03 m s^{-1} with 0.2-0.3 mm median grain size, 0.03-0.035 m s^{-1} with 0.3-0.4 mm median grain size and 0.045-0.06 m s^{-1} with 0.5-0.7 mm median grain size.

- The coarser bed sediment transportation pattern appears to be strongly influenced by the water depth. The critical threshold for entrainment velocity is about 0.28-0.32 m s^{-1} along the main channel and about 0.16-0.28 m s^{-1} in the shallower water.

The threshold current speed to erode bed sediment and the threshold settling velocities of the suspended sediment was computed using MATLAB software and showed in Figure 5-20 and Figure 5-21. In Figure 5-20, the higher the value, the higher current speed is needed to move the sand on water bed (erosion); and In

Figure 5-21, the lower the value, the easier the suspended sediment can settle down on bed (deposition). The bed sediment mainly erodes along the main channel during the maximum current velocity. And there appears to be a higher amount of erosion for spring tides than on neap tides. The suspended sediment is transported along the main channel. A large portion of the suspended sediment cannot be transported at the maximum neap current speed. This remaining suspended sediment tends to deposit along the bank and the intertidal flats. During high spring tides, more suspended sediment is transported comparing with high neap tides because of the higher flow velocity and the higher tidal range. There is almost no sediment transportation during low spring tides and low neap tides.

Effects of residual currents, threshold current speed of bed sediment motion, and suspended sediment settling were assessed and mapped in Figure 5-22a and Figure 5-22b. In Figure 5-22a, the locations with positive values (blue contour) indicates that the threshold bed sediment motion speed is higher than the residual currents, and hence bottom sediment starts to move and advect with water flows. Figure 5-22a shows that the sediment erosion and transportation predominately occurs along the main channel from the tidal inlet to the Tairua Wharf (the light brown area indicates the area of the sediment deposition).

The positive value with blue colour contour in Figure 5-22b presents the threshold sediment settling velocity higher than the residual current speed. Therefore, it also indicates the locations where the eroded and suspended sediment will deposit on the water bottom. Comparing the two plots in Figure 5-22, sediment is mostly suspended from the tidal inlet to the Tairua Wharf, and within the central part of Tairua Estuary there will be net sediment deposition. Thus, these two figures can be used to forecast the future bathymetry.

Sediment samples did not cover the area of the tidal inlet and the ebb delta. Therefore, no sediment sample plots could be used to interpret the sediment transportation from the tidal inlet to the ebb delta. Thus, the residual currents (Figure 5-7) were used to investigate the sediment transport pattern at the tidal inlet and ebb delta. Suspended sediment from the rivers and eroded from the estuary bed flows along the main channel of the estuary to the ocean along the northern side of the tidal inlet. Subsequently, suspended sediment tends to deposit on the terminal lobe of the ebb tidal delta due to lower current speeds. Meanwhile, the flow along the Pauanui Beach enters the estuary along the southern side of the tidal inlet, and the sediment deposits due to lower current speeds and forms the flood tidal delta. The flow entering the estuary and the flow exiting the estuary meet together, and form a large eddy at the corner of the Pauanui Spit outside of Tairua Estuary, which acts as a sediment deposition-centre. This phenomenon coincides well with the photo which was taken by Christian Winter in 2013.

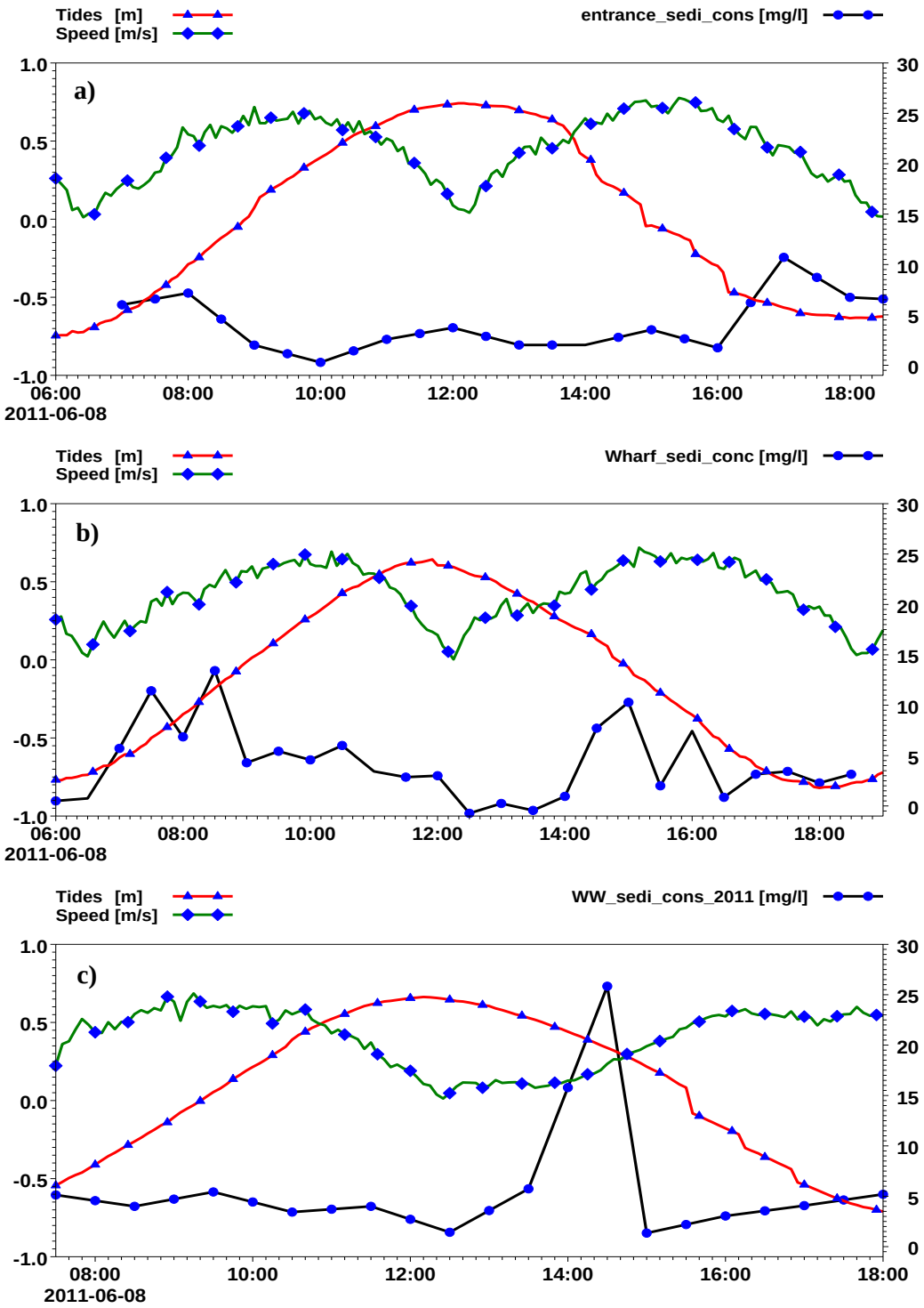

Figure 5-16 Suspended sediment concentration ( ) with tides ( ) and current speed ( ) at the a) Tairua tidal inlet, b) Tairua Wharf and c) Pauanui Waterway on 8 June, 2011.

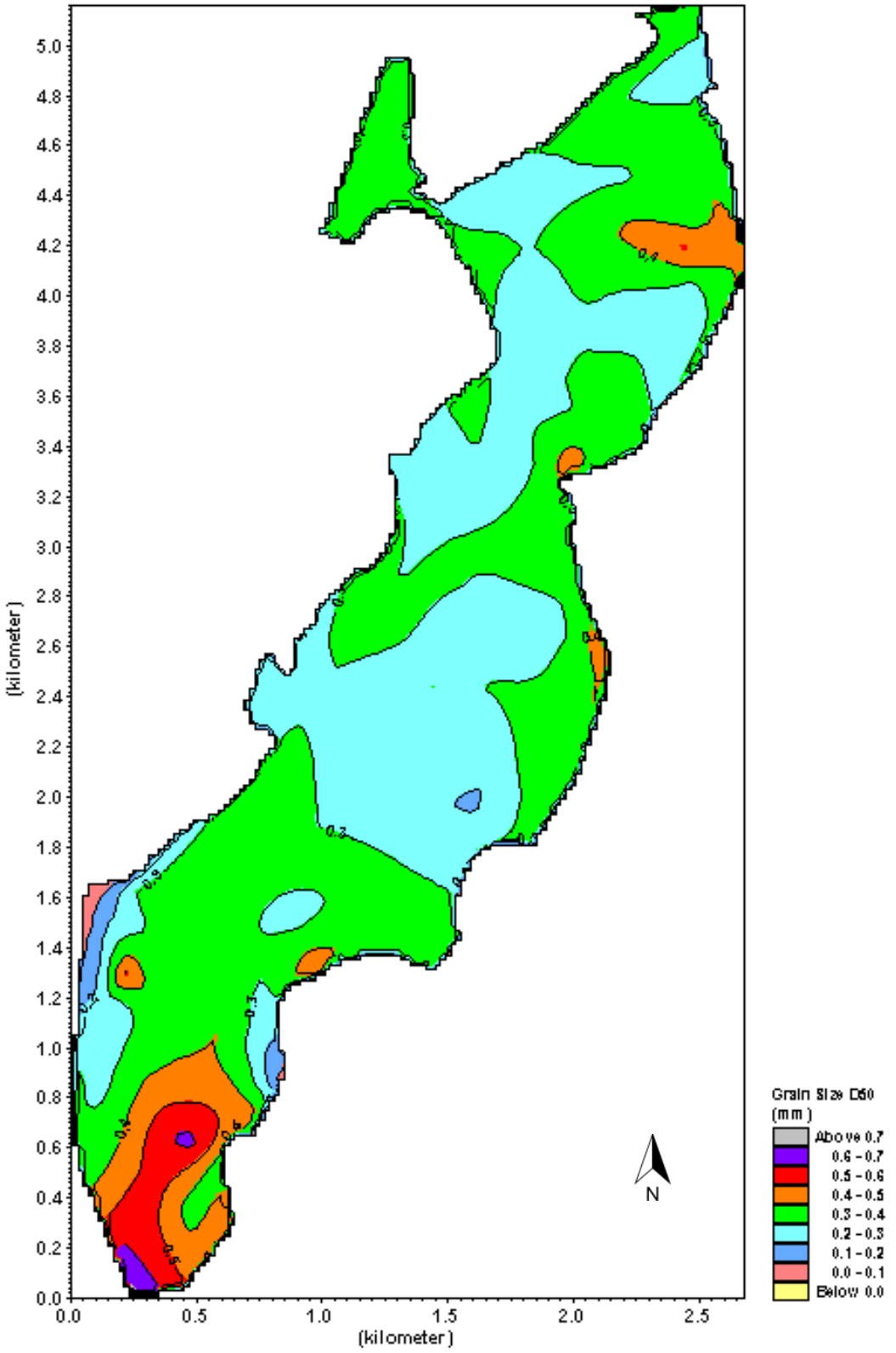

Figure 5-17 Median grain size D50 (mm) interpolated on the data from Waikato Regional Council's soil sampling by Robertson and Peters (2006).

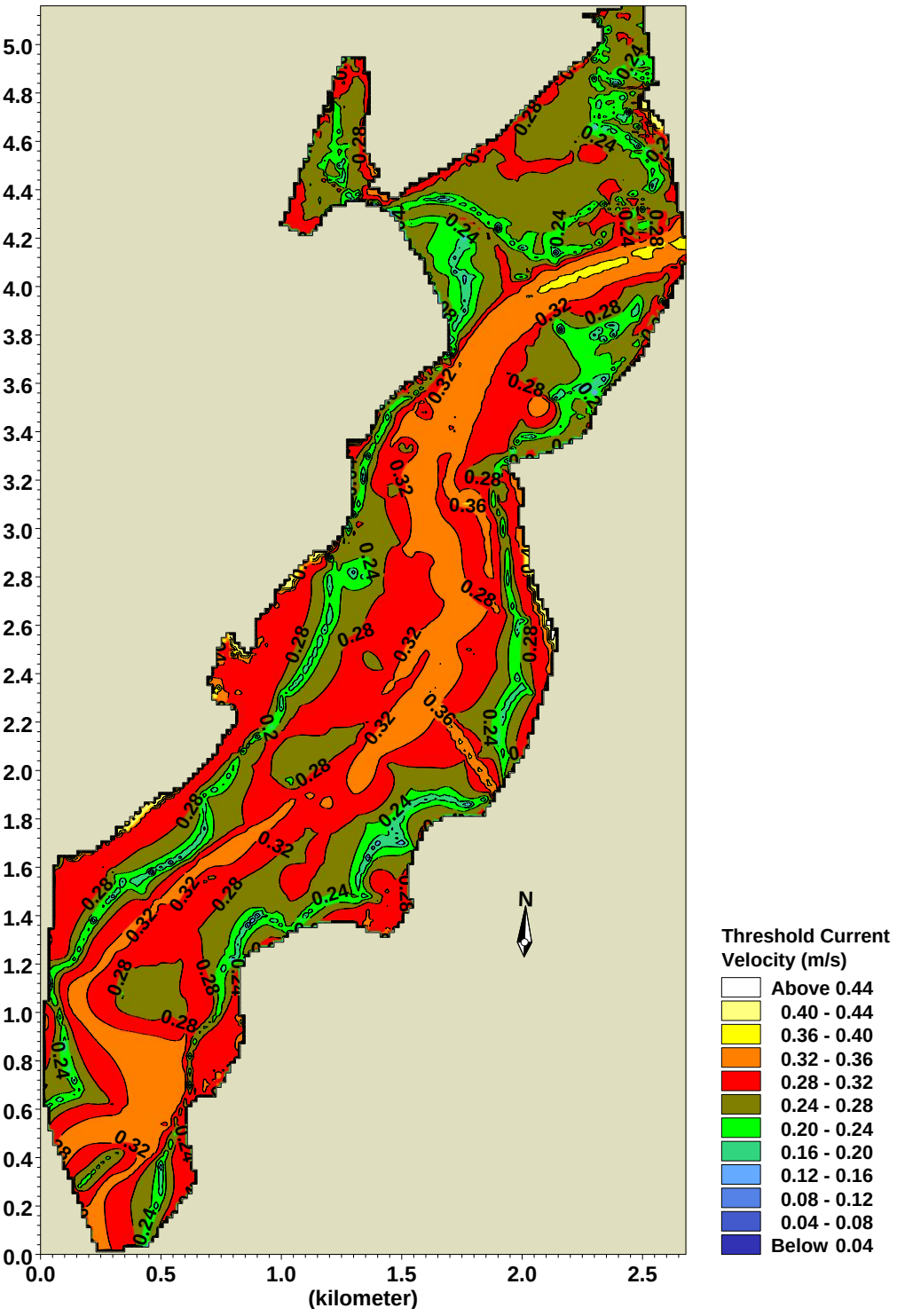

Figure 5-18 Threshold current speed of bed grain motions computed on the median grain size (D50) map shown in Figure 5-17.

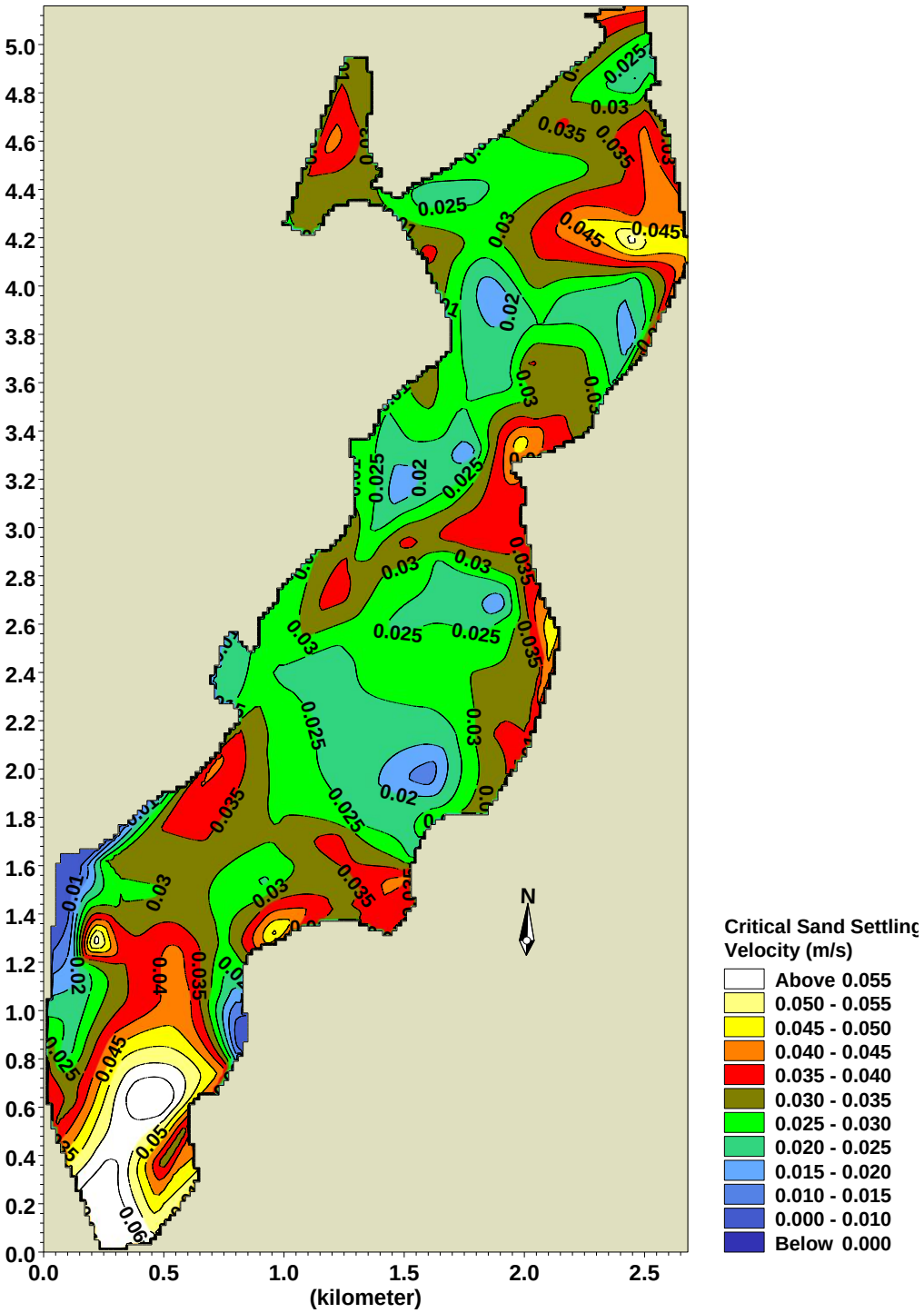

Figure 5-19 Calculated critical suspended sediment settling velocity with 10°C and 35 PSU sea water on the median grain size (D50) map shown in Figure 5-17.

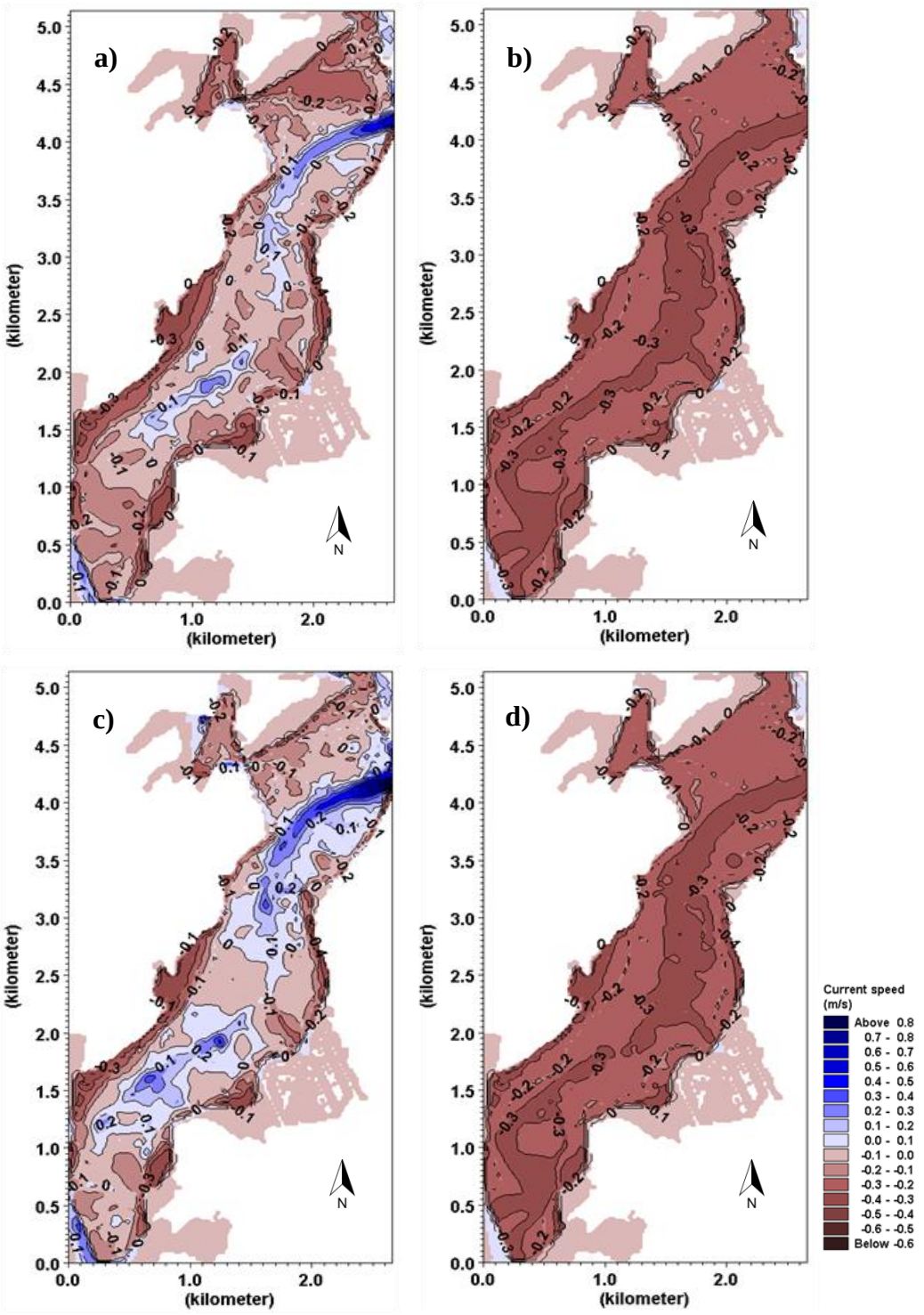

Figure 5-20 Threshold current speed of sand bed motions at Tairua Estuary for a) high neap, b) low neap, c) high spring and d) low spring tides.

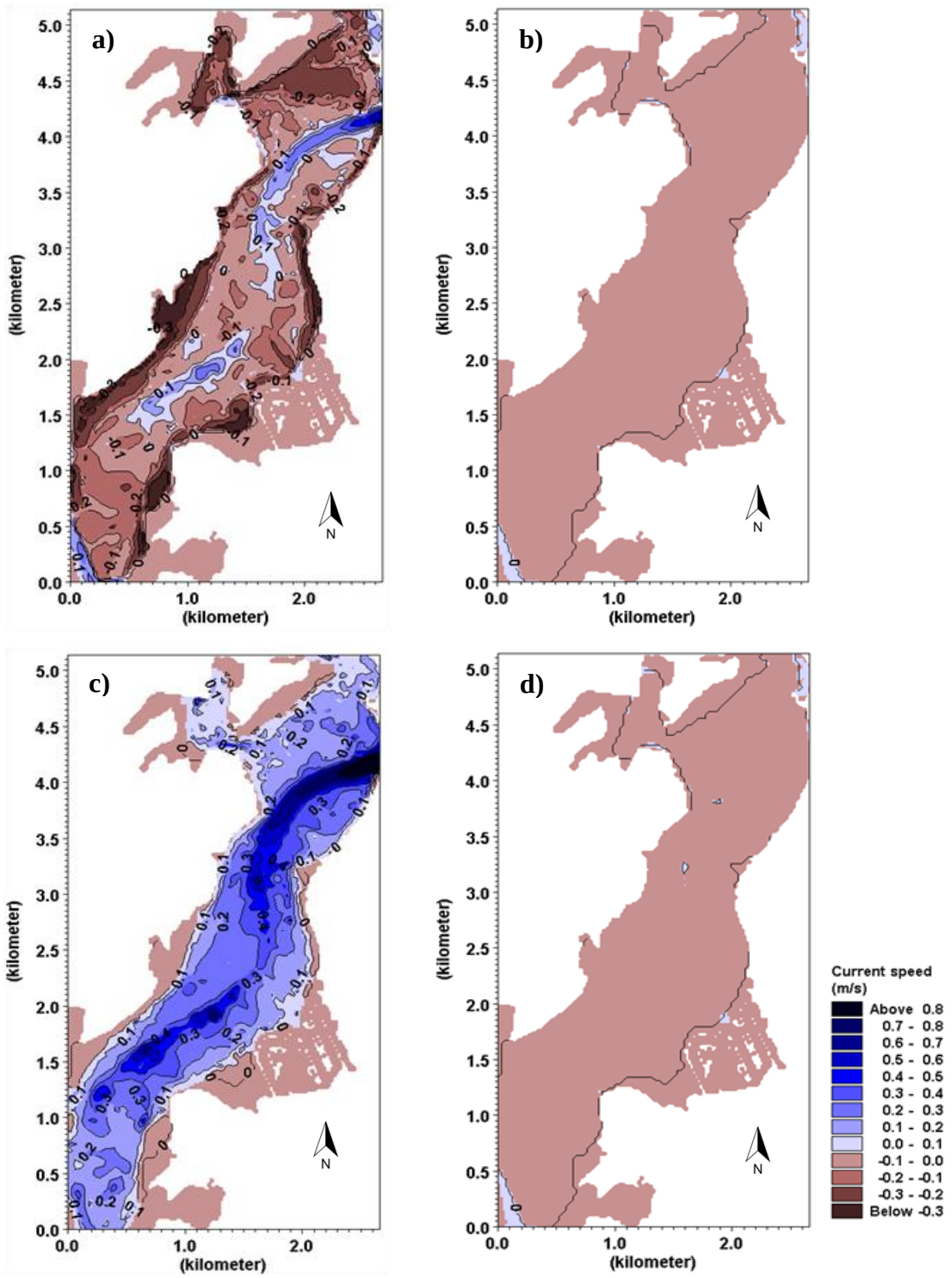

Figure 5-21 Threshold settling velocity of suspended sediment at Tairua Estuary for a) high neap, b) low neap, c) high spring and d) low spring tides.

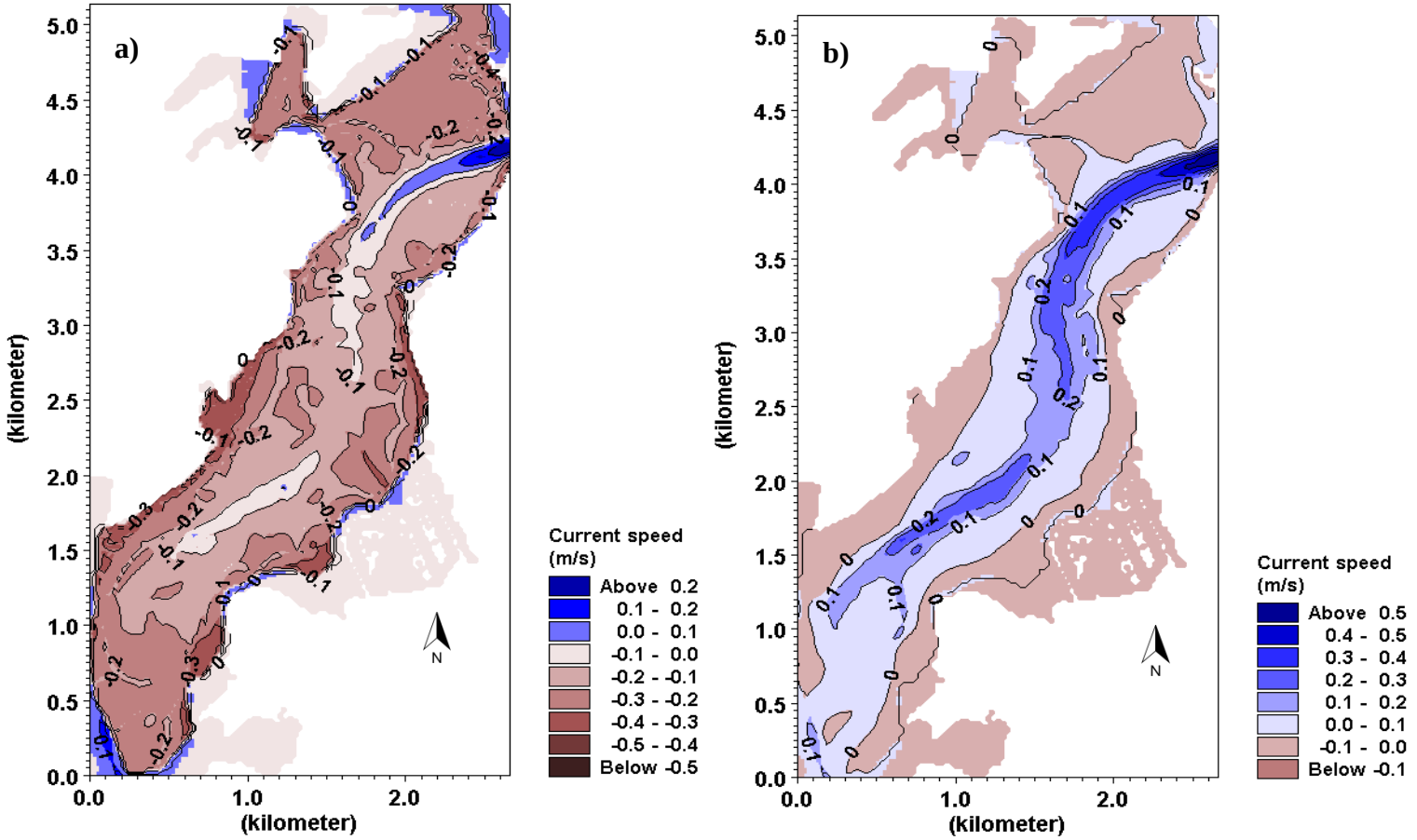

Figure 5-22 Difference a) between the residual current speed and the threshold current speed of sand bed motions and b) between the residual current speed and the threshold settling velocity of suspended sediment.

5.3.4 Waves

Waves around New Zealand's open coast were normally derived from two sources including the locally generated waves by local winds and distantly generated (swell) waves formed within the wider Pacific Ocean or Southern Ocean. Wind generated waves within the harbour can be a significant geomorphic agent with regard to sediment transport and could potentially play a significant role in the shaping of the estuary enclosed beaches especially at times of spring tide (Kirk, 1991) and Wind generated 2-D circulation, mixing and wave re-suspension is important where fetch is great and wind is strong (Hume et al., 2003). However, a large proportion of the energy of an ocean wave is lost on entering an estuary, with as little as 2% actually reaching beyond the estuary mouth (Nordstrom, 1992).

Within the Tairua Estuary, ocean swell waves are believed to be negligible (Kirk, 1991). However, swell waves have been observed to enter the harbour when coming from a southeasterly direction. The purely wave-induced sediment transport is relatively less important in estuaries than on the coastal shelf (Anderson, 1972; McDowell & O'Connor, 1977). Therefore, this research was more interested in tidal currents at the lower Tairua Estuary and there were no instruments deployed for measuring waves within the Tairua Estuary. A wind station was put up at the lower reach to measure wind for model environment condition.

5.4 CONCLUSIONS

5.4.1 Updated the Oceanography Parameters

The maximum current speed is 1.0-1.4 m s^{-1} at the location of the tidal inlet, and 0.4-0.6 m s^{-1} at the Pepe Stream, the Grahams Stream entrance and the northern corner of the Paku Hill which is close to the Tairua Beach. The minimum current speed is about 0-0.1 m s^{-1} along the main channel during flood tides.

At Tairua Estuary, the average high spring tide is 1.0 m, the average low spring tide is -0.82, therefore the average tidal range is 1.82 m during the spring tides; the average high neap tide is 0.6 m, the average low neap tide is -0.53 m, and the average tidal range is 1.13 m during the neap tides. The water surface area was calculated using the number of the grids covered by water multiplied by the area per grid (50 m×50 m). The calculated water surface during spring high water was 6.41 km^2, and 3.62 km^2 at low neap water. Therefore, the average water surface area is 5.02 km^2. As a result, the tidal prism at springs and neaps could be

calculated as 9.12×10^6 m^3 and 5.67×10^6 m^3 respectively. The field recorded and model calculated mean current speeds are 0.606 m s^{-1} and trough current speed is 0.005 m s^{-1} at the tidal inlet. As a result, the average water discharge from the estuary to the ocean is 131.37 m^3 s^{-1} with 430 m^2 mean tidal inlet cross area. Therefore, Tairua Estuary could be flushed only after 19.29 hours during the spring tides. This conclusion is consistent with the saline mixing research by Bell (1994) which calculated that 82% of incoming water into the estuary was new ocean water and that harbour flushing took 1.3 tidal cycles to replace the entire tidal prism volume.

The maximum and mean Tairua River discharge is 220 m^3 s^{-1} and 9.78 m^3 s^{-1} calculated on the one year weather station collected data; the maximum and mean discharge from the Pepe Stream is 1.46 m^3 s^{-1} and 0.23 m^3 s^{-1}; the maximum and mean discharge from the Grahams Stream is 0.75 m^3 s^{-1} and 0.17 m^3 s^{-1} respectively.

These oceanography parameters calculated in this research (value®) is listed in Table 5-8 for comparing with the data given by Hume & Herdendorf (1988) and Joynes & Barnett (1991).

Table 5-8 Main oceanography parameters of the Tairua Estuary (*Hume & Herdendorf, 1988; ^ Joynes and Barnett, 1991; ® Liu, 2013).

Description	value*	value^	value®
Catchment area	280 km^2		280 km^2
Surface area at MHWS	6.12 km^2		6.41 km^2
Surface area at MLWN			3.62 km^2
Mean surface area			5.02 km^2
Spring tidal range	1.6 m		1.82 m
Neap tidal range			1.13 m
Mean tidal range			1.48 m
Spring tidal prism	5.02×106 m^3		5.71×106 m^3
Neap tidal prism			3.55×106 m^3
Mean throat velocity	0.66 m s^{-1}		0.58 m s^{-1}
Peak throat velocity	1.01 m s^{-1}	1.6 m s^{-1}	1.38 m s^{-1}
Throat area (measured)	430 m^2		430 m^2
Mean throat discharge			249.4 m^3 s^{-1}
Peak Springs discharge	436 m^3 s^{-1}		593.4 m^3 s^{-1}

5.4.2 Features of Hydrodynamic and Sediment Transport

Entrainment, transport and deposition of sediment in an estuary are the results of a complex suite of river, tide, and wave processes operating over different temporal scales (Nicholes & Biggs, 1985).

Tairua Estuary is a micro-tidal with semi-diurnal tides dominated at the lower reach of the estuary, with a significant diurnal effect at the Tairua River mouth. The tidal wave undergoes more distortion during spring tides than during neap tides.

Tairua Estuary has shallow basin of various shapes with extensive intertidal area; narrow entrance to the sea, ebb and flood tidal deltas at mouth; tidally dominated circulation and mixing; small river influence compared to the tides; good flushing because much of the water leaves the estuary on the outgoing tide. These conclusions are same as Hume et al. (2003) who classified the New Zealand estuaries on the basis of factors such as climate, the catchments characteristics, oceanic and riverine conditions.

Tides can reach the Tairua River mouth. The higher the river discharges from the Tairua river mouth to the estuary, the smaller the tidal wave magnitude, as a result, the higher the water volume stratification. This conclusion agrees with Garel et al. (2009) who suggested that highly stratified conditions developed with increasing river discharge. A salt wedge with tidal motion was observed at the lower estuary during the river flood.

The relative impacts of tidal (neap, spring) and river discharge (including a flood event) forcing upon water and sediment circulation have been examined. Tidal asymmetry produced faster currents on the ebb than on the flood, especially at the mouth. This pattern of seaward current dominance was enhanced with increasing river flow, due to horizontal advection that was confined within the narrow estuarine channel. The freshwater inputs and, at a degree less, the tidal range controlled the vertical mixing and stratification importance. Depending on the intensity of turbulent mixing, the residual water circulation was dominantly controlled either by tidal asymmetry or gravitational circulation. The SSC was governed by cyclical local processes (re-suspension, deposition, mixing, advection) driven by the neap-spring fluctuations in tidal current velocities. More, intertidal variability in stratification indicated the significance of tidal pumping at the partially and highly stratified estuary. The estuary turbidity maximum (ETM) was enhanced with increasing current velocities, and displaced downstream during periods of high river discharge. During the flood event, the ETM was expelled out of the estuary, and the SSC along the estuary was controlled by the sediment load from the drainage basin. These conclusions coincide well with the study at the rock-bound Guadiana estuary by Garel et al. (2009).

The influence of tidal asymmetry on the residual fluxes of coarse and fine sediment is different: the suspension load of coarse sediment is strongly limited by the current speed and it adapts to changes in the current speed rapidly in comparison with the tidal time scale. For fine sediment, saturation of the suspended load seldom occurs. Most fine sediment settles only at very low current speed and the settling time delay is important.

Uncles (2001) concluded that the difference between the maximum tidal currents during ebb and flood is relevant for residual sediment transport, which in particular affects the residual flux of the coarse suspended fraction; and difference between the slack water periods preceding ebb and flood, which particularly influences the residual flux of the fine suspended fraction. Dronkers (1986) also contributed that estuarine morphology is to a large extent determined by the residual sediment transport pattern. The inverse statement is also true. Residual sediment transport depends on differences in magnitude and duration between ebb and flood tidal currents. Such differences named tidal asymmetry are produced by the distortion of tidal wave propagation on the coastal shelf and entering estuaries.

At the Tairua Estuary, the peak of the tide has an average 30 minutes delay and the trough of the tide has an average 40 minutes delay between the tidal inlet and the Pauanui waterway in the lower reaches of Tairua Estuary. Further upstream the time delays increase relative to the ocean, while the tidal asymmetry is also accentuated. The peak of the tide has an average 3 hour 40 minutes delay and the trough of the tide has an average 6 hour delay between the tidal inlet and the Tairua river mouth. Basing on the tidal asymmetry and propagation analysis, more water can accumulate in the upper part of Tairua Estuary during the spring tidal cycle than during a neap tide. It causes an increase of salinity. The net sediment moved landward during flood tides. As discussed above that tidal asymmetry produced faster currents on the ebb tides than on the flood tides, especially at the river mouth. This pattern of seaward current dominance was enhanced with increasing river flow, due to horizontal advection that was confined within the narrow estuarine channel. Highly stratified conditions developed with increasing river discharge. This result could be explained by the found of Dronkers (1986) that the river runoff produces a cross-sectional distribution of current velocities which enhances seaward transport in the near surface part, but counteracts seaward transport in the deeper parts of the channel.

Bed sediment is eroded mainly along the main channel during the maximum current velocity. There is higher amount of erosion occurring for spring tides than on neap tides. A big portion of the suspended sediment will deposit along the bank and the intertidal flats during neap tides. More suspended sediment will be transported because of the higher flow velocity and the higher tidal range during neap high tides. There is almost no bed sediment is moved to suspension or settles on water bed during spring low and neap low tides.

Healy et al. (1981) proposed that Pauanui Beach was in a long-term state of slow erosion with sediment being removed from the beach and deposited inside the estuary. However, Carryer (1982) showed that Pauanui Spit has been under a state of long term net accretion with sand taken out with the ebb flows from Tairua Estuary. In this research, both of the hydrodynamic and sediment transport simulation results and instrument data supported that the sediment erosion and transportation happens mainly along the main channel from the tidal inlet to the Tairua Wharf. The suspended sediment is transported along the main channel to the outside ocean along the north side of the tidal inlet and deposits at the ebb delta with lower current speed at the outside of the estuary. Meanwhile, the flow along the Pauanui Beach flows back to the estuary along the southern side of the tidal inlet and the sediment deposits due to lower current speed after entering the estuary and form the flood tidal delta. These two flows entering the estuary and the flow exiting the estuary meets together and forms a big eddy between the head of the Pauanui Spit and the ebb tidal delta outside of Tairua Estuary. A shallow area between the ebb tidal delta and the Pauanui Beach can be found in field.

5.4.3 Main Factors Influencing Sediment Transport

The main factors deciding the sediment supply and sediment transport pattern include the river flow, sediment characteristics, current velocity distribution and variation during tidal cycle, wind waves and swell.

The river inflow related to an input of sediment and a cross-sectional flow structure affected by density differences. The density differences tend to increase flood currents in the deepest parts of the channel, especially in the lower half of the vertical profile, and tend to decrease flood currents near the surface and in the shallow parts of the cross-section. The inverse holds for the ebb currents. This conclusion coincides with the other studies by Postma (1967) and Festa & Hansen, (1978).

For suspended sediment transport, the deposition patterns are strongly influenced by the grain size. The coarser the grain size, the higher the critical sediment settling velocity (Dronkers, 1986). This study found that the critical settling velocity of suspended sediment is about 0.025-0.03 m s^{-1} with 0.2-0.3 mm median grain size, 0.03-0.035 m s^{-1} with 0.3-0.4 mm median grain size and 0.045-0.06 m s^{-1} with 0.5-0.7 mm median grain size.

The influence of tidal asymmetry on the residual fluxes of coarse and fine sediment is different. The suspension load of coarse sediment is strongly limited by the current speed and it adapts to changes in the current speed rapidly in comparison with the tidal time scale. For fine sediment, saturation of the suspended load seldom occurs. Most fine sediment settles only at very low current

speed and the settling time delay is important.

The influence of tidal asymmetry on the residual fluxes of coarse and fine sediment is different. The suspended load of coarse sediment is strongly limited by the current speed and it adapts to changes in the current speed rapidly in comparison with the tidal time scale. Most fine sediment settles only at very low current speed and the settling time delay is important. The coarser bed sediment transportation pattern appears to be strongly influenced by the water depth. The critical threshold for entrainment velocity is about 0.28-0.32 m s^{-1} along the main channel and about 0.16-0.28 m s^{-1} in the shallower water.

The purely wave-induced sediment transport is relatively less important in estuaries than on the coastal shelf (Anderson, 1972; McDowell & O'Connor, 1977). Therefore, in this research, there were no instrument deployed within the estuary and no swell were considered in the modelling. However, the wind time series collected at the Slipper Island and the lower reach of the Tairua Estuary were input 10 m above water surface in both MIKE and 3DD models to simulate the impacts of the wind induced wave within the estuary.

CHAPTER SIX
SALINITY AND TEMPERATURE STRUCTURE

The main goal of this chapter is to investigate the cross sectional and vertical salinity and temperature structure within Tairua Estuary by using three dimensional hydrodynamic modelling and field observations (CTD and DataFlows). It is important for understanding the stratification features, and as a result, gaining a better understanding of the estuarine physical processes. Tairua Estuary was estimated as highly stratified with high river flow (>200 m^3 s^{-1}) but low current speed; and it is partially-stratified with high river flow (>200 m^3 s^{-1}) and a current speed higher than 0.5 m s^{-1}. The higher the river flow, the higher the possibility of water stratification for a given current speed at the Tairua tidal inlet. Less stratification occurs with higher current speed at a given river flows. This is because the higher tidal flow has higher energy and, therefore, mixes well with the river flow to generate turbulent flow and as a result a homogenous water column. Water temperature varies with tidal flow, river discharge, locations and air temperature over the intertidal flats. The MIKE 3 Flow FM model simulation results are consistent with the instruments (Dataflows) observations well.

6.1 INTRODUCTION

Estuaries are primarily characterised by their geomorphology and patterns of salinity stratification (Hansen & Rattray, 1966). Salinity and temperature structures in an estuary are primarily a consequence of water exchange due to the tides at the tidal inlet, and the freshwater input at the river mouth (Hardisty, 2007). Salinity studies are especially important in coastal research because changes in river discharge and wind control salinity at the coast and on the shelf. By understanding salinity we can better understand the coastal ocean density and circulation patterns. Water temperature in estuarine systems varies throughout the tidal cycle if the temperature of the seawater and the fresh water is different (Hardisty, 2007). The density differences tend to increase flood currents in the deepest parts of the channel, especially in the lower half of the vertical profile, and tend to decrease flood currents near the surface and in the shallow parts of the cross-section. The inverse holds for the ebb currents. This flow structure has an important impact on the sediment transport (Postma, 1967; Festa & Hansen, 1978).

Therefore, this case study discussed the structure of salinity and water temperature basing on the field instrument data for better understanding the physical process of Tairua Estuary, especially with the relationships between tidal flow and river discharge.

6.2 METHODS - MIKE 3 FM HD MODELLING

MIKE 3 Flow Model FM is a modelling system based on a flexible mesh approach. The system is based on the numerical solution of the three-dimensional incompressible Reynolds averaged Navier-Stokes equations invoking the assumptions of Boussinesq and of hydrostatic pressure. Therefore, the model consists of continuity, momentum, temperature, salinity, and density equations and is closed by a turbulent closure scheme. In the horizontal domain both Cartesian and spherical coordinates can be used. The free surface is taken into account using a sigma-coordinate transformation approach. The spatial discretisation of the primitive equations is performed using a cell-centred finite volume method. The spatial domain is discretised by subdivision of the continuum into non-overlapping element/cells. In the horizontal plane an unstructured grid is used while in the vertical domain a structured discretisation is used. The elements can be prisms or bricks whose horizontal faces are triangles and quadrilateral elements, respectively. An approximate Riemann solver is used for computation of the convective fluxes, which makes it possible to handle discontinuous solutions (MIKE 3 FM user manual, 2012).

6.2.1 Main Equations

The MIKE 3 FM flow module was used to simulate the salt and temperature distribution characteristics of Tairua Estuary. The main equations used in the modelling are listed below.

$$\frac{\partial T}{\partial t} + \frac{\partial uT}{\partial x} + \frac{\partial vT}{\partial y} + \frac{\partial wT}{\partial z} = F_T + \frac{\partial}{\partial z}\left(D_v \frac{\partial T}{\partial z}\right) + \widehat{H} + T_s S \quad (6\text{-}1)$$

$$\frac{\partial S}{\partial t} + \frac{\partial uS}{\partial x} + \frac{\partial vS}{\partial y} + \frac{\partial wS}{\partial z} = F_S + \frac{\partial}{\partial z}\left(D_v \frac{\partial S}{\partial z}\right) + \widehat{H} + s_s S \quad (6\text{-}2)$$

Where T is temperature, S is salinity, D_v is the vertical turbulent (eddy) diffusion coefficient, $\widehat{H}$ is a source term due to heat exchange with the atmosphere, T_s is the temperature of the source, s_s is salinity of the source. F is the horizontal diffusion term defined by

$$(F_T, F_s) = \left[\frac{\partial}{\partial x}\left(D_h \frac{\partial}{\partial x}\right) + \frac{\partial}{\partial y}\left(D_h \frac{\partial}{\partial z}\right)\right](T, s) \quad (6\text{-}3)$$

Where, D_h is the horizontal diffusion coefficient. The diffusion coefficients relate to the eddy viscosity by

$$D_h = \frac{A}{\sigma_T} \text{ and } D_v = \frac{v_t}{\sigma_T} \quad (6\text{-}4)$$

Where, σ_T is the Prandtl number.

In the open ocean the range of salinity is generally in the range of 34 ‰ to 38 ‰, with an average of about 35 ‰ (Hardisty, 2007), whereas the river water can be assumed to be fresh, so that salinity decreases in an upstream direction. The salinity distribution could be described as a Gaussian curve.

$$S(x) = 35exp\left[-\frac{x^2}{2\sigma_x^2}\right] \tag{6-5}$$

Where, x is the position, and σ_x is the variance used to describe the spread of the distribution.

The surface and bottom boundary conditions for the temperature are

$$\text{At } z = \eta,\ D_h\frac{\partial T}{\partial z} = \frac{Q_n}{\rho_0 c_p} + T_p\hat{P} - T_e\hat{E} \tag{6-6}$$

$$\text{At } z = -d,\ \frac{\partial T}{\partial z} = 0 \tag{6-7}$$

Where, Q_n is the surface net heat flux, and $c_p = 4217\ J/(kg\,°K)$ is the specific heat of water.

The surface and bottom boundary conditions for salinity are

$$\text{At } z = \eta,\ \frac{\partial s}{\partial z} = 0 \tag{6-8}$$

$$\text{At } z = -d,\ \frac{\partial s}{\partial z} = 0 \tag{6-9}$$

When heat exchange from the atmosphere is included, the evaporation is defined as

$$\hat{E} = \begin{cases} \frac{q_v}{\rho_0 l_v} & q_v > 0 \\ 0 & q_v \le 0 \end{cases} \tag{6-10}$$

Where, q_v is latent heat flux and $l_v = 2.5 \times 10^6$ is the latent heat of water vaporisation.

6.2.2 3D Flexible Mesh Grids

A three dimensional flexible triangular mesh was generated using the Mesh Generator tool in MIKE Zero. The digitized water-depth data were interpolated using the 'Natural Neighbor' method before smoothing and refinement by bisection and the final grid is shown in Figure 6-1. The mesh type in the vertical is 'sigma'. It includes 10 layers with equidistant 0.1m layer thickness. There are a total of 1973 nodes and 3044 elements in the mesh. The minimum depth cutoff is 2 m. The two boundaries are river discharge and offshore tidal elevation respectively. Map projection is NZGD_2000_New_Zealand_Transverse_Mercator.

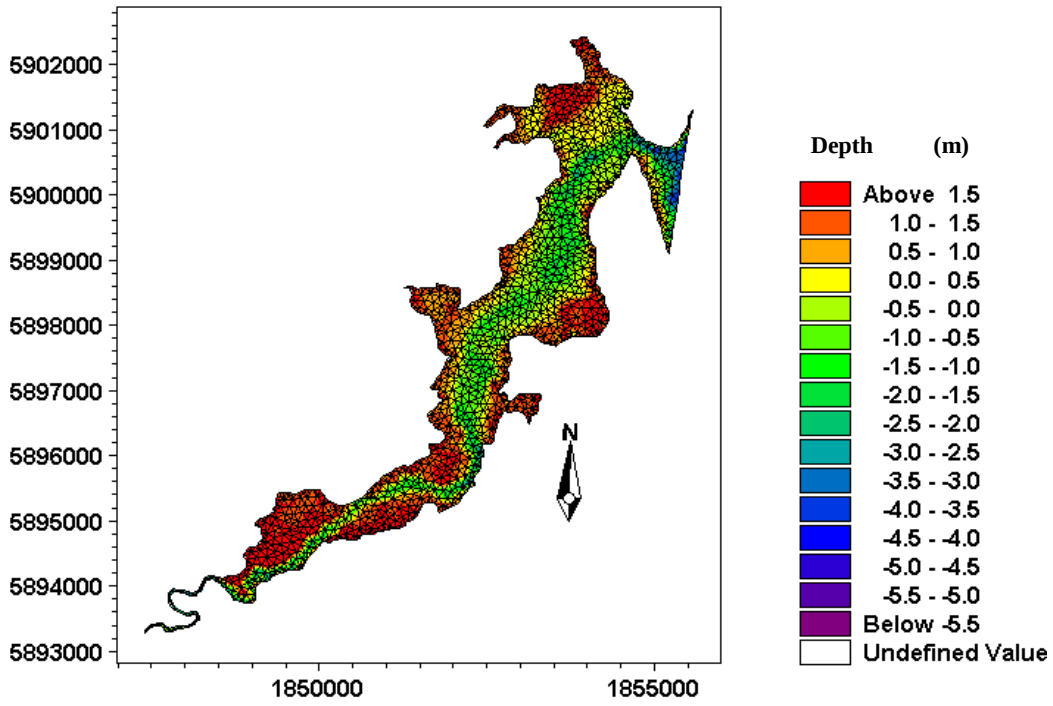

Figure 6-1 3-D flexible mesh generated for the MIKE 3 FM modelling. There are 10 layers with 0.1 m depth per layer from water bottom to water surface.

6.2.3 Simulation Period

The MIKE 3 FM hydrodynamic model simulation ran from 12.00am 29 July, 2010 to 10.00pm 26 August, 2010. The total number of time steps was 250000 with 10 second time step intervals. The time zone was in New Zealand Standard Time (NZST).

6.2.4 River Discharge and Tidal Elevation Boundaries

The time series river discharge data recorded at the Broken Hill station, which is 11 km upstream of the Tairua River mouth was used at the river boundary and the offshore boundary surface elevation was calculated by NIWA's regional RiCOM (River and Coastal Ocean Model). Its boundaries did not include a Coriolis correction and wind correction.

Figure 6-2 shows the tidal elevation during June in 2011. It was used as the tidal boundary of the MIKE 3 HD FM models. Salinity and temperature was calculated for the peak flood and peak ebb tides on spring and neap to analyse the impacts of the tides at Tairua Estuary.

6.2.5 Air Temperature

The air temperature data were downloaded from the NIWA's Cliflo website. It was recorded at the nearest permanent site to Tairua located at the Whitianga Aero Aws. Station (Network: 1520, Number: B65862, Latitude: -36.834º, Longitude: 175.677º) during June (winter) and December (summer) in 2011. The time series of the air temperature is shown in Figure 6-2. The average air temperature during December (summer) was 19.42°C and during June (winter) was 12.03°C, which were input as the model environmental boundary.

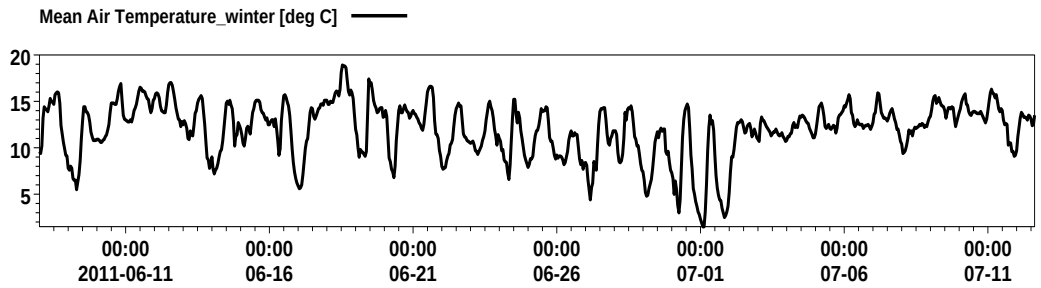

Figure 6-2 Air temperature time series observed during June (winter) in 2011 at the Whitianga Aero Aws Station (-36.834, 175.677).

6.2.6 Water Temperature, Salinity and Density

As introduced in Chapter 2, water temperature and salinity range were estimated according to the metrological data collected by other scientist or research group.

New Zealand waters are colder in the south and warmer in the north. As spring arrives, water warms gradually and reaches the peak temperature in late summer. Northern waters have more fish species than cooler southern waters. Mean seawater surface temperature (SST) is 12-14°C in winter and 18-20°C in summer around New Zealand (www.surf-forecast.com).

Continuous water temperature was recorded by the Waikato Regional Council from 1991 at the Broken Hills station on the Tairua River, 11 km upstream from the Tairua Bridge. The highest recorded water temperature was 28.7°C on 7 February 1998 and the lowest water temperature was 4.4°C on 26 June 1992.

The evaporation, precipitation, river inflow, and confined circulation are the key factors influencing seawater salinity. The density of surface seawater ranges from about 1020 to 1029 kg m^{-3}, depending on the temperature and salinity. Deep in the ocean, under high pressure, seawater can reach a density of 1050 kg m^{-3} or higher (Ridgway, 1968).

6.2.7 Model Parameters

The minimum time step was 0.01 second with the maximum time step set to 10 second in order to keep the critical Courant-Friedrichs-Levy (CFL) stability number as 0.8 for the shallow water and transport equations. The drying depth was 0.01 m, the flooding depth was 0.05 m and the wetting depth was 0.1 m. The density type is 'function of temperature and salinity'. The horizontal eddy viscosity type depends on the Smagorinsky formulation, which in this case was set to 0.1. The Bed resistance type was constant 0.1 m 'roughness height'. The Coriolis force was applied in the model and varied across the domain. The wind recorded at the Slipper Island Station was applied 10 m above the water surface. Both of the horizontal and vertical dispersion was specified as the 'scaled eddy viscosity' formulation with constant value 1 $m^2 s^{-1}$. Heat exchange was considered in the modeling. The precipitation data recorded at the Whitianga were applied. There is no ice coverage and wave radiation was considered. The initial temperature was 15°C and salinity was 34.5 PSU respectively. The time series of water temperature recorded by the ADP at the tidal inlet and the RBR at the Tairua river mouth were used as the offshore boundary and the river mouth boundary respectively. The low order, fast algorithm solution technique of the time integration and space discretisation was used in the shallow water equations.

6.2.8 Field Data

Two DataFlows temperature and salinity probes were deployed at the water bottom and surface at the Tairua Wharf and two more DataFlows were attached on the structure used to secure the ADV at the power pole (37° 01.30´S, 175° 51.07´E) close to the Pauanui Waterway from 8 June to 12 July, 2011, to collect water temperature and salinity data. The details of these deployments are provided in Chapter 3.

Figure 6-3 shows the water temperature recorded by the ADCP at the tidal inlet and the Dataflow at the Tairua Wharf located at the lower Tairua Estuary for one tidal cycle. The two instruments show agreement.

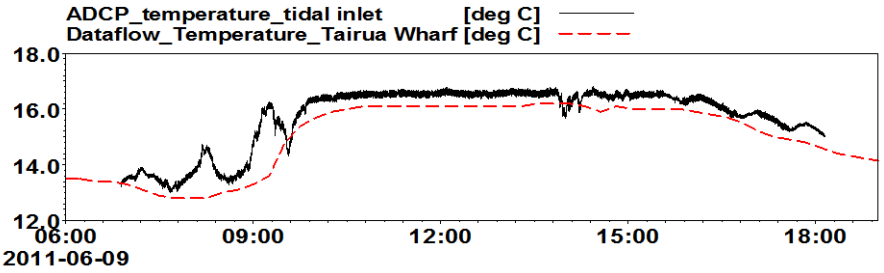

Figure 6-3 the observed water temperature by ADCP at Tairua tidal inlet and by Dataflow at Tairua Wharf which is close to Tairua tidal inlet.

6.3 RESULTS AND DISCUSSIONS

6.3.1 Estuarine Stratification

The estuarine Richardson number R_{iE} was used to evaluate the effect of stratification at the entrance of Tairua Estuary under different tidal and river inflow conditions. This number expresses the ratio of the potential energy gain due to freshwater discharge to the mixing power of tidal currents (Vaz and Dias, 2013).

$$R_{iE} = g\left(\frac{\Delta\rho}{\rho}\right)\left(\frac{Q_f}{bU_{RMS}^3}\right) \quad (6\text{-}11)$$

Where, $\Delta\rho$ is density difference between sea and freshwater; ρ is mean density; Q_f is river flow; b is width of the section where the data were collected; and U_{RMS} is root-mean-square tidal velocity. If R_{iE} is greater than 0.8, the estuary is highly stratified; if it is smaller than 0.08, the estuary is considered as well-mixed; and if $0.08 < R_{iE} < 0.8$, the estuary is considered as partially mixed (Fischer et al, 1979).

The Tairua tidal inlet comprises of a main channel that is 130 m wide with a mean depth of 2.79 m at mid-tide (Hume and Herdendorf, 1992). The mean throat (tidal inlet) velocity is 0.58 m s^{-1}, and the peak throat velocity is 1.38 m s^{-1} calculated by the calibrated 'estuary-20m' hydrodynamic model. The average Tairua River inflow is 9.78 m^3 s^{-1} and the peak value is 220 m^3 s^{-1} was recorded by the Waikato Regional Council's station (discussed in Chapter 5). Four scenarios were calculated: R_{iE} is 0.048 with 9.78 m^3 s^{-1} mean river flow and 0.58 m s^{-1} mean throat velocity, it is well-mixed; R_{iE} is 0.99 with 200 m^3 s^{-1} peak river flow and 0.58 m s^{-1} average throat velocity, and it is highly stratified; R_{iE} is 0.013 with 9.78 m^3 s^{-1} average river flow and 1.38 m s^{-1} peak throat velocity, it is well-mixed; and R_{iE} is 0.269 with 200 m^3 s^{-1} peak river flow and 1.38 m s^{-1} peak throat velocity, it is partially-mixed. This data indicates that Tairua Estuary is well-mixed with mean current speed and river flow.

Tidal current speed and river flow are the two key factors impacting on the estuarine stratification. To investigate the relationships between the estuarine stratification and the key factors of the current speed and river flow, the Richardson number R_{iE} was calculated and the results are plotted in Figure 6-4. This plot demonstrates that the higher the river flow, the higher the possibility of water stratification for a given current speed at the Tairua tidal inlet. It also demonstrates that less stratification occurs with higher current speed at a given river flows. This is because the higher tidal flow has higher energy and, therefore, mixes well with the river flow to generate turbulent flow and as a result a homogenous water column. Tairua Estuary is well-mixed or partially-mixed with

a current speed higher than 0.5 m s^{-1}, even when the river discharge reaches its peak value (200 m^3 s^{-1}). Dyer (1979) also classified Tairua Estuary as a partially-mixed estuary and there is considerable friction between water and estuary bottom to create turbulence. Turbulence tends to mix the water column more effectively than entrainment, causing the salinity to decrease to the head of the estuary in the lower layer and to increase progressively towards the sea in the surface layer; though there is no water movement, there is salt exchanging vertically; the landward flow at the bottom can be of order 0.05 m s^{-1} with tidal oscillations of 0.5 m s^{-1}.

The tidal currents are sufficiently strong to destroy the salt wedge interface and cause some vertical mixing of salt and fresh water. This pattern is also observed in a ROMS model for the Hudson River Estuary (Warner et al, 2005). Bell (1994) found that 82% of the incoming water on the flood tide is new salt water, indicating a large input of salt water on the flood tide and an efficient flushing system on the ebb tide.

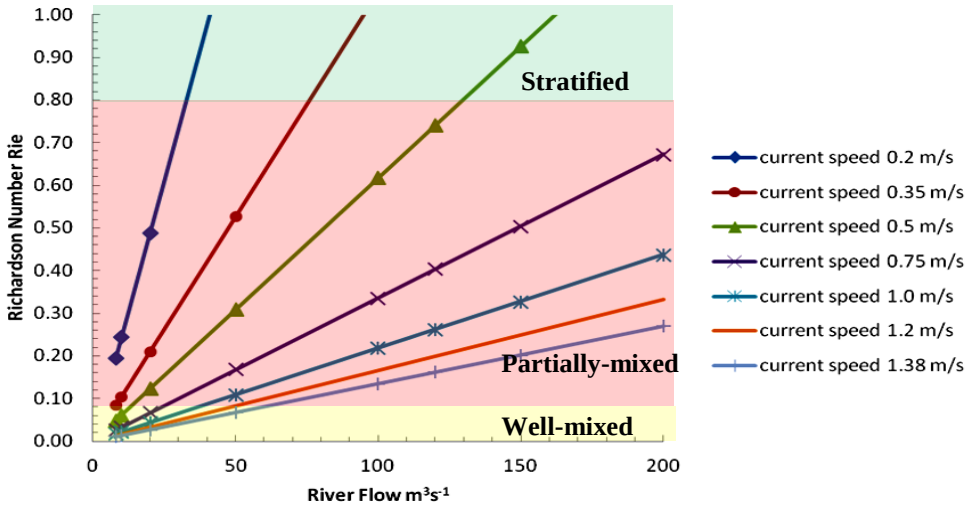

Figure 6-4 The Richardson number calculated based on current speed and river flow of Tairua Estuary. The estimated well-mixed, partially mixed and stratified Richardson Numbers are in yellow, pink and blue respectively.

6.3.2 Field Observations

6.3.2.1 *Water Salinity*

Figure 6-5 is water salinity observed by the four DataFlows at the water bottom and surface in front of Tairua Wharf (close to the tidal inlet) and the power pole at the upper reach of the estuary. The tidal elevation and the river discharge are also plotted in Figure 6-5. The plots showed that water salinity is about 3-4 PSU higher on water bottom than at water surface in front of the Tairua Wharf.

However, there is little difference in the salinity between the water bottom and water surface at the power pole location. This indicates that seawater mixes well with river fresh water at the upper reach of the estuary and there is a salt wedge during peak flood and ebb flow at the lower reach.

As discussed in Chapter 5, Tairua Estuary is a tide-dominated estuary and tides have higher energy than river discharge. At the lower reach of the estuary, especially close to the estuary entrance (tidal inlet), salty water from the outside ocean flows into the estuary during flood tides and river freshwater discharge from the river mouth to the estuary in the opposite direction. The heavier salty water flows under river fresh water and results in a salt wedge in front of the Tairua Wharf.

Water salinity changes with tidal flow and river freshwater discharge. At the Tairua Wharf, the maximum salinity at peak flood tide is similar to the ocean seawater outside, but the minimum salinity differs with the peak ebb flow in each tidal cycle. The heavier saltier seawater flows under river freshwater and results in salinity stratification from the tidal inlet to the Tairua Wharf at peak flood tides. It increases with flood tides and decreases with ebb tides along the main channel within Tairua Estuary. Water salinity at the tidal inlet and its vicinity is higher with flood tides on the spring than neap tides, however, lower salinity with ebb tides on the spring than neap tides. For the same tidal flow, the higher the river discharge, the lower the water salinity. The plot also shows several floods that discharged from the Tairua River mouth during this period, e.g. the 59 $m^3 s^{-1}$peak floods discharged on 18 June and 20 $m^3 s^{-1}$ discharged on 22 June, 2011. These floods did not influence salinity at peak flood tides, however, salinity decreased with the river floods at peak ebb flow. This indicates that tidal flows have higher energy than river flows at peak flood tides. Compared with salinity features close to the tidal inlet, salinity values are more sensitive to river discharge at the location close to river mouth because the tidal energy decreases and the river energy increases from the estuary entrance to the river mouth gradually. In general, the higher the river freshwater discharge is, the lower the salinity at the upper estuary.

Water salinity also varies with the spring and neap tidal cycles. This is because tidal range is bigger during spring tides than during neap tides and results in the lower salinity with the peak ebb flow on spring (~15 PSU) than on neap (~20 PSU).

Three CTDs were used to observe the profiles at tidal inlet, Tairua Wharf and Pauanui Waterway for investigating the relationships between the tidal flow and water salinity stratification. Figure 6-7 summarises the tidal elevations, tidal currents, and wind at the three locations observed on 9 June, 2011. Figure 6-8 are the CTDs observed salinity values with water depth on the same day. Salinity

distribution features with water depth are investigated and discussed in four time segments (the segment A, B, C and D refer to Figure 6-7).

- **Segment A - low tide to slack tide during flooding**

Water salinity is the lowest after the ebb flow because the river flow has higher energy than the tidal flow at this moment. At the beginning of the flood flow, the salt seawater starts to come back into the estuary. However, the current speed is still not strong enough to mix the seawater with fresh water input from the river and it results in heavier seawater flowing beneath the lighter fresh river water at the tidal inlet at about 8.00am (Figure 6-8a). This is termed the salt wedge. The salt wedge extends landward, where it reaches the Tairua Wharf at about 8.30am (Figure 6-7b). However, the salinity difference between the water surface and bottom decreases from 10 PSU at the tidal inlet to about 3-4 PSU at the Tairua Wharf indicating some mixing has occurred. At the Pauanui Waterway, close to the river mouth, there is no salinity stratification because the seawater is well mixed with the river water and salinity increases from about 10 PSU to 25 PSU.

- **Segment B - slack tide to high tide during flooding**

During this period, surface elevations keep rising until the highest tidal elevation (0.6 m) is reached at about 1.00pm. The current speed increases to a maximum of 0.62 m s^{-1} at about 10.40am and decreases to the minimum of about 0 m s^{-1} at 1.18pm. During this period, the strength of flood tidal currents is higher than the river flow and as a result the estuary is well-mixed with salinity of about 35 PSU along the main channel.

- **Segment C - high tide to slack tide during ebbing**

After reaching the high water level during flooding, tides started to withdraw and flow seawards. Fresh water from the river mouth flows over the salt wedge at the Tairua Wharf and results in salinity stratification being established by 2.20pm (Figure 6-7b).

- **Segment D - slack tide to low tide during ebbing**

During this period, seawater mixes well with river fresh water and results in a rapid decrease of salinity from the upper estuary to the tidal inlet. Figure 6-9, Figure 6-10 and Figure 6-11 showed salinity variation with water depth observed by three CTDs at the tidal inlet, the Tairua Wharf (lower estuary) and the Pauanui

Waterway (upper estuary), respectively. These plots showed that river discharge causes an inflow with lower density and salinity above the heavier salty seawater, which resulted in the salinity stratification. Meanwhile, tidal flow induced mixing of the two layers due to the turbulence generated by the friction. At the area close to the estuary entrance, the tidal currents speed was higher; as a result, better mixing conditions occurred there. It could explain the water column is more homogenized with higher tidal currents at the tidal inlet and along the main channel at the lower reach of the estuary.

6.3.2.2 *Water Temperature*

Figure 6-6 is water temperature recorded by the four DataFlows at the Tairua Wharf and the Pauanui Waterway. The tidal elevation and air temperature are plotted in the same figures to investigate the impacts on the water temperature. At the Tairua Wharf, the maximum water temperature is 30.8°C, the minimum water temperature is 10.7°C, and the average water temperature is about 14.2°C. At the Pauanui Waterway, the maximum water temperature is 31°C, the minimum water temperature is 2.8°C, and the averaged water temperature is 12.7°C from 8 June to 12 July, 2011 (winter in New Zealand).

Model calculated vertical water temperature profiles were extracted from the tidal inlet to the upper estuary during one modelled tidal cycle on 10 June, 2011 (winter in New Zealand) and plotted in Figure 6-12 to investigate the water temperature regimes with tidal flow. In the lower estuary (e.g. the Tairua Wharf), the water temperature for water column is 13.5°C with the slack tides and 14.8°C at the high water during flood tides; water temperature is 14°C at the slack tides and 13.6°C at low water during ebb tides; and the mean water temperature at water surface during one tidal cycle is 14.0°C. In the upper estuary (e.g. the Pauanui Waterway), water temperature is 12°C at the slack tides and 12.4°C at high water during flood tides; water temperature is 12.25°C at the slack tides and 12°C at low water during ebb tides; and the mean water temperature on the water column during one tidal cycle is 12.2°C.

Figure 6-13 to Figure 6-16 present the model calculated horizontal distribution of water temperature from 10.40pm on 10 June to 8.20am on 11 June, 2011 (winter in NZ). On the slack tides during flooding, warmer seawater enters into the estuary. It increases water temperature to 13°C at the water surface and 12.75°C at the water bottom of tidal inlet and in the general vicinity. Water temperature is 11.75°C along the main channel and 12°C in the shallow water (i.e. the rectangular area in Figure 6-13). With high water during flood tides, more seawater comes into the estuary and distributes towards the river mouth. It is 14.6°C at the surface and 14°C at the water bottom. The seawater mixes well with

colder freshwater along the main channel and water temperature increases to 12.2-12.4°C, the shallow water increases to 12.4-12.6°C. On the slack tides during ebb tides, seawater flows seawards. Water temperature is 14.5-14.75°C at the surface and 14-14.25°C at the water bottom of tidal inlet and in the general vicinity. Water temperature is 11.75-12°C along the main channel and 12.25°C in the shallow water. And on the low tides during ebbing, water temperature is 14.4-14.8°C at the surface and 14-14.4°C at the water bottom of the tidal inlet. Water temperature is 11.6°C along the main channel and 12°C at shallow water.

These instrument data and model results suggest that the water temperature changes mainly with tidal flow at the lower estuary and with river discharge at the upper estuary. At the intertidal flat close to the Pauanui Waterway, water temperature varies not only with tidal flow and river discharge, but also with air temperature due to shallow water at this location.

However, the Dataflow observed at the Pauanui Waterway was 1% higher than the model results because the water is shallow and hence, sensitive to air temperature, however, air temperature is not considered in the model.

Water temperature is higher at water surface and distributes into estuary faster along the main channel, than the water at the bottom during flooding. It demonstrates that water temperature at water surface is more sensitive to air temperature and incoming radiations than on water bottom. Seawater at water surface withdraws seawards faster than the seawater at the water bottom during ebb tides and results in higher water temperatures at the water bottom than the water surface; water along the shoreline is colder than along the main channel within the estuary during flood tides and is warmer during the ebb tides. It is because of the higher friction of the shallow water along the shoreline and the hence slower flow velocity when compared to the water flow speed along the main channel, it also because of the shallower water depth.

6.3.3 Model Simulation Results

6.3.3.1 *Vertical Water Temperature*

Model calculated vertical water temperature profiles were extracted from the tidal inlet to the upper estuary during one tidal cycle on 10 June, 2011 (winter in New Zealand) and plotted in Figure 6-12 to investigate the water temperature regimes with tidal flow.

In the lower estuary (e.g. the Tairua Wharf), the model calculated water temperature for the water column is 13.5°C with the slack tides and 14.8°C at the

high tides during flooding; water temperature is 14°C at the slack tides and 13.6°C at low tides during ebbing; and the mean water temperature on the water surface during one tidal cycle is 14.0°C. In the upper estuary (e.g. the Pauanui Waterway), water temperature is 12°C at the slack tides and 12.4°C at high tides during flooding; water temperature is 12.25°C at the slack tides and 12°C at low tides during ebbing; and the mean water temperature on the water column during one tidal cycle is 12.2°C. The modelled results of water temperature was very close to the average water temperature recorded by the Dataflow deployed at the Tairua Wharf which was about 14.2°C and at the Pauanui Waterway which was about 12.7°C (discussed in Section 3.1). The water temperature observed by the Dataflow at the Pauanui Waterway was 1% higher than the model results because the water is shallow and hence, sensitive to air temperature, however, air temperature is not considered in the model.

The observed mean water temperature is 12°C within Tairua Estuary during winter. It is higher with high tides than with low tides. The averaged water temperature varies at different locations within the estuary. The maximum water temperature was 14.8°C at the tidal inlet with high tides and the minimum water temperature was 9.2°C at the upper estuary with low tides. The temperature gradient is strongest in the lower estuary (0-2 km from the tidal inlet), and in the river channel (about 6-8 km from the tidal inlet). The maximum water surface temperature was 1.8°C higher than the bottom temperature at the lower estuary and about 0.4°C for the river channel with peak flood tides. Water temperature in the upper estuary (2-6 km from the tidal inlet) is homogenous because the water is shallow and well-mixed there. However, there is temperature stratification found at high water level in the river channel because of the colder river water located at the junction between the tidal dominated lower estuary and the river dominated upper estuary.

6.3.3.2 *Horizontal Water Temperature*

Figure 6-13 to Figure 6-16 present the horizontal profiles of water temperature for slack tides and high tides during flooding, slack tides and low tides during ebbing from 10.40pm on 10 June to 8.20am on 11 June, 2011 (winter in NZ).

On the slack tides during flooding, warmer seawater goes into the estuary; it increases water temperature to 13°C at the water surface and 12.75°C at the water bottom of the tidal inlet and in the general vicinity of the tidal inlet. Water temperature is 11.75°C along the main channel and 12°C in the shallow water (i.e. the rectangular area in Figure 6-13). On the high tides during flooding, more seawater comes into the estuary and distributes towards the river mouth. It is 14.6°C at the surface and 14°C at the water bottom. The seawater mixes well with

colder freshwater along the main channel and water temperature increases to 12.2-12.4°C, the shallow water increases to 12.4-12.6°C. On the slack tides during ebbing, seawater flows seawards. Water temperature is 14.5-14.75°C at the surface and 14-14.25°C at the water bottom of the tidal inlet and in the general vicinity of the tidal inlet. Water temperature is 11.75-12°C along the main channel and 12.25°C in the shallow water. And on the low tides during ebbing, water temperature is 14.4-14.8°C at the surface and 14-14.4°C at the water bottom of the tidal inlet. Water temperature is 11.6°C along the main channel and 12°C in the shallow water.

Figures 6-13 to Figure 6-16 presented the horizontal and vertical water temperature at the Tairua tidal inlet and within the Tairua Estuary. Water temperature is higher at the water surface and distributes into the estuary faster along the main channel, than the water at the bottom during flooding; seawater at the water surface withdraws seawards faster than the seawater at the water bottom during ebb tides and results in higher water temperatures at the water bottom than the water surface; water along the shoreline is colder than along the main channel within the estuary during flood tides. It is because of the higher friction of the shallow water along the shoreline and the hence slower flow when compared to the water flow speed along the main channel.

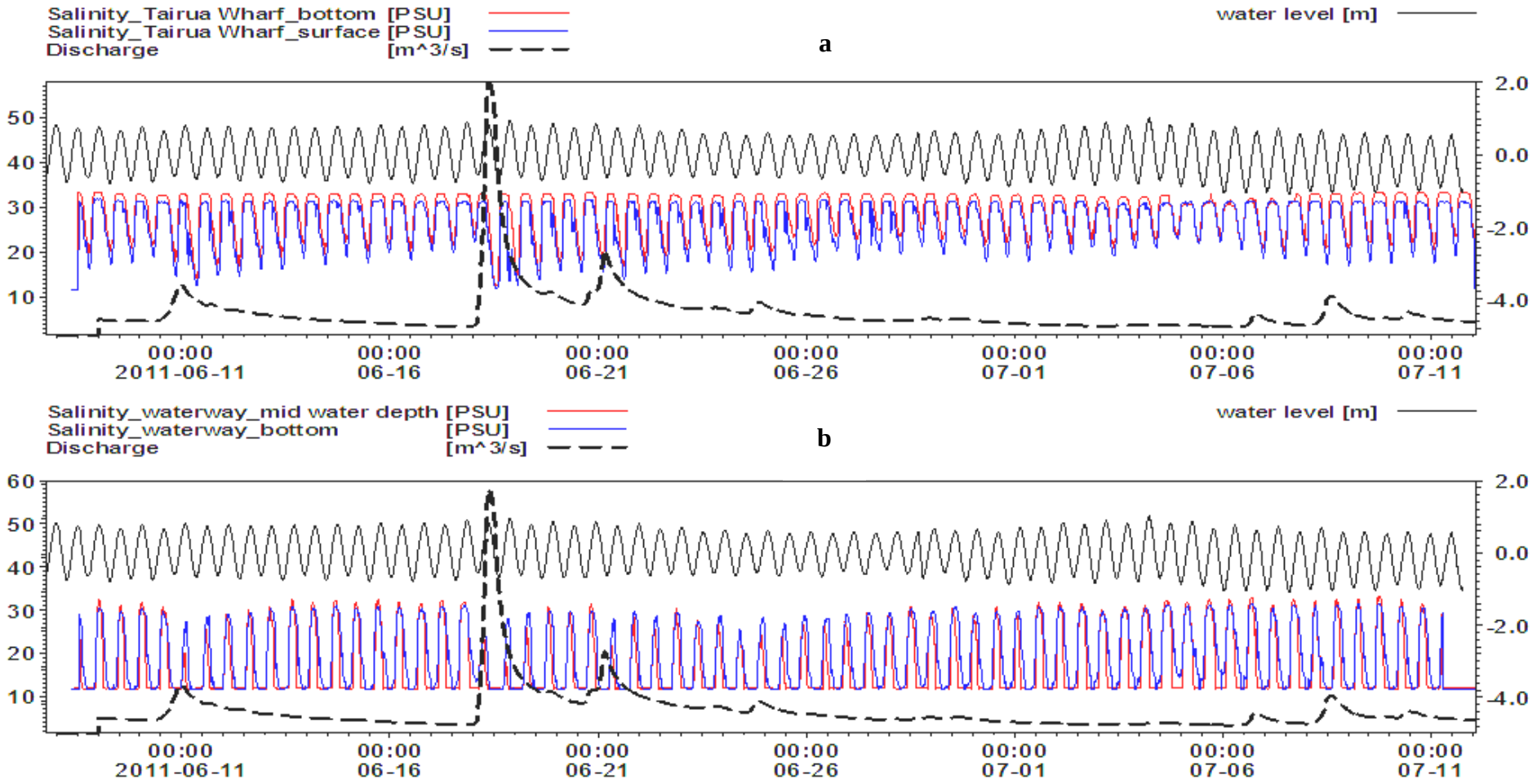

Figure 6-5 Dataflows recorded salinity on water bottom (blue solid), salinity at mid water depth (red solid) comparing with tidal elevation (black solid) and Tairua River freshwater discharge (black dot) at (a) Tairua Wharf and (b) Pauanui Waterway.

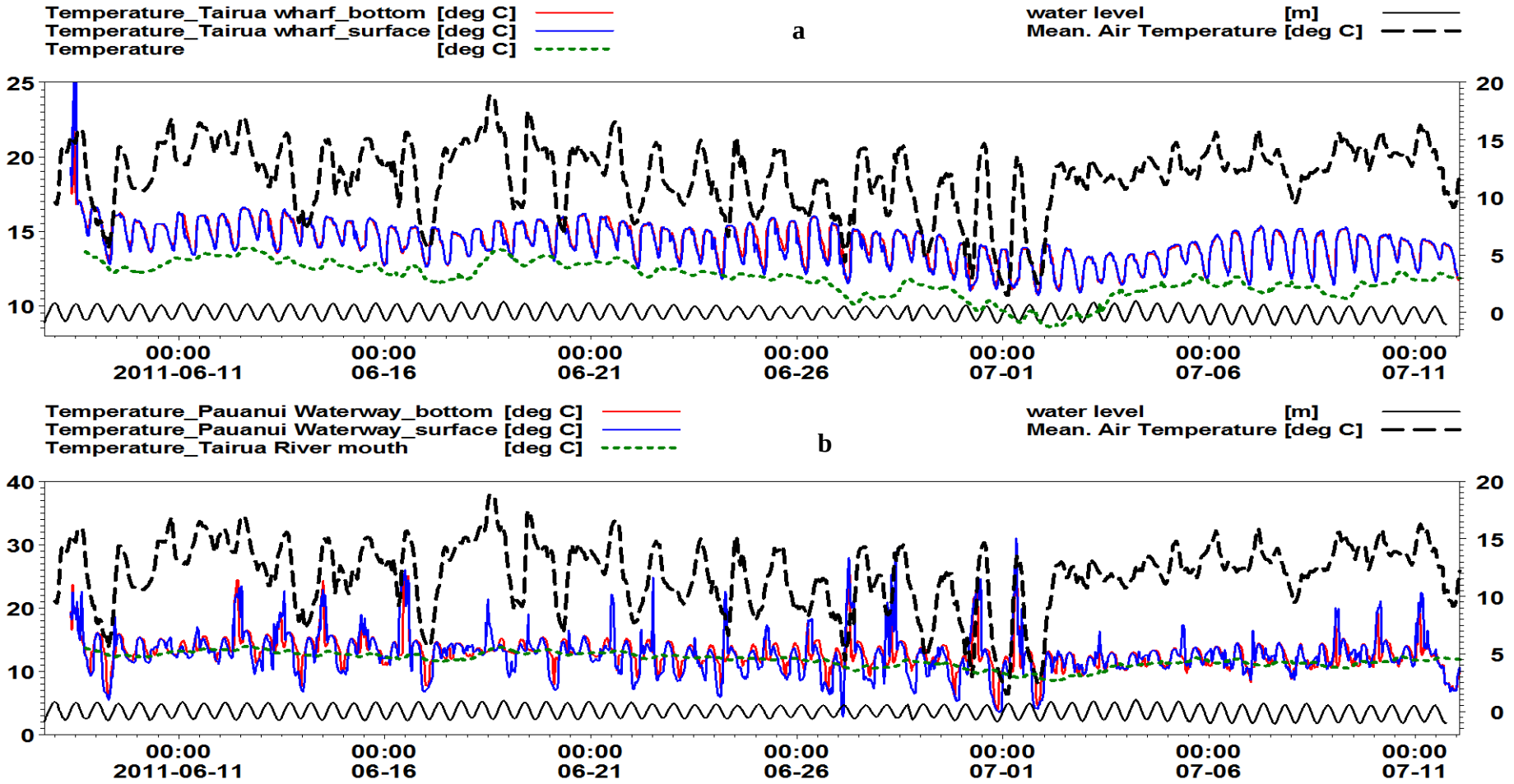

Figure 6-6 Dataflows observed water temperature on water bottom (red solid), water temperature at water surface (blue solid) comparing with tidal elevation (black solid), mean air temperature (black dot) and water temperature at Tairua River mouth (green dot) at (a) Tairua Wharf and (b) Pauanui Waterway..

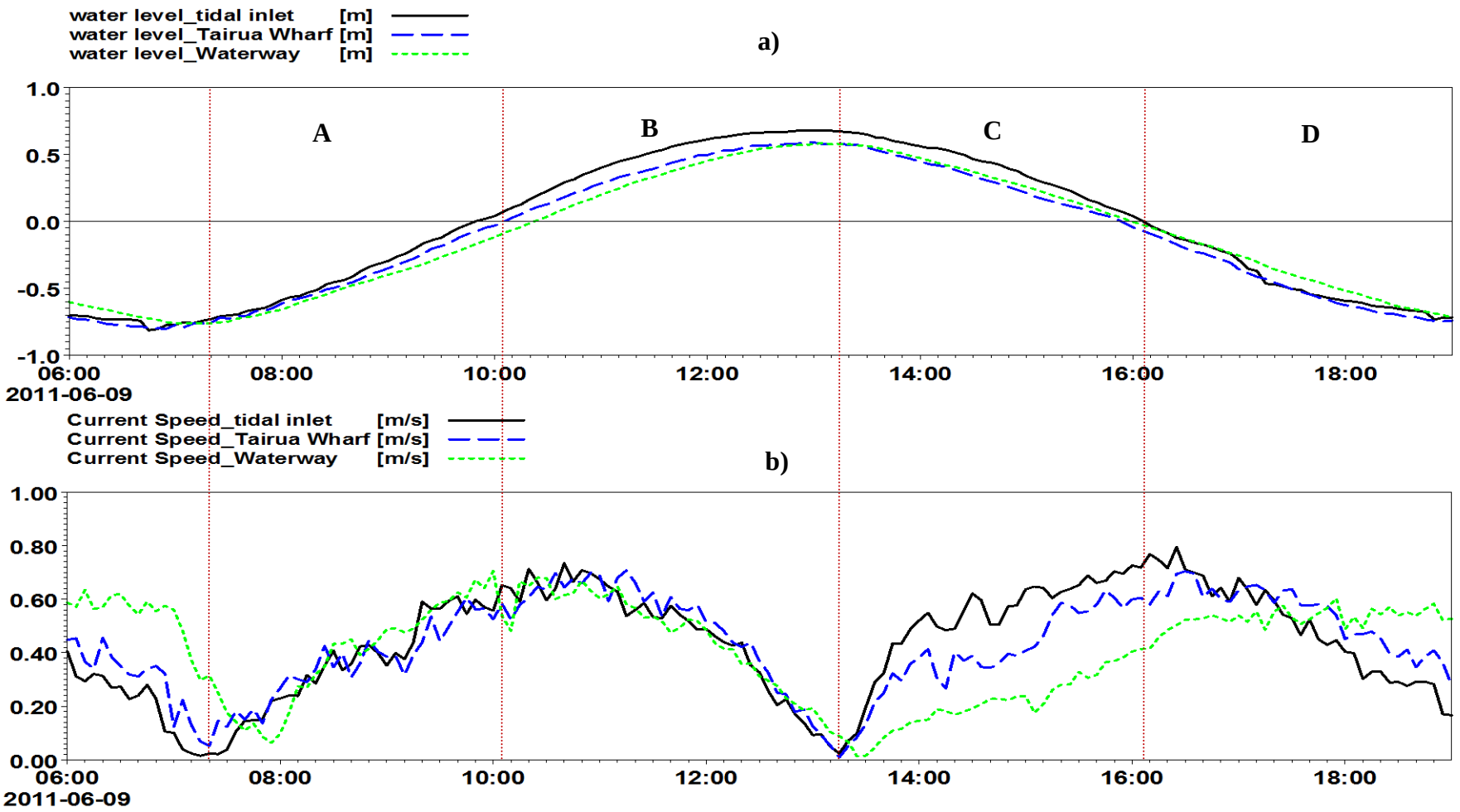

Figure 6-7 (a) Surface elevations and (b) current speed observed by the three ADVs from 6.00am to 7.00pm on 9 June, 2011 at Tairua tidal inlet, Tairua Wharf and Pauanui Waterway where the CTDs were cast.

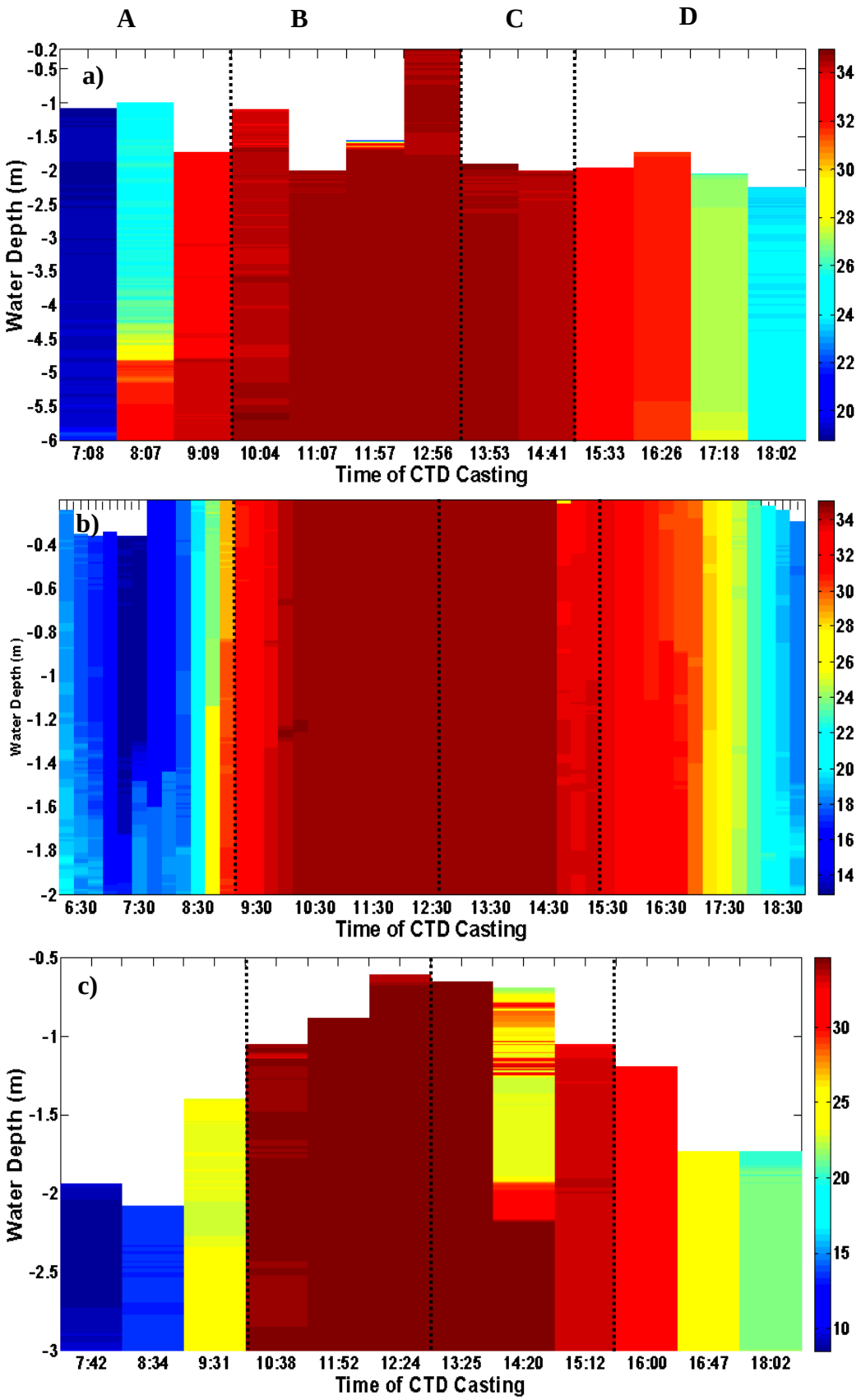

Figure 6-8 CTD observed water salinity at a) Tairua tidal inlet, b) Tairua Wharf, and c) Pauanui Waterway at the lower estuary on 9 June 2011. The areas A, B, C and D are four different periods in one tidal cycle shown in Figure 6-7.

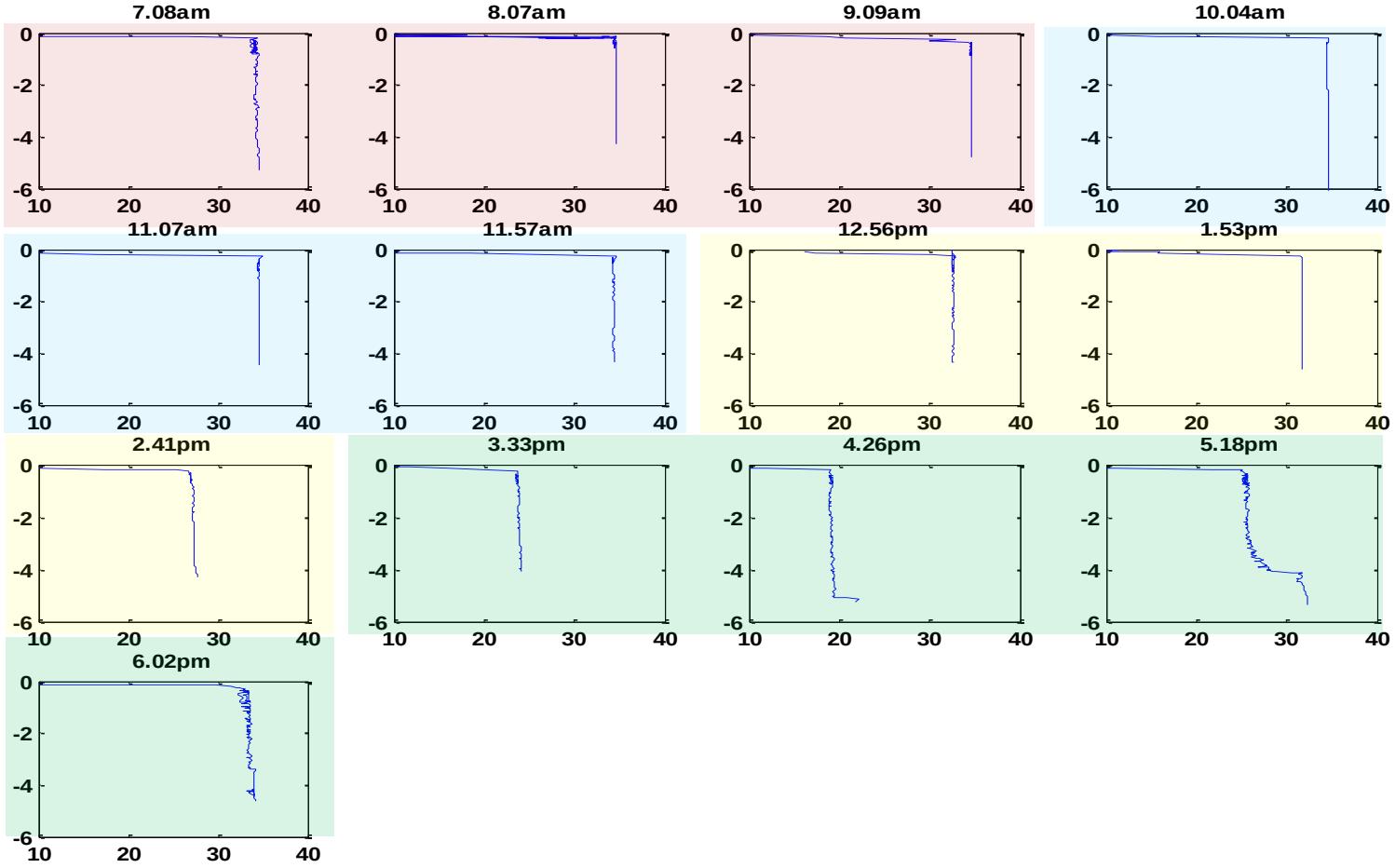

Figure 6-9 Vertical profile of CTD observed water salinity every 1 hour at Tairua tidal inlet on 9 June, 2011. The red, green, yellow and blue background present the different periods A, B, C and D in one tidal cycle which were shown in Figure 6-7 and Figure 6-8.

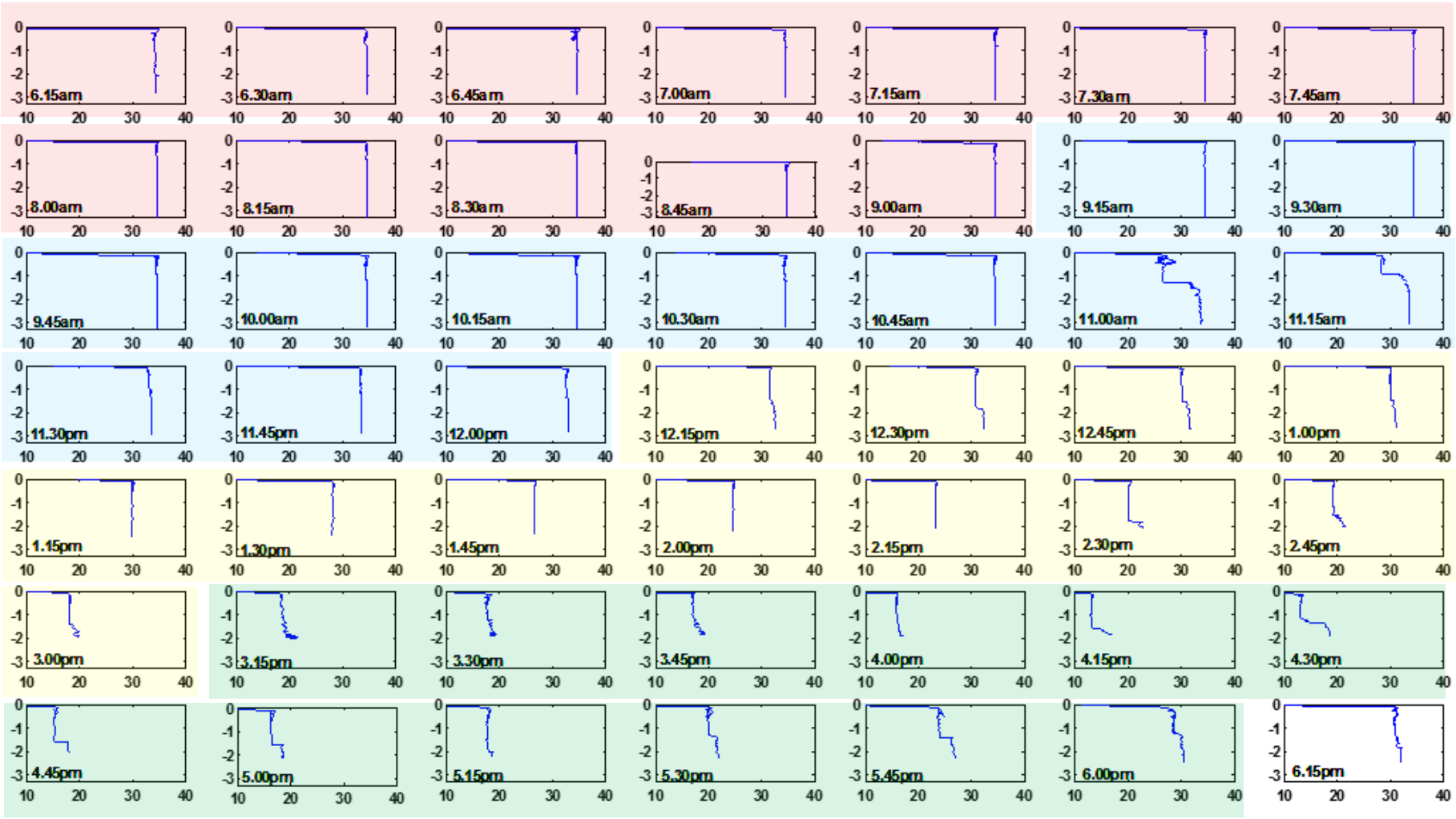

Figure 6-10 Vertical profile of CTD observed water salinity every 15 minutes at Tairua Wharf on 9 June, 2011. The red, green, yellow and blue background present the different periods A, B, C and D in one tidal cycle which were shown in Figure 6-7 and Figure 6-8.

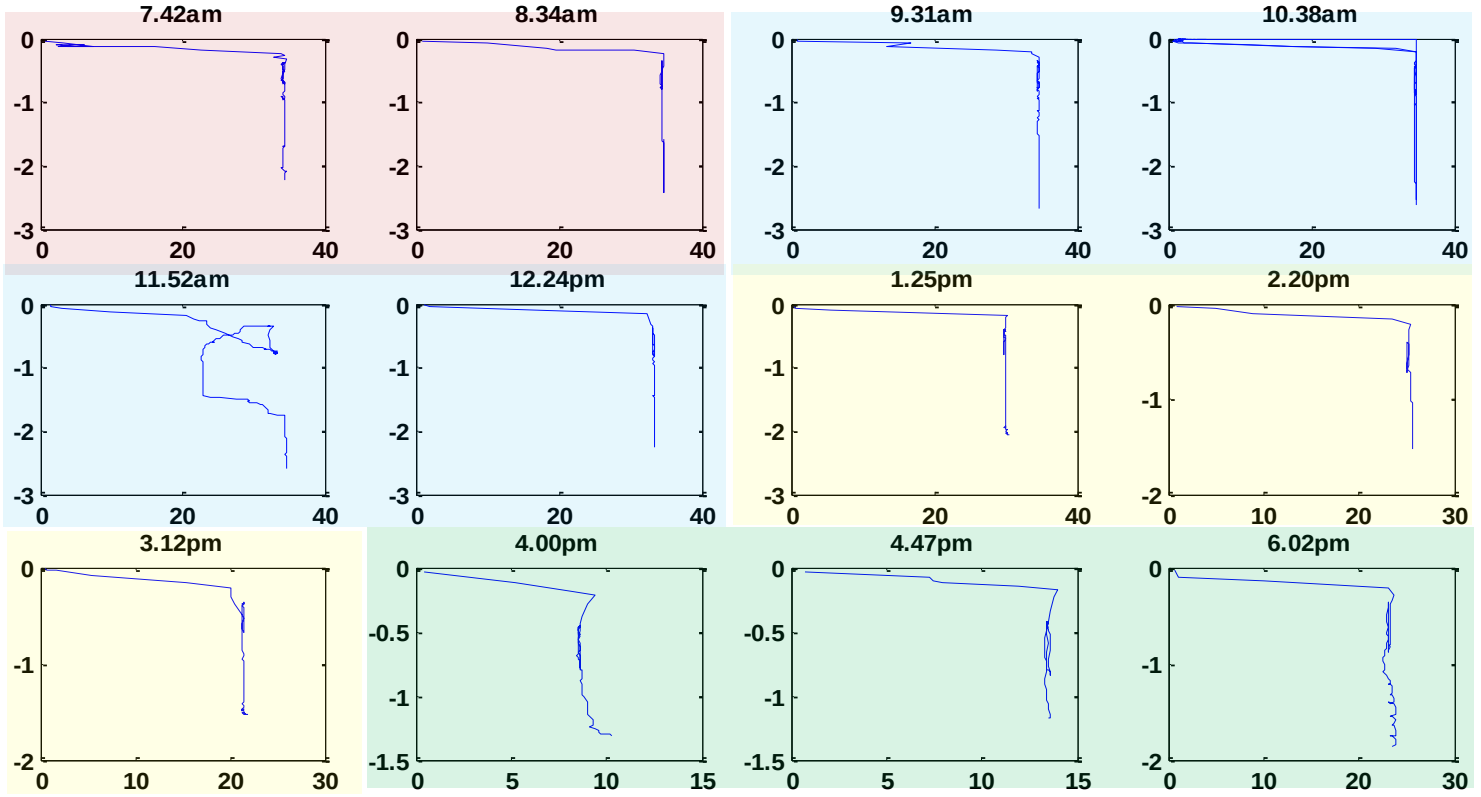

Figure 6-11 Vertical profile of the CTD observed water salinity every 1 hour at Pauanui Waterway on 9 June, 2011. The red, green, yellow and blue background present the different periods A, B, C and D in one tidal cycle which were shown in Figure 6-7 and Figure 6-8.

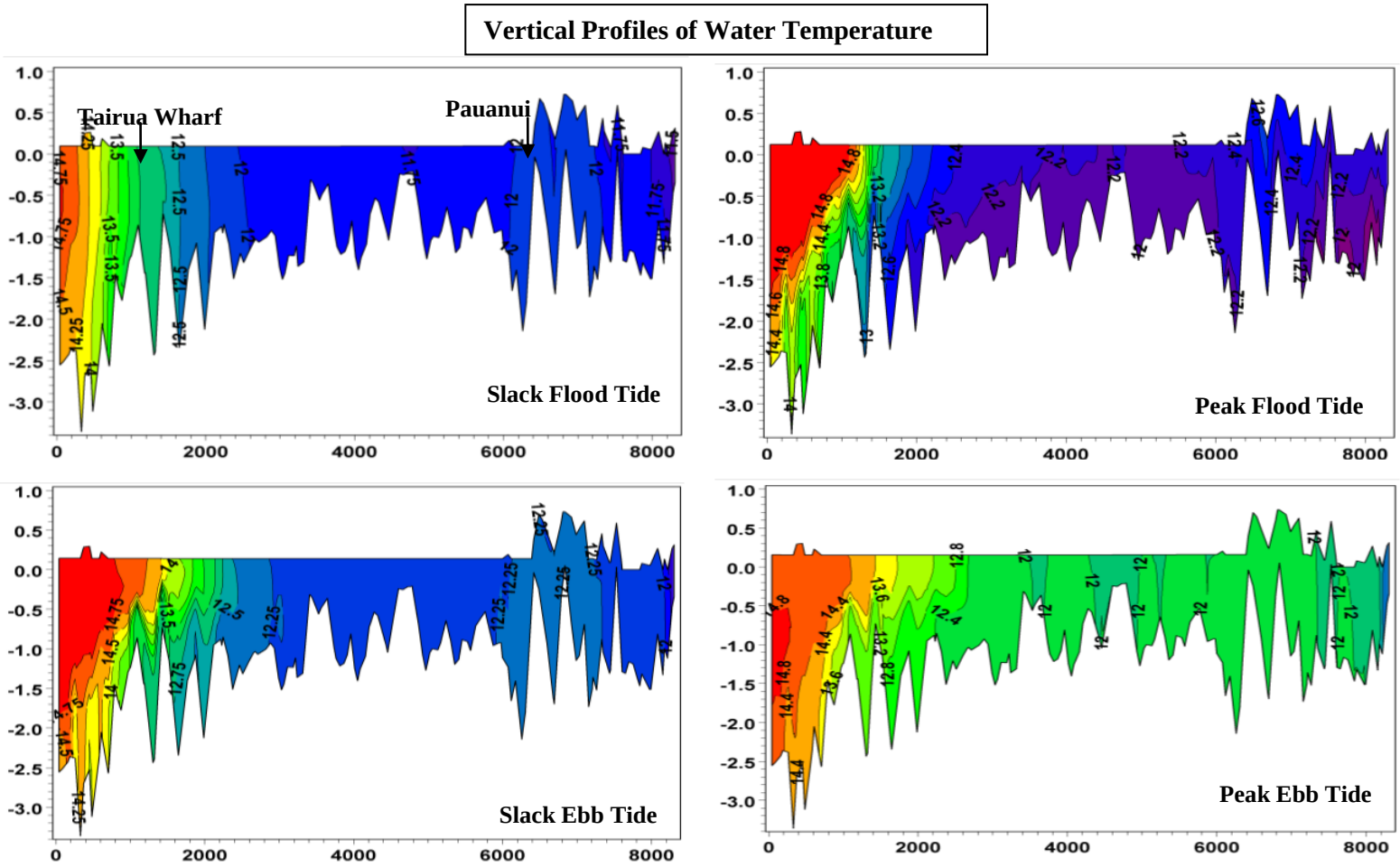

Figure 6-12 Vertical profiles of water temperature calculated by the MIKE 3 FM Flow model from Tairua tidal inlet to Tairua River mouth at a) slack flood, b) peak flood, c) slack ebb and d) peak ebb from 10.40pm 10 June to 8.20am 11 June, 2011 (winter in NZ).

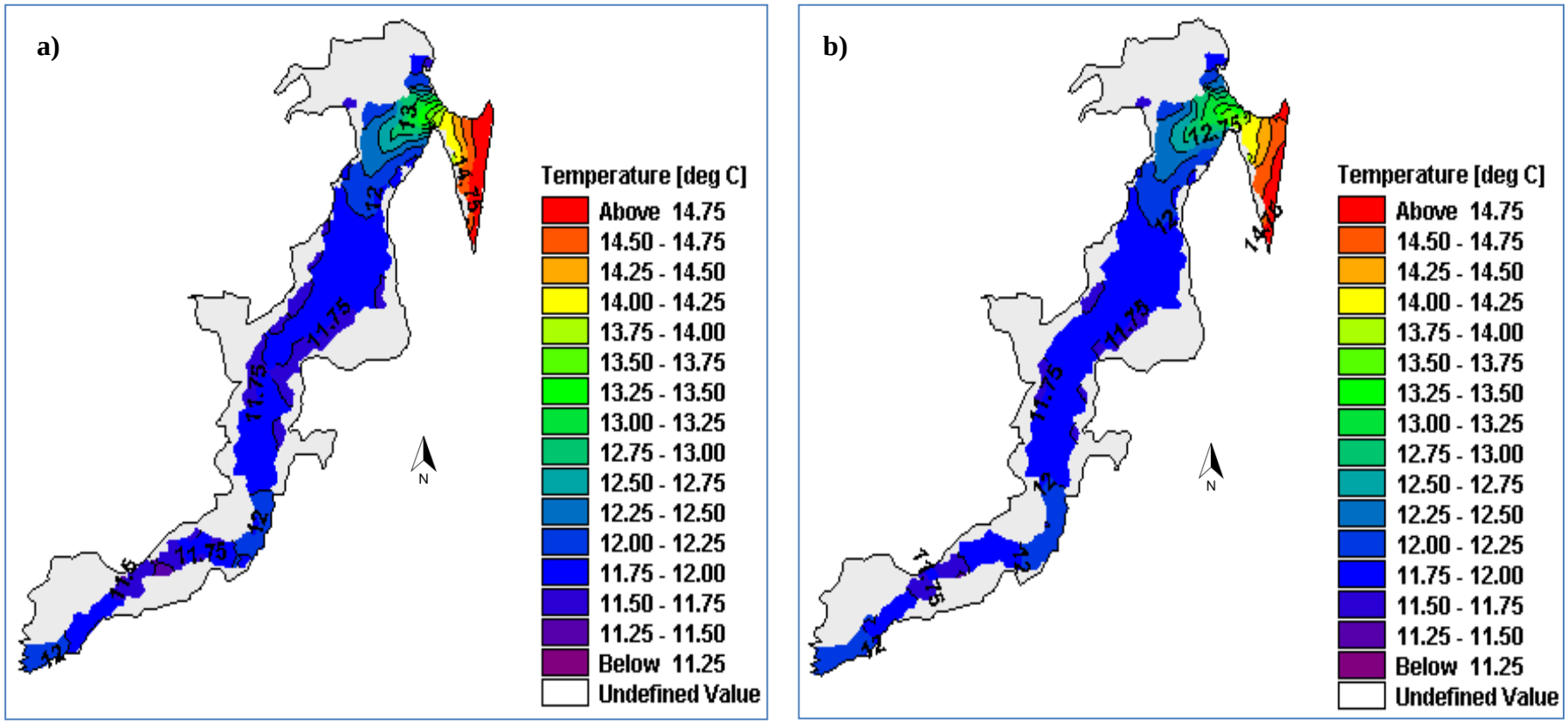

Figure 6-13 Horizontal water temperature at (a) water surface and (b) water bottom calculated by the MIKE 3 FM flow model at the slack flood tides from 10.40pm 10 June to 8.20am 11 June, 2011 (winter in NZ).

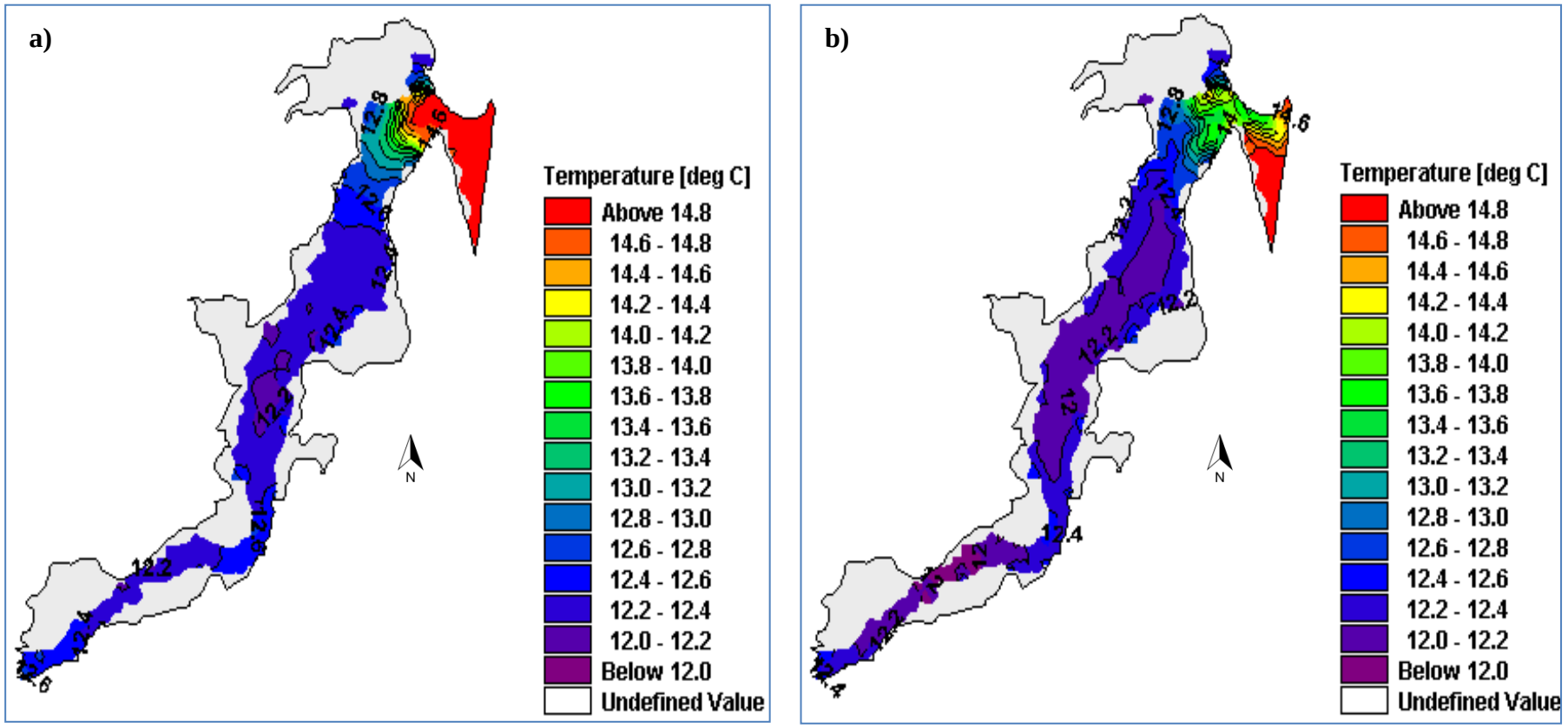

Figure 6-14 Horizontal water temperature at (a) water surface and (b) water bottom calculated by the MIKE 3 FM Flow model at the peak flood tides from 10.40pm 10 June to 8.20am 11 June, 2011 (winter in NZ).

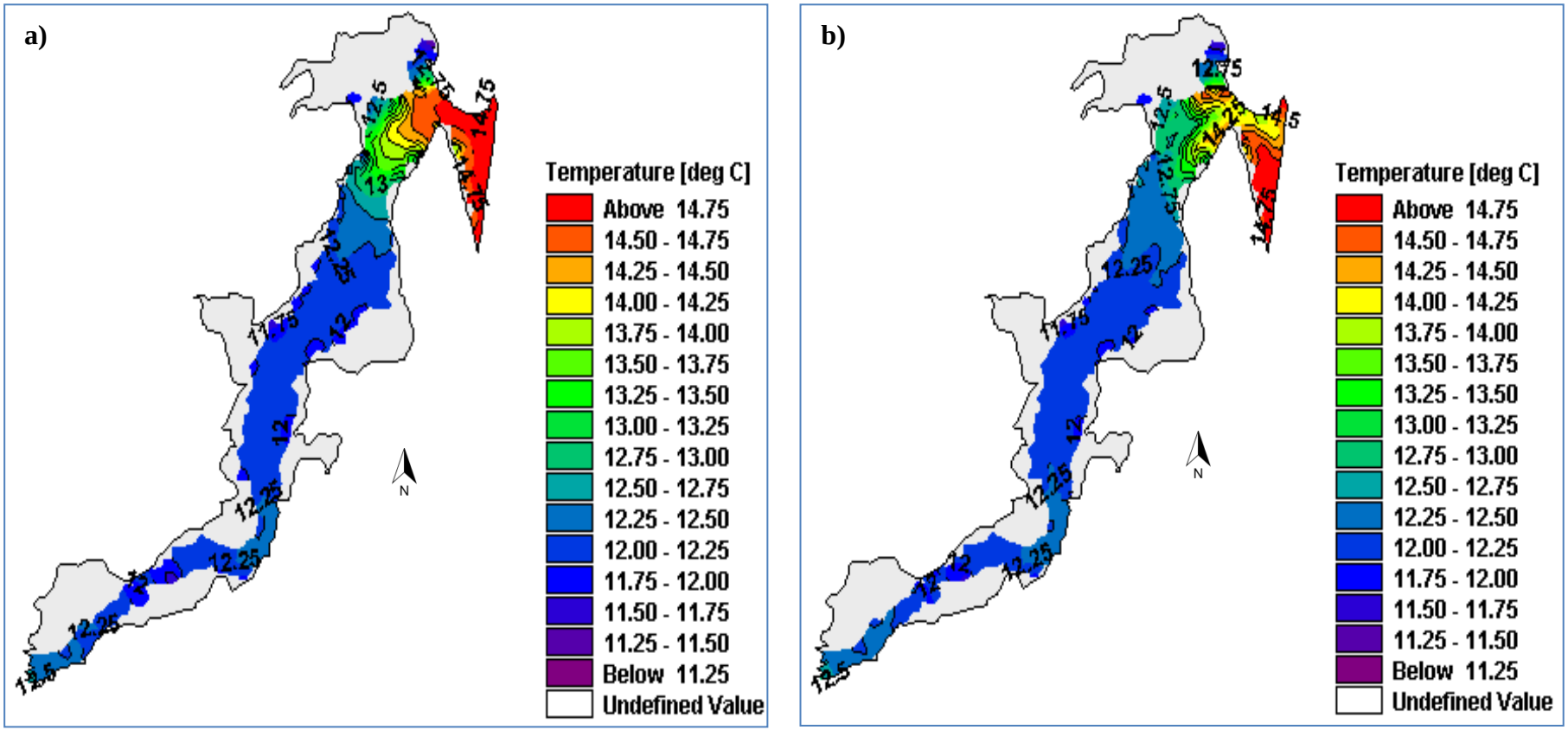

Figure 6-15 Horizontal water temperature at (a) water surface and (b) water bottom calculated by the MIKE 3 FM Flow model at the slack ebb tides from 10.40pm 10 June to 8.20am 11 June, 2011 (winter in NZ).

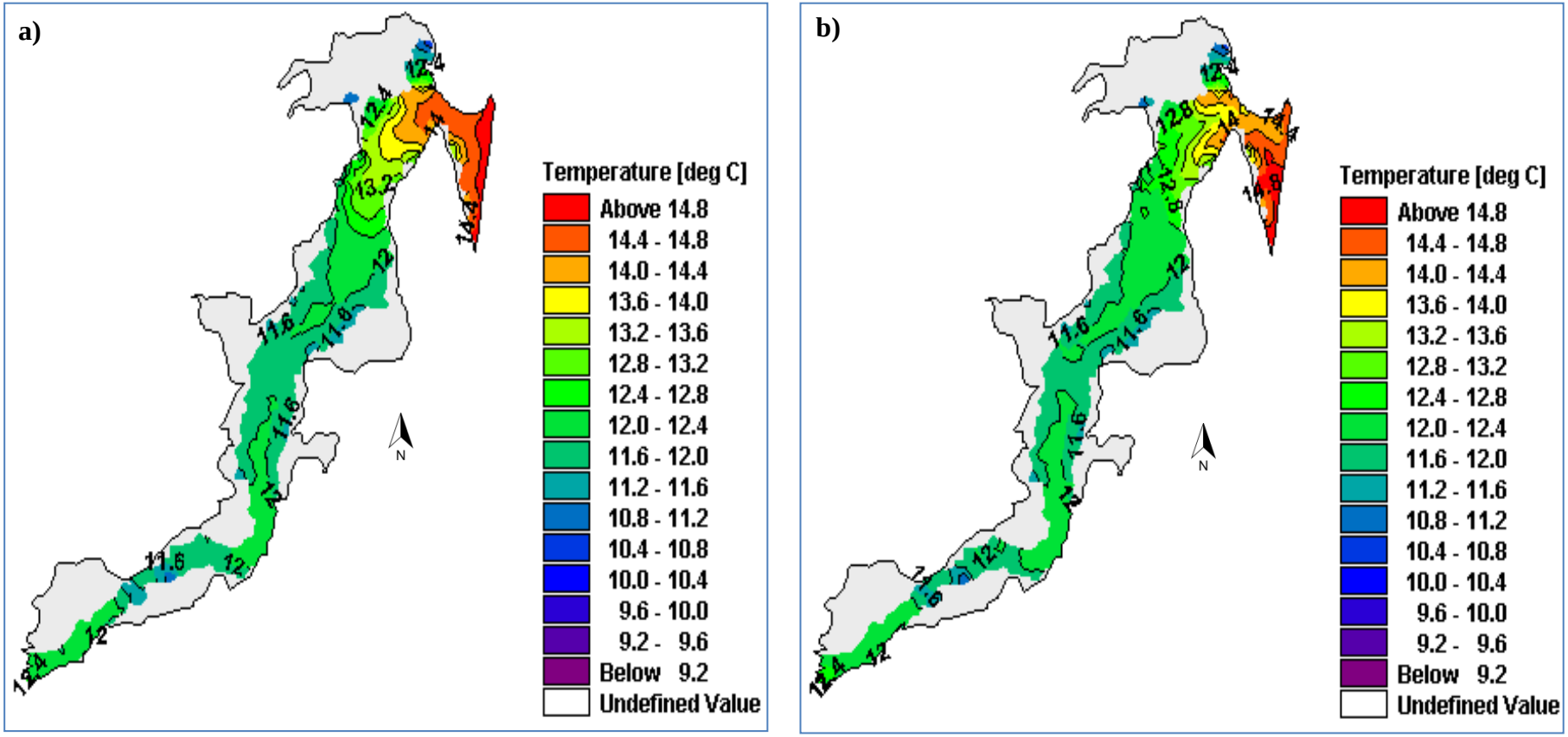

Figure 6-16 Horizontal water temperature at (a) water surface and (b) water bottom calculated by the MIKE 3 FM Flow model at the peak ebb tides from 10.40pm 10 June to 8.20am 11 June, 2011 (winter in NZ).

6.4 CONCLUSIONS

A MIKE 3 Flow FM Model were run, the boundary files included time series of tidal flow, river discharge, wind conditions and air temperature. The original water temperature and salinity were input at the two ends of the estuary, they are the tidal inlet and the Tairua River mouth.

Basing on the Richardson equation, Tairua Estuary was estimated as highly stratified with high river flow (>200 $m^3 s^{-1}$) but low current speed; and it is partially-stratified or well mixed with high river discharge (>200 $m^3 s^{-1}$) and a current speed higher than 0.5 m s^{-1}. It also indicates that tidal current speed and river flow are the two main factors impacting on the estuarine stratification. The higher the river flow, the higher the possibility of water stratification for a given current speed at the Tairua tidal inlet. Less stratification occurs with higher current speed at a given river flows. This is because the higher tidal flow has higher energy and, therefore, mixes well with the river flow to generate turbulent flow and as a result a homogenous water column. Dyer (1979) classified Tairua Estuary as a partially-mixed estuary. He also suggested that there is considerable friction between water and estuary bottom to create turbulence. Turbulence tends to mix the water column more effectively than entrainment, causing the salinity to decrease to the head of the estuary in the lower layer and to increase progressively towards the sea in the surface layer; though there is no water movement, there is salt exchanging vertically; the landward flow at the bottom can be of order 0.05 m s^{-1} with tidal oscillations of 0.5 m s^{-1}.

Water temperature varies with tidal flow, river discharge, locations and air temperature over the intertidal flats. It is higher at water surface than water bottom, and distributes from the tidal inlet to the upper estuary with tidal flow. The averaged water temperature varies at different locations within the estuary. The maximum water temperature was 14.8°C at tidal inlet with high tides and the minimum water temperature was 9.2°C at the upper estuary with low tides. The temperature gradient is strongest in the lower estuary (0-2 km from the tidal inlet), and in the river channel (about 6-8 km from tidal inlet). The maximum water surface temperature was 1.8°C higher than the bottom temperature at the lower estuary and about 0.4°C for the river channel with peak flood tides. Water temperature in the upper estuary (2-6 km from the tidal inlet) is homogenous because the water is shallow and well-mixed there. However, there is temperature stratification found at high water level in the river channel because of the colder river water located at the junction between the tidal dominated lower estuary and the river dominated upper estuary.

The MIKE 3 Flow FM model simulation results are consistent with the instruments (Dataflows) observations indicating that the MIKE 3 HD FM module

is a suitable tool for the study on horizontal distribution and vertical profiles of water salinity and temperature within the estuaries.

CHAPTER SEVEN
FORCING MECHANISMS OF SEICHE HAZARD AND IMPACTS ON SEDIMENT TRANSPORT

A seiching event was observed from 4th to 5th of August, 2010. This chapter analyses the water elevation and current speed data with the spectrum analysis tool of MATLAB and calibrates a depth-averaged hydrodynamic model to study the potential forcing mechanisms of this observed event; and develops a three dimensional non-cohesive sediment transport model to investigate the impacts of seiche on the sediment transport in Tairua Estuary. A heavy wind together with a sediment-laden flood discharged from the Tairua River mouth to the lower reach of Tairua Estuary, pulses of turbid water migrated to the lower reach of Tairua Estuary in a salt wedge under the river flow and resulted in density stratification before the seiche event, which resulted in flow instability with the pycnocline, forming the seiche event. The absence of seiche in the rest of the recorded floods suggested that flood, sediment stratification and heavy wind are the three forcing mechanics of the seiche occurred on 4 August, 2010.

7.1 INTRODUCTION

7.1.1 Research Background

During the field campaign undertaken from 27 July, 2010 to 4 September, 2010, the RBR tide gauge captured three significant flood events at the Tairua River mouth. The Acoustic Doppler Velocity meters (ADV) also captured water elevation and current speed fluctuations from about 5.00pm on 4 August, 2010 to 4.15am on 5 August, 2010 in the lower reaches of Tairua Estuary (Figure 7-1).

Understanding the forcing mechanisms of a seiche event is important because seiches affect the residual circulation, and hence the regions of potential sediment deposition. And a seiche plays a significant role in determining the position and strength of the salt wedge, the thickness of the diffusive bottom boundary layer and the overall dispersion characteristics of the system (Luettich, 2000). However, the forcing mechanisms of a seiche event within estuaries and its impacts on estuarine sediment transport pattern had not been studied and published. This study supplied a method to study the seiche hazard within estuary basing on numerical modelling. It is valuable in the case of not enough data.

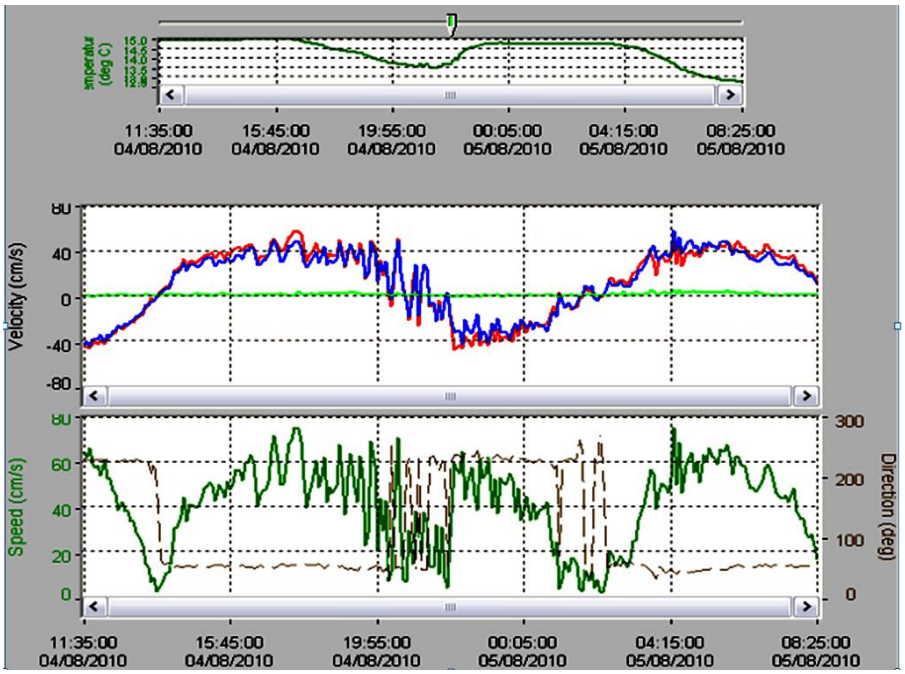

Figure 7-1 Water temperature (°C), water pressure (dBar) and current speed (cm s^{-1}) & direction (°) recorded by the three Acoustic Doppler Velocity meters (ADV) during the flood discharge from Tairua River upstream on 4 Aug., 2010.

7.1.2 Seiche Characteristics

A seiche is an oscillating response of an enclosed or semi-enclosed water body to external forcing that occurs in order to return the system to equilibrium (Luettich et al, 2000). The official definitions of a seiche event from the U.S. Army Corps of Engineers (2006) include

- A standing wave oscillation of an enclosed water body that continues, pendulum fashion, after the cessation of the originating force, which may have been either seismic or atmospheric;
- An oscillation of a fluid body in response to a disturbing force having the same frequency as the natural frequency of the fluid system;
- Any sudden rise in the water of a harbour or a lake whether or not it is oscillatory.

The seiches in harbours can generate strong and unpredictable currents affecting the safety of ships entering or leaving the harbor, and under extreme conditions these can also cause damage to moored vessels.

Understanding the forcing mechanisms of a seiche event is important because it has been recognized that seiches affect the residual circulation, and hence the regions of potential sediment deposition. A seiche plays a significant role in

determining the position and strength of the salt wedge, the thickness of the diffusive bottom boundary layer and the overall dispersion characteristics of the system (Luettich, 2000). On the Murray River, Australia, wind-forced seiche events induced hydraulic damming of the river and flow reversals that resulted in flooding of a local lagoon and replenishment of wetlands proximal to the river. Most of the great floods of Venice were associated with seiches caused by low air-pressure and the strong long-lasting Adriatic Sirocco wind, and appear mostly in the October–December period (Raicich, 2003).

7.1.3 Research Objectives

This study analysed the observed water elevation and current speed with the spectrum analysis tool of MATLAB to define the seiche event. A depth-averaged hydrodynamic model was set up and calibrated to investigate the potential forcing mechanisms using the field meteorological data and the numerical models simulation results. A three dimensional non-cohesive sediment transport model was developed to investigate the impacts of seiche on the sediment transport in Tairua Estuary.

7.2 METHODS

7.2.1 Spectrum Analysis

The observation data collected contains a lot of non-seiche components. For example, currents or changes in pressure due to tides and waves. Therefore, the water level data needs to be extracted to provide relevant information. This may be done in various ways, including wavelet analysis, detrending or filtering the data, or simple observation of the data.

Eight ocean tidal constituents (M2, S2, N2, K2, K1, O1, P1, and Q1) are the principal tides presented for the New Zealand area (Pugh, 1987).

In this research, the MATLAB ‘Butter’ function was used to filter the M2, S2, N2, K2, K1, O1 and P1 lower frequency oscillations from water elevations and currents, so that only the high frequency seiche was left. And then the MATLAB ‘FFT’ function was used to calculate the seiche periods.

7.2.2 MIKE 21 HD Model Development

The MIKE 21 HD model was developed and calibrated as discussed in Chapter 4. Four MIKE 21 HD models were run to study the impacts of the wind and the river discharge on the surface elevation and current speed. Model 1 and 2 were run with and without a river discharge boundary; Model 3 and 4 were run with and without wind input, respectively (Table 7-1).

Table 7-1 Scenarios to study the effects of Tairua River flow and wind conditions

Model	Bathymetry	Grid	Boundary	Wind
1	Estuary_River_20m	20 m	Offshore Tides	Yes
2		20 m	Offshore Tides + River Discharge	Yes
3		20 m	River Discharge	Yes
4		20 m	River Discharge	No

7.2.3 MIKE 3 FM HD and MIKE 3 FM ST Model Development

A MIKE 3 FM HD model was developed using a 10 sigma layer bathymetry (Figure 7-2), the fresh water salinity was set as 0, the sea water salinity was 32, the offshore tides boundary was extracted from the MIKE 21 HD model, and the river discharge boundary was same as the one used in the MIKE 21 HD model. It was run from 12.00am on 1 August 2010 to 12.00am on 8 August 2010 to make sure the model was stable enough before seiche analyses during the seiche event from 4 August 2010 to 5 August 2010. The time step was 10 seconds to keep the critical CFL lower than 0.8. Bed resistance was 0.1 and eddy viscosity was 0.1 based on the Smagorinsky formulation.

To better understand the impacts of the seiche event on the sedimentation in the lower estuary, a MIKE 3 FM ST (sand transport) model was run based on the MIKE 3 FM no-cohesive sediment transport model. The sediment properties were set in the model including the sand median grain size (0.39 mm), porosity (0.4) and relative density (2.65). The horizontal and vertical sediment dispersion was set as constant 1 based on the scaled eddy viscosity formulation. The heat exchange parameter was set as a constant 0.5 for Dalton's Law. The initial water temperature and water salinity were set as 10°C and 34 PSU, respectively. Nineteen points from the tidal inlet to Tairua Waterway were selected to extract the vertical profile (Figure 7-3).

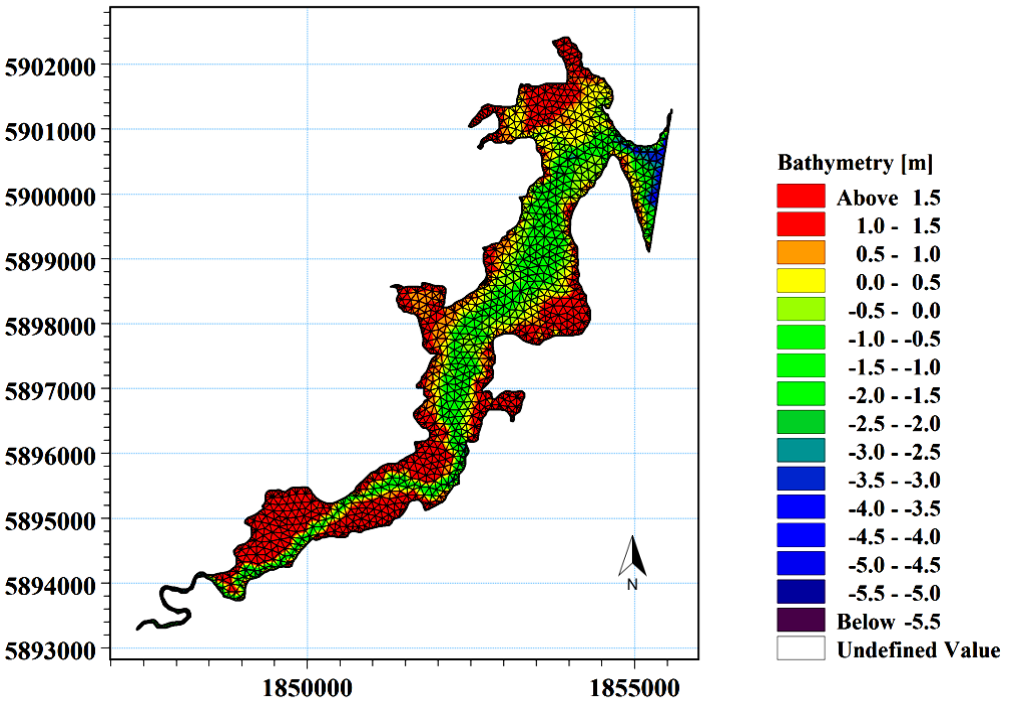

Figure 7-2 The bathymetry with flexible triangle meshes generated for the MIKE 3 FM ST model.

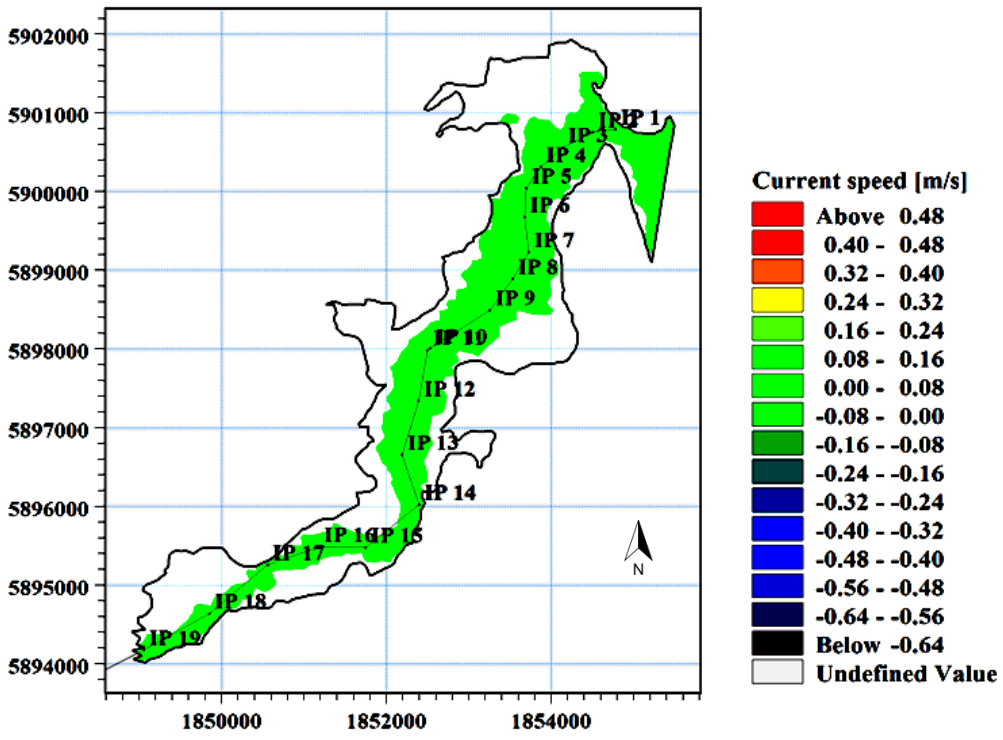

Figure 7-3 The points for vertical profile extracting.

7.2.4 Meteorological and Field Data

As discussed in Chapter 3, a field deployment was undertaken from July 27 to September 4, 2010. The instruments consisted of two InterOcean S4ADWs, one Sontek ADP, three Sontek ADVs, one DOBIE tide gauge, one SCUFA Fluorometer, and one RBR Tide Gauge (Figure 3-1). Additional meteorological data were obtained including the rainfall data from the Pinnacles Mountain Station, wind speed and direction from Slipper Island, atmosphere pressure and daily air temperature from Whitianga. The Waikato Regional Council supplied the tidal elevations at Thames and Whitianga.

7.3 RESULTS

7.3.1 Results of Spectral Analyses

The water elevations and the current speed observed by the three ADVs after filtering at the M2, S2, N2, K2, K1, O1 and P1 tides are plotted in Figure 7-4 and Figure 7-5. There are obvious pulses of water elevation and current speed during the seiche event. Figure 7-6 showed the phase difference between water elevations and current speed. And the results of the spectral analysis shown in Figure 7-7 indicate that water level fluctuations observed by the ADV current meter has an average period of 20.89 minutes with the maximum magnitude of 0.18 m at the moorings close to the tidal inlet; an average period of 17.78 minutes with the maximum magnitude of 0.14 m observed at the Tairua Wharf; and an average period of 20.93 minutes with the maximum magnitude of 0.07 m at the Pauanui Waterway.

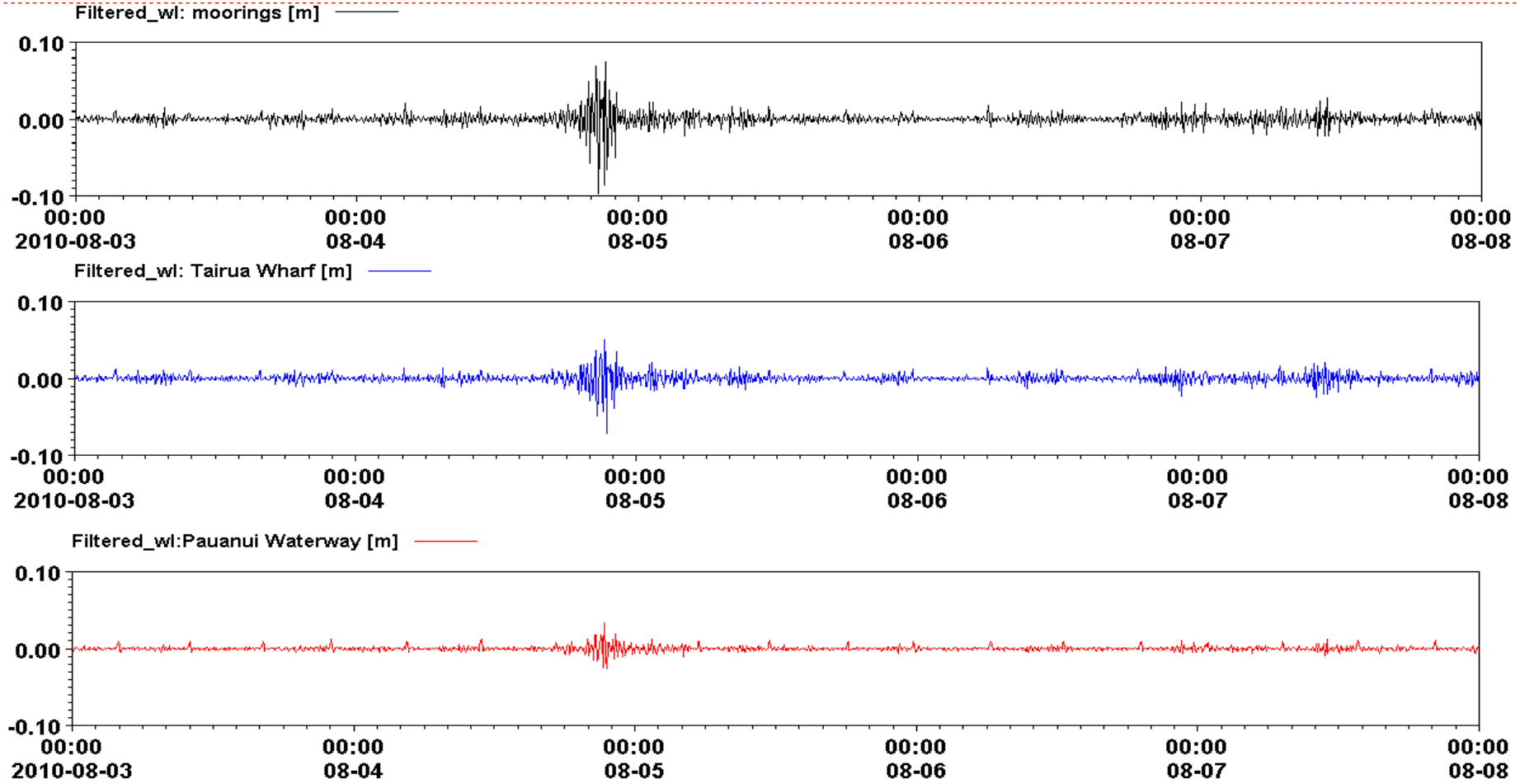

Figure 7-4 Surface elevation observed by the ADV1, ADV2 and ADV3 after filtering the M2, S2, N2, K2, K1, O1 and P1 tides

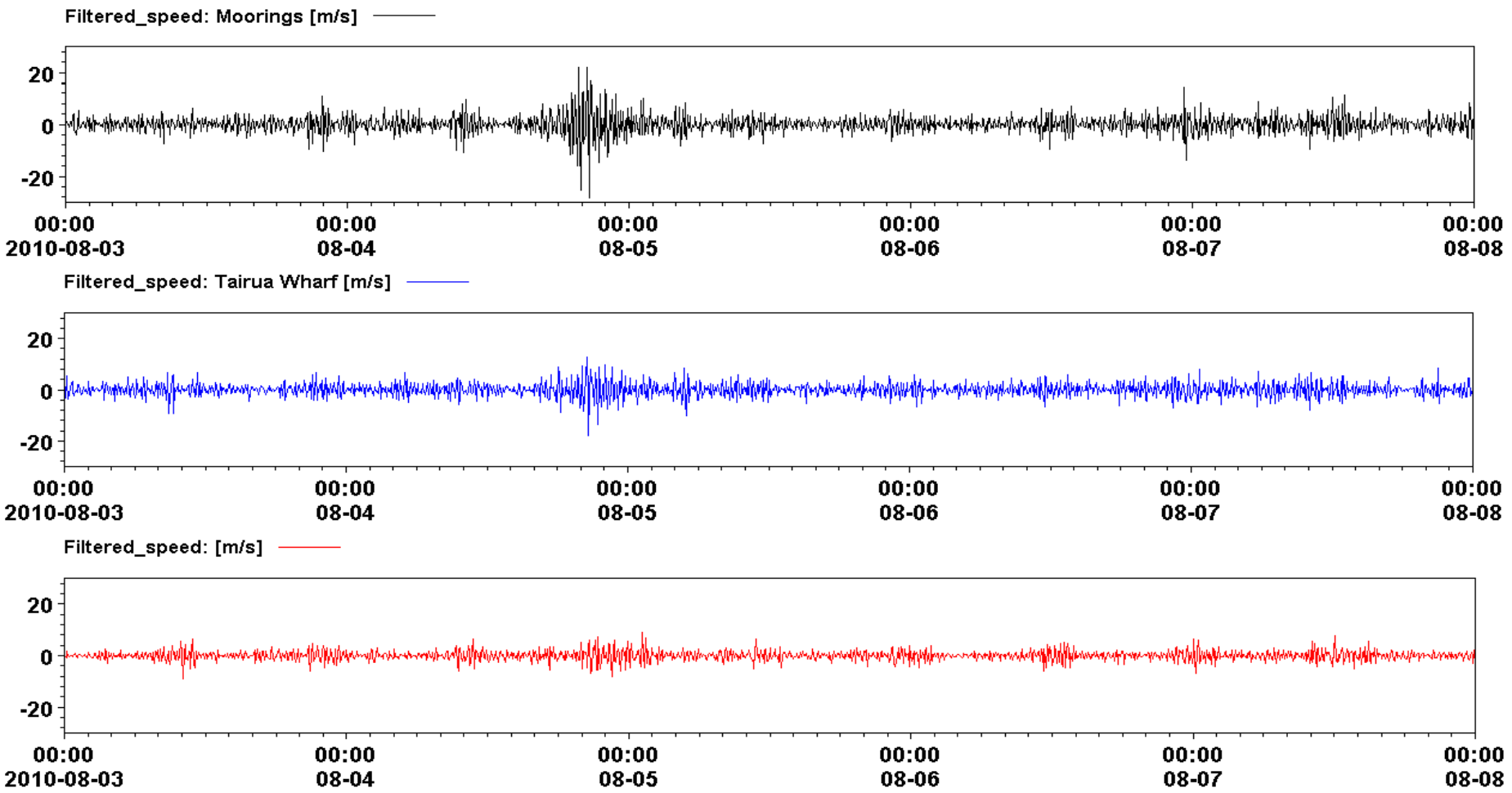

Figure 7-5 ADV1, ADV2 and ADV3 observed current speed after filtering the M2, S2, N2, K2, K1, O1 and P1 tides.

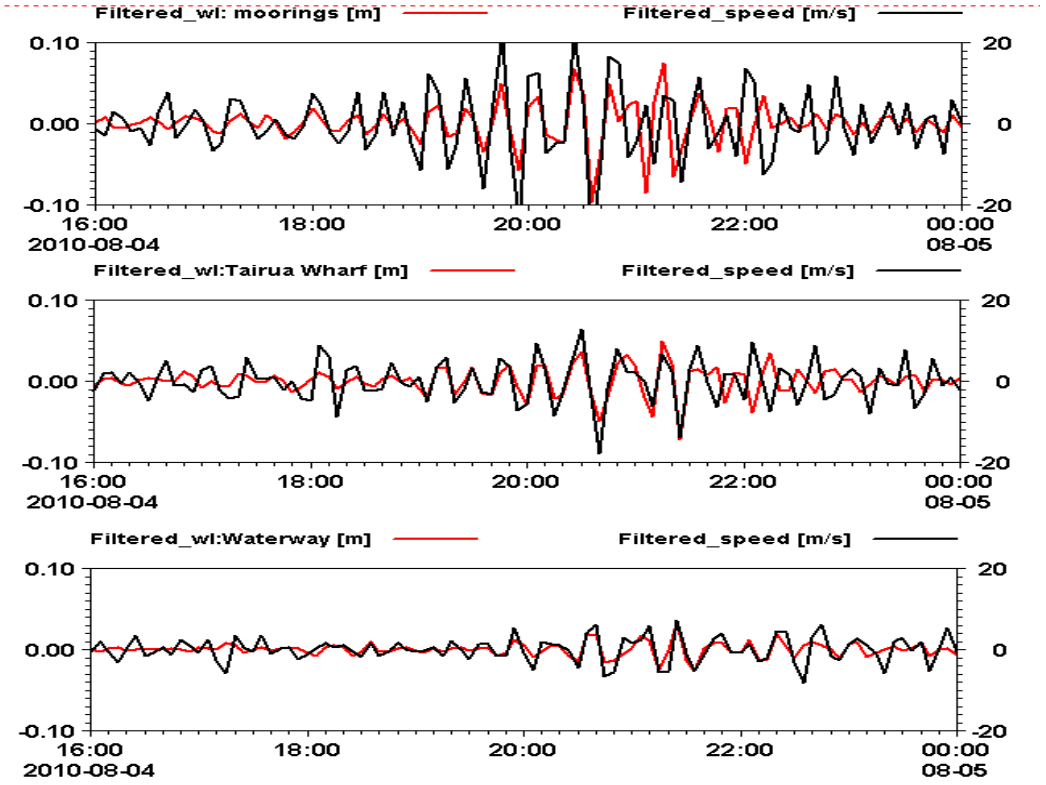

Figure 7-6 Filtered water level and current speed during the seiche to show their phase difference.

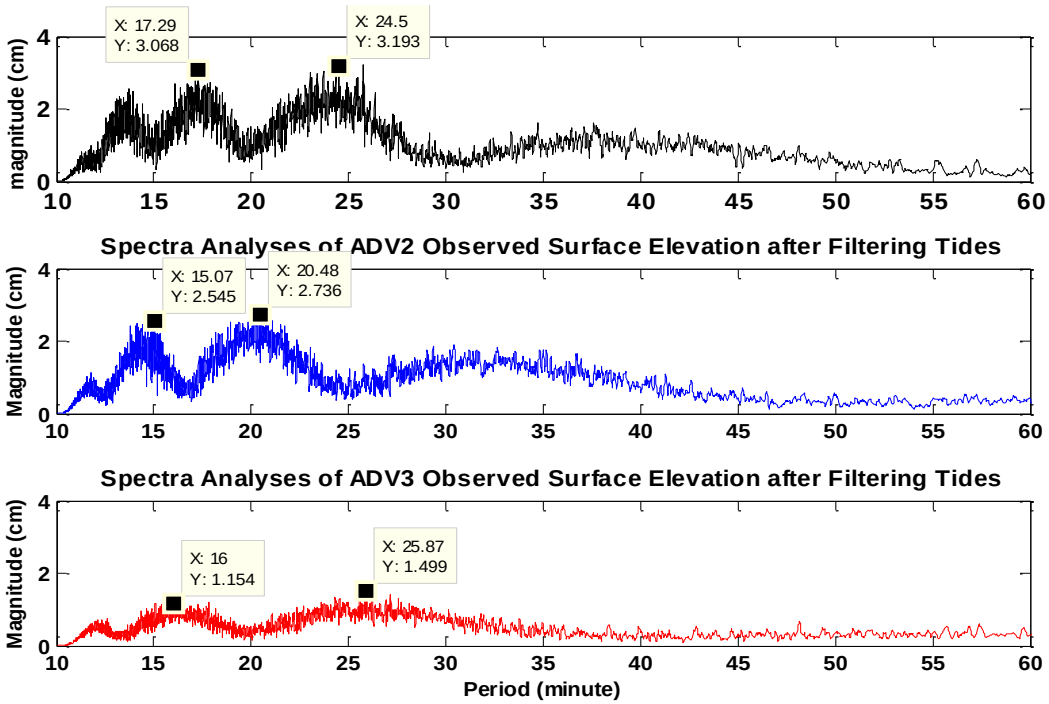

Figure 7-7 Spectral analyses results of the surface elevation observed by the ADV1, ADV2 and ADV3 after filtering the tides to calculate the seiche period and magnitude.

7.3.2 Meteorological and Field Data

The available meteorological data from 12.00am on 3 August, 2010, to 12.00am on 8 August, 2010 are plotted in Figure 7-8 as well as the current velocity and direction, and turbidity data. The hourly barometric pressure time series recorded at the Whitianga Airport station showed a sudden change in barometric pressure before the seiche event. The barometric pressure decreased from 1017.1 hPa at 10.00am on 3 August 2010 to 1004.2 hPa at 4.00pm on 4 August 2010, and then jumped to 1005.6 hPa at 10.00pm on 4 August 2010. The barometric pressure gauge stopped working from 11.00am on 6 August (Figure 7-8c).

The rainfall rate was recorded on the top of Pinnacles Mountain that is close to the Tairua River Mouth. The time series presented a heavy rainfall starting from 1.05am at a rate of 6 mm h^{-1} and continuing with an increase to 12 mm h^{-1} until 11.45am, reaching 24 mm h^{-1} at 2.45pm, then increasing to the maximum rate of 54 mm h^{-1} at 4.50pm on 4 August 2010 (Figure 7-8d). The time series of river discharge recorded at the Broken Hills Station (11 km upstream of the Tairua River) shows a flood started with a flow of 8.45 m^3s^{-1} at 10.40am, before the seiche event, and it reached the maximum value of 45.17 m^3s^{-1} at 7.25pm on the same day (Figure 7-8e).

Pulses of water turbidity were recorded by the DOBIE equipped with an OBS turbidity meter. The time series shows that the turbidity increased at around 3.00pm and declined 9 hours later (Figure 7-8f). The hourly wind speed and direction was recorded on the Slipper Island station. Wind speed increased from 7.1 m s^{-1} at 11.00am to 10.9 m s^{-1} at 12.00pm and reached the maximum speed of 15.8 m s^{-1} at 1.00pm on 4 August 2010. It kept up an average speed of 12.5 m s^{-1} until 7.00pm. Wind directions changed from north to south in 1 hour and kept to the southern direction for 4.5 hours, suddenly it changed from south to north in only 0.5 hours (Figure 7-8g).

Water depth information was collected by the S4 ADW current meter offshore from Pauanui Spit near Tairua Estuary tidal inlet at 12.00pm on 4 August, 2010 and at 8.00pm on the same day. These data show the presence of wave groups that result in fluctuations in mean water level, and a hint of an infragravity wave with a period of about 200 s at 8.00pm. Although these observed mean sea level fluctuations are similar to the amplitude of the seiche, these occurred after the seiche became established. Further, wave group occurs at other times in the record without seiche in Tairua Estuary.

The ADV current meters captured three floods on 4 August, 13 August and 26 August, 2010 respectively. However, seiche occurred during the flood that happened on 4 August, 2010 but not the other two floods (Figure 7-9).

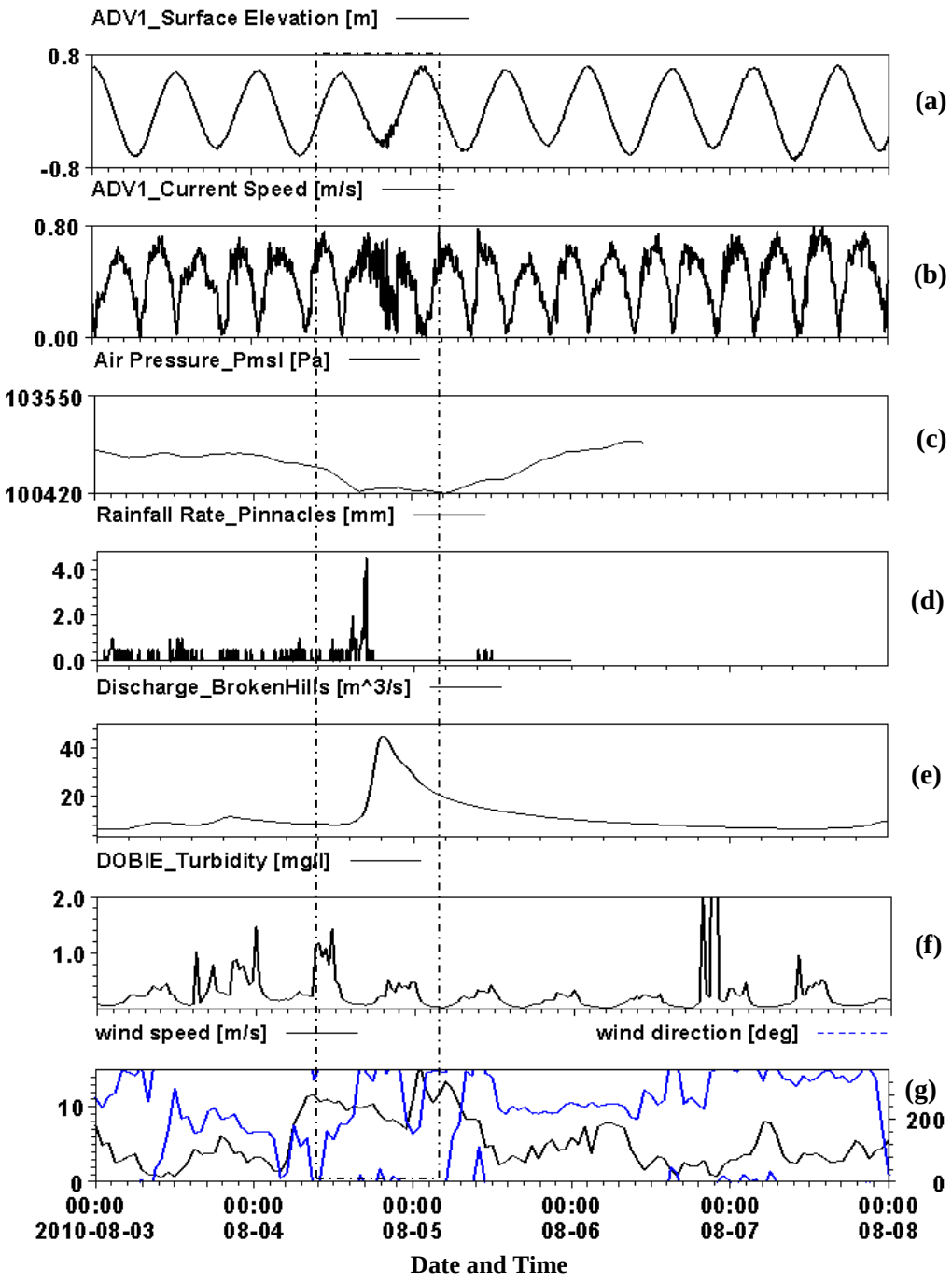

Figure 7-8 Time series of the meteorological data include (a) surface elevation, (b) current speed, (c) air pressure, (d) rainfall rate, (e) river discharge, (f) water turbidity, and (g) wind speed (in black) and direction (in blue) observed during the seiche event happened on 4 August, 2010.

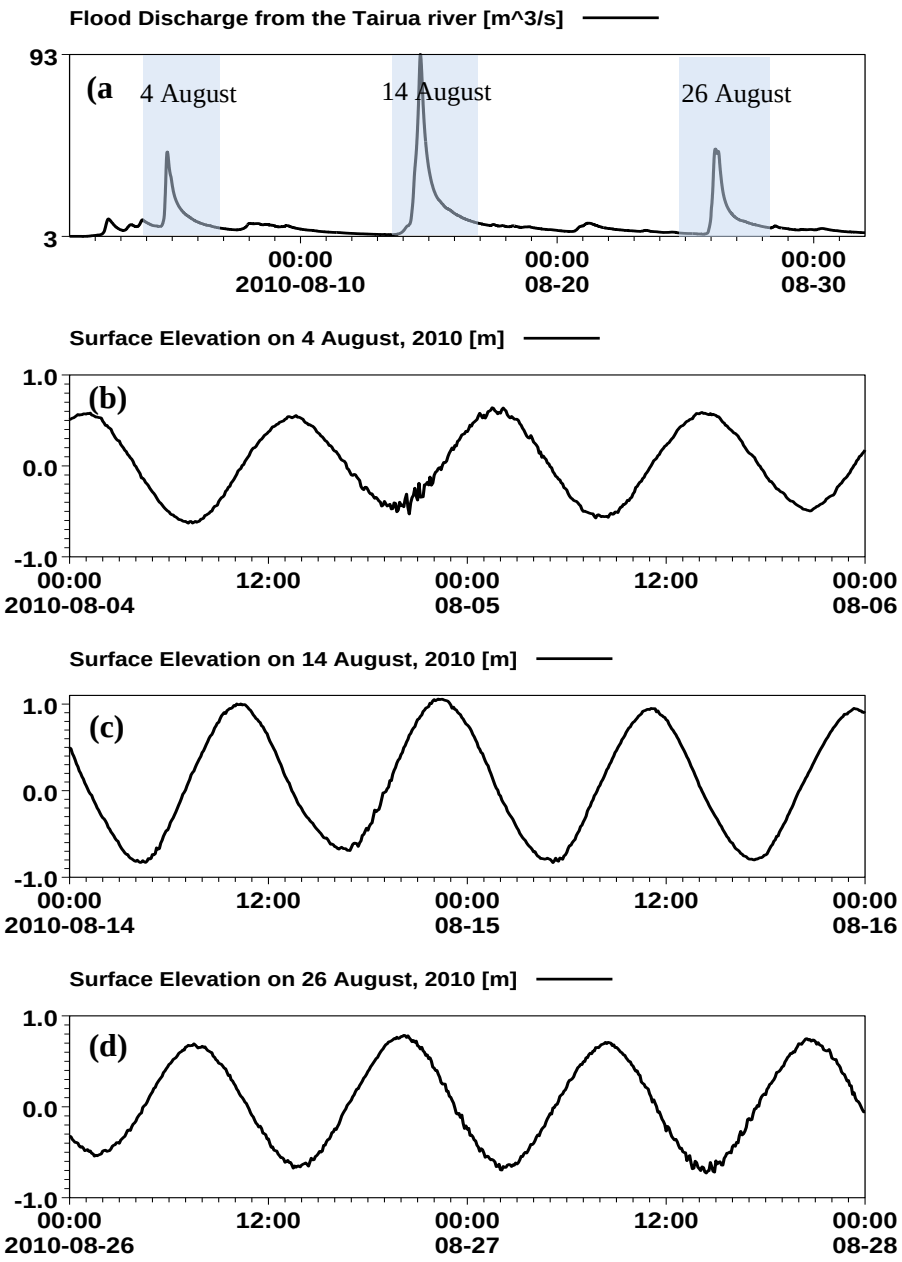

Figure 7-9 (a) The three floods captured by RBR current metre from 1 August, 2010 to 1 September, 2010 at the Tairua River mouth and surface elevation observed at the lower Tairua Estuary during these three floods on (b) 4 August, 2010; (c) 14 August, 2010; and (d) 16 August, 2010.

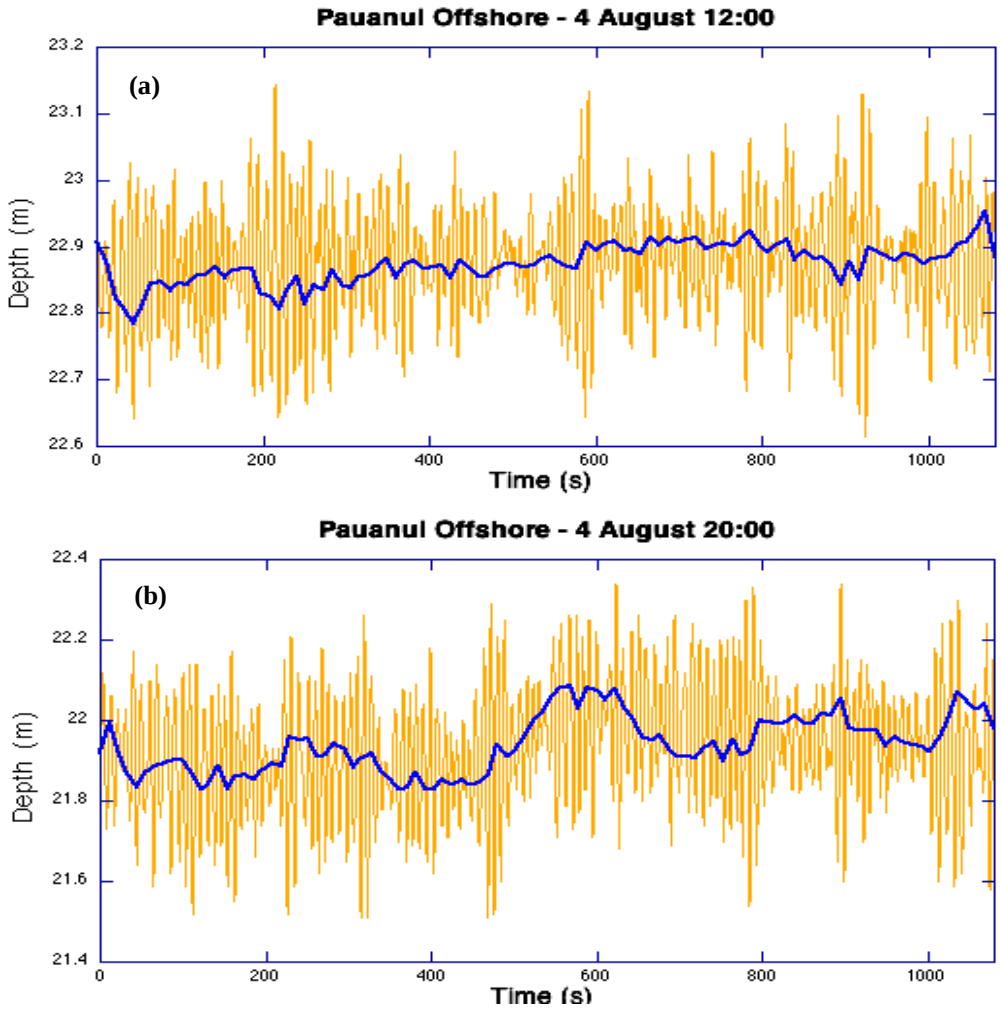

Figure 7-10 Water depth collected by the S4 current metre close to the Pauanui Beach (a) at 12.00pm and (b) at 8.00pm on 4 August, 2010.

7.3.3 Simulation Results

The Model 1 and Model 2 (Table 7-1) simulation results of the water level and current speed were extracted and are plotted in Figure 7-10 to study the impacts of the river flood on the lower reaches of Tairua Estuary. The Model 3 and Model 4 simulation results of the water level and current speed were extracted and are plotted in Figure 7-11 and used to investigate the effects of wind conditions.

The vertical profiles of the salinity and density calculated by the MIKE 3 FM ST (sediment transport) models are extracted for 2.30pm (Figure 7-12a) and 4.00pm (Figure 7-12b) on 4 August, 2010. The plots present density stratification at 2.30pm and 4.00pm on 4 August, 2010.

The model calculated suspended sediment concentration in g m^{-3} which was compared with the turbidity data recorded by the DOBIE equipped with an OBS from 12.00pm on 1 August to 12.00pm on 6 August, 2010 (Figure 7-13).

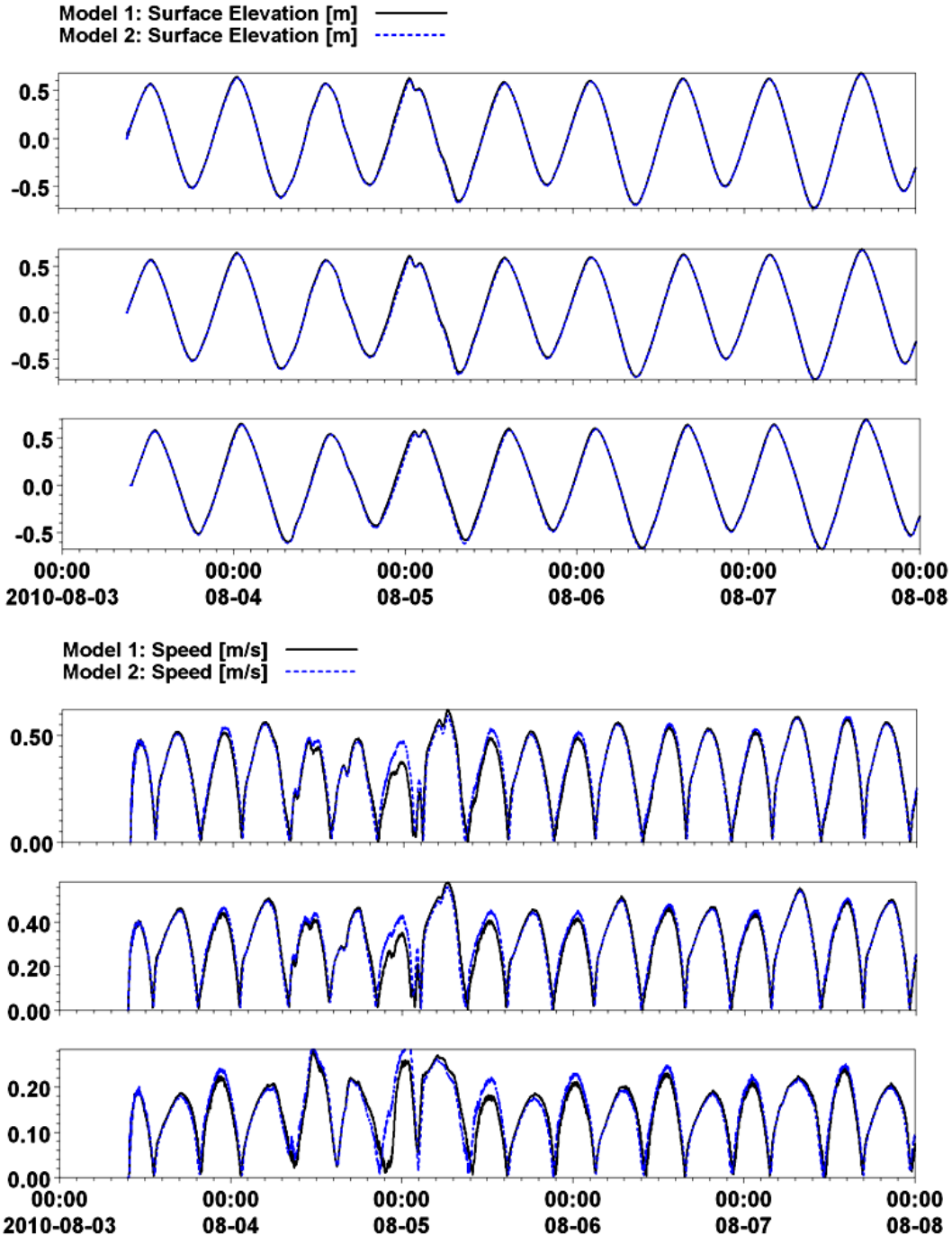

Figure 7-11 Simulation results of Model 1 (black solid) and Model 2 (blue dot) used to simulate the effects of river discharge to the surface elevations and current speed. Model 1 was run with offshore tidal boundary; however, model 2 was run with offshore tidal boundary and Tairua River discharge with wind (Table 7-1).

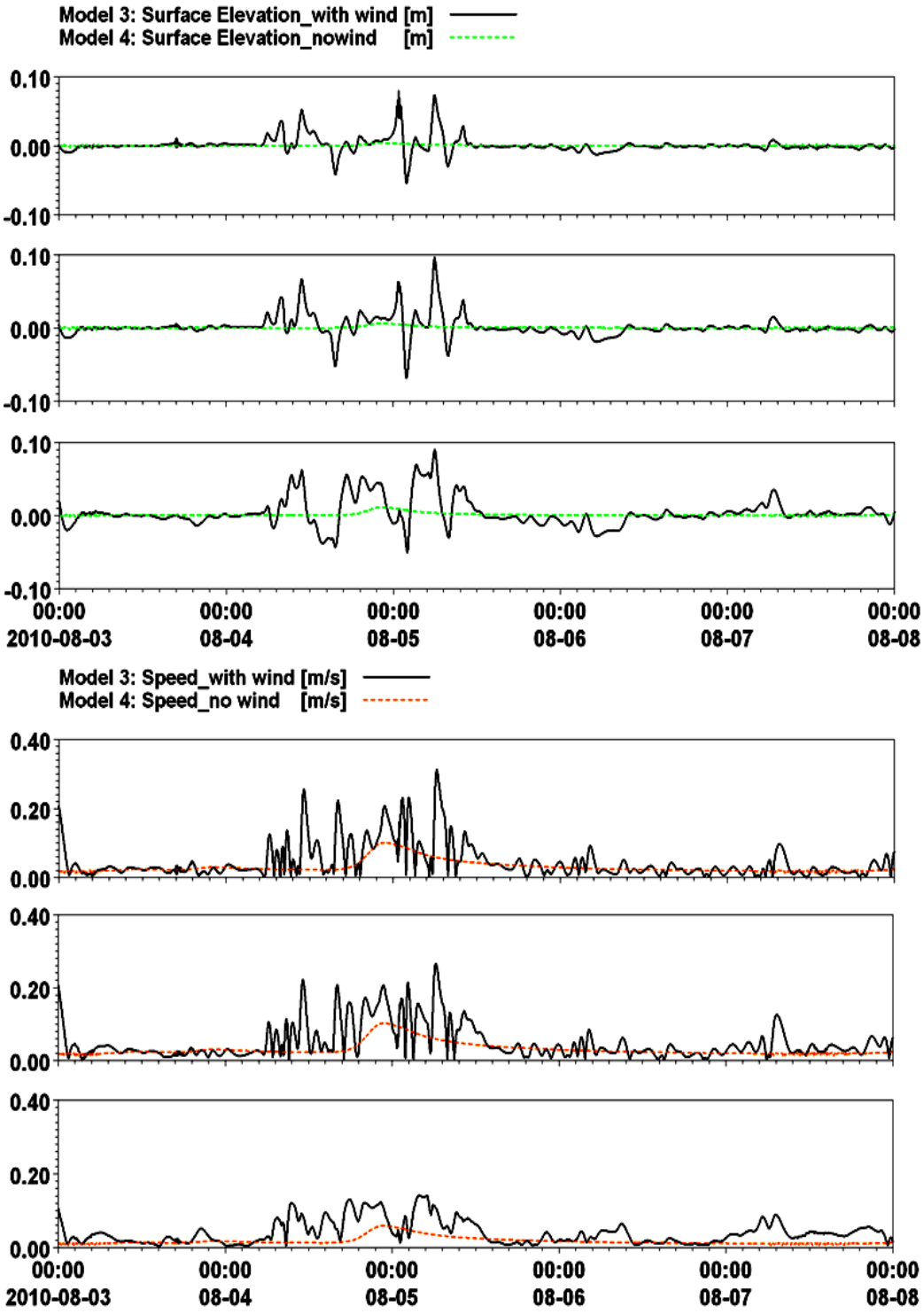

Figure 7-12 Simulation results of the Model 3 (black solid) and Model 4 used to simulate the effects of wind conditions to surface elevations (green dot) and current speed (red dot). Model 3 (with wind) and Model 4 (without wind) were also run with Tairua River discharge boundary (Table 7-1).

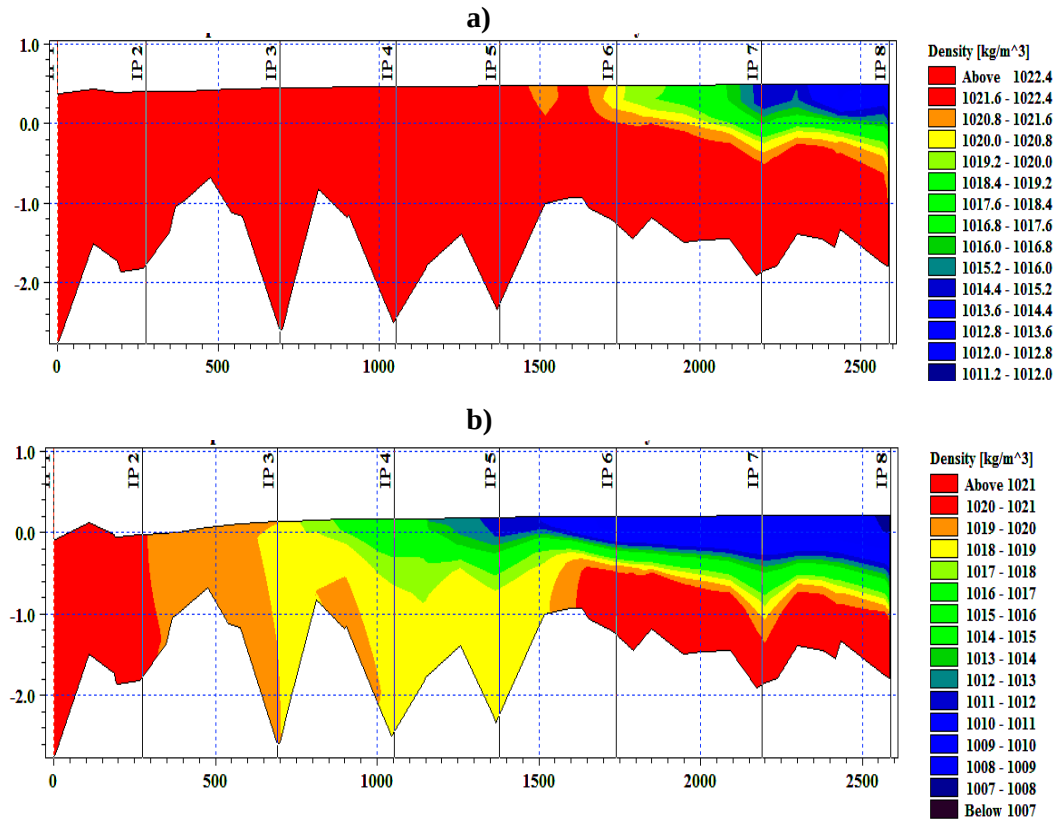

Figure 7-13 Vertical profile of water density from Tairua tidal inlet to Tairua River mouth at a) 2.30pm and b) 4.04pm on 4 August 2010, which was calculated by the MIKE 3 FM ST model.

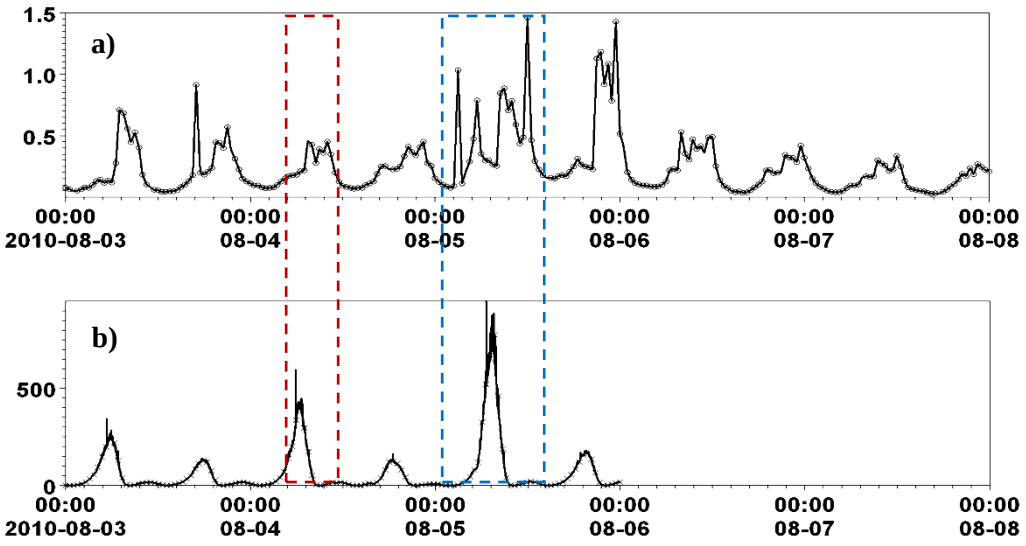

Figure 7-14 a) Water turbidity collected by DOBIE with OBS, kg m-3, b) suspended sediment concentration calculated by the MIKE 3 FM ST model, g m-3. The red rectangular shows the pulse of water concentration before the seiche and the blue rectangular shows the pulse of water concentration after the seiche.

7.4 DISCUSSION

7.4.1 Event Definition

The phase difference between the water elevation and velocity can be used to define it as a progressive oscillation or a standing wave. A true seiche should be a standing wave, so there should be a 90° phase shift between the elevation and the horizontal velocities (e.g. peak velocities occur when the water surface gradient is highest. There should also be a spatial displacement – so the strongest seiche currents will not occur where the largest displacements occur – so maximum displacements and vertical currents at antinodes and strongest horizontal currents and no displacement at nodes. Progressive waves don't have a phase shift.

Figure 7-6 showed that there is no or little phase shift before 8.40pm at the location of ADV1 (Moorings), before 9.40pm at ADV2 (Tairua Wharf), and before 10.20pm at ADV3 (Pauanui Waterway). However, after 8.40pm at ADV1, 9.40pm at ADV2 and 10.20pm at ADV3, the phase difference between the water elevation and current speed is about 90°. They were real seiche, a standing wave. Therefore, this seiche event was progressive oscillation with little resonance in the beginning, and this progressive oscillation resulted in a real standing wave (seiche).

Tairua Estuary is a barrier enclosed, elongated estuary and connects with the sea through a narrow tidal inlet on the eastern boundary. Therefore, Tairua Estuary could be considered as a closed system. Hence, the seiche period can be calculated according to Marian's equation

$$T = \frac{2L}{n\sqrt{gh}} \qquad (7\text{-}1)$$

The total length of the lower part of the estuary is around 3.4 km with an average water depth of 3 m, taking n as 1, the seiche period is 20.9 minutes according to Equation (7-1). This result is very close to the spectral analysis results of 20.89 minutes and 20.93 minutes (Figure 7-7). Therefore, the observed water levels and current speed fluctuations in the lower reaches of Tairua Estuary are consistent with the seiche event.

7.4.2 Forcing Mechanisms of the Seiche Event

There are various causes of seiche. In both lake and harbour systems, seiche can be caused by the passage of small barometric fluctuations, with a period close to the natural seiche period of the system. Other mechanisms include a rapid change in air pressure due to a squall; the impacts of wind gusts on the water surface; a

lapse in strong onshore winds, causing pent-up water at the shore to be released; heavy rain, snow or hail over a portion of the water body; flood discharge from a river at one end of the system; and tilting or movement of the lake or sea bed resulting from earthquakes (Chrystal, 1909). In semi-enclosed micro-tidal water bodies, the prime mechanisms driving seiche is changes in wind speed and direction (Luettich et al, 2000).

7.4.2.1 *Flood Discharged from Tairua River Mouth*

Flood discharge at one end of a system will increase the water level initially at that end (Chrystal, 1909). The meteorological and field data in Figure 7-8e shows a maximum 45.17 $m^3 s^{-1}$ flood discharge from the Tairua River mouth to the lower reach of Tairua Estuary at the time the seiche occurred.

The computed results of Model 1 and Model 2 presented in Figure 7-11 show that the river flood discharge to the estuary is related with the fluctuations of water level and current velocity. The results also indicate that the flood discharge from the Tairua River mouth increases the current velocity in the lower estuary resulted in the density stratification happening in the lower reaches of the estuary before the seiche event. It also transported fine sediment into the estuary, increasing the turbidity. This result coincides well with and supports the found of Garel et al. (2009) that highly stratified conditions developed with increasing river discharge. A salt wedge with tidal motion was observed at the lower estuary during the flood event.

The vertical profile of water density computed by the MIKE 3 FM ST (Three Dimensional Flexible Mesh Sand Transport) model and recorded by the DOBIE with OBS in Figure 7-13 suggest that pulses of turbid water migrated to the lower reach of Tairua Estuary in a salt wedge under the river flow and resulted in density stratification before the seiche event on 4 August, 2010. It indicated that flood discharged from Tairua River taken big load of sediment and discharge to the lower reach of Tairua Estuary. This pycnocline generated an unstable flow at the lower estuary. And the oscillation of surface elevation and current velocity is the response of the equilibrium of the water system. Such a mechanism has been suggested in the literature, but no data have been published to support it. The model calculated the suspended sediment concentration shown that pulse of water concentration increased also after the seiche event (Figure 7-14), which indicates that the seiche does increase the sediment transport at the lower Tairua Estuary.

However, the flood at the river mouth is not the only mechanisms capable of forcing a seiche event. Figure 7-9 shows that three floods occurred on 4 August, 14 August and 26 August in 2010, but a seiche only occurred on 4 August.

7.4.2.2 ***Wind at the Water Surface***

Wilson (1972) indicated in his research that the main causes of seiche are wind friction on the water surface or rapid barometric changes. A wind-forced seiche event begins when a sustained wind acts on a water surface to initiate water movement after a brief frictional lag (Csanady, 1972). Thompson (1982) found that wind-induced water set-up caused significant differences in water elevation between upstream and downstream locations on the River Thames. Ordinary wind-driven surface waves roughen the surface, but wind piles water against the windward shoreline where a small portion of its volume causes the lake surface to rise. While the surface tilts upward at the windward end, the thermocline tilts in the opposite direction and at a much steeper angle (Korgen, 1995). The increase in wind speed leads to a decrease in atmospheric pressure. If the decrease in pressure is only on one end of a water body, it can induce a seiche (Chrystal, 1909).

The force to be considered is water level set-up by wind, and the role that water depth plays in this occurrence. The change in water level associated with wind stress is quantified by

$$\frac{f\eta}{fx} = \frac{C_D \rho_A w_{10}^2}{\rho g h} \qquad (7\text{-}2)$$

Where, C_D is drag coefficient, ρ_A is air density, W_{10} is wind speed 10 m above water surface, ρ is water density, g is acceleration due to gravity, $g = 9.81$ ms^{-2}, and h is water depth (Chrystal, 1909).

The meteorological data in Figure 7-8g shows the hourly surface wind speed recorded at NIWA's station on Slipper Island. The plot shows that the wind speed increased from 7.1 m s^{-1} at 11.00am to 10.9 m s^{-1} at 12.00pm, reaching the maximum speed of 15.8 m s^{-1} at 1.00pm. It continued at 12.5 m s^{-1} until 7.00pm on 4 August, 2010. The main wind direction is around 350° (from NW to SE). According to Equation 7-2, a higher wind speed induces a higher increase of the water level if all other conditions are same, and deeper water produces smaller water level set-up. Therefore, strong winds blowing in changing directions can affect the water surface within the estuary more than the offshore ocean.

The MIKE 21 HD model 3 and model 4 computed results show that the wind generated both water level and the current velocity fluctuations (Figure 7-12). It also indicates that wind variations at the time scale of minutes could affect the strength of the seiche oscillation. On the other hand, a sudden increased mean wind speed lasting for at least several minutes could cause local atmospheric pressure changes, and as a result, impact the seiche.

7.4.2.3 ***Rapid Changes of Barometric Pressure***

When the atmospheric pressure is higher, it restricts the ability of the water level to rise. This is known as the inverse barometric effect. It is quantified by the sea level response, which indicates that a change in the atmospheric pressure by 1 hPa will induce a change in the water level by 1 cm (Pattiaratchi, 2001). The pressure decreased by 13 hPa from 3 August to 4 August resulted in water surface increase of 13 cm. The sudden increase in pressure at 4.00pm on 4 August re-increased the water level adjustment and resulted in the oscillations returning the system to equilibrium. Goring (1995) analysed the sea level data from 15 tide gauges and concluded that variation in sea level is caused by waves propagating into the area instead of changes in barometric pressure for north-eastern sites of New Zealand.

7.4.2.4 ***Rainfall***

The rainfall rate data suggest that a heavy rainfall occurred just before the seiche event on 4 August, 2010. The hourly rainfall time series were used to force the numerical model to verify the effects of the rainfall. However, no water level and current speed fluctuations were found to be generated. The rainfall is not the main factor generating the seiche directly. However the meso-scale storm associated with the wind, sudden barometric pressure changes, and heavy rainfall resulted in the river flood.

7.4.2.5 ***Long Period Ocean Waves***

Long period oceanic waves generated by abrupt atmosphere pressure changes or surf beat may force seiche within an estuary (Wilson, 1972). Figure 7-14 shows that the wave groups and an infragravity wave with a period of about 200 s were present after the seiche. Therefore, it may also be a factor in the seiche. However, the wave group's period is too short compared to the 20.8-minute seiche period.

Edge or shelf waves on the continental shelf may also force seiche. These shelf waves are often caused by severe storms such as tropical cyclones (Pattiaratchi, 2001). However, the data collected for this study were not suitable for analysing the impacts of the edge waves.

7.4.2.6 ***Seismic Activity***

The final mechanism for generating long period ocean waves capable of forcing

seiche is remote seismic activity, which may generate tsunami. A Mw 5.8 earthquake occurred near the Kermadec Islands, New Zealand (29°57'48.39"S, 178°19'26.15"W) about 905 km to the NNE of Tairua Estuary on 4 August, 2010. However, historical data indicates that it needs a minimum of Mw 8.5 to create a measurable effect for the Coromandel Peninsula. A tsunami generated by the 1946 Mw7.4 earthquake in the Aleutian Islands is the only distant earthquake under Mw8.5 to have had a significant effect in New Zealand (Power, 2013). And no tsunami was detected by the tsunami network around New Zealand including Raoul Island in the Kermadec (Pacific Tsunami Warning Centre, 2010). Therefore, seismic activity is not one of the seiche generating factors.

7.5 CONCLUSION

The phase difference between water elevations and current speed is about 0º in the beginning and is about 90º afterwards. It indicated that this water fluctuation event is a forced oscillation (most progressive) with little resonance in the beginning and it resulted in the real seiche, a standing wave. The spectrum analysis results of the observed fluctuations coincides well with the calculated seiche period based on Marian's Equation and indicate these fluctuations are a seiche that happened on 4 August, 2010.

The vertical profile of water density recorded by the DOBIE and SCUFA suggested that pulses of turbid water migrated to the lower reach of Tairua Estuary in a salt wedge under the river flow and resulted in density stratification before the seiche event on 4 August, 2010. Such a phenomenon has been suggested in the literature, but no data have been published to support it. The data showed that an intense, meso-scale storm produced heavy precipitation, resulting in a sediment laden flood discharging from the Tairua River mouth to Tairua Estuary. A MIKE 3 FM ST model was also developed to compute the vertical profile of water density. The results present two density stratification events which occurred at 2.30pm and 4.00pm during the seiche event on 4 August, 2010. The estuary turbidity maximum (ETM) was enhanced with increasing current velocities, and displaced downstream during periods of high river discharge. During the flood event, the ETM was expelled out of the estuary, and the SSC along the estuary was controlled by the sediment load from the drainage basin.

Considering all these related information, this water elevations and current speed oscillation with little resonance and finally a real seiche was forcing by a heavy wind together with a sediment-laden flood discharged from the Tairua River mouth to the lower reach of Tairua Estuary, which resulted in flow instability with the pycnocline, forming the seiche event. The absence of seiche in the rest of the record floods suggested that flood, sediment stratification and heavy wind are the three forcing mechanics of the seiche occurred on 4 Aug, 2010.

CHAPTER EIGHT
EFFECTS OF SEA LEVEL RISE ON ESTUARINE PHYSICAL PROCESS

To study the impacts of sea level rise on the hydrodynamics and sediment transport within Tairua Estuary, a set of MIKE 21 HD (hydrodynamic) and MIKE 21 ST (sediment transport) numerical models were set up as extensions of the calibrated 'estuary_20m' hydrodynamic model. These models were mainly forced by tides, wind and river discharges, with different sea level rise scenarios at the local region of Tairua Estuary as a case study. The chosen sea level rise scenarios are within the range of projections for the period 2010-2115 relative to 1980-1999. Three scenarios of annual average river discharge based on flow rate observations at Broken Hills Station from 1975 to 2012 were applied in the models. The impacts of SLR on tidal range, water depth, water surface area, residual current and thirty-day average sediment flow rate and their interaction were analysed through comparing the 13 SLR scenarios with the present situations. Under various SLR scenarios the degree of flood dominance along the main channel to the river mouth of the estuary increases. The more sinusoidal shapes of surface elevation and the less asymmetry between flood tides and ebb tides of the simulation results can support this point. As a result, longer salt seawater intrusion and more sediment to the Tairua River upstream. Despite the flood tides dominant nature of flow regime along the main channel from tidal inlet to the river mouth, the net sediment transport is in the flood tide direction. As a result, with higher SLR, the stronger flood tides can take more sediment into the estuary and deposit at the lower reach of the estuary, but less sediment will be flushed outside of the estuary with ebb tides.

8.1 INTRODUCTION

Estuaries are formed in response to sea level stabilization over the past 6000 years. Sea level is the result of changes in the volume of ocean water due to thermal expansion and contraction, glacial advance and retreat, as well as changes in the elevation of the Earth's surface (Jackson, 2013). Estuaries and lagoons are formed under conditions where relative sea level rise (SLR) exceeds the rate of sediment infilling (Boyd et al., 1992).

Local SLR has the potential to accelerate processes such as shoreline erosion, land inundation, saltwater intrusion, and increase storm surge risk (Nicholls, 2003). Understanding how the hydrodynamics change within estuaries in response to SLR is also likely to have implications for biological and chemical processes occurring in estuaries, as these processes are tightly coupled with estuarine physical processes (Hong and Shen, 2012). The variation of this effect depends on

bathymetry, tide ranges, as well as properties of wave and wind. Due to nature of multi-scale and unsteadiness in coastal hydrodynamic and morphodynamic processes, this effect can be predicted by using integrated coastal/ocean processes-based models. The modeling processes and parameters have to be properly based on flow conditions since the modeled conditions represent projected future scenarios beyond the calibrated conditions (ASCE, 1992). Validated computational processes-integrated models can be applied to assess the SLR impacts on a local/regional scale coast (Ding et al., 2013).

Studying the effects of SLR in local is of vital importance because the impacts of SLR can vary significantly from place to place (Kettle, 2012). The effects of sea-level rise on coasts are not uniform, but vary considerably from region to region and over a range of temporal scales (Nicholls et al., 2010; Weiss et al., 2011).

For the purpose of coastal flood management and infra-structure planning, it is essential to take into account SLR under dynamic storm/hurricane conditions for assessing temporal and spatial variation of SLR impact on coasts and estuaries (Ding, 2011). The Paku marina was proposed to be constructed on the lee side of Paku Hill within Paku Bay (now it is under constructing). It is important to consider the impacts of SLR on sediment transportation over long term, and the effects of a marina or the other coastal structures before construction taking place (Ding, 2011).

The study of SLR-related impacts has been performed in previous studies. Based on the regional SLR, US-CCSP (2008) proposed three projected SLR scenarios (0.3, 0.5, and 1.0 m of SLR by 2100) to evaluate several aspects of SLR impacts for the mid-Atlantic US coast. Cooper et al. (2005) also applied digital elevation models (DEM) to study the impact of projected sea level rise to the New Jersey coast using two relative sea level rise projections, 0.61m and 1.22 m to study what areas could be chronically inundated. Valentim (2013) used his numerical modelling results of the MOHID 2D model and determined the residual circulation, tidal asymmetry and tidal dissipation considering the actual SLR. Lopes et al. (2011) had used sea level rise scenario projection to force the morphodynamic model MORSYS2D, previously implemented for the Ria de Aveiro, and computed the lagoon hydrodynamics, residual sediment transport and its balance at the lagoon inlet, and predicted the tidal asymmetry. Local/regional assessment of impacts of sea-level rise usually is required for coastal hazard management in coastal zones (USACE, 2011), for which the variation of waves, tides, and geomorphology has to be included. However, the primary SLR impacts on coastal hydrodynamics such as waves and currents, as well as morphological changes due to sediment transport have not been fully studied (Ding, 2013).

This research used integrated coastal/ocean processes-based well-calibrated ‘estuary_20m’ MIKE 21 HD and MIKE 21 ST models, with modeling processes and parameters properly based on flow conditions, based on the local small-scale Tairua Estuary, for which a set of sea-level rise scenarios (SLR 0 m, 0.5 m, 0.8 m

and 1.2 m) and local extreme hydrological forcing including tides, river floods, wind and sediment transport are taken into account, to find the impacts of SLR on estuarine tidal flow, current speed, tidal range, residual circulation, sediment transport processes and their interactions.

8.2 SEA LEVEL CHANGE FORCASTING

The MfE New Zealand local government guidance (NZ Coastal Policy Statement, 2010) suggests a base value SLR of 0.5 m relative to the 1980-1999 average, accompanied by an assessment of the potential consequences from a range of possible higher SLR scenarios for planning and decision timeframes out to the 2090s (2090-2099). At the very least, all assessments should consider the consequences of a mean SLR of at least 0.8 m relative to the 1980-1999 average (Table 8-1). Over the 20th century, the linear least squares trend in SLR was 1.7 mm yr^{-1} (Church and White, 2006). Records and other sea level proxies indicate that SLR at an average rate of 1.7 mm yr^{-1} rise and an acceleration of 0.013±0.006 mm yr^{-1} from 1870 to 2004 (Church & White, 2006). However, confirmation of acceleration in SLR trend may take a few decades because of the long-period natural cycles in sea level (Bell, 2001). Hannah and Bell (2012) estimated that the average relative SLR is 1.7±0.1 mm yr^{-1} derived from tide gauges around New Zealand. In this study, 0.5 m, 0.8 m and 1.2 m SLR for the time period 2010-2115 were selected as the three sea level rise scenarios. Figure 8-1 presents the low lying area potentially affected by different sea level rise scenarios at Tairua Estuary and urban residential area in blue solid line (data from WRC, 2012).

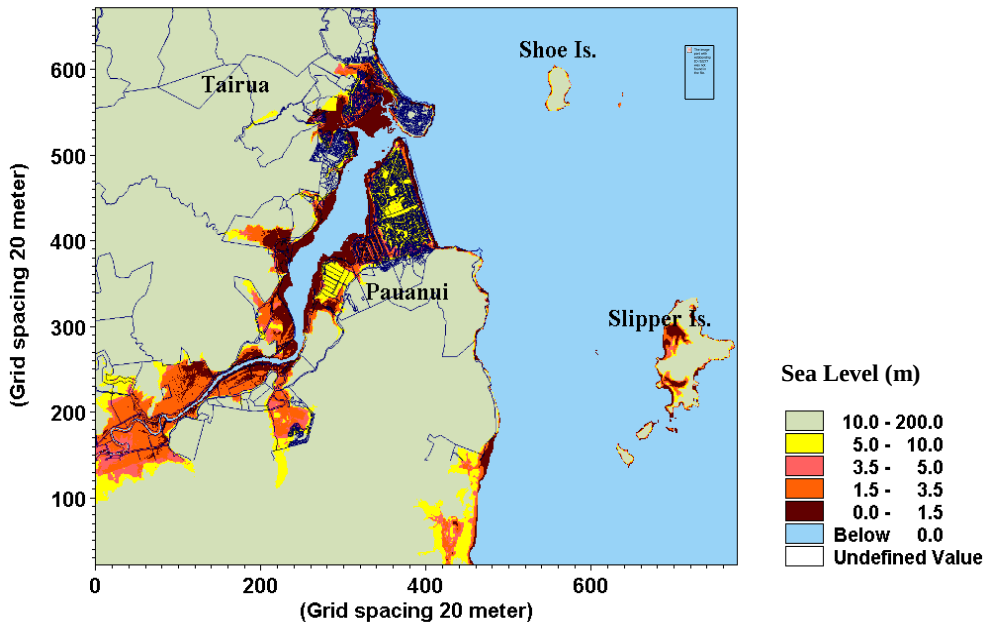

Figure 8-1 Low-lying areas and urban residential area at Tairua Estuary (data from Waikato Regional Council).

Table 8-1 SLR baseline for different future timeframes (preceded by NIWA based on MfE table, 2010)

Timeframe	Base sea-level rise allowance (m relative to 1980-1999 average)	consider the consequences of sea-level rise of at least (m relative to 1980-1999 average)
2030-2039	0.15	0.20
2040-2049	0.20	0.27
2050-2059	0.25	0.36
2060-2069	0.31	0.45
2070-2079	0.37	0.55
2080-2089	0.44	0.66
2090-2099	0.50	0.80
> 2100	10 mm per year	10 mm per year

8.3 RIVER DISCHARGE

Climate change is projected to result in increased westerly winds in winter and spring, along with more rainfall in the west of the North and the South Island and drier to the east and north of the country. Conversely, in summer and autumn, climate models suggest a decreased frequency of westerly conditions, with drier conditions in the west of the North Island and a possible increase in rainfall in the Gisborne and Hawke's Bay regions at the end of the 21st century (MfE, 2008).

The duration percentiles data of Tairua River flow at the Broken Hills Station 11 km upstream from the Tairua Bridge from 2 July, 1975 to 1 May, 2012 were recorded by WRC. The annual Tairua River discharge averaged over 37 years show that 20% of the Tairua River discharge were below 1.48 $m^3 s^{-1}$, 50% of the Tairua River discharge were below 2.82 $m^3 s^{-1}$ and 80% of the Tairua River discharge were below 6.11 $m^3 s^{-1}$ (Figure 8-2). The annual Tairua river discharge to Tairua Estuary averaged over one year in 2012 is about 8 $m^3 s^{-1}$ observed at the same station. Therefore, the annual averaged Tairua River discharge of 2.5 $m^3 s^{-1}$ (with less rainfall), 5 $m^3 s^{-1}$ (at present) and 10 $m^3 s^{-1}$ (with higher rainfall) were selected as the river discharge scenarios.

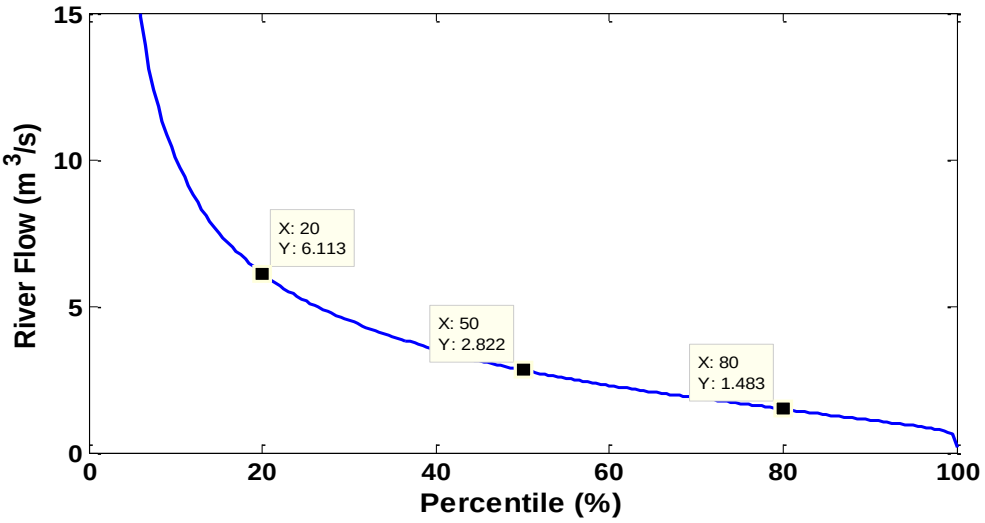

Figure 8-2 Duration percentiles of Tairua River flow observed at the Broken Hills station from 15.30 on 2 July 1975, to 13.00 on 1 May 2012 (Data from Waikato Regional Council).

8.4 SCENARIOS MODELLING

The review of MfE (2008) suggested that increased rainfall and sea-level rise will result in changes of groundwater level and lead to more saltwater intrusion in coastal zones. Therefore, four models were run with 0 m, 0.5 m, 0.8 m and 1.2 m SLR and the same river discharge time series to study the impacts of SLR (Table 8-2); nine models were run with not only 0 m, 0.5 m, 0.8 m and 1.2 m SLR scenarios but also 2.5, 5 and 10 $m^3 s^{-1}$ fixed river discharge scenarios to study the effects of river discharge and SLR on saltwater intrusions (Table 8-3). The influence of wind observed from the NIWA Station on Slipper Island from 28 July 2010 to 27 August 2010 was also incorporated into the model runs.

Table 8-2 Potential SLR modeling scenarios, summary of forcing conditions

Model	Bathymetry	Sea Level Rise (m)	River Discharge	Wind Speed
S1	whole_50m & Estuary_20m	+0.0	Time series observed at the Broken Hills Station July 28 - Aug.27 2010	Time series observed at the Slipper Island July 28 - Aug.272010
S2		+0.5		
S3		+0.8		
S4		+1.2		

With sea level rise, there is more possibilities of increased sediments coming down to the river due to catchment run-off changes, as a result, the bathymetry used in the modelling should change with sea level rise. However, in this study, the bathymetry kept same with sea level rise in the four modelling scenarios.

Table 8-3 Potential SLR and Tairua River discharge modelling scenarios, summary of forcing conditions

Model	Bathymetry	Sea-level Rise (m)	River Discharges ($m^3 s^{-1}$)	Wind Speed
S5	whole_50m & Estuary_20m	+0	2.5 (less rainfall)	Time series observed at the Slipper Island 28 July - 27 Aug, 2010
S6		+0	5 (present)	
S7		+0	10 (more rainfall)	
S8		+0.5	2.5	
S9		+0.5	5	
S10		+0.5	10	
S11		+0.8	2.5	
S12		+0.8	5	
S13		+0.8	10	

The thirteen scenarios were modeled based on the same bathymetry which was used in the calibrated and validated 'estuary_20m' model. It means that the modelling in this research assume the bathymetry will not change or change very little because the MIKE module could only simulate the short-term morphodynamics.

8.5 RESULTS AND DISCUSSION

Tidal elevations and current speed were extracted from the model scenarios S1 to S4 at the locations of the deployed ADCP, ADV1, ADV2, ADV3 and RBR every half hour with 0 m SLR (black solid line), 0.5 m SLR (blue dashed line), 0.8 m SLR (red dotted line) and 1.2 m SLR (green dash-dot line) during spring tides in flood season (Figure 8-3). From the Tairua River mouth to the estuary entrance the shapes of tidal elevations are more and more sinusoidal at the same stations with SLR (Figure 8-3a). This result coincides with the other related research (Aubrey and Speer, 1985; Dronkers, 1998). The increased sinusoidal tidal shape at the river mouth with SLR implies that tidal flow has more energy than river discharge and Tairua Estuary will likely be dominated more by tides rather than river discharge as SLR occurs. This will influence the long-term residual sediment transport in the system, and salt water intrusion length within estuaries. Significant salinity changes will occur in the saltwater and freshwater confluence area. This will be of particular concern for drinking water supplies and coastal ecosystems during droughts.

Figure 8-3b shows a comparison of the current speed at different locations within Tairua Estuary with the S1 to S4 SLR scenarios. It shows that both of the ebb and flood current speed increases with SLR, and it increases faster during flood tides than ebb tides with SLR. With the same river discharge, the estuary is dominated

more by flood tides than ebb tides. More sediment will be taken into estuary from the Pauanui Beach and ebb tidal delta, and result in bigger size flood tidal delta and smaller ebb delta.

As discussed above, the higher the SLR, the stronger the flood tidal flow will enter the estuary which dominating over river discharge within the estuary will be closer to the river mouth with SLR than the present. Figure 8-3 shows that the shapes of the surface elevation and current speed at the Tairua River mouth are more and more similar to the estuary entrance. And also the river flood effects to the estuary will decrease for the same river discharge and wind conditions with higher SLR (0.8 m and 1.2 m).

Tidal elevation (Figure 8-3a) at each of the instruments deployment locations for the different SLR scenarios show that tidal elevation does not change very much at the tidal inlet except for a depth offset. However, the closer to the Tairua River mouth, the tidal asymmetry decreases, and the phase lag from estuary entrance up to river mouth within estuary also decreases with increasing SLR. The low and high water tends to arrive earlier as a consequence of SLR (Figure 8-3, 8-7 and Table 8-4). These phenomena had also been found in similar studies of Sinha and Rao (1997).

Comparing the scenarios S2 to S4 with the present situation (S1), tidal range increases 0.012 m (0.66%) at the tidal inlet, 0.188 m (11.94%) at the moorings, 0.209 m (13.45%) at the Tairua Wharf, 0.286 m (19.28%) at the Pauanui Waterway and 0.889 m (107.97%) at the Tairua River mouth with SLR 1.2 m but keep the same river discharge (Figure 8-3a). The scenarios S5 to S13 models computed surface elevations every 10 minutes also at the tidal inlet (black), moorings (blue), Tairua Wharf (light green), Waterway (light blue) and Tairua River mouth (red) with both sea level rise and increased river discharge (Figure 8-7). Tidal range at the Tairua River mouth was calculated and summarized in Table 8-4. These results indicate that the interaction between tidal flows entering from the open ocean to the estuary and the river discharge through the river mouth to estuaries will influence the tidal range. Further into the estuary, the increased variation in tidal waves due to SLR becomes more prominent. Tidal range will decrease with increased river discharge when sea level is same, and tidal range will increase with SLR when river discharge keeps same. The effects of SLR on the change of tidal range will be more than the effects of river discharge for Tairua Estuary (Table 8-4 and Figure 8-7). This also indicates that Tairua Estuary will likely be dominated more by tides and less by river discharge with SLR.

Equation (8-1) as proposed by O'Brien (1969) could be used to calculate the changes in tidal prism due to inundation related to the tidal range (T_r), shoreline length of the bay (C), the relative SLR (S) and an average shoreline slope (s).

$$P = \frac{T_r C S}{2s} \tag{8-1}$$

As discussed above, with SLR, the tidal range within the estuary increases, the shoreline length increases with larger surface area, and the average shoreline slope is small. Therefore, the tidal prism increases and results in a higher average current speed with SLR. This coincides with the simulation results (Figure 8-4b). Dean et al. (1987) also suggested that the increase of mean sea level likely resulting in increased tidal prisms is expected intertidal bays and lagoons, therefore the average current speed increases with SLR.

The percentage change in cross-sectional area of the tidal inlet (A_c) is directly proportional to the percentage change in tidal prism (P) as demonstrated by Equation (8-2). The constant m is in the order of unity.

$$\frac{dA_c}{A_C} = m\frac{dP}{P} \tag{8-2}$$

Therefore, as the tidal prism increases, the tidal entrance will increase in area. The Paku hill is located on the western side of the tidal inlet limits an increase in width, but the head of the Pauanui sand Spit is relatively flat (the slope is about 1.8 degree) allowing the inlet to be widen. With SLR, the tidal inlet will also be deeper and this result in less bottom friction.

Average water depth was extracted from the 30-day depth-averaged scenarios S1, S2, S3 and S4 at the five instruments locations (Figure 8-4). The results indicate that the average water depth increases more at the lower reach of the estuary to a lesser degree at the Tairua River mouth with the same SLR. It is probably because the estuary is dominated more by tides from outside ocean than river discharge and more sediment will be taken into the estuary and deposit at the river upstream. Therefore, the average water depth at the river mouth will increase less with SLR. Bruun (1962) also assumed his conceptual model that the thickness of sediment deposited on the near shore profile equals to the increase of SLR.

Figure 8-4b showed the intertidal zone area within Tairua Estuary from tidal inlet to river mouth increases during spring water with 0.5 m and 0.8 m SLR scenarios. However, it decreases with 1.2 m SLR even though the average water depth increases with higher SLR at the Tairua River mouth, e.g., 13.6% with SLR 0.5 m, 9.06% with SLR 0.8 m, and 6.46% with SLR 1.2 m comparing with the present. This might be due to the intertidal zone being fairly flat (about average 1:4.3 slope) at approximately 0.9 m above mean sea level and hence the intertidal flat will actually decrease with a SLR of 1.2 m. This is likely to be under-estimation for the decrease in intertidal zone because any significant rise in sea level is likely to prompt a response from the local township to build shoreline constraining protection structures and embankments. This was not accounted for in the model results as a static terrestrial environment was assumed for each SLR scenario.

The residual circulation is the remains after the tidal currents have been removed (Carter and Pritchard, 1988). Residual flow plays an important role in the long-

term material transport process in the coastal area (Manh and Yanagi, 2000). The residual circulation indicates the long-term fate of water and particles in a given sub-domain and could be used for a qualitative estimation of the ultimate fate of passive particles released (Lopes et al., 2006). Figure 8-5 presents the residual currents calculated using the MIKE Zero toolbox over two tidal cycles based on the calibrated 'estuary-20m' MIKE 21 hydrodynamic model for 13 August 2010 (spring tides in dry season). The hatched area in the figure is dry land. The vectors are residual current speed and direction. Zone A is the intertidal flat close to tidal inlet and Paku Bay, which is close to the Paku marina (in the process of constructing).

Residual current effects were analysed for four main zones within Tairua Estuary.

-A large eddy is generated in Zone A with 0.5 m SLR by the increased current speed in shallow water. The higher discharge from Paku Bay with SLR can also contribute to this large eddy. As a result, sediment will be deposited on the tidal flat close to the flood tidal delta. The eddy size decreases more with SLR, because of the deeper water.

-The large eddy found in Zone B is associated with the sudden change in the channel direction. Therefore, it is less affected by SLR, but still affects sediment transport. The computed residual currents indicate that eroded sediment will be carried out from the river upstream and the water/land boundary, and will be pushed in Zone B. Part of the sediment will be deposited at Zone B and some will be carried seawards along the bank. Deposition will decrease with SLR because the ebb tidal currents along the main channel will decrease with increased water depth.

-Another large eddy is present in Zone C where the lower reach of the estuary meets the river and finer sediment is carried by the river deposited in this zone. With flooding from the Tairua River upstream, more bottom sediment could be stirred; the suspended sediment together with the sediment taken from river upstream will be carried to the lower estuary with high speed river flow.

-Zone D is the flood tidal delta within Tairua Estuary, where the tidal flow from the open sea outside, the main channel within the estuary, and Paku Bay discharge converge on the inner side of the tidal inlet. Simulation results in Figure 8-5 shows that speed and direction of residual currents will change with SLR in Zone D. SLR will result in flooding and hence shallow water at the head of the Pauanui Spit, the flood tide will have higher energy than the present situation. Therefore, the average current speed at the tidal inlet will increase and the direction will change. However, the residual current speed from Paku Bay and intertidal flat will decrease. As a result, the flood tidal delta will possibly move north-west. The residual currents indicate that more sediment erosion along the channel margins.

To calculate the changes of average sediment transport rate with SLR, four MIKE 21 ST (depth-averaged sediment transport) models were set up based on the 'estuary_20m' MIKE 21 HD model for different SLR scenarios and run for thirty days. Non-cohesive sand with 0.36 mm median grain size (d50) was applied in the model based on the sediment sampling results. The simulation results were extracted and plotted in Figure 8-6. The positive values represent net seaward sediment transport and negative values represent net sediment transport entering the estuary. The total residual flow includes wind-driven currents, density-driven currents and tide-induced residual currents (Manh & Yanagi, 2000). In this study, a two-dimensional numerical model forced by the tides, river discharge and wind was used for calculating the residual current, and the density-driven residual currents were ignored here.

The simulation results showed that the highest sediment transportation occurs at the inner side of the tidal inlet; when SLR is 0 m, the sediment at the tidal inlet and the lower estuary is mainly transported seaward and will deposit at the ebb tidal delta. With SLR, more sediment will be transported into the estuary and most will deposit at the flood tidal delta and intertidal flat close to the tidal inlet inside the estuary. However, Pauanui Beach is a pocket beach with limited sediment sources, so increased sediment inflow to the estuary may result in erosion of the beach. Figure 8-6 also showed that there will be more sediment taken to the Paku Bay from the tidal inlet. A Paku Marina will be constructed at the Paku Bay when this case study was carrying on. It is helpful for a better design of the Paku Marina to consider the impacts of sea level rise.

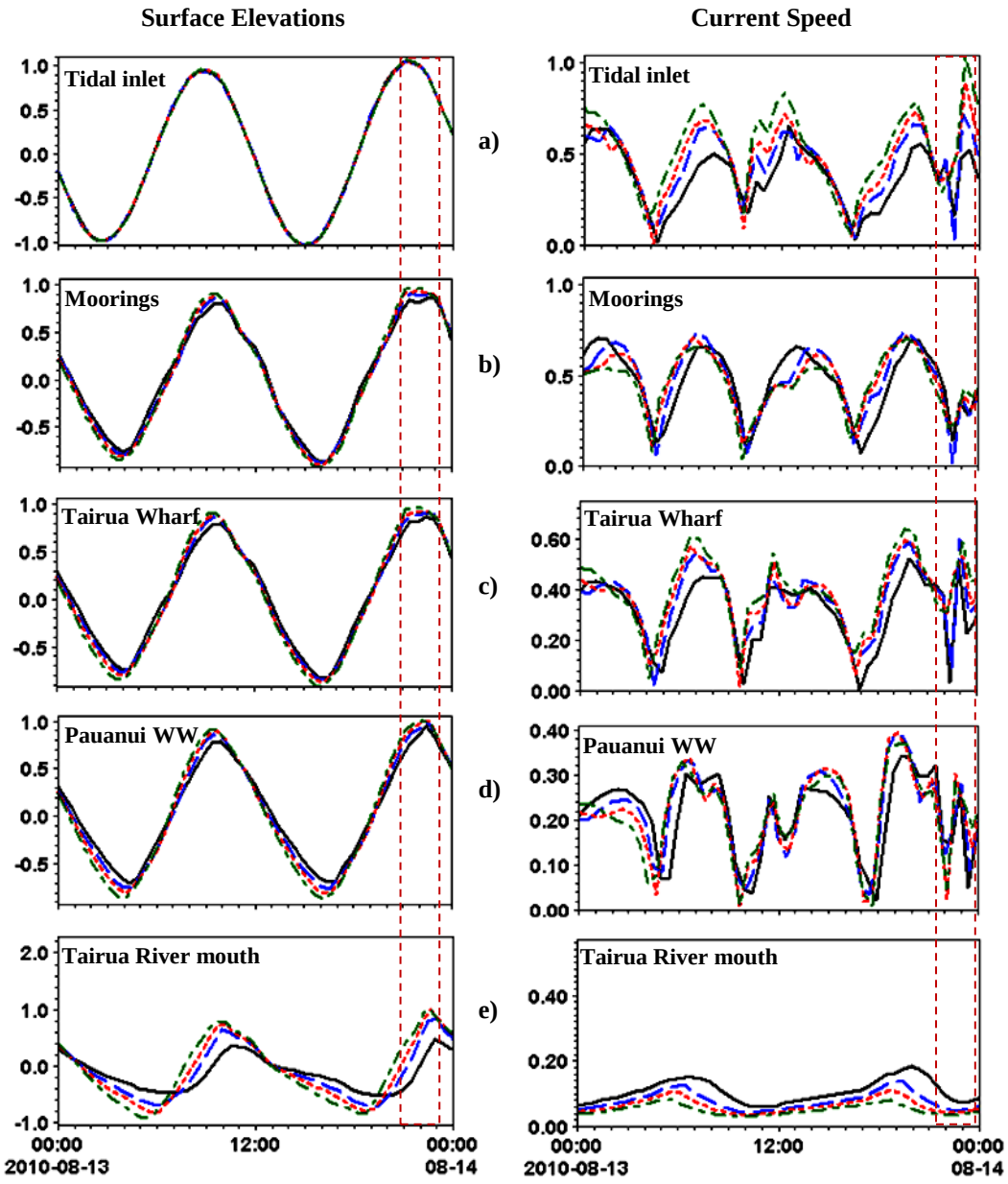

Figure 8-3 Surface elevations and current speed with SLR 0 m (black solid), 0.5 m (blue dash), 0.8 m (red dot) and 1.2 m (green dash-dot) at a) estuary entrance, b) moorings, c) Tairua Wharf, d) Pauanui Waterway and e) Tairua River mouth at Tairua Estuary

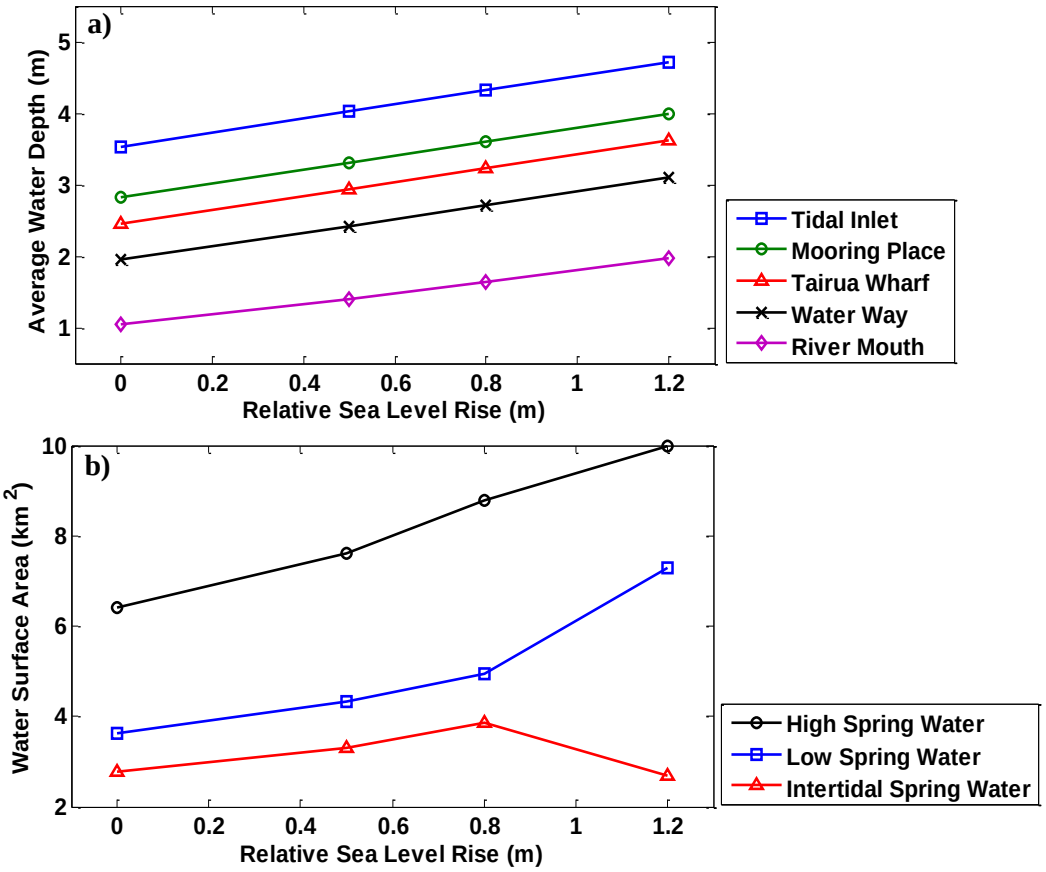

Figure 8-4 MIKE 21 HD model calculated 30-day a) mean water depth at the instruments locations from Tairua tidal inlet to Tairua River mouth, and b) mean water surface area during high spring, low spring and intertidal spring water with SLR 0m, 0.5 m, 0.8 m and 1.2 m.

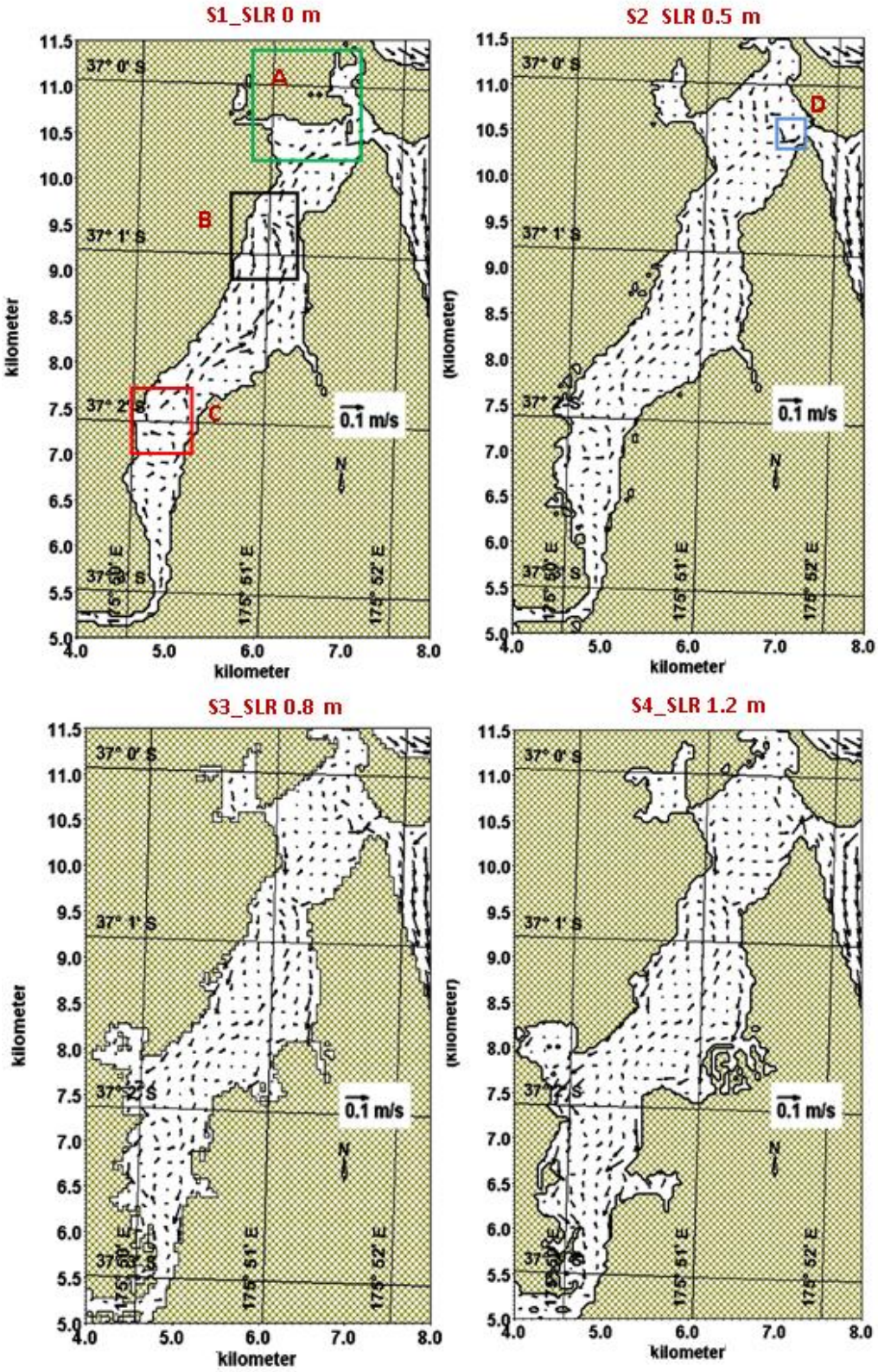

Figure 8-5 Residual currents with SLR 0 m, 0.5 m, 0.8 m and 1.2 m which were calculated based on two tidal cycles during high spring tides in 2010.

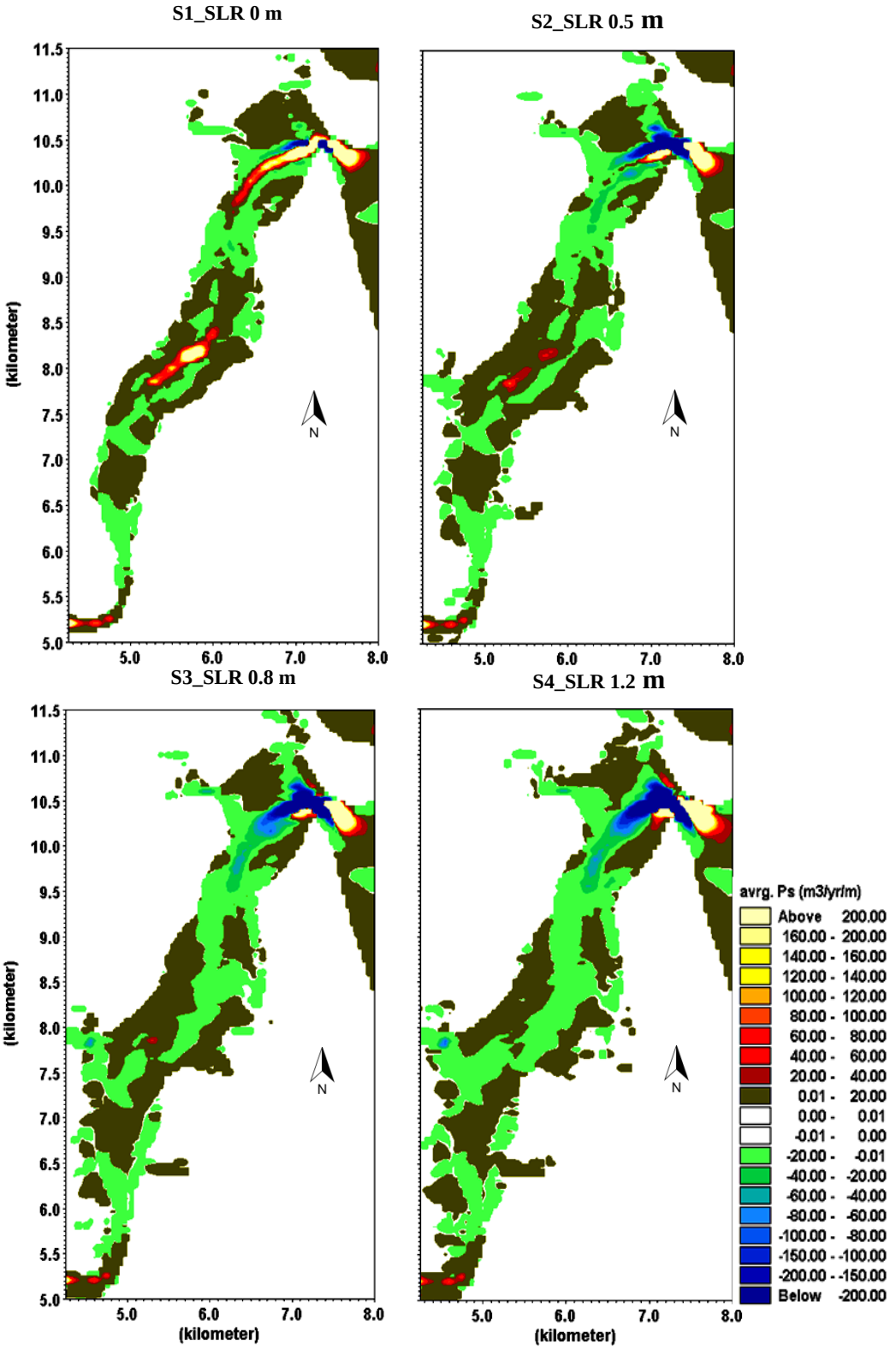

Figure 8-6 Mean sediment transport rate (m3 year-1 m-1) with SLR 0 m, 0.5 m, 0.8 m and 1.2 m calculated based on two tidal cycles during high spring tides in 2010.

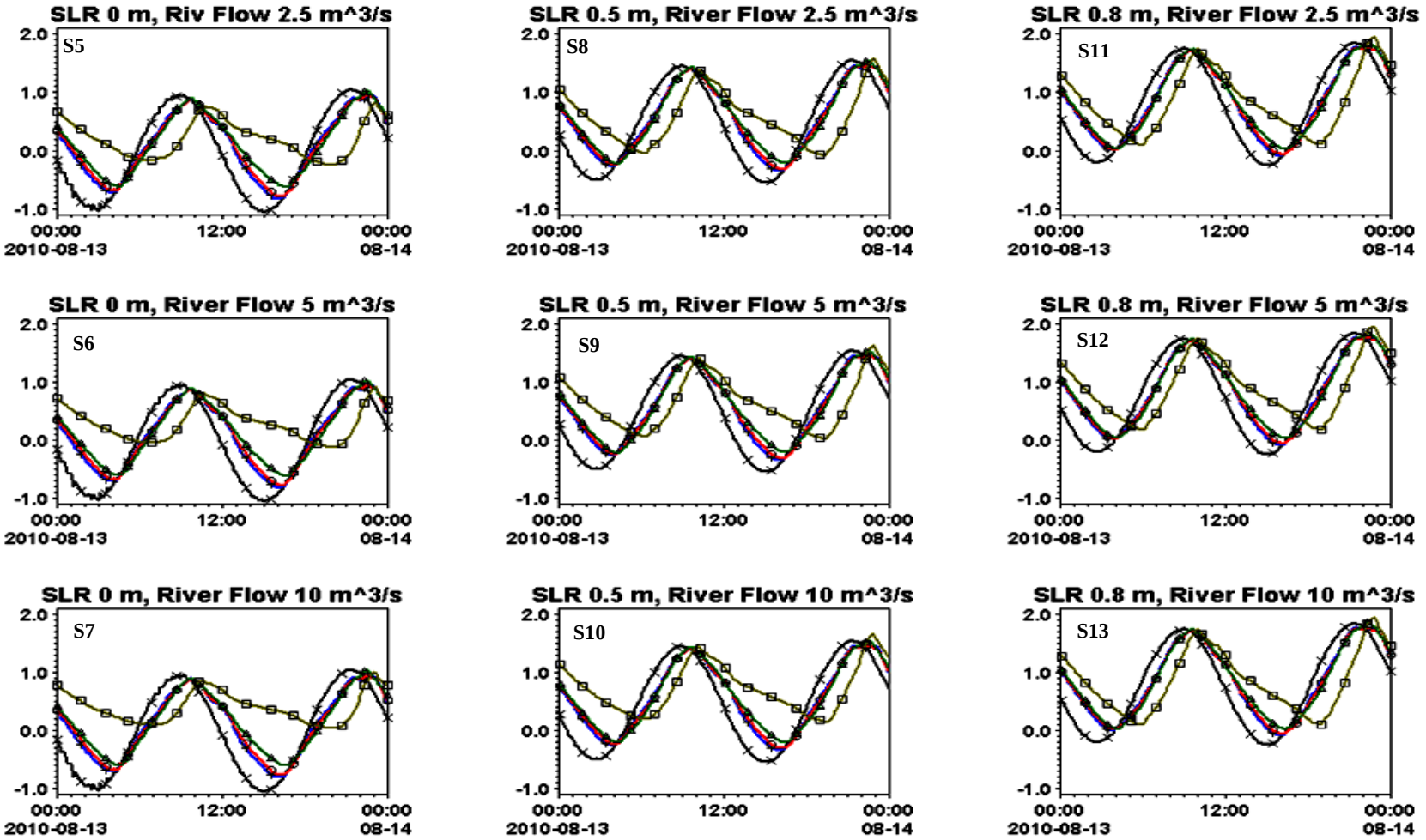

Figure 8-7 MIKE 21 HD Model calculated surface elevations at Tairua tidal inlet (black), moorings (blue), Tairua Wharf (red), Pauanui Waterway (green) and Tairua River mouth (yellow) with SLR and river discharge scenarios on 13 August, 2010.

Table 8-4 Computed tidal range at Tairua River Mouth (high spring tides in summer) with SLR and annual mean Tairua River discharge.

SLR (m)	River Discharge ($m^3 s^{-1}$)	Low Tides (m)	Time	High Tides (m)	Time	Tidal Range (m)
0	2.5	-0.407	6.20am	0.509	10.50am	0.916
0	5	-0.364	6.50am	0.462	10.40am	0.826
0	10	-0.343	7.20am	0.400	10.20am	0.743
0.5	2.5	-0.662	6.05am	0.749	10.15am	1.411
0.5	5	-0.619	6.15am	0.718	10.05am	1.338
0.5	10	-0.568	6.15am	0.666	9.45am	1.234
0.8	2.5	-0.777	5.58am	0.867	9.58am	1.644
0.8	5	-0.747	5.58am	0.822	9.48am	1.569
0.8	10	-0.667	6.08am	0.752	9.48am	1.420

8.6 CONCLUSIONS

SLR can modify current hydrodynamic and morphodynamic features at coasts and estuaries, due to increasing of wave setup, tidal prisms and currents, and shoreline changes (Douglas, 1997). The well-calibrated and validated MIKE 21 HD hydrodynamic model were used to simulate for various sea level rise (0 m, 0.5 m, 0.8 m and 1.2 m) with different river discharge (2.5 $m^3 s^{-1}$, 5 $m^3 s^{-1}$ and 10 $m^3 s^{-1}$) scenarios to estimate the impacts of local (Tairua Estuary) SLR on estuarine physical process, e.g. surface elevation, current speed, tidal range, water depth and river flow velocity. Four MIKE 21 ST (depth-averaged sediment transport) models were set up based on the 'estuary_20m' MIKE 21 HD model for different SLR scenarios and run for thirty days, to calculate the changes of average sediment transport rate with SLR. Non-cohesive sand with 0.36 mm median grain size (d50) was applied in the model based on the sediment sampling results.

The result of hydrodynamic modeling indicates that the estuary is ebb tides dominant over river discharge at present. Under the four SLR scenarios the degree of flood dominance along the main channel to the river mouth of the estuary increases. The more sinusoidal shapes of surface elevation and the less asymmetry between flood tides and ebb tides of the modelling simulation results with SLR can support this point. As a result, more salt seawater intrusion landward and more sediment transporting to the Tairua River upstream. This conclusion is very important information for water quality estimation and river bank protection with SLR. Hansen & Rattray (1965) also get the conclusion that SLR can likely result in changes in groundwater level and an increase in saltwater intrusion in coastal zones. The changes in the salinity gradient will alter the estuarine circulation.

Despite the flood tides dominant nature of flow regime along the main channel from tidal inlet to the river mouth with SLR, the net sediment transport is in the

flood tide direction. As a result, with higher SLR, the stronger flood tides can take more sediment into the estuary and deposit at the lower reach of the estuary, but less sediment will be flushed outside of the estuary with ebb tides. The sediment taken into the Tairua Estuary is mainly come from the Pauanui Beach. It implies that the Pauanui Beach will retreat. Pethick (2001) also concluded that changes occurred to the estuaries are a result of the redistribution of sediment within the estuaries as well as inputs from the marine environment.

The strength of flood flow is substantially increased more than that of ebb flow and as a result the net sediment transport is in the flood tide direction, resulting in infilling of estuary, especially the Paku Bay, where the Paku Marina is under constructing. This result helps to understand the SLR impacts on local area and a good design for it.

Accommodation space available for sediment infilling or water volume in an estuary, will influence estuarine transgression and is a function of relative SLR changes, freshwater flow, hypsometry and sediment supply (Cooper, 1993). At present, the Tairua Estuary is dominated by ebb tidal flow; with SLR, it is dominated by flood tidal flow more and more basing on the numerical modelling results. It is well known that estuaries were dominated by flood flow 6000 years before because they had more accommodation space available. It indicates that the Tairua kinds of estuaries will become younger with relative sea level rise.

Dominic (2009) suggested that if the estuary has an abundant influx of external sediment on a continuous basis, then the estuary is able to maintain its geomorphology and reach a stable state. Therefore, the future work should be carried out is to estimate the influx of external sediment to predict the estuary stability.

PART IV. MODEL APPLICATION

CHAPTER NINE
IMPACTS OF MARINA CONSTRUCTION, CHANNEL REALIGNMENT AND DREDGING ON ESTUARINE PROCESS

The Paku marina project including a 95-berth marina construction, Grahams Channel realignment and marina access channel dredging is being carried out at Paku Bay, Tairua Estuary. This study investigates the impacts of the project on the hydrodynamics and sedimentation of the lower reaches of Tairua Estuary. The peak tidal elevations, tidal currents, residual currents and sediment transport rate are calculated to compare before and after the marina project based on the calibrated MIKE 21 HD (Hydrodynamic) and MIKE 21 ST (non-cohesive sediment transport) models. The model results indicate that the impacts of the marina construction and the related activities on the lower Tairua Estuary system are less than minor.

9.1 INTRODUCTION

9.1.1 Research Background

As discussed in Chapter 5, the lower reach of Tairua Estuary is a dynamic system, affected by tidal exchange and river flows. Sedimentation appears to be concentrated around the sediment sources (i.e. river and stream mouth) as well as within the tidal delta system.

Tairua Marine Ltd (TML) proposed to extend an existing marina to 95 berths within Paku Bay (Figure 9-1), which is a small intertidal embayment situated on the lee side of the volcanic cone of Paku Hill, adjacent to Paku Drive near the entrance to Tairua Estuary. Residential development is directly related to the marina project.

Tonkin & Taylor Ltd (T&T) were commissioned by TML to study the impacts of the marina construction and related activities on the coastal physical processes in 2008. T&T identified likely sediment transport pathways and deposition patterns using a sediment textual model developed by McLaren (1981).

9.1.2 Marina Construction Project

This marina extending project mainly includes three activities (A, B and C in Figure 9-1).

- **95-berth Marina Construction**

A 95-berth structure, a concrete boat ramp and floating pontoon for general public use, with added breakwater protection and a sand roosting area; a public footpath around the Spit linking the boat ramp to Paku Drive, an extension of the existing footpath north along Paku Drive, a public footpath on the Marina road alongside the site frontage, and a ferry landing. The breakwater is separated from the marina piling by 10 m and the total area occupied by the structure is 960 m^2. A sand roosting area is proposed to be built outside of the marina sheet piling to provide a high tide beach at the entrance of Paku Bay, this will occupy an area of 2,600 m^2 (~4,200 m^3).

- **Grahams Channel Realignment**

The Grahams Channel is proposed to be realigned between the Causeway Bridge and the dredged marina access channel, to follow the historic channel alignment (1941). Once the new channel has been formed, the existing channel will be filled in with clean sand. The new channel will be 5 m wide at the stream bed with a total length of approximately 1,130 m. At the northern side of the bay, the channel will have a bank depth of 0.8 m and a stream bed at 0 m (relative to LINZ Mean Sea Level vertical datum). Bank depth reduces to 0.5 m in the south-eastern corner of the bay, and the channel bed at this point is at -0.2 m. The entire channel will have a slope varying between 1:1500 and 1:2500.

- **Marina Access Channel Dredging**

The marina basin and access channel are proposed to be constructed by dredging approximately 40,000 m^3 of sediment to create the marina facility, 32,000 m^3 of which will come from the marina basin, with the balance coming from excavations associated with access channel widening. The marina basin will be contained within PVC sheet piling driven to a finish level of 1.6 m above the existing seabed. The marina will be linked to the harbour entrance by a 320 m long access channel that will widen and deepen the current navigation channel serving the boat ramp and pole moorings in the area. A relative gentle slope of 1 to 6 (V:H) will be maintained on the landward side of the channel with a 1 to 3 (V:H) slope constructed on the seaward side.

9.1.3 Research Objectives

This case study is primarily to investigate the potential effects of the proposed marina construction and related activities on hydrodynamics and sedimentation in the lower Tairua Estuary. In particular, the following matters are to be assessed.

- Sedimentation changes within Paku Bay, with a focus on the south-eastern corner, which could lead to a change in substrate conditions.
- The potential effects that the widening and deepening of the access channel will have on the flood tide delta located in close proximity to the marina access channel, the harbour entrance and the ebb tidal delta.
- The potential effects on the intertidal flat and any sea grass or shellfish habitat present in this area.
- The circulation and flushing features within the proposed marina and implication for monitoring water quality inside the marina.

9.1.4 Methodologies

A MIKE 21 HD (hydrodynamic) model and MIKE 21 ST (non-cohesive sediment transport) model were developed with finer grid size (10×10 m), then used to simulate Tairua estuary. The current speed, residual currents, maximum current speed, peak flood/ebb flow and mean sediment transport rate were calculated and compared before (M1) and after (M2) the marina project.

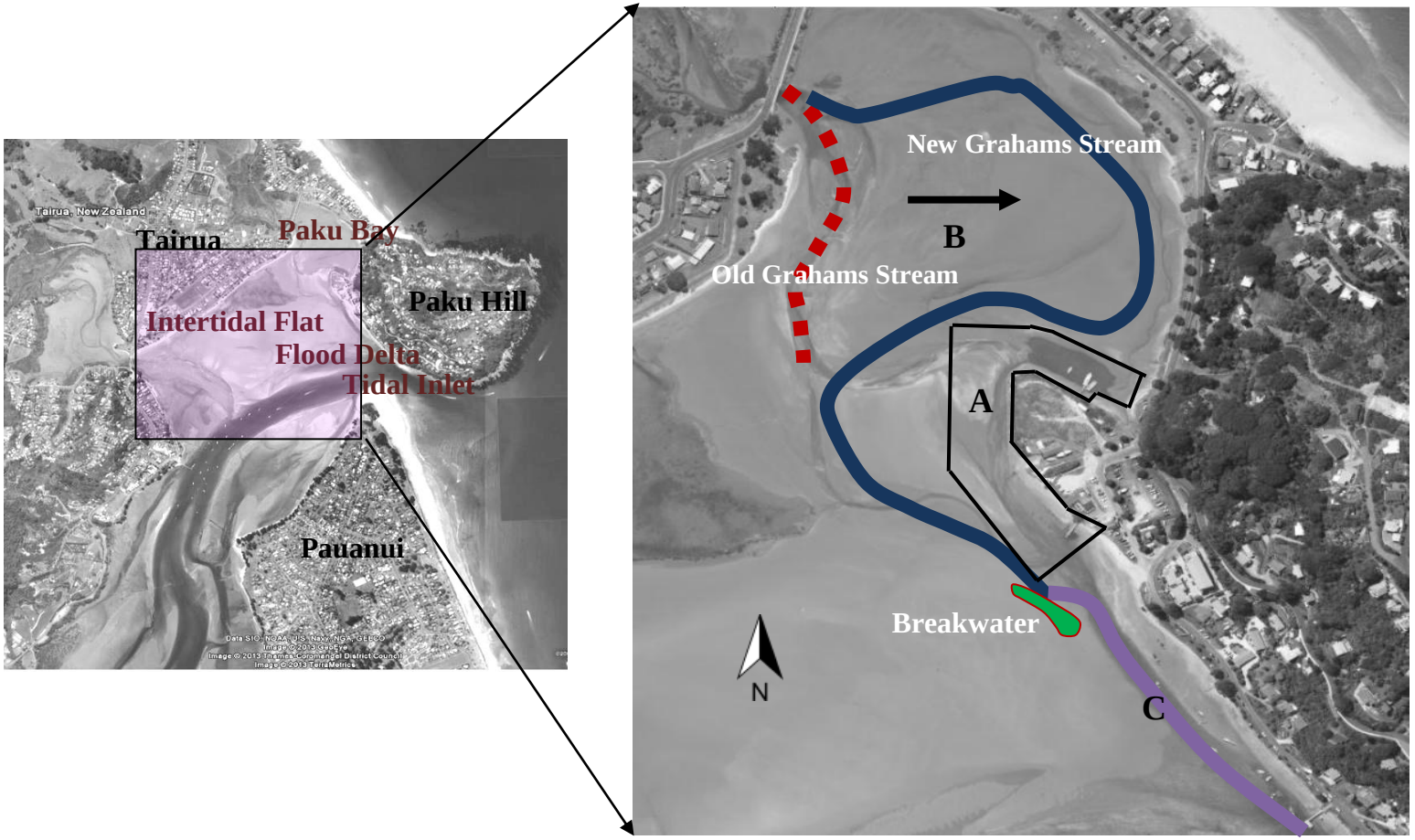

Figure 9-1 Aerial photograph of Paku Bay with the Paku Marina Zone to the western of Paku Hill. The marina construction includes: A. a 95-berth marina, B. a realigned Grahams channel and C. a dredged marina access channel.

9.2 NUMERICAL MODELLING

9.2.1 Bathymetries Development

The ‘estuary-20m’ depth-averaged MIKE 21 and 3DD hydrodynamic models with 20×20 m grid size were discussed in Chapter 4.

An ‘intertidal_10m’ (Figure 9-2 purple) and a ‘Paku_2m’ bathymetries were developed based on the 1×1 m original grids using the software of Manifold. Both bathymetries include the realigned 5 m wide Grahams Stream. Figure 9-3 shows the stages of the ‘marina project’ developed on the ‘intertidal-10m’ bathymetry. O1 is Paku Bay at present; O2 is after the construction of the Marina in the south-eastern corner of Paku Bay and dredging the marina access channel from the tidal inlet to the marina entrance; O3 is after relocating the original Grahams Channel to reduce fine sediment depositing at the back of the Marina Wall; O4 is after filling the original Grahams Channel.

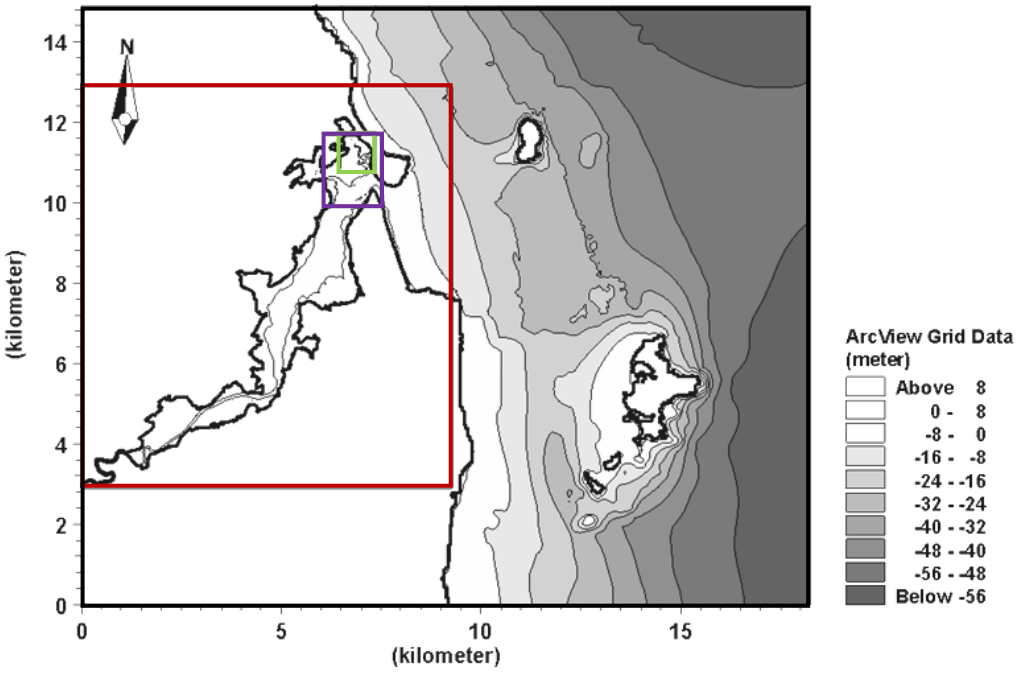

Figure 9-2 The four-resolution bathymetries with different extent developed considering the scenario requirements and simulation time, which include ‘whole_50m’ grids (black), ‘estuary_20m grids’ (red), ‘intertidal_10m’ grids (purple), and ‘Paku_2m’ grids (green). The plot is generated using the tool of MIKE Zero Plot composer and Grid Plot.

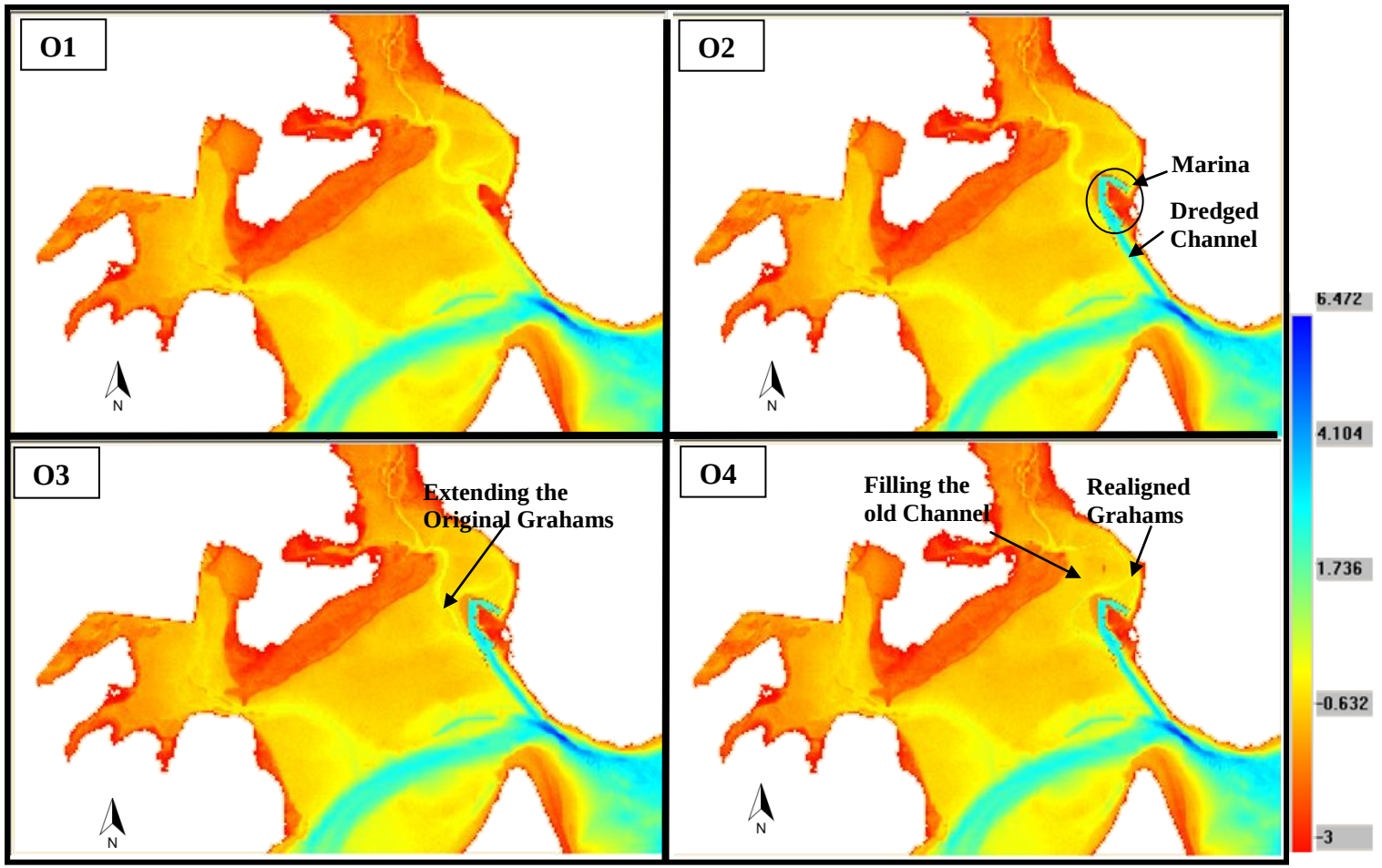

Figure 9-3 The 'intertidal_10m' bathymetries covering the Tairua intertidal flat, tidal inlet and Paku Bay at different stages of the marina construction process. The grid resolution is 10×10 m. I, J cell numbers are 300×200.

9.2.2 Model Boundaries

9.2.2.1 *River and Streams*

The Tairua River, Grahams Stream and Pepe Stream are the main fresh water discharging into Tairua Estuary (Figure 9-4). Grahams and Pepe Stream directly discharge into Paku Bay close to the marina site.

Sediment transport and deposition is largely determined by the bay's hydrodynamics. The company Tonkin & Taylor (2008) analysed the sediment samples and concluded that the contributing forces resulting in sediment transport are predominantly river and tidal flows. Together with freshwater discharge from Grahams Stream, the tidal Grahams Channel meanders through the eastern sector of Paku Bay providing drainage and influencing hydraulic circulation and sedimentation patterns in this area. At times the Grahams Stream is likely to carry significant volumes of fine sediments including sands, silts and clays.

The maximum and average river flow values for the three main fresh water sources are listed in Table 9-1, and the mean values were used as input into the hydrodynamic model as river flow boundaries.

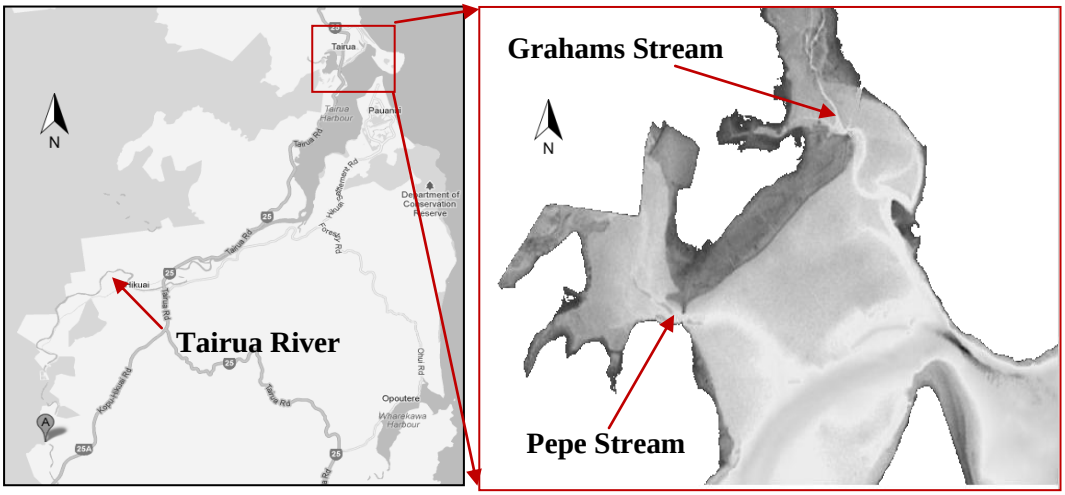

Figure 9-4 The Tairua River, Pepe stream and Grahams Stream discharging to Tairua Estuary.

Table 9-1 Mean and maximum Tairua River water level and discharge

Rivers	Mean Surface Elevation (m)	Max. Surface Elevation (m)	Mean River Flow (m^3/s)	Max. River Flow (m^3/s)
Tairua	-	-	9.7784	220
Pepe	0.52772	1.46	0.23346	1.46
Graham	0.25745	1.34	0.17698	0.75

9.2.2.2 *Tidal Boundaries*

The eastern and southern tidal boundaries are extracted and interpolated from the calibrated estuary_20m MIKE 21 HD model output. To reduce the eddies on the boundaries because of the shallow water, e.g., the intertidal area on the 'South 1' boundary and the shallow water close to the beach on the 'East' and 'South 2' boundary, the water depth was changed to be deeper.

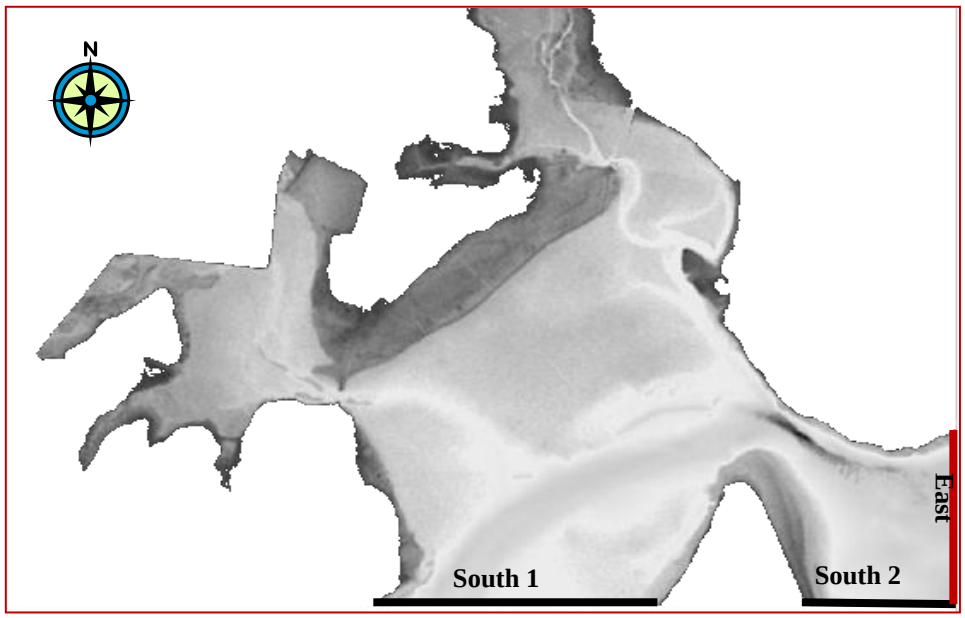

Figure 9-5 Eastern and southern tidal boundaries in the intertidal-10m model.

9.2.3 MIKE 21 HD Model Parameters

The hydrodynamic model time step was 5 s to make the maximum Courant number less than 5 and to keep the model stable. The simulation period was from 12.00pm 28 July, 2010 to 12.00pm 2 Aug., 2010, for a total of 501120 steps. The drying depth and flooding depth were 0.2 m and 0.3 m, respectively. The initial surface elevation was 0 m, the eddy viscosity was given as Smagorinsky Formula and the velocity-based coefficient was 0.5. The resistance was given as a constant Manning number of 32. No wind and wave was input into the modelling as Tonkin &Taylor (2008) suggested that waves are relatively mild within Paku Bay on the lee side of Paku Hill.

9.2.4 MIKE 21 ST Model Parameters

The 'intertidal_10m' MIKE 21 ST models were set up based on the MIKE 21 HD model. The simulation type of the model is 'current only' as waves were ignored.

The time step was 1 s. The simulation period is from 12.00pm 28 July, 2010 to 12.00pm 26 August, 2010, for a total of 4176 steps. The Engelund & Hansen pure current theory was used as the sediment transport theory with 2.65 relative density of sediment, sediment porosity of 0.4, average grain size of 0.36 mm, and sedimentation gradation of 1.25. The critical shields parameter was 0.045. Water temperature was 10°C. Bed friction was set as a constant Manning number of 32. The Lax-Wendroff theory was accepted as the morphological scheme with Courant based filter coefficients. A scaling factor of bed slope diffusivity effect of 1 was selected including a bed level update scheme. The lateral boundary condition was zero sediment flux gradient for outflow and specified gradient/extrapolation for inflow.

9.2.5 Model Scenarios

A MIKE 21 HD model and a MIKE 21 ST model were run based on the O4 bathymetry (M2) to compare the changes after the marina project within Paku Bay (M1). The model scenarios are listed in Table 9-2.

Table 9-2 Model scenarios to study the impacts of marina project

Model	Bathymetry				Boundaries		Wind
	Name	Grid size	Marina	Re-channel	Rivers	Offshore Tides	
M1	O1	10m	no	no	yes	yes	no
M2	O4		yes	yes	yes	yes	no

9.3 RESULTS AND DISCUSSIONS

9.3.1 Peak Flood/Ebb Flows

Figure 9-6 shows the peak flood flow and peak ebb flow for the lower Tairua Estuary before (M1) and after the marina project (M2) on spring tides. The flood flow branches into three flows after entering the tidal inlet. One branch flows along the main channel to the Tairua River upstream, one flows along the marina access channel into Paku Bay and one crosses the flood tidal delta to the intertidal flat. The branch to Paku Bay re-branches to the intertidal flat and further into Paku Bay. The flood flow is stronger than the ebb flow for Paku Bay and the neighbouring intertidal flat. This indicates that the area is dominated by flood flow and results in sediment infilling.

The differences of peak flood flow and peak ebb flow (M2-M1) for spring tides were calculated and mapped in Figure 9-7. During the peak flood flow, the vectors along the flood direction present a faster flood flow after the marina project (red arrow), the vectors in the ebbing directions present a faster flood flow before the marina (blue arrow), and vice versa. Both the peak flood flow and the peak ebb flow are slower along the marina access channel after the marina project. The breakwater increases the flood flow to Paku Bay mouth and the ebb flow to the marina entrance. More flood flow from the dredged marina access channel to the intertidal flat and tidal inlet. There are no significant changes in the flood and ebb flow at the inner intertidal flat.

Figure 9-8 are higher resolution maps of peak flood flow and peak ebb flow in Paku Bay before (M1) and after the marina project (M2) for spring tides. It shows that Paku Bay will be filled with sediment because flood flow dominates Paku Bay after the marina construction. The flood and ebb flow velocity will increase after the marina project because the marina piling wall constructed at the marina point Paku reduces the cross-sectional at the entrance of Paku Bay, and also because of the accelerating effects of the breakwater beside the marina entrance. The ebb flow from the causeway will flow across the new Grahams Channel beside the sand bird roost. It is likely to result in the channel infilling and reshaping after many years. Therefore, frequent maintenance dredging will be required. Current speed behind the marina wall will increase along the realigned Grahams Channel at the south-eastern corner within Paku Bay. It does not reduce the shielding effects as much the Grahams Channel realignment as expected.

The peak flood flow and peak ebb flow are plotted for the region of the flood tidal delta, the tidal inlet and the marina access channel in Figure 9-9. The flood flow is stronger than the ebb flow over the intertidal flat. The flood and ebb flows along the marina access channel are slower after the channel is dredged deeper and wider.

The peak flood and peak ebb flows within the marina are shown in Figure 9-10, and were used to investigate the water circulation and hence the water quality within the marina structure. The plot shows that the flood and ebb flow velocity decreases at the end of the marina furthest from the entrance (area B) because of the shielding effects of the sudden change in channel direction and distance from the channel. The breakwater at the right side of the marina entrance constricts the mouth with the marina piling wall. It increases the water flow velocity from the access channel to the Grahams Channel because of the reduced cross-sectional area. With ebb flow, channel restrictor increases the water flow velocity from the Grahams Channel to the marina access channel at the marina entrance. This increased current flow tries to flow toward the bank at point A after passing the breakwater. The strength of the flow is great enough to generate a turbulent flow at the marina entrance and forms a large eddy together with the ebb flow from the marina. This potentially results in sediment deposition in front of the marina

entrance, and also reduces the water quality with less water flushing out from the marina.

9.3.2 Tidal Currents

Time series of current speeds were extracted from the M1 and M2 model outputs with realigned Grahams Channel, through the dredged marina access channel and to the tidal inlet from 10 August, 2010, to 15 August, 2010 (for spring tides) and are presented in Figure 9-11.

Point P1 is located in the re-aligned Grahams Channel behind the marina at the south-eastern corner of Paku Bay. The results show that after the marina construction there is an overall increase in velocity and the flood velocity is stronger than the ebb velocity. Therefore, more tidal flow is likely to reach this corner after the channel is relocated. The mean peak flood velocity is about 0.2 m s^{-1} and the mean peak ebb velocity is 0.11 m s^{-1}, which represents increases of about 0.18 m s^{-1} for the flood flow and 0.08 m s^{-1} for the ebb flow after the project.

Point P2 is located in the realigned Grahams Channel at the mouth of Paku Bay. The velocities have increased but there is not much difference between the flood velocity and the ebb velocity. The model forecasts the mean peak flood and ebb velocity to increase by about 0.34 m s^{-1} and 0.29 m s^{-1} respectively after the project. More ocean water will flow through the deepened access channel into Paku Bay. The accelerating effect of the breakwater increases the flood velocity. Ebb flow velocity increases with the reduced cross-sectional area at Paku Bay entrance.

Point P3 is located inside the marina access channel and close to the flood tidal delta. The forecasted mean peak flood and ebb velocity at P3 is 0.42 m s^{-1}, which is about 0.08 - 0.1 m s^{-1} slower after project implementation. At this point, there is always a slack from ebb flow to flood flow.

Point P4 is located at the tidal inlet inside the estuary. At this point, the mean peak flood and ebb flow velocity does not change significantly after the marina construction project with the 0.92 m s^{-1} mean peak flood velocity and 0.75 m s^{-1} mean peak ebb velocity.

Point P5 is at the tidal inlet outside of the estuary. The M1 and the M2 model current speed results are also the same as each other with a 1.03 m s^{-1} peak tidal velocity. This coincides well with the conclusions of Hume and Herdendorf (1993).

Hence it is clear that the effects of the marina on tidal currents is relatively localised and result from flow constrictions and redirections at the end of structures.

9.3.3 Residual Currents

Residual currents are commonly defined as the tidal-cycle average of tidal currents. A residual current map is useful for assessing the locations of sediment deposition and erosion, and also forecasting the locations of the contaminated deposits.

For this case study, residual currents were calculated from the mean tidal currents over the tidal cycles from 5.50pm 28 July, 2010, to 10.40am 25 August, 2010. The residual currents and their differences are mapped for the area of the intertidal flat (Figure 9-12), Paku Bay, (Figure 9-13) and the flood tidal delta including the tidal inlet (Figure 9-14) before (M1) and after (M2) the marina construction, respectively.

In Figure 9-12, the residual flow from the upper estuary separates into two net flows at the tidal inlet inside the estuary. One branch flows to the outside ocean through the tidal inlet and one branch flows into Paku Bay, together with a residual flow from the ocean. These two flows meet and generate a large eddy at the flood tidal delta. The differences between the M1 and M2 residual currents indicate that there are no significant impacts on intertidal flat residual currents due to the marina construction. However, flood flows are faster along the marina access channel close to the flood tidal delta and flows slower along the access channel on the Esplanade bank site. The flood flow velocity also increases after flowing through the breakwater on the western side of the marina entrance.

Figure 9-13a shows the residual currents in Paku Bay computed before the marina construction (M1) on the basis of the 'intertidal_10m' hydrodynamic model from 5.50am 28 July, 2010, to 10.40am 25 August, 2010. The flood flows into Paku Bay entrance meet the ebb flow discharging from the mouth of the Grahams Stream and generate a large eddy at the south-eastern corner of Paku Bay. As a result, sediment is likely to be transported from the access channel, intertidal flat and the Grahams Stream to this area. Figure 9-13b summarises the surficial sediment texture in Paku Bay. Coarser sediment is found at M2, while finer sediments occur at N2 in the middle of the eddy and O1 which has lower flow velocities.

The other branches shown in Figure 9-13a will flow from the Bay entrance to the Manaia Road direction and reaches the point K2. It will re-branch into two flows at K2 upward to Paku Bay and downwards to the intertidal flat along the bank parallel to the Manaia Road. Therefore, fine sediments will deposit at K2 with

slower current speed, coarser sediments are taken to the points K1 and J2. These results coincide well with the T&T's sediment sample composition analyses results in 2008 (Figure 9-13b).

Figure 9-14a presents the residual currents at Paku Bay computed after the marina project (M2) basing on the 'intertidal_10m' hydrodynamic model from 5.50am 28 July, 2010, to 10.40am 25 August, 2010. The residual currents were increased at points A, D and H than at points C, E, G and F. It is likely that sediment will be taken into Paku bay, and the coarser sediment will be transported through the Grahams Channel to the Causeway. Finer sediment will deposit on the Paku beach behind the marina, and on the side of the Grahams Channel at points E and G. At the point B, where the realigned Grahams Channel changes direction and flows toward Paku Bay. The arrows across the channel suggest that the channel will be filled or the Grahams Channel will migrate away from the bird roost after a number of years. Flood flow dominates the interior of the marina. Hence, the marina will be infilled with fine sediment particularly at the end of the marina (Point F). Eddies and the turbulent flow at the marina entrance will reduce water circulation and affect water quality.

9.3.4 Mean Sediment Transport Flux

The mean sediment transport flux was calculated using the MIKE 21 ST (non-cohesive sediment transport) module.

Figure 9-15 shows the difference between the averaged sediment transport flux ($m^3yr^{-1}m^{-1}$) before (M1) and after the marina construction (M2). The results indicate that the main changes in sediment transport are on the flood tidal delta and in the tidal inlet. More sediment will be transported to the intertidal flat from the dredged marina access channel, all about 10 m3 yr^{-1} m^{-1}. Sediment will be transported at higher rate (16-24 m^3 yr^{-1} m^{-1}) from the flood tidal delta to the tidal inlet and will result in an increase of the ebb delta volume. This result coincides with the forecasting of T&T (2008).

Within the marina, the sediment transport rate is about 0.2-0.4 m^3 yr^{-1} m^{-1} at the entrance. Along the realigned Grahams Channel, the sediment transport rate is about 0.1–0.3 m^3 yr^{-1} m^{-1} at the mouth of Paku Bay. As shown in Figure 9-14a the water flow changes directions suddenly by the bird Roost adjacent to the marina wall, and flows back perpendicular to the bird Roost. This results in the sediment being pushed away from the Grahams Channel. The breakwater beside the marina entrance reduces the channel cross-sectional area with the piling of the marina, which accelerates the water flow from the access channel to the Grahams Channel and results in more erosion.

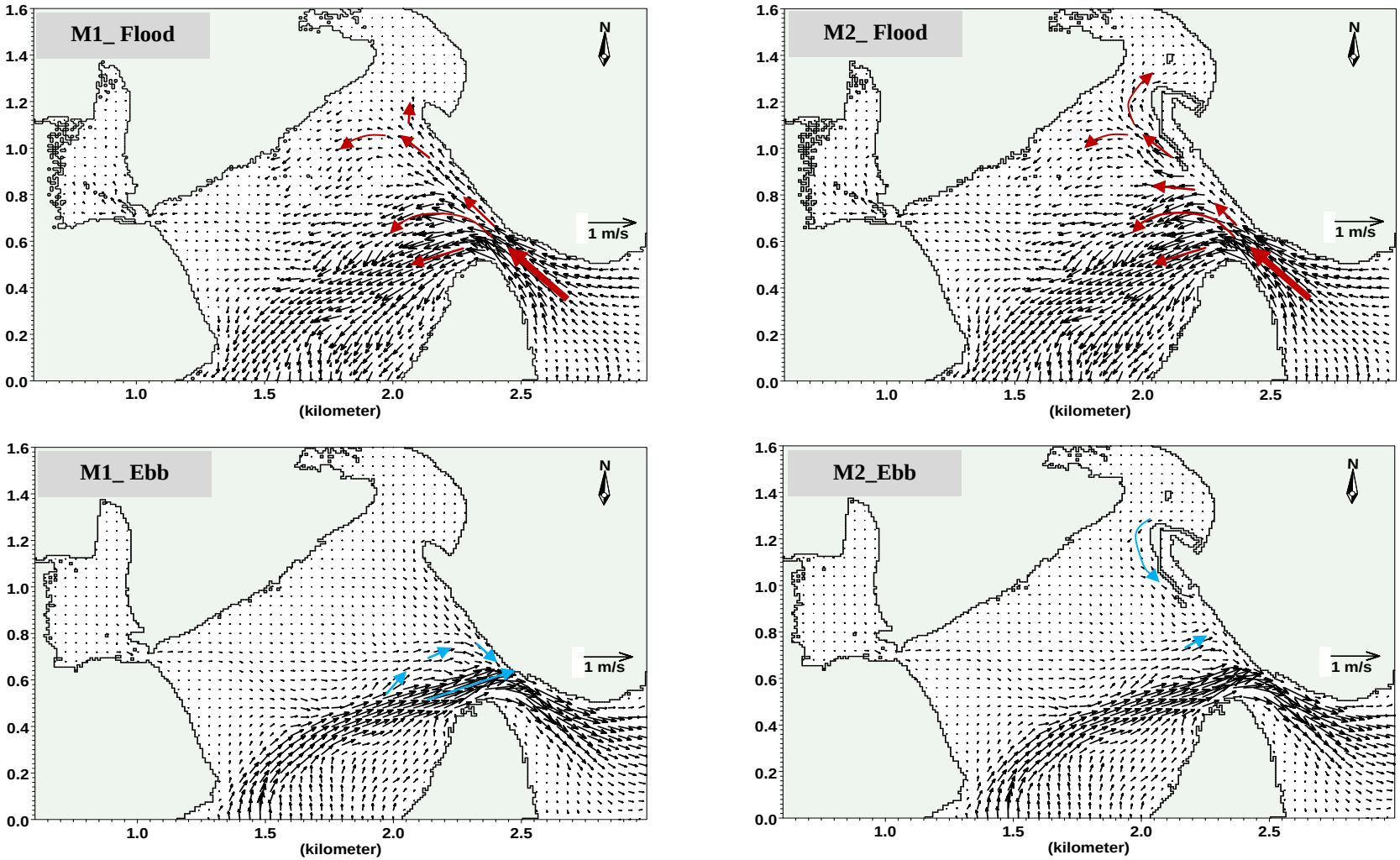

Figure 9-6 Peak flood flow and peak ebb flow at the lower reach of Tairua Estuary before (model M1) and after the Paku marina construction (model M2) on spring tides. The main flood and ebb flows are indicated as red and blue vectors respectively.

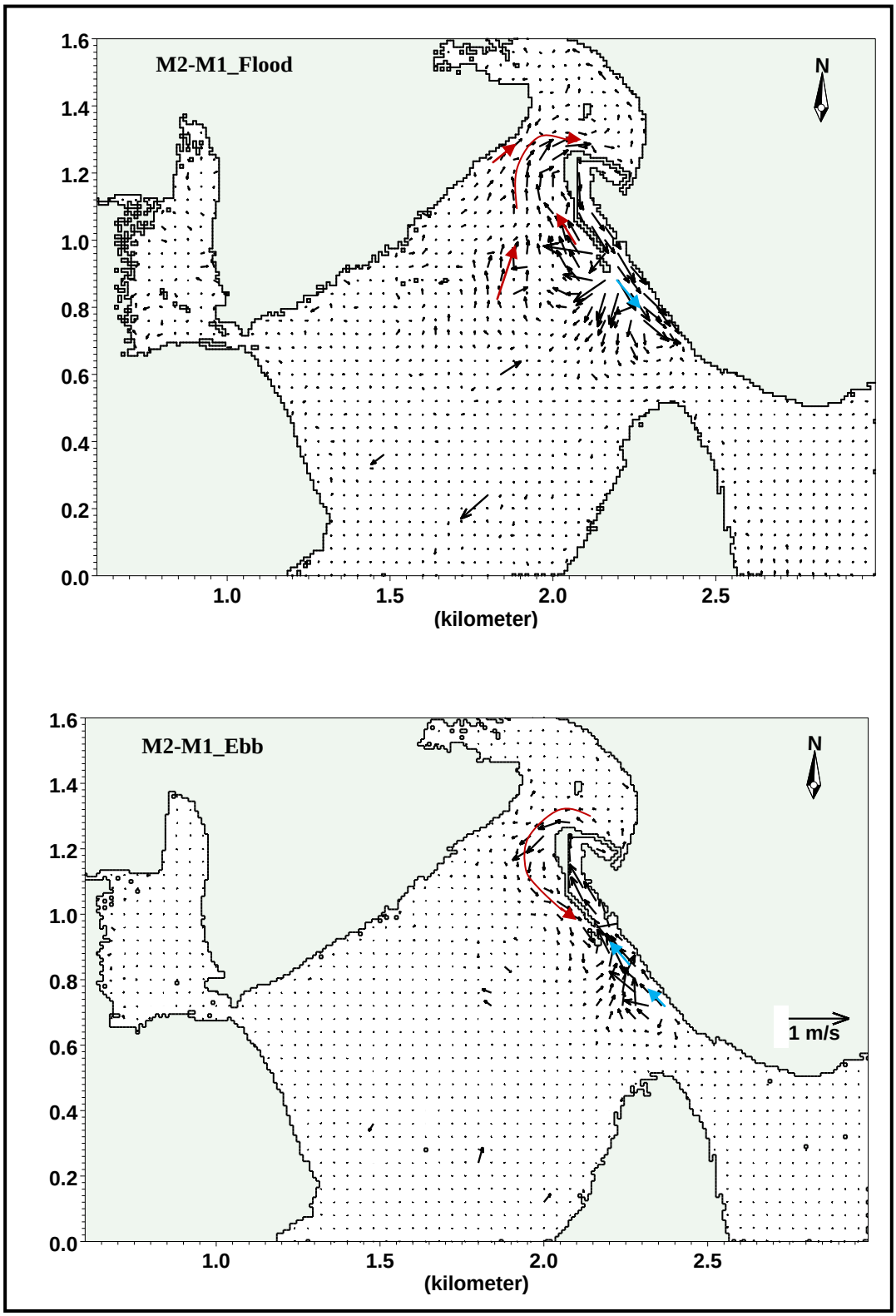

Figure 9-7 Difference between the peak flood currents (top) and peak ebb currents (bottom) before (model M1) and after the Paku marina construction (model M2) over the intertidal flat for Spring tides. The red vectors indicated the flow out from the Paku Bay and blue vectors presented the flow into the Paku Bay.

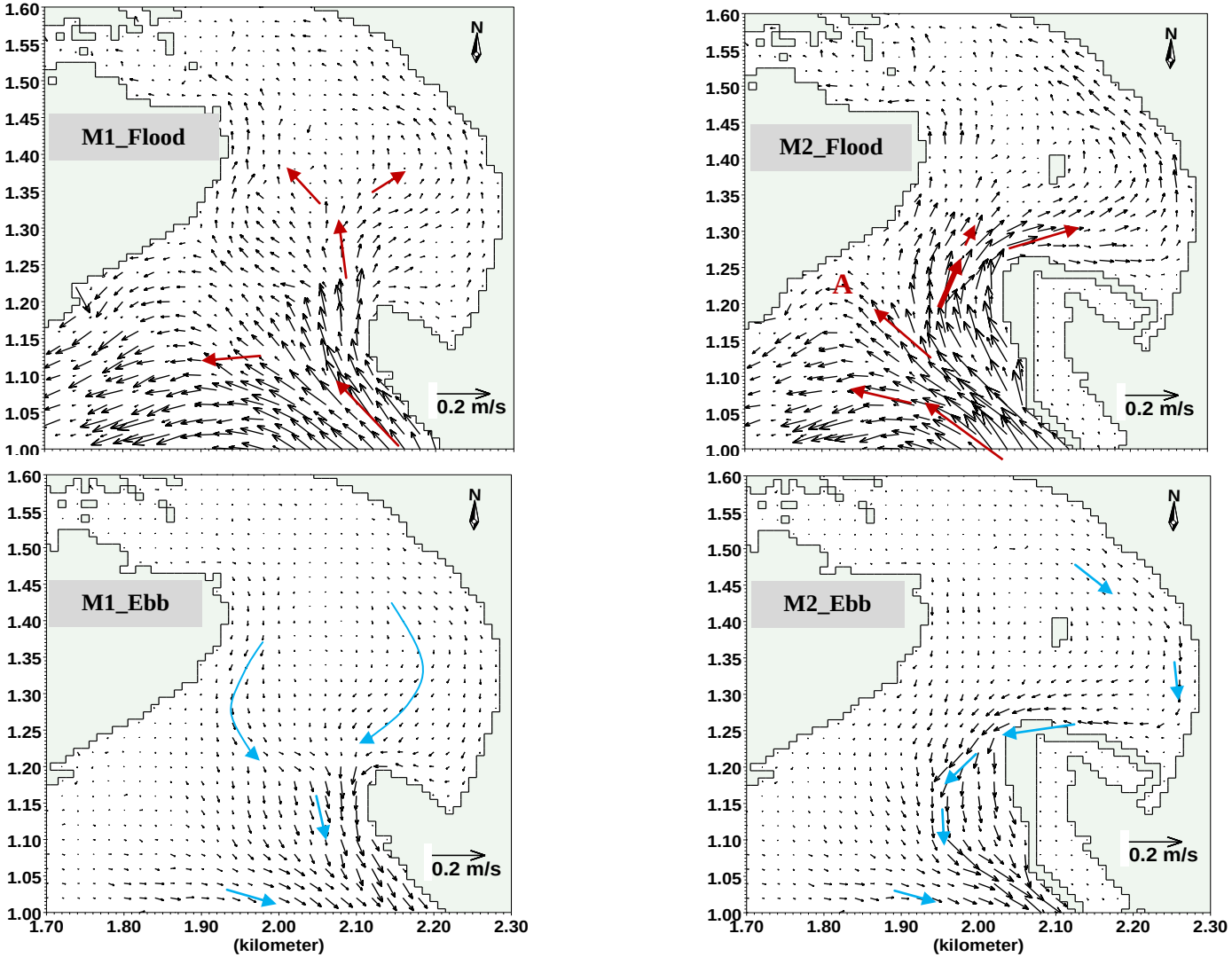

Figure 9-8 Peak flood and ebb flow at Paku Bay before (model M1) and after the Paku marina construction (model M2) for Spring tides. The red vector s indicated the flow out from the Paku Bay and blue vectors presented the flow into the Paku Bay.

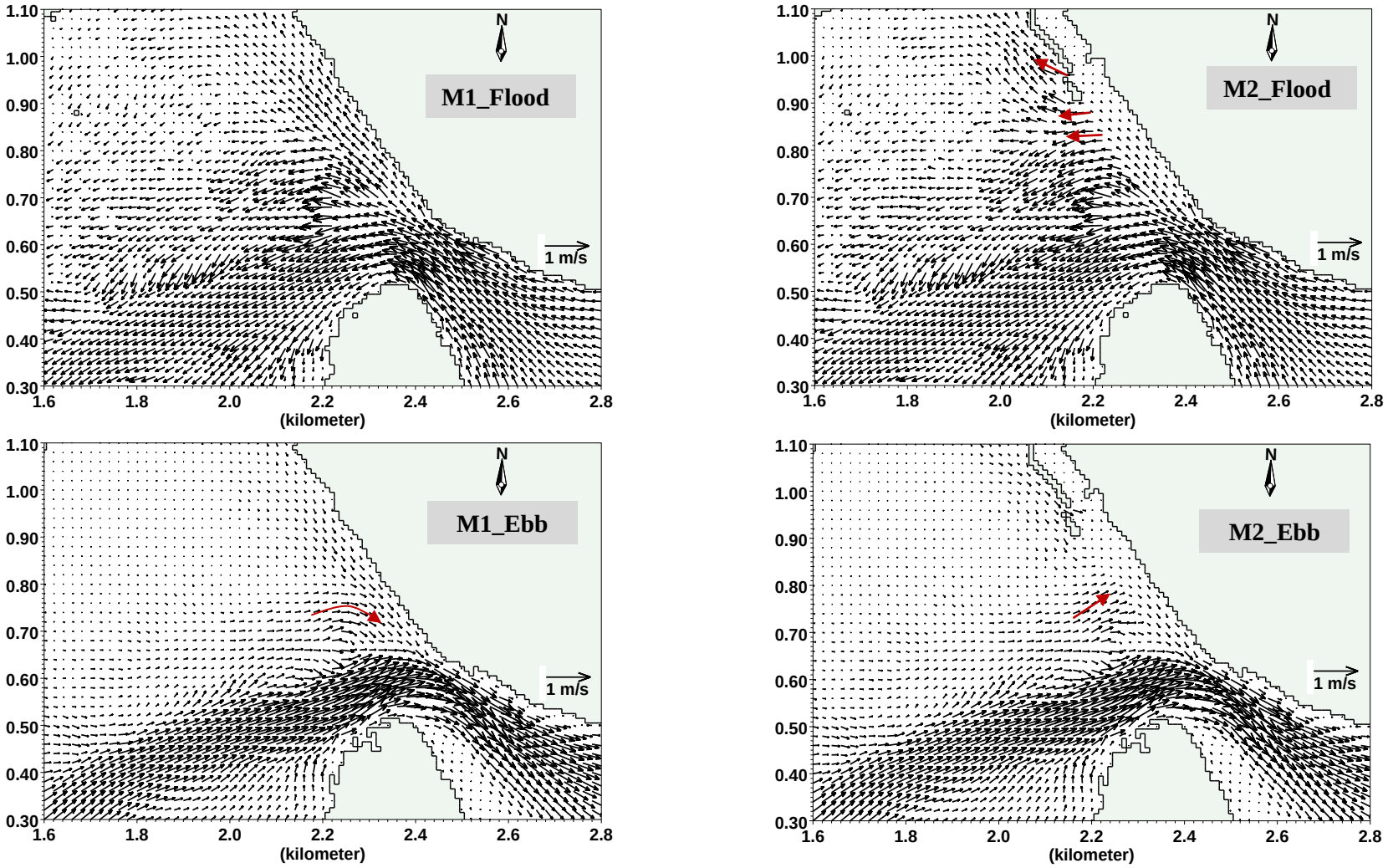

Figure 9-9 Peak flood flow and ebb flow over the flood tidal delta and through tidal inlet before (model M1) and after the marina construction (model M2) for spring tides. The red vector s indicated the flow out from the Paku Bay and blue vectors presented the flow into the Paku Bay.

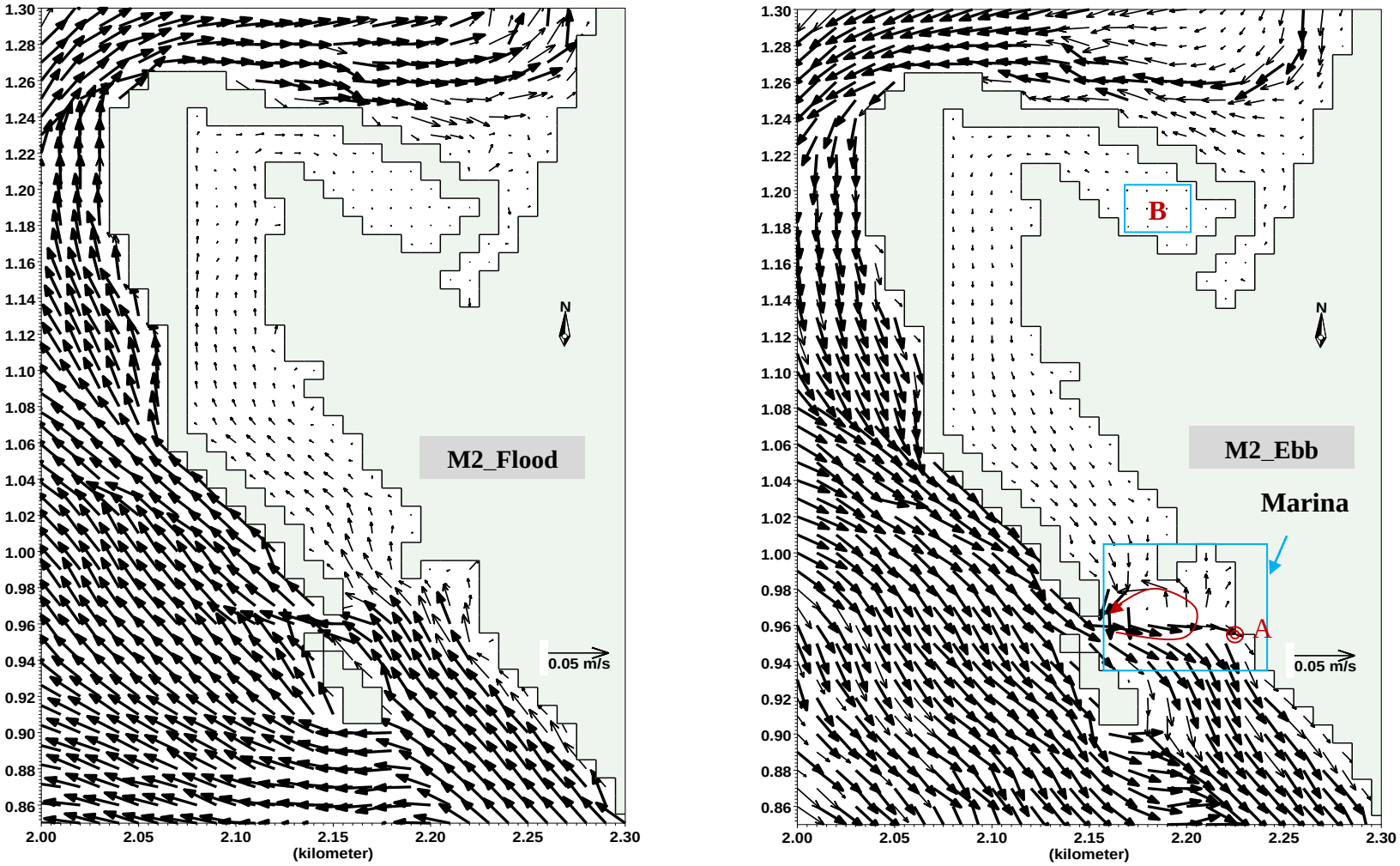

Figure 9-10 Peak flood flow and ebb flow inside the Paku marina after marina construction (model M2) for spring tides.

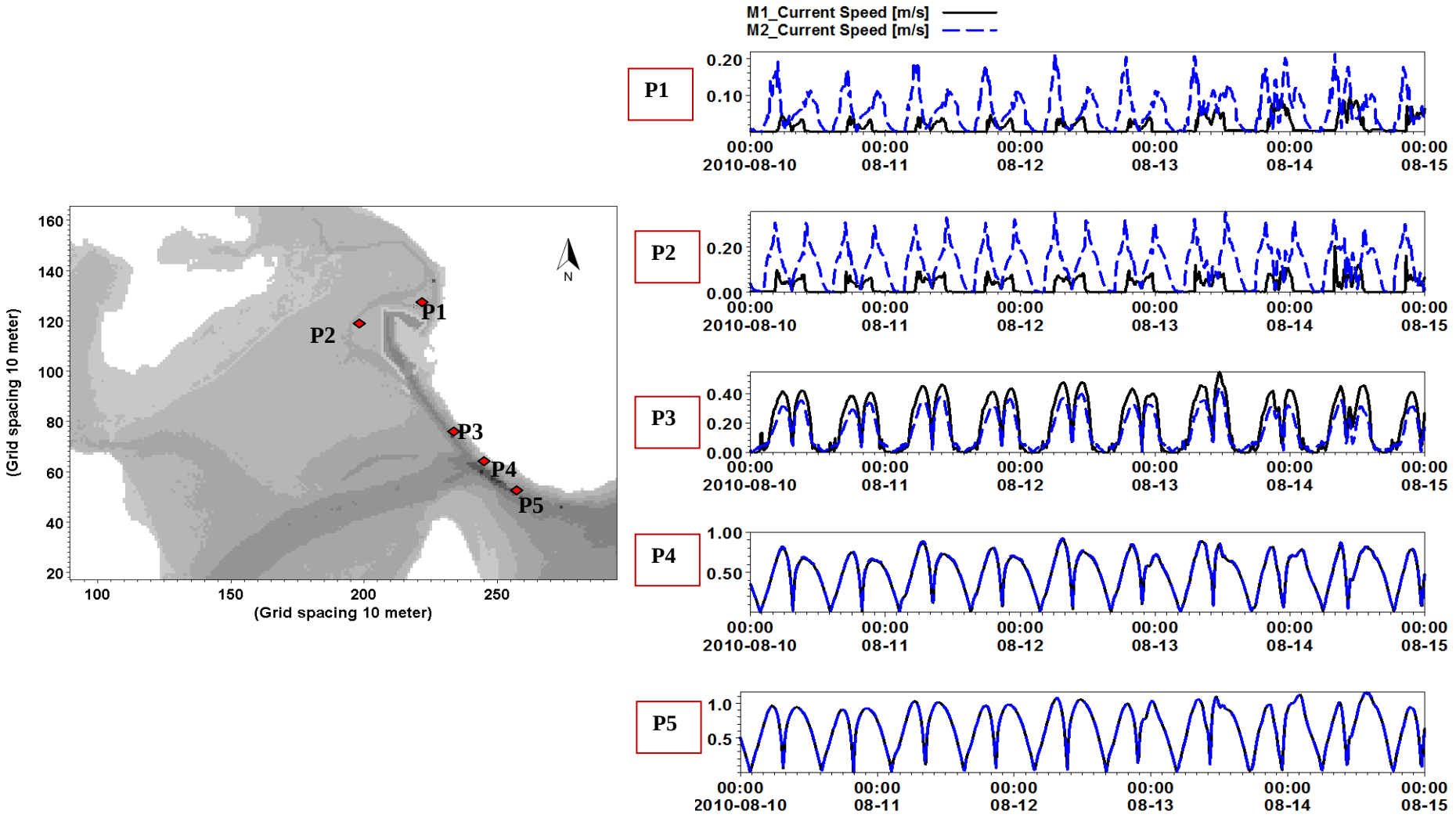

Figure 9-11 MIKE 21 HD Model calculated current speed at five selected points from Paku Bay to tidal inlet before (black solid line) and after the marina construction (blue solid line) for spring tides.

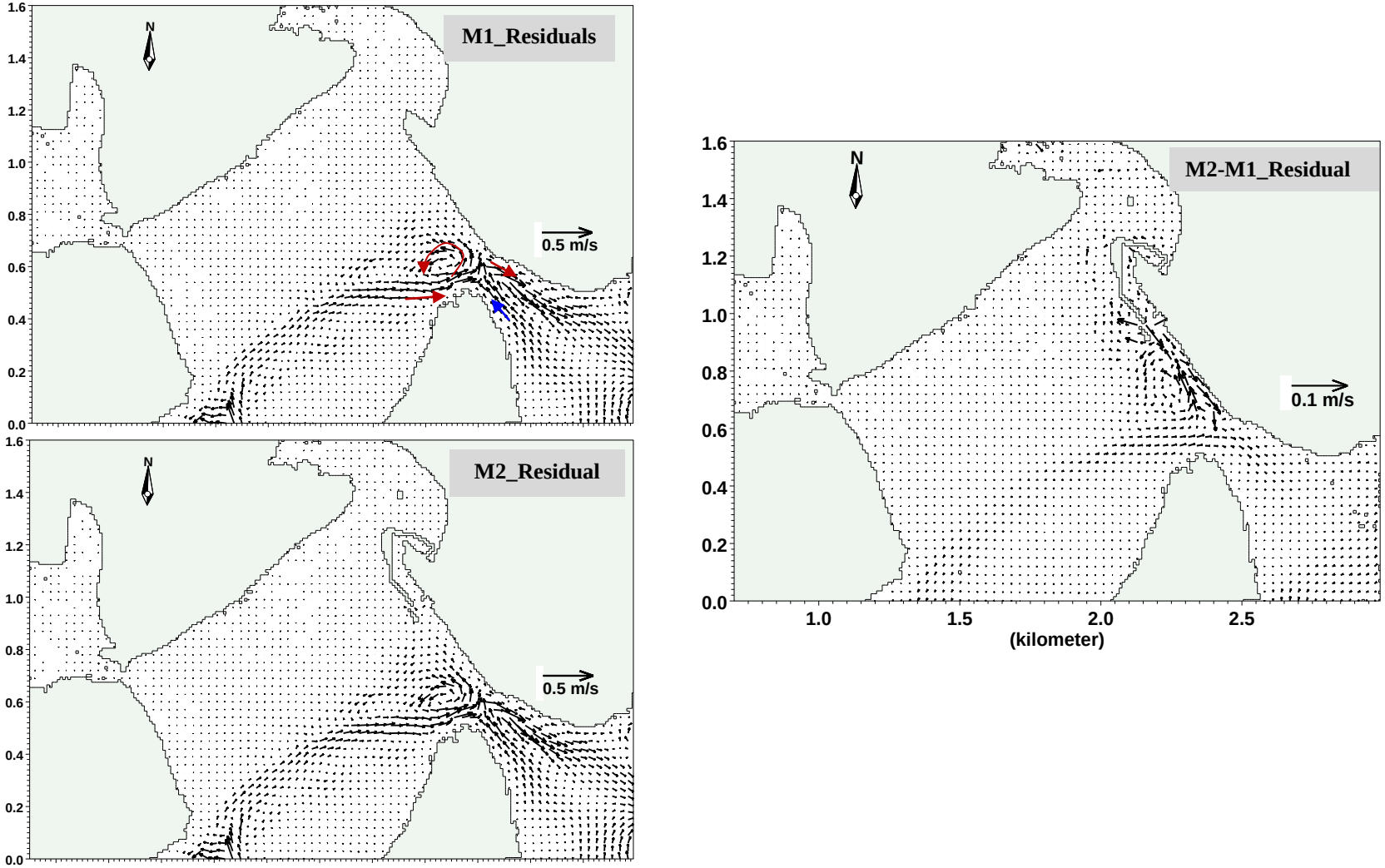

Figure 9-12 Residual currents of the lower Tairua Estuary computed by the 'intertidal_10m' hydrodynamic model from 2.50pm 28 July, 2010, to 10.40am 25 Aug., 2010 before (model M1) and after the Paku marina construction (model M2).

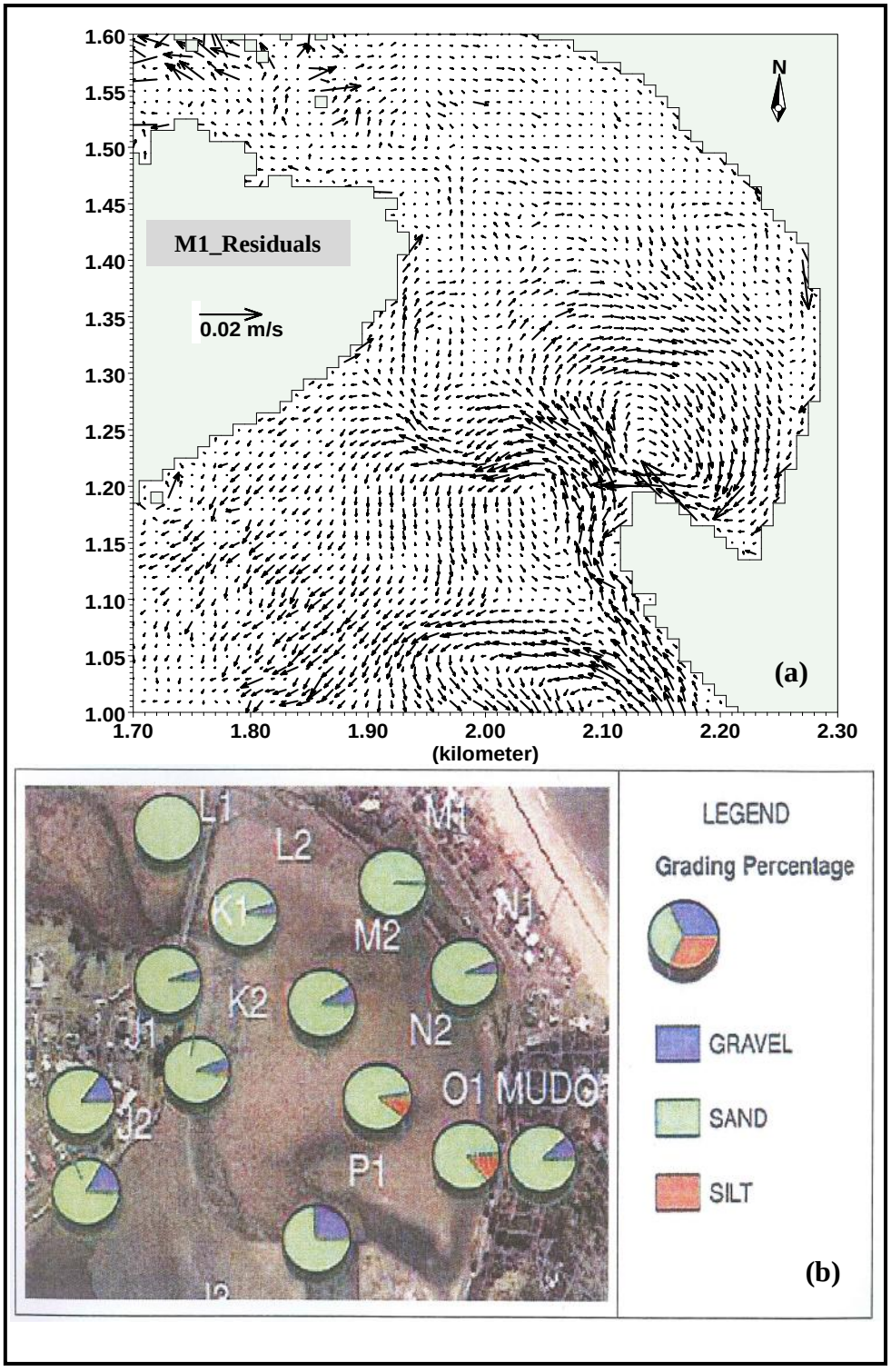

Figure 9-13 a) Residual currents at Paku Bay computed before the marina construction (model M1) by the 'intertidal_10m' from 2.50pm on 28 July, 2010, to 10.40am on 25 Aug., 2010, and b) the locations of sediment samples and textural analysis results within Paku Bay by Tonkin & Taylor in 2008.

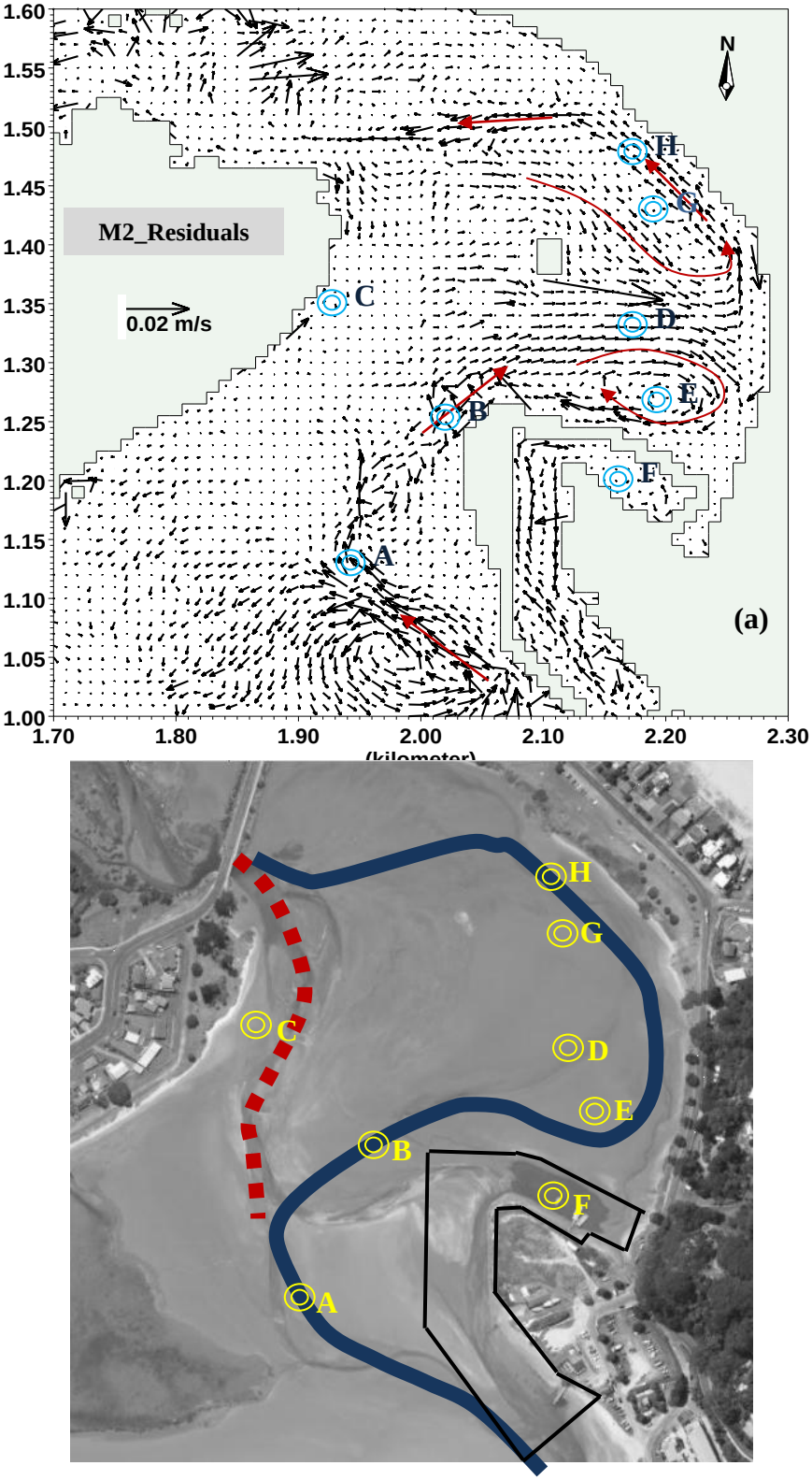

Figure 9-14 Residual currents at Paku Bay computed after the Paku marina construction (model M2) based on the 'intertidal_10m' MIKE 21 HD model from 17.50am 28 July, 2010, to 10.40am 25 August, 2010.

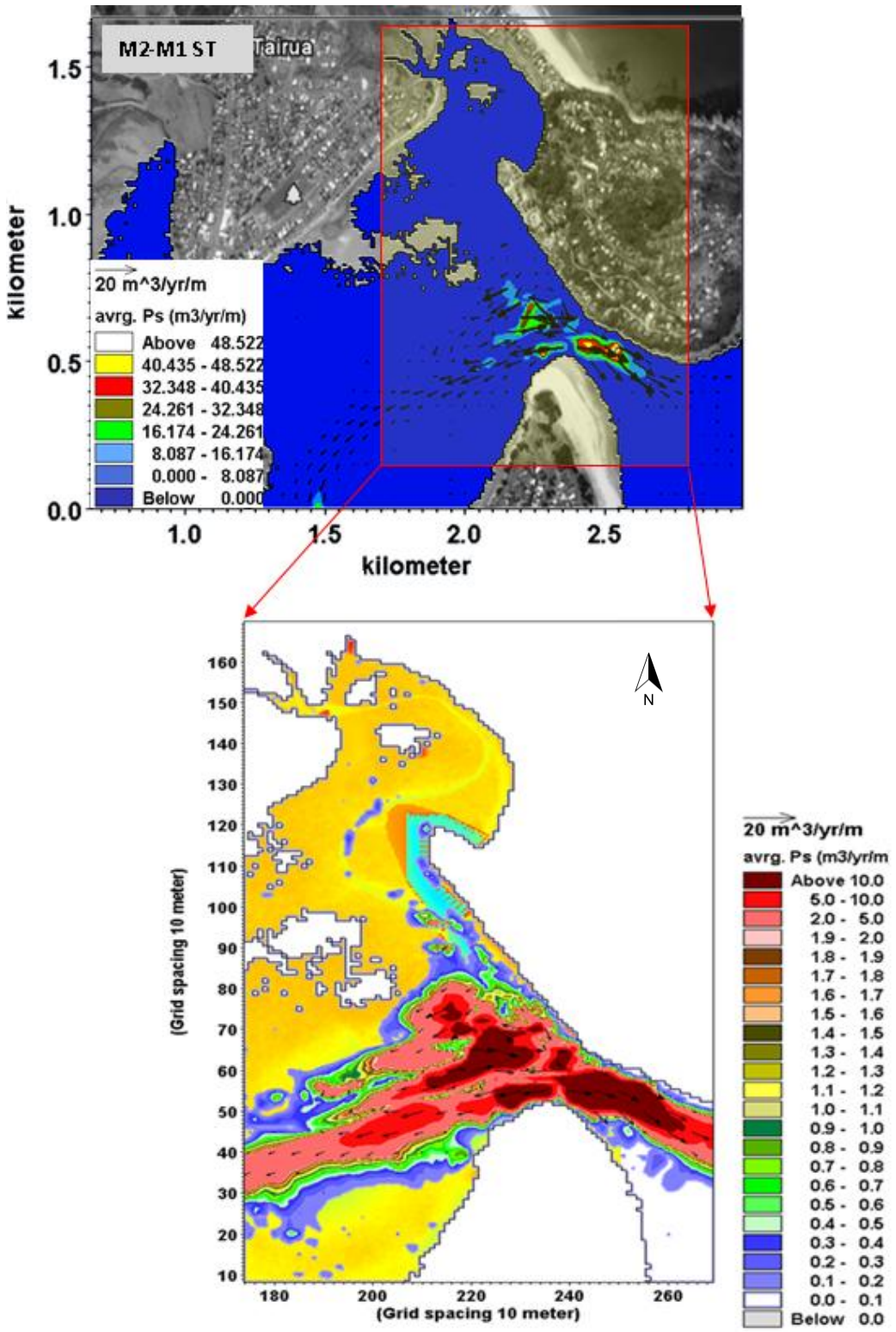

Figure 9-15 The difference of the mean sediment transport flux (m3 yr^{-1} m^{-1}) before (model M1) and after the Paku marina construction (model M2).

9.4 CONCLUSIONS

The 'intertidal_10m' hydrodynamic and sediment transport models were developed to enable comparison of the scenarios of before and after the marina construction project (including associated structures and realigned Grahams Channel). The results indicate that there are no significant changes in the flood/ebb tidal flow, current speed and residual currents over the intertidal flat after the marina project. However, the net flood flow velocity close to the marina will increase by about 0.05 m s^{-1} after going through the gap between the breakwater and the marina piling wall; as a result, sediment will be eroded from the marina entrance, the Esplanade beach and the intertidal flat. However, it will potentially not affect any sea grass or shellfish habitat present in this area because the sediment transport flux is very small.

Within Paku Bay, the velocity gradients and circulation eddies created by the Grahams Stream flow and tidal inflows will influence overall sedimentation patterns over time. Before the marina construction, during peak ebb tides, a portion of the sediments carried by the Grahams Stream are distributed to the lower Tairua. A portion of the sediment likely deposited at the south-eastern corner of Paku Bay because of the sheltering effects of the marina point Paku. River flows dominate over tidal flow, and the discharge from the Grahams Stream will become homopycnal, as density contrasts between seawater and stream water are small, causing the discharge to mix and spread out as an axial turbulent jet. Under these conditions coarse grained sediment will deposit near the river mouth at the Grahams Stream Bridge, and finer sediment will settle with increasing distance from the river mouth.

At other times tidal flows are expected to dominate over river inputs, resulting in potential density stratification and hypopycnal flows (where less dense fresh water overrides denser marine water) in which fine silts and clays again settle out with increasing distance from the river mouth as flocs, with coarser material such as sands deposited near the river mouth. In either case, tidal inflows into Paku Bay under current conditions are likely to deflect the Grahams Stream jet to the left and into the bay on the flood tide resulting in sediment accumulation within the bay, with finer sediments settling out in the more isolated eastern and south eastern margins of the bay.

After the marina construction, the Grahams Channel is re-aligned to reduce the fine sediment deposition because of the shielding effects of the Marina point Paku and Paku Marina. The results indicate the current speed at the south-eastern corner of Paku Bay is faster than the current speed before the channel realignment. However, finer sediment will deposit close to Paku Beach and the area between the historical Grahams Channel and the realigned channel. With increased flood flow from Paku Bay mouth into the bay after marina construction, the sediment

flushed through the Grahams Channel could not leave the bay. Instead it will be carried back to the beach at the south-eastern corner of the bay or flow along the new channel and deposit on the sides of the Grahams Channel and the causeway. As a result, the realigned Grahams Channel will be migrate and adjust over a number of years.

The marina access channel is dredged deeper and wider between the bank of the Paku hill and the flood tidal delta. This will result in slower flood and ebb flow along the deeper access channel. However, the channel dredging also changes the topography of the flood tidal delta. This results in changes to the hydrodynamics and sedimentation of the flood tidal delta, and also the tidal inlet system. More sediment will be flushed from the flood tidal delta to the ocean and deposit on the ebb tidal shoal; a portion of sediment taken from Pauanui Beach and the vicinity is taken back to the tidal inlet with flood tides and deposits on the southern side of the main estuary channel where the Pauanui Wharf is located. More sediment will be also transported from the access channel to the intertidal flat.

Flood flow will dominate the interior of the marina. As a result, the marina will be filled with fine sediment, and these fine sediments most likely will deposit at the end of the marina. The increased current speed across the front of the marina entrance near the breakwater will generate a turbulent flow at the front of the marina entrance, and obstruct the water exiting the marina during ebb tides. As a result, less water circulates within the marina and this, in turn, lowers water quality.

All the model calculated results suggest that the potential changes in the dimensions of the tidal inlet and tidal delta system due to the proposed marina redevelopment will not be significant compared with the 22125.27 ton per year catchments sediment yield (Mead *et al*., 2005) and 5.3×10^6 m^3 spring tidal prism of Tairua Estuary.

9.5 FUTURE WORKS

Future work will be to study the impacts of natural hazards on the marina area, because the site is exposed to natural hazards including wave effects, river flooding, tsunami, accelerated sea level rise and also the harbour seiche. These factors have been recognised as very important in the marina design, because any significant changes to flow patterns in this area as a result of the dredging could cause potential adjustments to the form and locations of the delta, with consequential effects on the inlet configuration and adjacent shorelines.

The dredged material from the marina construction is proposed to be deposited inside 5 and 8 m water depth offshore of the Pauanui Beach so that the material

could gradually return onshore to increase sub-aerial beach volumes along Pauanui Spit. The sediment distributing pathways are proposed to be simulated after collecting wave data offshore, as this study suggests the sediment could return into Tairua Estuary.

The marina structure in the model is not smooth enough because of the grids resolution (10×10 m). Therefore, finer grids (1×1 m) numerical models are necessary to be developed in the future, even though the model will run for long period and results in a very large output file.

CHAPTER TEN
CONTINUOUS OIL SPILL DISPERSAL PATHWAY AND FATE FORCASTING WITHIN TAIRUA ESTUARY

Based on particle tracking and a tidal flow model, this chapter studies the behaviour of oil slicks in Tairua Estuary. In order to track the oil slicks motion, a two dimensional oil trajectory model was developed using POL 3DD based on the well calibrated 3DD flow model introduced in Chapter 4. Five model scenarios predict the tracks of oil slicks, the variation in the shapes and size of the oil slicks, and the evaporation rate under the impacts of the tidal flow, air/water surface temperature, oil type, wind direction and speed. It also predicts the areas where oil slicks would be deposited at the shoreline. These results could be used as a reference for planning suitable response to oil spill accidents at Tairua Estuary.

10.1 INTRODUCTION

Oil spills may be due to releases of crude oil from tankers, offshore platforms, drilling rigs and wells. Oil enters estuaries in a number of ways, including spills from freighters, tankers, barges, small recreational and commercial craft going around and colliding with other structures; the oil is carried from highways, cities transportation, and industrial area into the estuary by the runoff of rainfall and snowmelt; oil leakage or seepage lead by the coastal refineries, factories and mills adjacent to estuaries. Estuaries are usually dense with vegetation and access is always tricky, so any clean-up operation would be extremely difficult.

The various levels of biological effects of oil include human hazards through eating contaminated seafood; decrease of fisheries resources and damage to wildlife such as sea birds and mammals; decrease of aesthetic values due to unsightly slicks and oiled beaches; modification of marine ecosystems by elimination of certain species with an initial decrease in diversity and productivity; modification of habitats, delaying or preventing re-colonisation (Doerffer, 1992).

Once the spill occurs, then accurate forecasts of the speed and direction of the slick, as well as the spreading rate, are of great importance. Based on that information the best method of clean-up can be determined and implemented. It helps in selecting eco-sensitive regions for preparedness and planning suitable response strategies whenever spill incident occurred (Quang et al. , 2013). Simulating the oil distribution with random motions induced by waves, wind and tidal currents is benefit for protecting the environment (Doerffer, 1992).

Various oil spill models have been developed by Cohen al. (1980), Huang (1983), Yapa et al. (1994), Spaulding (1995), ASCE Task Committee (1996), Li and Mead (1999) focusing on the surface oil movement and distribution. Many field, laboratory and modeling studies by Johansen (1984), Elliot et al. (1986), Delvigne and Sweeney (1988), Singsaas and Daling (1992), Reed et al. (1994a) have demonstrated the importance of natural oil entrainment to both the mass balance calculations and the spatial and temporal distribution on sea surface. Quang et al. (2013) used MIKE 21 SA model to simulate oil spill transport with five scenarios. The results of simulation showed that spill trajectory and slick area depend on analysis hydraulic regime, wind direction and wave in the study area. However, the factors influencing oil spill distribution, especially the relationship between the oil spill distribution pathway and estuarine physical process had not been studies so much.

In this chapter, an oil spill accident resulted from a boat collision in front of the Tairua Wharf was 'generated' for case study. Five POL3DD oil spill models were developed on the basis of the well calibrated estuary_20m 3DD Flow model forced by the offshore tides, river discharge and wind. The models simulated not only the oil spill trajectory (distributing pathways), oil slicks shape and size on the water surface, the oil particles distribution, but also the oil deposition along shoreline, for better understanding the factors influencing the oil spill distribution and the impacts of the estuarine process on oil spill distribution.

10.2 OIL SPILL SCENARIOS

An oil spill accident scenario was developed located on a ferry grounded on the rock close to the Tairua Wharf after filling the petrol/diesel at 2.00pm on 12 August, 2010. The oil tank of the ferry held 60 m^3 and leaked at a rate of 5 $m^3 h^{-1}$ for 12 hours.

The Tairua Wharf was selected for this study as the oil spill location because of its key locations in the middle of the lower reach of Tairua Estuary (Figure 5-10). It is influenced by the tidal flow from the outside ocean and also the Tairua River, Pepe Stream and Grahams Stream. The tidal inlet is to the north-east and the Pauanui Waterway is to the south-east; the Hahei and hot water beach are to the north; and Whangamata, is to the south. There are regular ferries between Tairua Wharf, Paku Wharf and Pauanui Wharf; it is a popular spot for fishing in Tairua Harbour; and there is a fuel company located here to supply petroleum products (Figure 10-1).

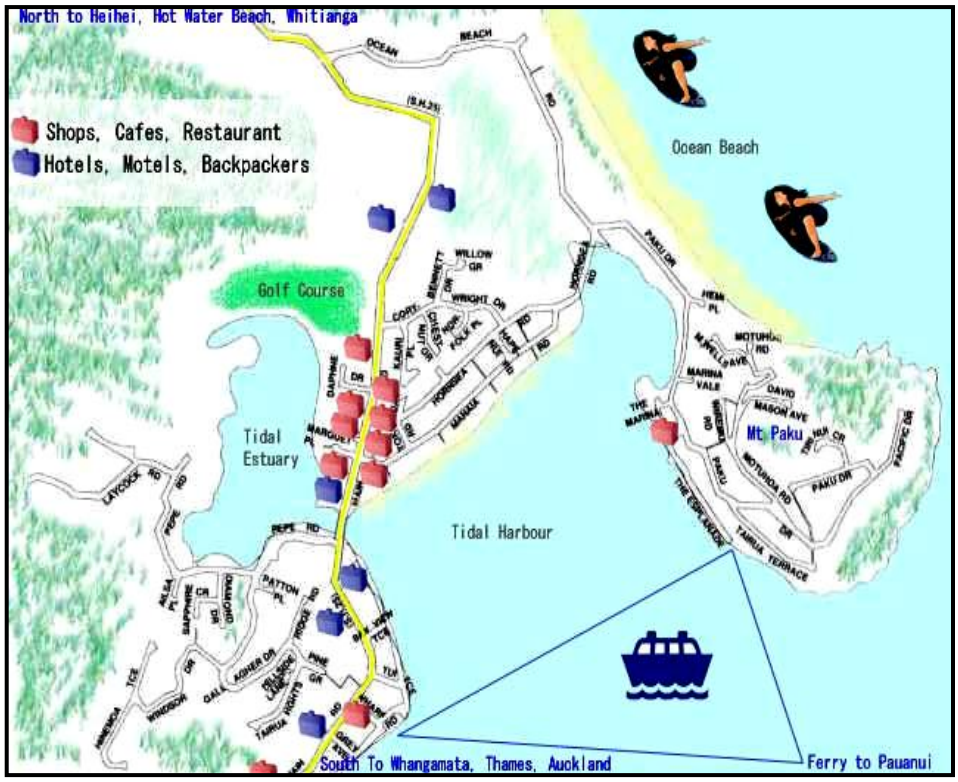

Figure 10-1 Tairua Wharf is located within the main Tairua urban area, where it is a ferry transport centre and close to the tidal inlet.

10.3 OIL DISPERSAL MECHANISMS

Figure 10-2 summaries the main mechanisms that govern the trajectory and the fate of an oil spill at sea are spreading, evaporation, dispersion, emulsification and biodegradation (Shen and Yapa, 1988).

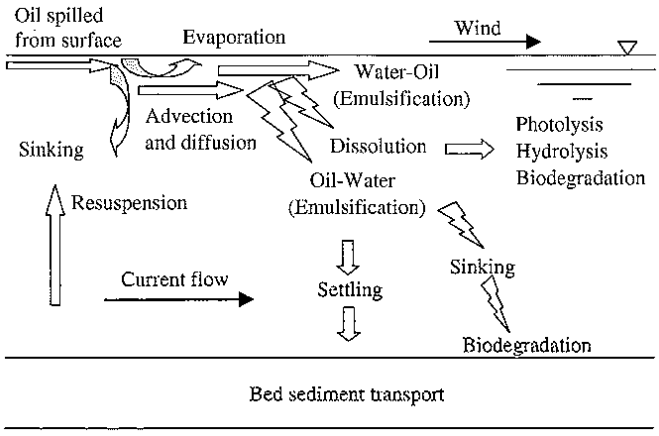

Figure 10-2 Oil slicks transformations at sea (Shen and Yapa, 1988)

10.4 EQUATIONS USED IN POL3DD OIL SPILL MODULE

The POL3DD Oil Spill models are developed for simulating the rate of oil discharged or accidentally spilled at the selected locations. In POL3DD Oil Spill, Lagrangian particles with three-dimensional coordinates represent the cloud of oil. These particles are tagged with a position, volume, concentration, Carbon number and a variety of other parameters. The particle volumes are subject to decay by dissolution and evaporation.

The methods adopted for dissolution and evaporation follow the procedures of Rye (1995); the evaporation rate is dependent on a mass transfer coefficient, area of sea surface covered by condensate, the molecular weight of each component, saturation vapour pressure, gas constant and absolute temperature; for dissolution, the model considers the entrained oil to be in droplets, with a size that depends on the Carbon Number. The dissolution depends on a mass transfer coefficient, surface area of the droplets and seawater solubility of each constituent.

The buoyancy of the droplets is found with the Gibb (1971) formula, which is commonly adopted for sediment transport studies. For small droplets, this reduces to the well-known Stokes relationship for buoyant spheres. Vertical diffusion is modeled as a random walk, which is the standard procedure within POL3DD. With the combination of diffusion (acting to inject the particles into the water column) and buoyancy (acting to bring the particles to the surface), the model applies evaporation to particles at the surface and dissolution to the particles in the water column.

The oil/condensate advects downwind at a fixed percentage of the wind speed. This is normally taken as 3-3.5% of the wind speed at the surface and reduces into the water column, in accordance with an imposed cubic velocity profile. If currents are not known, a higher level of horizontal diffusion may be applied to compensate. Given that the along shore currents at any instant can be directed up or down the coast, the diffusion can act to simulate this back and forth movement over the long time scales of the model simulation. However, the results are expected to be better if currents are taken from a 3DD model simulation.

On reaching a shoreline, oil/condensate can be re-suspended and carried to other locations. While this can be simulated by POL3DD model, alternatively the modeler can consider the first point of impact for contingency planning and rapid clean-up operations. In this case of a “sticky shoreline”, the model sums the total volumes reaching each length of coast, and does not allow re-suspension (POL3DD User Guide, 2006).

10.4.1 Initial Surface Spreading of the Spill

The formulas used in POL3DD Oil Spill module for the surface spreading are also according to Fay (1975). Fay predicted that the hydrocarbons will spread through three different stages (Rye, 1995).

- First, the gravitational forces, caused by the density difference between oil and water, will dominate.
- Next, the viscosity of the water will play a dominant part.
- And finally, when the slick has become sufficiently thin, the surface tension will dominate the further spreading.

10.4.2 Evaporation

In POL3DD, the equation given by Harrison et al. (1975) has been used. The evaporation is from the slick is given by

$$\frac{dQ_i}{dt} = -k_E A_{x_i} M_i P_i/(RT) \quad (10\text{-}1)$$

Where, $\frac{dQ_i}{dt}$ is the rate of evaporation of component I, g s^{-1}; k_E is the mass transfer coefficient for evaporation, m s^{-1}; A is the surface area covered by the spill, m^2; x_i is the mol fraction of component i present; P_i is the saturation vapor pressure of component i, atm; R is the gas constant, 82×10^{-6} m^3 atm (mol K)$^{-1}$; and T is the absolute temperature, K.

The mass transfer rate coefficient k_E is related to the wind velocity by means of

$$k_E = C_D U_{wind} \quad (10\text{-}2)$$

C_D is the surface drag coefficient. C_D is given the value 0.0012 by Smith (1988); and U_{wind} is the wind velocity, m s^{-1}.

10.4.3 Dissolution of Oil into Water

The dissolution (entrainment) rate from the slick was calculated in POL3DD Oil Spill Module based on Harrison et al. (1975),

$$\frac{dQ_i}{dt} = -k_D \alpha_i A(x_i S_i - c_i) \quad (10\text{-}3)$$

Where, $\frac{dQ_i}{dt}$ is the rate of dissolution of component i, g s^{-1}; k_D is the mass transfer coefficient, dissolution, m s^{-1}; α_i is the empirical constant that expresses the difference between the solubility of component i in fresh- and salt-water; S_i is the fresh water solubility of component i, g m^{-3}; c_i is the concentration of component i dissolved or already present in the water, g m^{-3}.

10.4.4 Hydrocarbon Toxicity to Organisms

It is generally believed that the dissolved hydrocarbons cause immediate toxic effects on marine and fresh water organisms (McAuliffe, 1987).

The linear calculations are used in POL 3DD Oil Spill module according to the work of McAuliffe (1987) for the field exposure.

10.5 NUMERICAL MODELLING

10.5.1 Model Parameters

The POL 3DD Oil Spill model was developed on the basis of the estuary_20m 3DD Flow model. It covers about 9.3×10 km^2 with 20×20m cell size (Figure 4-3). The vertical mixing is well-mixed using a five-layer model with 0.1 m layer depth on top of the four layers and 200 m of the bottom layer. Three wind scenarios were set up; the simulation period for the oil spill is 26 hours from 12.00am on 12 August 2010 to 12.00am on 13 August 2010 during spring high tide; time step for the oil spill simulation was set to 10 s, 60 time steps between disk output; the horizontal diffusion was calculated on the basis of the roughness length, and a uniform roughness length 0.001 m was applied; the vertical diffusion was based on mixing length, and the mixing length gradient was set as 0.4 with the minimum mixing length 0.05 m and maximum mixing length 2 m; oil evaporation and dissolution were considered; the wind speed percentage was 3.5%; and the 'sticky shoreline' approach was used so abstracted oil could not be remobilized.

The oil spill origin centre was at (318, 353), assuming a source of rectangular 1×4 cells; and located 1 layer down from the water surface; the settling velocity was 0.001 m s^{-1}; 20 oil particles were released per step; the mass transfer coefficient scaled the rate of evaporation of oil particles residing at the surface, using the default value 0.012. The carbon number varied with oil types. The higher the carbon number, the less the oil will evaporate. Four oil type scenarios are applied in the model with different carbon number (6 for petrol and 12 for diesel).

10.5.2 Model Scenarios

An ADP current meter was deployed at the tidal inlet as discussed in Chapter 3 to observe the water depth and the current speed from 27 July, 2010, to 14 September, 2010. The time series of surface elevations (tides) for spring and neap tides are plotted in Figure 10-3. The red points in the figures present the peak flood tide, peak ebb tide and slack tide. The time and tides height are listed in Table 10-1. Residual currents calculated for one month were discussed in Chapter 5 (Figure 5-6 to Figure 5-9).

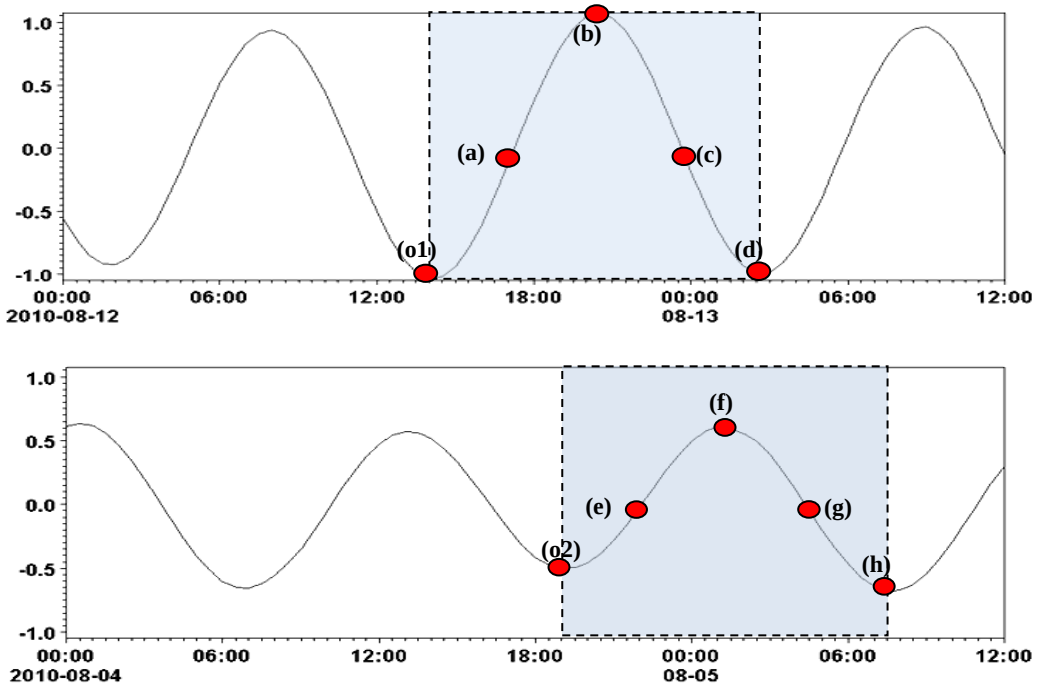

Figure 10-3 Current meter ADV observed spring tides from 2.00pm 12 August, 2010 to 2.30am 13 August, 2010 (top), and neap tides from 7.00pm on 4 August, 2010 to 7.30am on 5 August, 2010 (bottom) at tidal inlet.

Table 10-1 Spring and neap tide conditions for the oil spill modelling in Tairua Estuary in 2010. Point locations refer to Figure 10-3.

Spring Tides				Neap Tides			
Point	**Time Date (2010)**		**Tides height**	**Point**	**Time Date (2010)**		**Tides height**
o1	12 Aug.	14.00	-1.034	o2	4 Aug.	19.00	-0.5009
a	12 Aug.	17.30	0.1252	e	4 Aug.	22.00	-0.0212
b	12 Aug.	20.30	1.0736	f	5 Aug.	1.00	0.6105
c	12 Aug.	23.30	0.0724	g	5 Aug.	4.30	-0.0478
d	13 Aug.	2.30	-0.9905	h	5 Aug.	7.30	-0.6844

10.5.3 Wind

Two wind conditions were used to force the oil spill models. They include the wind from the north-east direction with 10 m s^{-1} speed, from the south-west direction with 5 m s^{-1} speed.

10.5.4 Air Temperature

Hourly air temperature data were downloaded from NIWA's Cliflo website. The air temperature was recorded at the Auckland Ardmore Airport (Agent number: 1965. Latitude: -37.03, Longitude: 174.96. Height above MSL: 23 m) from 7 June, 1990 to 6 July, 2012. The average air temperature and relative humidity from 1 January, 1991 to 31 December, 2011 was calculated and discussed in section 3.3.3. The results indicate that the highest dry bulb air temperature was 18.49°C in January and the lowest was 9.47°C in July.

10.5.5 Seawater Temperature

Two temperature conditions were considered in the model scenarios to simulate the impacts of the water and air temperature on the oil spreading, they are 25°C in summer and 10°C in winter.

10.5.6 Oil Properties

Oil is an imprecise term covering various petroleum products. Petroleum pumped out of the ground is normally called crude oil, which is a black liquid before the refining and distilling. The products after the refining and distilling are gasoline, diesel fuel, kerosene and so on. Petroleum products contain aliphatic hydrocarbons and the different lengths of the hydrocarbon molecules results in different properties and behaviour of the products such as their boiling points also. The main characteristics of these three fuels most commonly used are listed in Table 10-2.

Table 10-2 Main properties of petrol, diesel and kerosene fuel

Oil Type	Characteristics
Petrol (fuel for motors)	• Liquid • mix of alkanes and cycloalkanes (5 to 12 carbon atoms) • boiling range = 40°C to 205°C
Gas oil or Diesel (fuel for motors)	• Liquid • alkanes (12 or more carbon atoms) • boiling range = 250°C to 350°C
Kerosene (fuel for jet engines)	• Liquid • mix of alkanes (10 to 18 carbon atoms) and aromatics • boiling range = 175°C to 325°C

Two oil type conditions, including the petrol (carbon number 6) and diesel fuel (carbon number 12) were considered in the oil spill modeling. These two kinds of oils are the most common fuel used in the boats within Tairua Estuary, and due to their different carbon number, they may behave differently. Products with carbon numbers less than 10 tend to evaporate quickly.

10.5.7 Model Scenarios

A continuous oil spill was simulated from the Tairua Wharf. Five scenarios were modelled to investigate the influence of air temperature (winter conditions at 10 degrees Celsius (°C) and summer conditions at 25°C), tidal range (spring and neap tides), wind (direction and speed), and oil properties (diesel and petrol) on the oil slicks shape and oil spreading trajectory on water surface (Table 10-3).

Table 10-3 Modelling scenarios for oil spill trajectory

Model	Grid Size	Tides	Temperature	Wind	Type of oil
O1	20m	Spring	10°C	from SW, 5 m s^{-1}	Petrol (c=6)
O2		Spring	25°C	from SW, 5 m s^{-1}	Petrol (c=6)
O3		Neap	10°C	from SW, 5 m s^{-1}	Petrol (c=6)
O4		Spring	10°C	from NE, 10 m s^{-1}	Petrol (c=6)
O5		Spring	10°C	from SW, 5 m s^{-1}	Diesel (c=12)

10.6 RESULTS AND DISCUSSION

10.6.1 Oil Slick Distribution

Oil slicks area and thickness are the key variables for the computation of evaporation in oil weathering and transport models, which determines the changes in oil composition and properties with time. Oil film thickness is also used to compute the oil dispersion rate, which determines the spilt oil persistence on the water surface. In addition, the assessment of the oil slicks area and thickness are important for evaluating the potential efficiency of different oil spill combat methods, and for assessments of environmental impacts (Reed *et al*, 1999).

The numbers of oil particles per cell are plotted in Figure 10-10, which represents the extent of the oil slicks after 12 hours for the five scenarios (Table 10-3). These data define the oil slick area and thickness. The simulation results presented that

-The oil slick is thicker at the oil resource and elongated with thin film trailing around in all the five models. Model O3 results show that the oil slick is thicker at the spill resource, with less spreading during neap tides.

-The oil slicks are elongated with the NE wind during flood tides, and it is compressed with the NE wind during ebb tides. The SW wind pushes the oil film out of the Tairua Estuary; however the NE wind extends the elongated oil slicks upstream as far as the Swampy Stream. Comparing model O4 with the other models, it shows that the river upstream will be easier to be contaminated with wind from north-east.

-The extent of the slick is proportional to the wind speed.

-The slick area and thickness is also influenced by the tidal range. The larger the tidal range (spring tides), the more oil slicks spread out on water surface, and vice versa. The oil slicks mainly spread to the intertidal flat close to the flood tidal delta, and to the opposite site close to the Pauanui Waterway.

-The air temperature did not obviously influence the oil slicks thickness and area (model O1& O2). However, air temperature does accelerate the oil evaporation and emulsifications.

-For lower carbon numbers, the oil is easier to evaporate. However, the oil type did not influence the oil slicks thickness and area obviously for the simulation of model O1& O5.

-The long axis of the oil slicks is elongated during flood tides, and is compressed during ebb tides when the wind direction coincides with flood flow.

Figure 10-4, 10-5, 10-6, 10-7 and 10-8 show the oil particle distribution during one tidal cycle for spring tides with the oil spill located at the Tairua Wharf for the five scenarios. In each figure, the oil particle distributions at the middle of flood tide (point a), peak flood tide (point b), middle of ebb tide (point c) and peak ebb tide (point d) (Figure 10-3 and Table 10-1) were plotted for comparison.

-During the tidal process the dominant flow characteristic is the change of the current direction. The total particles are reduced because that portion of oil film on water surface evaporates, and portion of the oil diffuses, dissolves and sinks into the water.

-Comparing the five scenarios, air temperature does not change the oil particle numbers and distributions maybe because of the short simulation period (O1 & O2).

-Some oil particles could be flushed outside of the estuary during flood tides on spring, however, the oil will spread on the water surface within the estuary until it is stranded on the shoreline or sinks to the bottom (O1 & O3).

-The oil particles are distributed outside of the estuary and stick to the Pauanui Beach right to the Tairua tidal inlet (O1 & O4).

-Oil properties don't change the oil slicks trajectory (Figure 10-4), however, the diesel (carbon number is 12) has more oil particles on water surface than the petrol (carbon number is 6) because the oil with less carbon number is easier to be evaporated.

10.6.2 Oil Deposits along Shoreline

It is important to forecast the locations of the oil stranded on the shoreline for fast response to an oil spill accident. There are sea-grass, salt-marsh, mangrove and rocks along the estuary shoreline. It will be more difficult to clean up the oil film after it strands In POL3DD, the shoreline at the minimum time taken for the oil to reach the coast are generated in the 'impacts' file during oil spill simulations. These results are plotted in Figure 10-10 to Figure 10-14 for the five scenarios. They are also useful to estimate the length of shoreline affected by oil.

-Scenario O1. Figure 10-10 shows that the oil reaches the shoreline between Tairua Wharf and the Pepe Stream during the slack following flood tides. At the peak flood tide, the oil slick reaches the Swampy Stream in the upper harbour and strand on the shoreline there. Some of the oil spreads to the area around Pleasant Point opposite to Tairua Wharf, and some oil could also be found at the intertidal flat close to the tidal inlet. During slack tide following ebb tide, the oil slicks is

compressed and flows with the ebb tide to the tidal inlet. Therefore, oil could be found at the flood tidal delta and along the Esplanade Beach on the west side of Paku Hill. At the same time, the oil film becomes thicker because of oil accumulation around the Tairua Wharf. At peak ebb tide, more oil strands on the intertidal flat and could not be flushed outside of the estuary. The oil film will evaporate, emulsify and sink from the water surface, reducing the impact in the upper harbour.

-Scenario O2. The air temperature did not change the locations of oil stranding on the shoreline, because it had no influence on the oil slick distribution.

-Scenario O3. For neap tides, the oil slicks distribution area is smaller than for spring tides. And so less shoreline is affected. However, the oil reaches the shoreline more quickly.

-Scenario O5. There is not much difference between the diesel and the petrol in terms of shoreline affected.

The impacts of wind on oil stranding are obvious. Wind and water movement breaks up the slicks into windrows of thicker layers of oil aligned in the direction of the prevailing wind. This results in slicks extending for several kilometres in length, but only a few hundred meters in width. Within this slick, oil is unevenly spread and its thickness varies considerably. Oil will strand along the intertidal area from the Pauanui jetty to Pleasant Point.

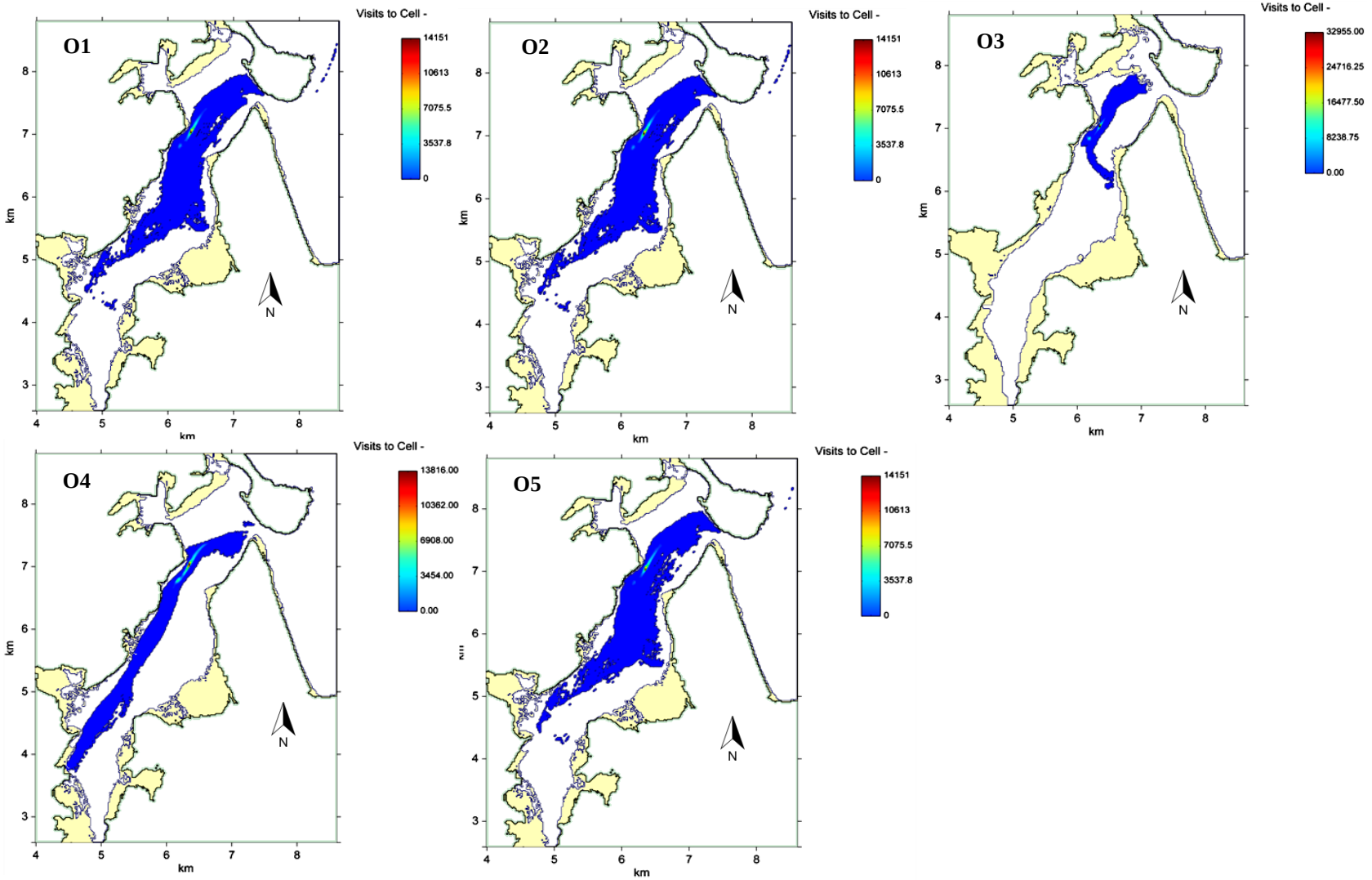

Figure 10-4 Distribution of oil slicks after12 hours for each of the five scenarios (Refers to the Table 10-3).

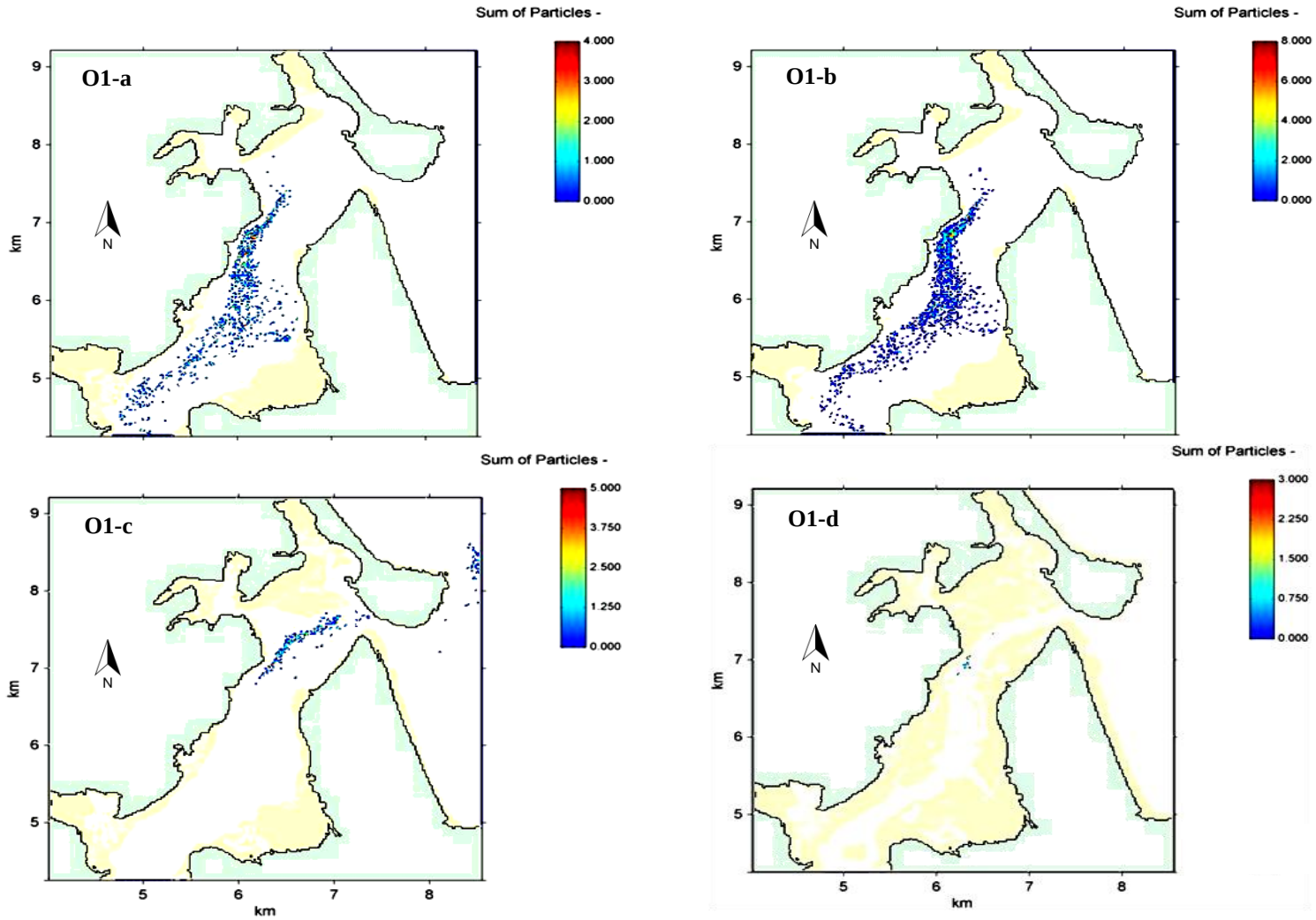

Figure 10-5 Distribution of oil particles on the water surface during one spring tidal cycle on 12 Aug., 2010 (Model O1), with petro, 5 m s^{-1} SW winds and 10°C air temperature.

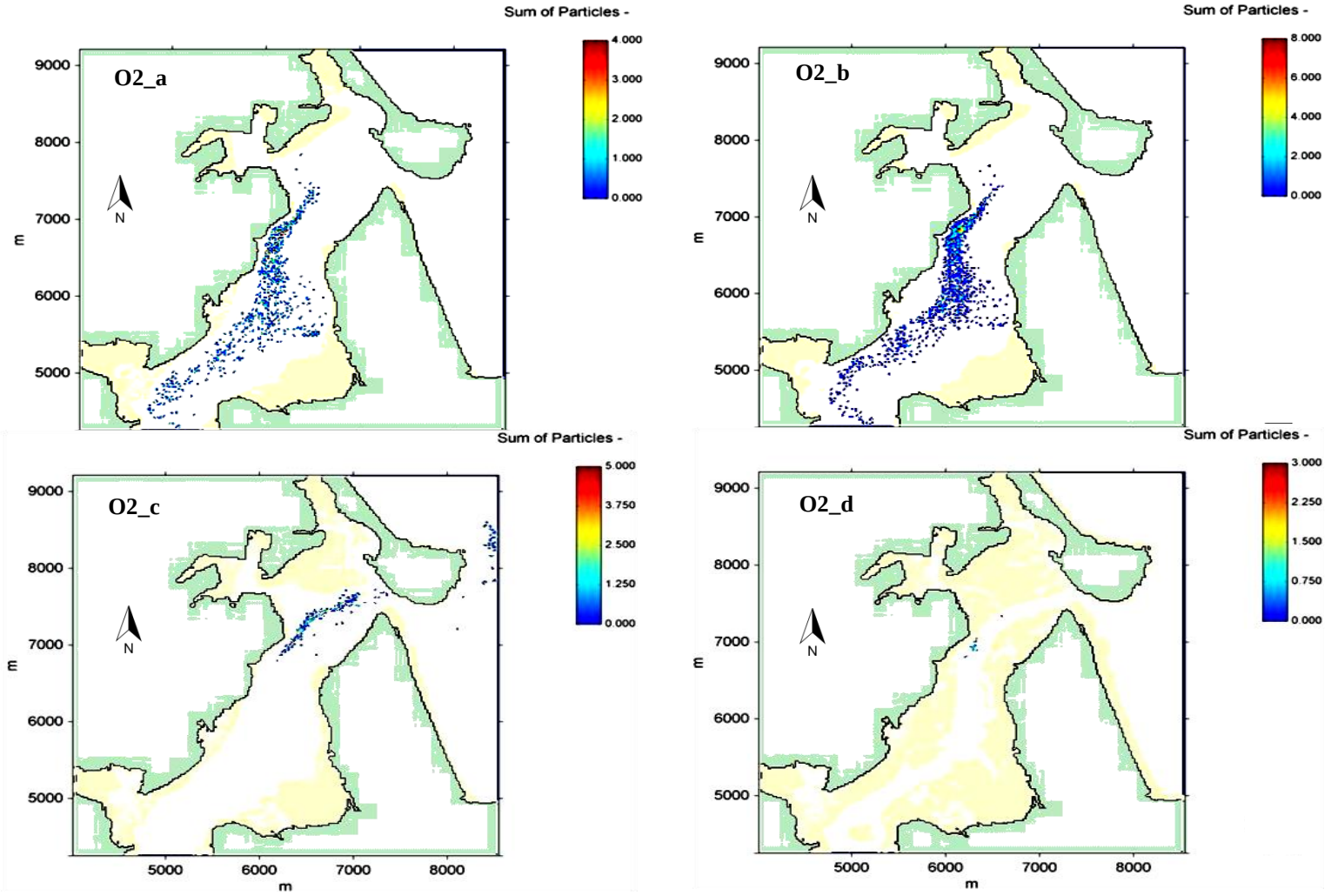

Figure 10-6 Distributions of oil particle on the water surface during one spring tidal cycle on 12 Aug., 2010 (Model O2), with petrol, 5 m s^{-1} SW winds and 25°C air temperatures.

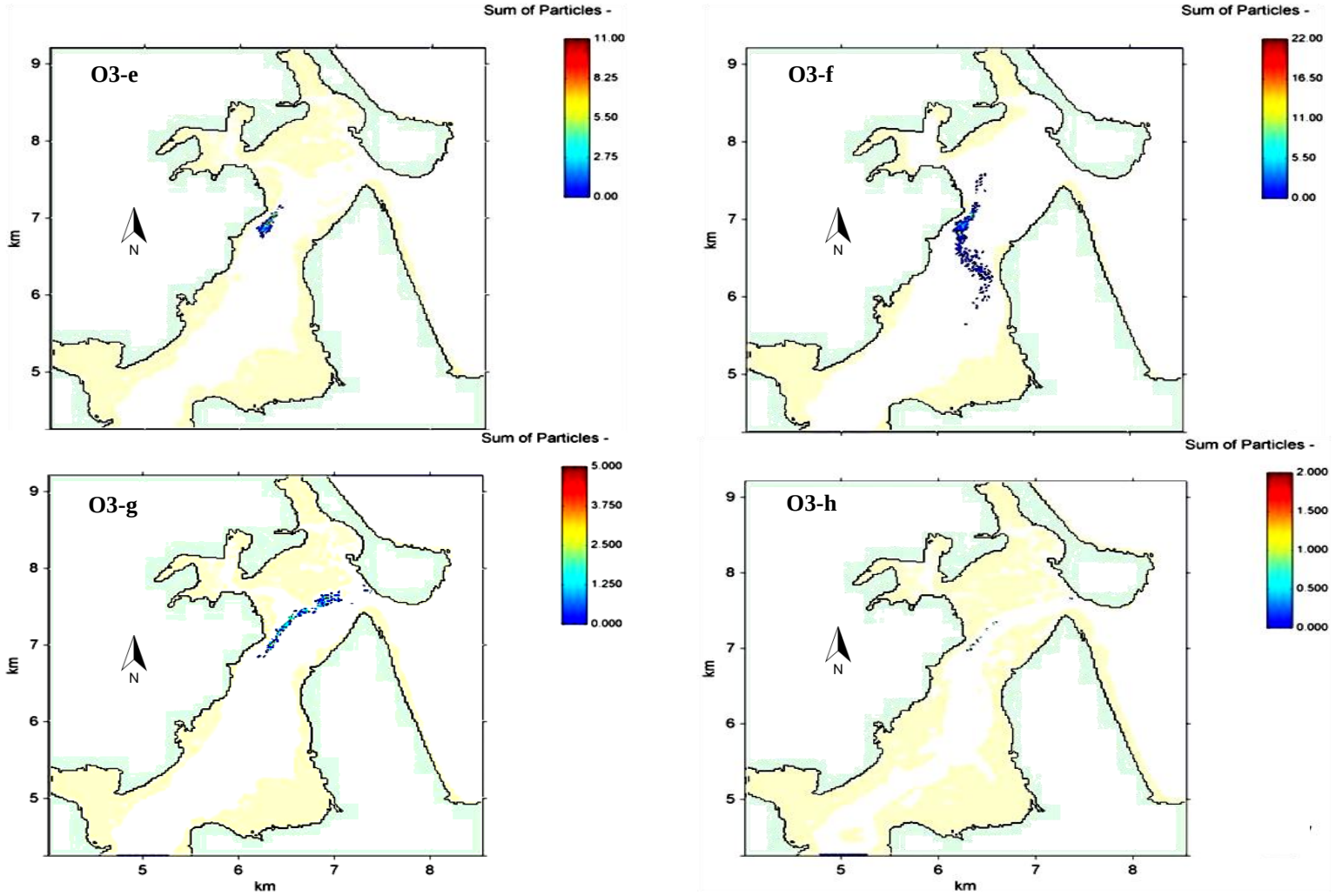

Figure 10-7 Distributions of oil particle on the water surface during one neap tidal cycle on 4 Aug., 2010 (Model O3), with petrol, 5 m s^{-1} SW winds and 10°C air temperatures.

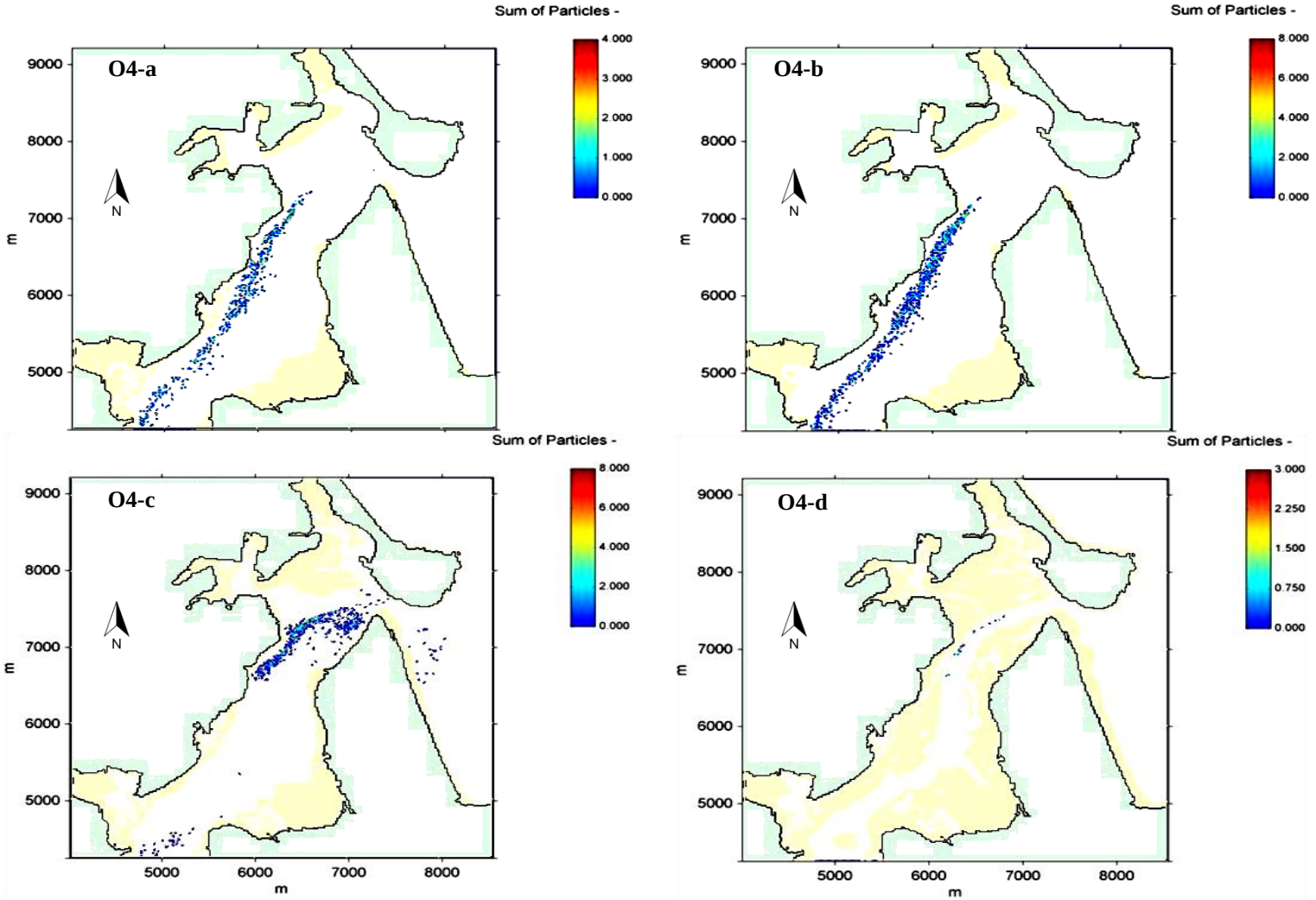

Figure 10-8 Distributions of oil particle on the water surface during one spring tidal cycle on 12 Aug., 2010 (Model O4), with petrol, 10 m s^{-1} NE winds and 10°C air temperatures.

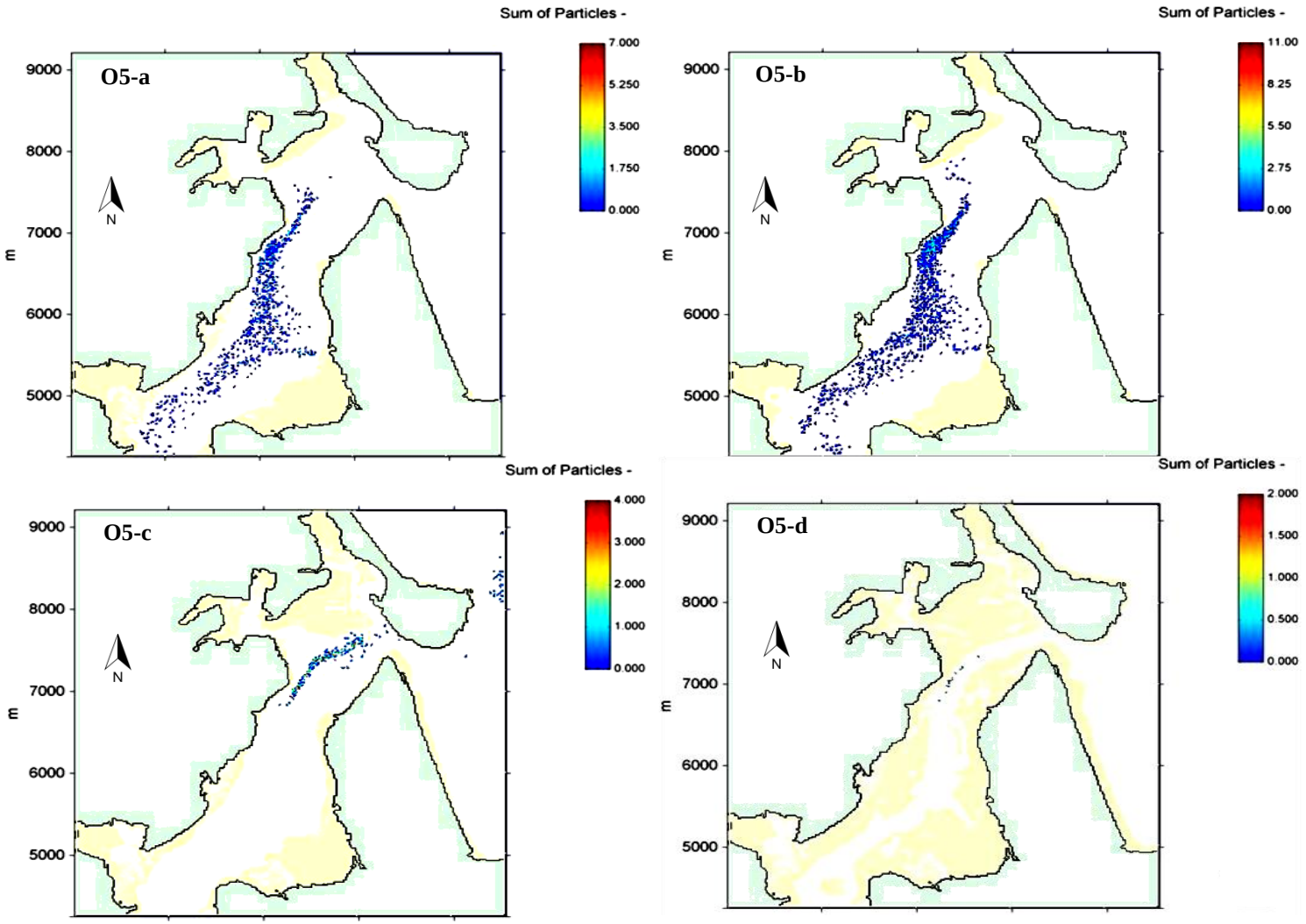

Figure 10-9 Distributions of oil particle on the water surface during one spring tidal cycle on 12 Aug., 2010 (Model O5), with diesel, 5 m s^{-1} SW winds and 10°C air temperatures.

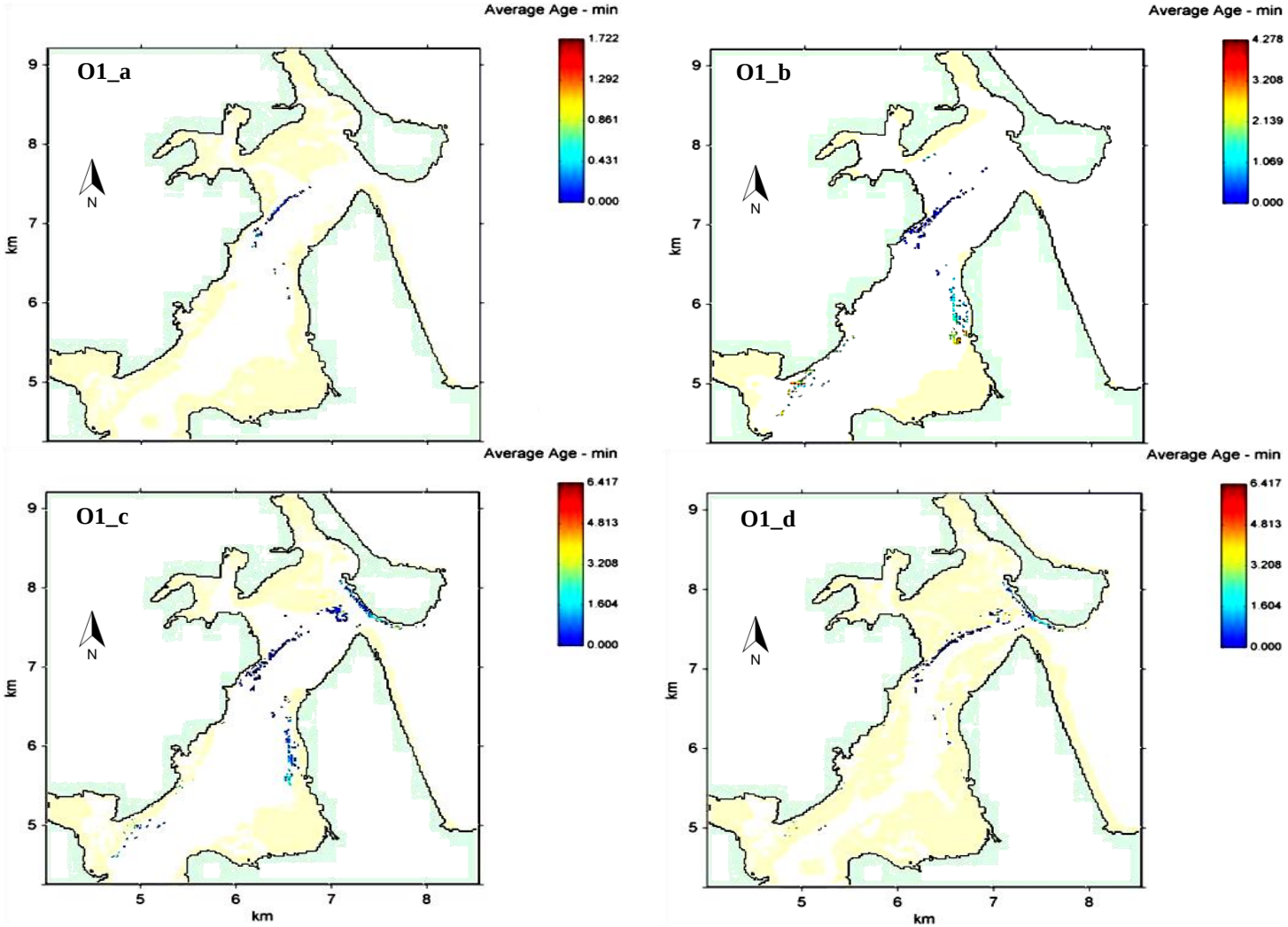

Figure 10-10 Minimum hours taken for the oil to reach and strand on the shoreline (Model O1) for spring tides, with petrol, 5 m s^{-1} SW winds and 10°C air temperatures.

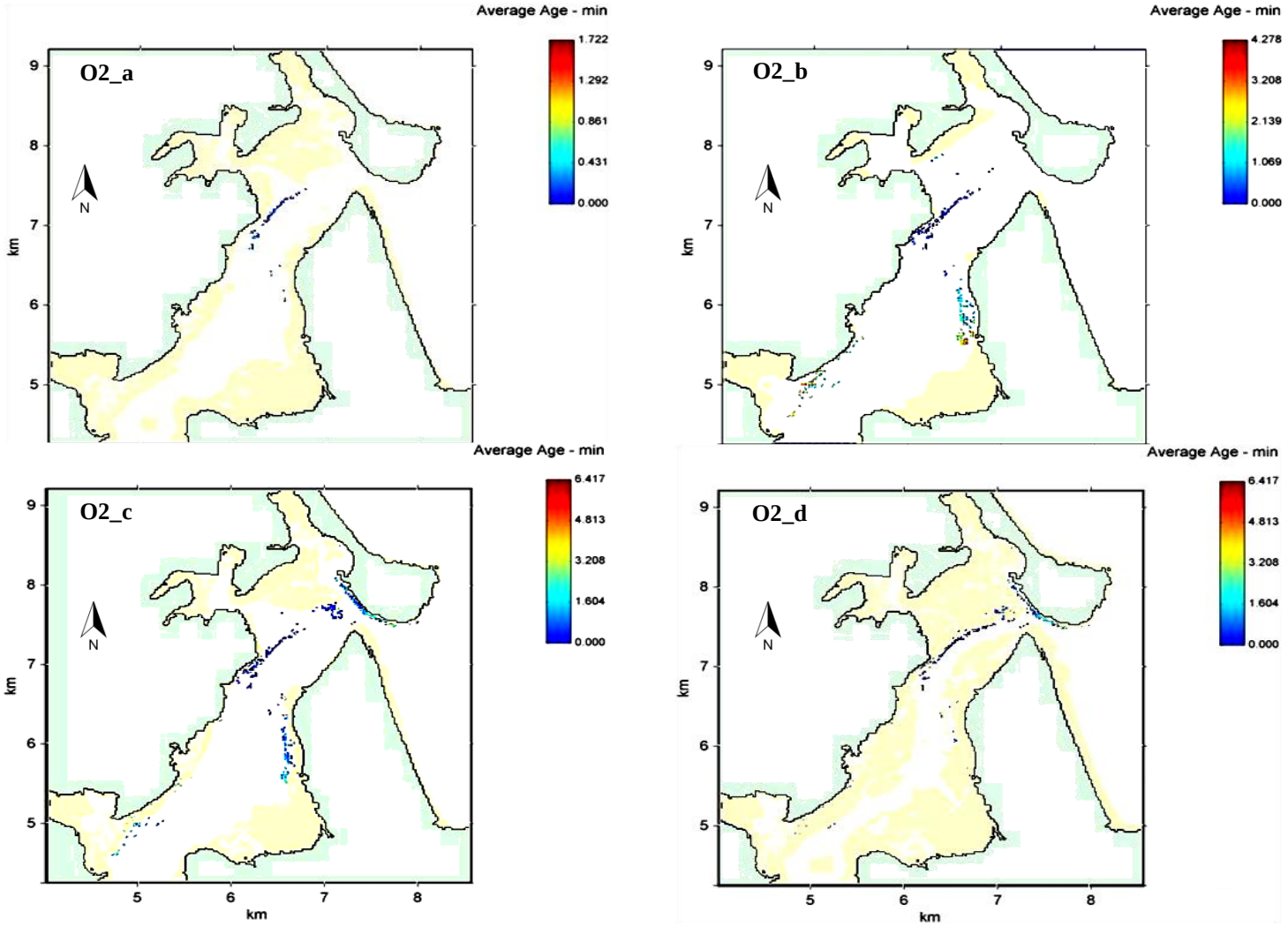

Figure 10-11 Minimum hours taken for the oil to reach and strand on the shoreline (Model O2) for spring tides, with petrol, 5 m s^{-1} SW winds and 25°C air temperatures.

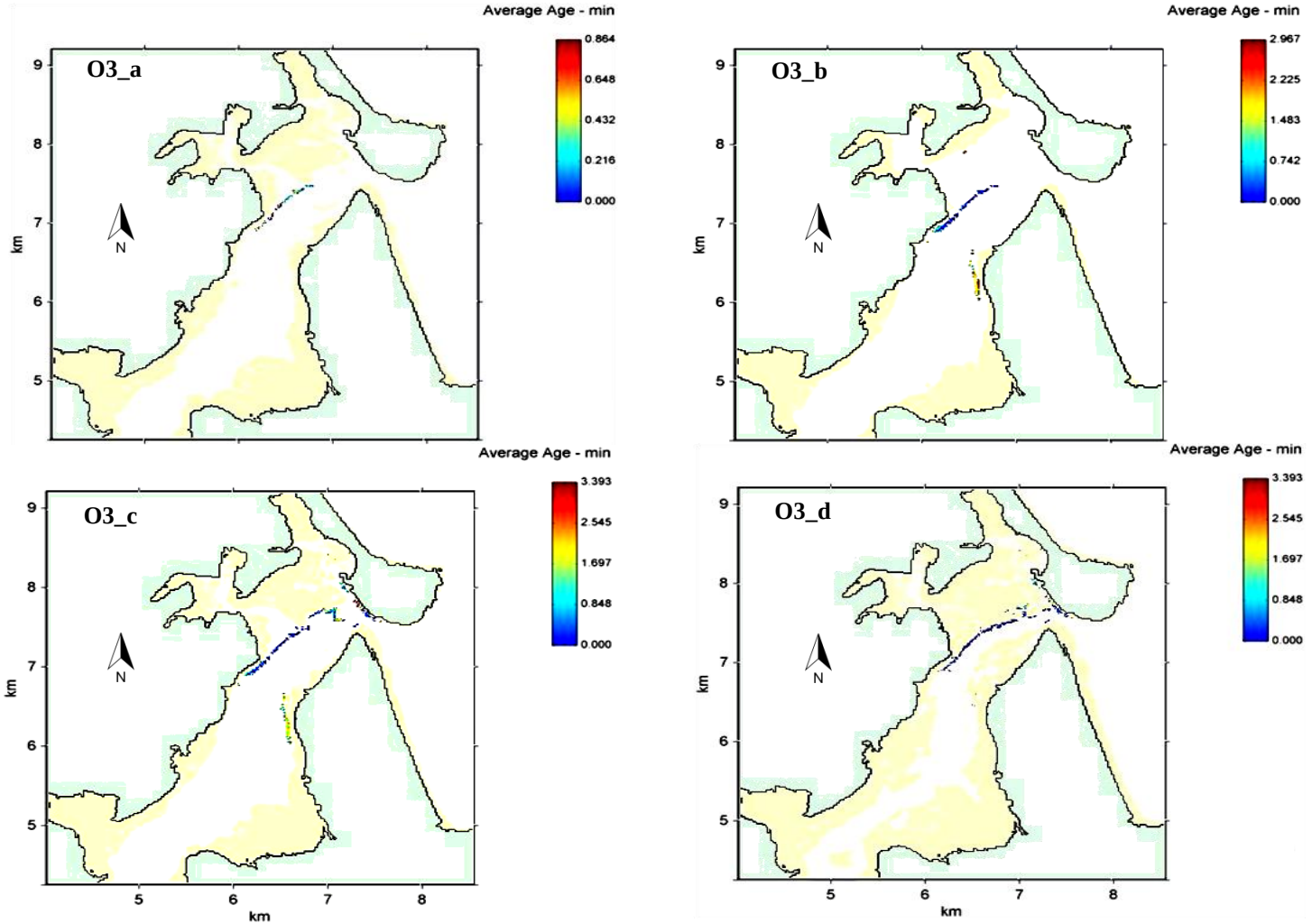

Figure 10-12 Minimum hours taken for the oil to reach and strand on the shoreline (Model O3) for neap tides, with petrol, 5 m s^{-1} SW winds and 10°C air temperatures.

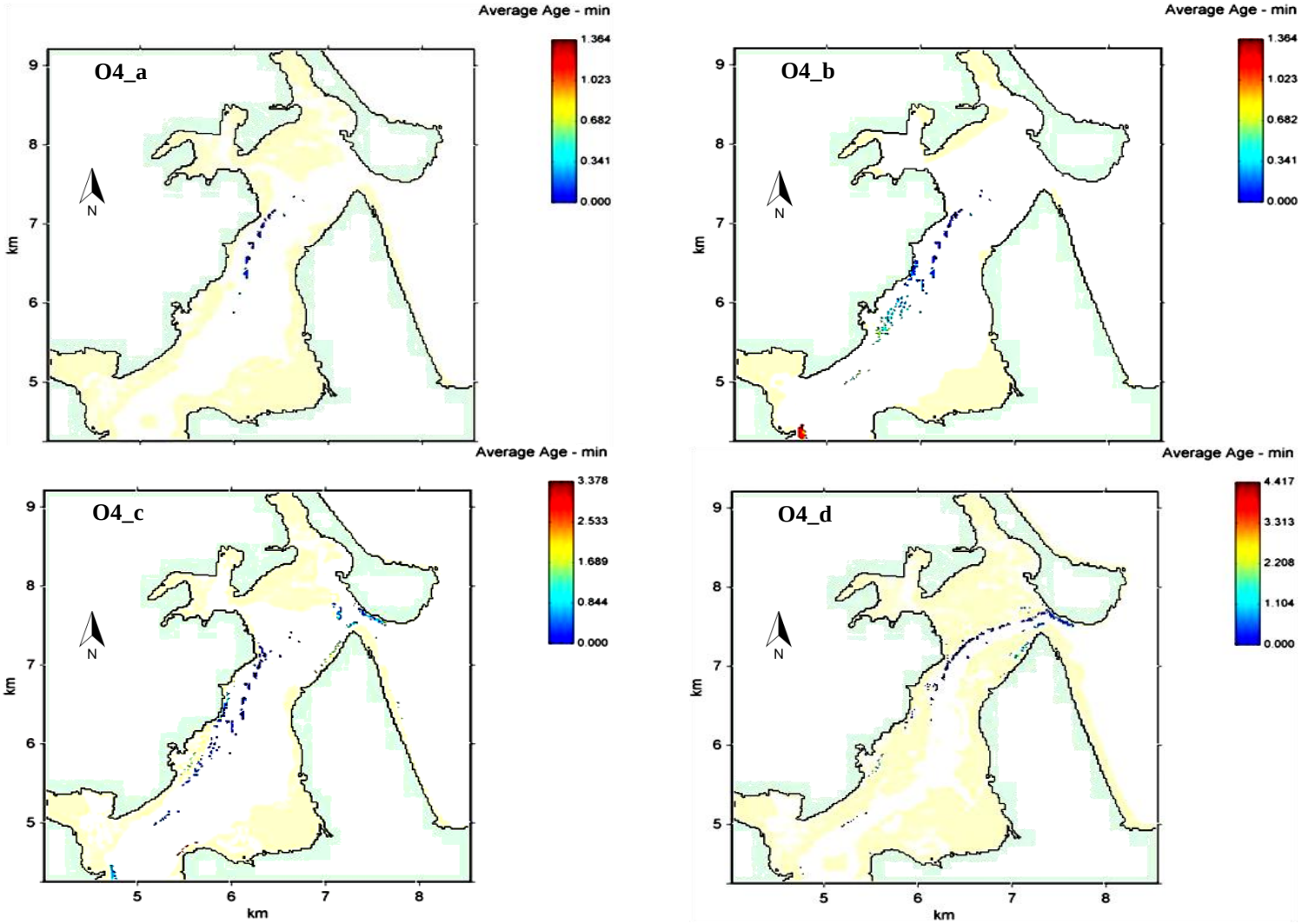

Figure 10-13 Minimum hours taken for the oil to reach and strand on the shoreline (Model O4) for spring tides, with petrol, 10 m s^{-1} NE winds and 10°C air temperatures.

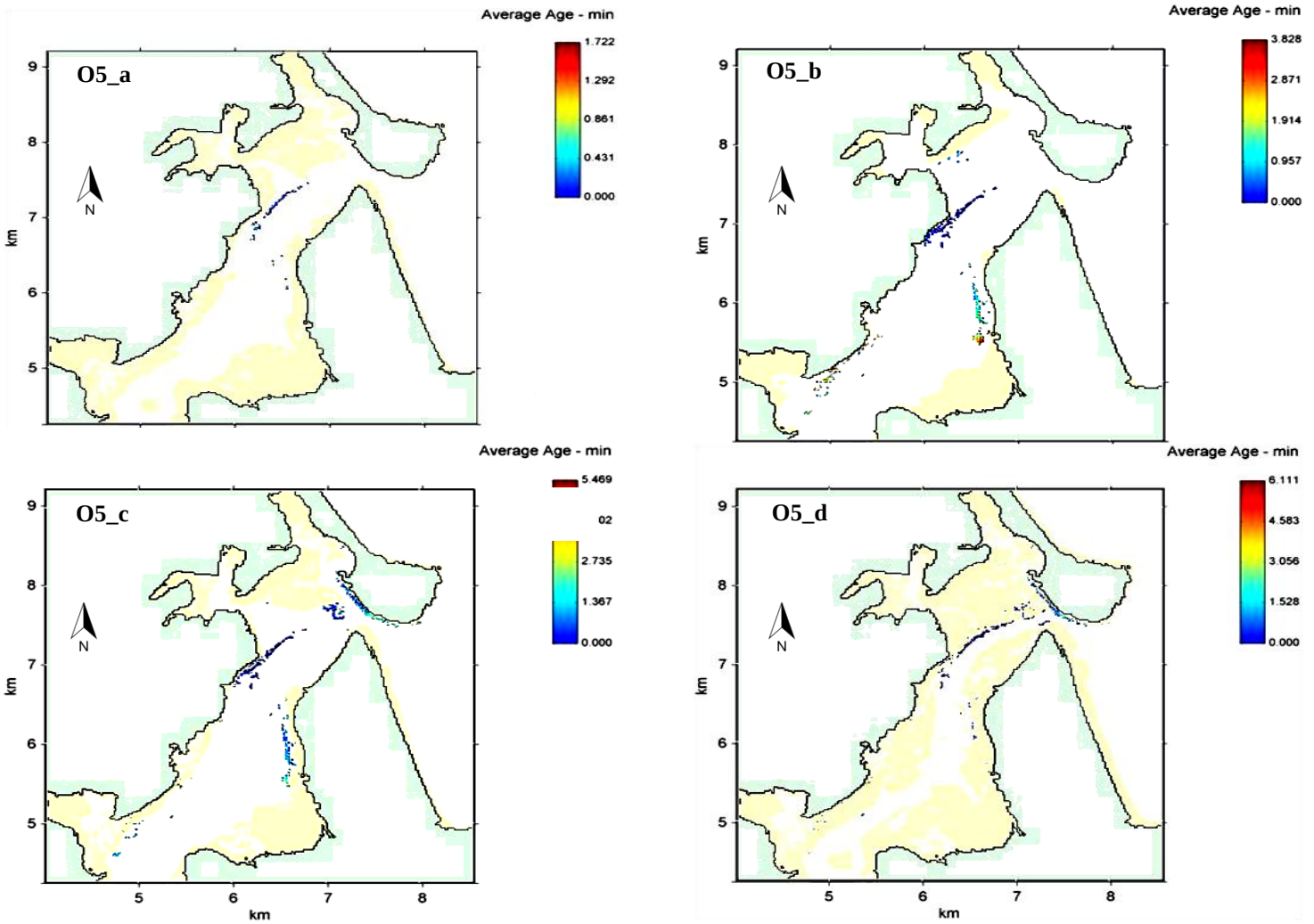

Figure 10-14 Minimum hours taken for the oil to reach and strand on the shoreline (Model O5) for spring tides, with diesel, 5 m s^{-1} SW winds and 10°C air temperatures.

10.7 CONCLUSIONS

The factors influencing oil movement and fate processes were analysed qualitatively based on the simulation results. This study found that not only air temperature, the locations of oil spill resource and oil properties influence the oil spill trajectory which had been found by other scientists, such as Doerffer (1992), Cohen al. (1980), Huang (1983), Yapa et al. (1994), but also the estuarine physical features such as tidal currents, wind direction, wave, wind speed, tidal range, will have effects on oil spill trajectory.

The larger the tidal range, the larger area the oil slicks spread out on water surface, and vice versa. Long axis of the oil slicks is elongated during with wind directions. The extent of the slick is proportional to the wind speed. The oil slicks are thicker at the oil resource and elongated with thin film trailing. Wind directions interact with tidal flow direction during oil spilling. Some oil particles could be flushed outside of the estuary during ebb tides on spring, and some will stayed at the water surface within the estuary until it is stranded on intertidal areas or after evaporation, emulsification and biodegradation. Air temperature does not obviously influence the oil slicks thickness and distribution area in this study, it maybe because of the short simulation period. Oil properties do not influence oil slicks thickness and area obviously, however, the diesel (carbon number is 12) has more oil particles on water surface than the petrol (carbon number is 6) because the oil with less carbon number is easier to be evaporated. There is not much difference between the diesel and the petrol in terms of shoreline affected.

These conclusions are in preparation to be published. Though this study focused on Tairua Estuary, it will supply a method of forecasting oil spill trajectory within estuaries for better coastal management and environment protecting.

PART V. SUMMARY

CHAPTER ELEVEN
CONCLUSIONS AND FUTURE WORK

This chapter summarises the answers to the main questions of this study and identifies possible future directions for further research.

11.1 FEATURES OF HYDRODYNAMIC AND SEDIMENT TRANSPORT OF TAIRUA ESTUARY

The maximum current speed is 1.0-1.4 m s^{-1} at the location of the tidal inlet, and 0.4-0.6 m s^{-1} at the Pepe Stream, the Grahams Stream entrance and the northern corner of the Paku Hill which is close to the Tairua Beach. The minimum current speed is about 0-0.1 m s^{-1} along the main channel during flood tides. At Tairua Estuary, the average high spring tide is 1.0 m, the average low spring tide is -0.82, therefore the average tidal range is 1.82 m during the spring tides; the average high neap tide is 0.6 m, the average low neap tide is -0.53 m, and the average tidal range is 1.13 m during the neap tides. The water surface area was calculated using the number of the grids covered by water multiplied by the area per grid (50 m×50 m). The calculated water surface during spring high water was 6.41 km^2, and 3.62 km^2 at low neap water. Therefore, the average water surface area is 5.02 km^2. As a result, the tidal prism at springs and neaps could be calculated as 9.12×10^6 m^3 and 5.67×10^6 m^3 respectively. The field recorded and model calculated mean current speeds are 0.606 m s^{-1} and trough current speed is 0.005 m s^{-1} at the tidal inlet. As a result, the average water discharge from the estuary to the ocean is 131.37 m^3 s^{-1} with 430 m^2 mean tidal inlet cross area. Therefore, Tairua Estuary could be flushed only after 19.29 hours during the spring tides. This conclusion is consistent with the saline mixing research by Bell (1994) which calculated that 82% of incoming water into the estuary was new ocean water and that harbour flushing took 1.3 tidal cycles to replace the entire tidal prism volume. The maximum and mean Tairua River discharge is 220 m^3 s^{-1} and 9.78 m^3 s^{-1} calculated on the one year weather station collected data; the maximum and mean discharge from the Pepe Stream is 1.46 m^3 s^{-1} and 0.23 m^3 s^{-1}; the maximum and mean discharge from the Grahams Stream is 0.75 m^3 s^{-1} and 0.17 m^3 s^{-1} respectively.

Estuarine morphology is to a large extent determined by the residual sediment transport pattern. However, the inverse statement is also true. Residual sediment

transport depends on differences in magnitude and duration between ebb and flood tidal currents. Such differences named tidal asymmetry are produced by the distortion of the tidal wave propagating on the coastal shelf and entering bays and estuaries (Dronkers, 1986). Tidal oscillations were recorded upstream the Tairua River as far as the Tairua Bridge. Numerical model results and field data indicate that as the river discharge increases, the smaller the tidal wave amplitude at the upper estuary because of the higher energy of the freshwater input. Major time delays of the tidal wave are evident at the river mouth region due to the propagation of the tide through the estuary. The peak of the tide crest has an average of 30 minutes delay and the trough of the tide has an average of 40 minutes delay between the tidal inlet and the Pauanui Waterway at the lower estuary. Further upstream the time delays increases relative to the ocean and the tidal asymmetry is also accentuated. The peak of the tide crest has an average 3 hours and 40 minutes delay and the trough of the tide has an average delay of 6 hours between the tidal inlet and the Tairua River mouth. This asymmetric tidal variation is typical of tidal estuaries (Aubrey and Speer, 1985).

Basing on the tidal asymmetry and propagation analysis, more water can accumulate in the upper part of Tairua Estuary during the spring tidal cycle than during a neap tide. As a result, an increase of salinity during spring tides than neaps. It also indicates that net sediment movement landward during flood tides. Garel et al. (2009) found that tidal asymmetry produced faster currents on the ebb tides than on the flood tides, especially at the river mouth. This pattern of seaward current dominance was enhanced with increasing river flow, due to horizontal advection that was confined within the narrow estuarine channel. Highly stratified conditions developed with increasing river discharge. This result could be explained by the findings of Dronkers (1986) that the river runoff produces a cross-sectional distribution of current velocities which enhances seaward transport in the near surface part, but counteracts seaward transport in the deeper parts of the channel.

Tairua Estuary is a partially mixed estuary where denser salty seawater flows under the fresh river discharge and results in salinity stratification from the tidal inlet to the Tairua Wharf at peak flood tides. The amount of stratification changes with tidal range and river discharge. Salinity stratification increases with flood tides and decreases with ebb tides along the main channel within Tairua Estuary, and salinity are lower during peak ebb flow for spring tides than for neap tides. Tairua Estuary is partially-mixed with a current speed higher than 0.5 m s^{-1}, even when the river discharge reaches its peak value (200 $m^3 s^{-1}$). The tidal currents are sufficiently strong to destroy the salt wedge interface and cause some vertical mixing of salt and fresh water. This pattern is also observed in a ROMS model for the Hudson River Estuary (Warner et al, 2005). Bell (1994) found that 82% of the incoming water on the flood tide is new salt water, indicating a large input of salt water on the flood tides and an efficient flushing system on the ebb tides. Dyer

(1979) also classified Tairua Estuary as a partially-mixed estuary and there is considerable friction between water and estuary bottom to create turbulence. Turbulence tends to mix the water column more effectively than entrainment, causing the salinity to decrease to the head of the estuary in the lower layer and to increase progressively towards the sea in the surface layer; though there is no water movement, there is salt exchanging vertically. The landward flow at the bottom can be of order 0.05 m s^{-1} with tidal oscillations of 0.5 m s^{-1}.

Water surface temperature within the Tairua Estuary is higher than the bottom water temperature from the tidal inlet to the upper estuary because of shallow channel. Tidal impacts on water temperature also occur faster at the surface than at depth within the lower estuary. Water temperature not only varies with tidal flow and river discharge, but also with air temperature, particularly in shallow water.

For suspended sediment transport, the deposition patterns are strongly influenced by the grain size. The coarser the grain size, the higher the critical sediment settling velocity. With coarser bed, the sediment transportation pattern appears to be strongly influenced by water depth. The bed sediment mainly erodes along the main channel during the maximum current velocity. And there appears to be a higher amount of erosion for spring tides than on neap tides. A large portion of the suspended sediment cannot be transported at the maximum neap current speed. This remaining suspended sediment tends to deposit along the bank and the intertidal flats. During high spring tides, more suspended sediment is transported comparing with high neap tides because of the higher flow velocity and the higher tidal range.

11.2 NUMERICAL MODELLING AND COMPARISONS

Tairua Estuary hydrodynamic numerical models with 50 m and 20 m grid size were developed. According to the statistics qualification results based on the methods of Winter (2007) and Van Rijn (2002). The results show that coarser grids supply less bathymetric information, and as a result, the less accurate model. This is due to the calibration being based on average values calculated for each of the grids, and hence the finer the grid, the closer the calculated results are coincided with the observed data. The current speed at the location of tidal inlet is not as good as the others. This might be because that the model is run on a fixed bed, however, the hydrodynamics of the estuary will change the sediment transport characteristics in reality, especially at the tidal inlet.

The calculated RMAE value of the two models with different resolutions (50 m and 20 m) using the same software (MIKE). The results indicate that the two models are ‘excellent’ in calculating the surface elevation and the ‘estuary-20m’

model is more accurate than the ‘whole-50m’ model, possibly because the coarser grids lose more bathymetry information during calculations. The RMAE results of the models with same resolution (20 m) but different software modules (MIKE 21 HD and 3DD Flow) were compared, too. The surface elevations calculated by the two modules both coincide well with the instruments data. The current speed computed by the 3DD Flow model is better than the MIKE 21 HD model. Their similar results indicated that both of the MIKE 21 HD module and the 3DD flow module were feasible.

However, the software of MIKE and 3DD also has different strengths. Both of MIKE and 3DD modules calculated the depth averaged results, however, MIKE takes less calculating time than 3DD; MIKE is less accurate in calculating along the curved river than 3DD; it is more feasible to nest boundaries from coarse model to fine model using 3DD than MIKE; some of the modules of 3DD have not been well calibrated; MIKE supplies a better and logical man-machine communication frontend. Therefore, both of the MIKE and 3DD were used for this study for their different abilities.

11.3 COMPLETION THE THESIS MAIN QUESTIONS

Q1: Whether the estuary is receiving greater net sediment from Pauanui Beach than is being transported out of the estuary, especially after relative sea level rise?

Sedimentation in Tairua Estuary has long been a concern. Even though it is clear that Tairua Estuary is infilling, it is uncertain whether the estuary is supplying sand to Pauanui Ocean Beach or vice-versa. The flood and ebb tidal delta indicate "the presence of two-way sand transport through the inlet where reversing tidal flows are dominant" (Kirk, 1991). Healy et al. (1981) proposed that Pauanui Beach was in a long-term state of slow erosion with sediment being removed from the beach and deposited inside the estuary. However, Carryer (1982) showed that Pauanui Spit has been under a state of long term net accretion with sand taken out with the ebb flows from Tairua Estuary.

Numerical model results indicate that the suspended sediment is predominantly transported out of the estuary along the main channel at the northern side of the tidal inlet by ebb currents. The coarser sand-sized suspended sediment is deposited on the ebb delta as the current speed dissipates outside of the estuary. Meanwhile, the flood flow along the Pauanui Beach returns to the estuary predominantly along the southern side of the tidal inlet, and the sediment is mostly deposited to form the flood tidal delta as the velocity decreases after

entering the estuary. The combination of the offset ebb and flood flows through the inlet forms a big residual current eddy at the corner of the Pauanui Spit outside the Tairua Estuary inlet. The fine sediment from the ebb tidal delta and the Pauanui Beach deposited at the centre of the eddy, and coarser sediment flowed into the estuary and deposited at the flood tidal delta and intertidal flat.

The directions of the flow depend on the waves from the open ocean, too. However, there were no waves were considered into the modelling. In the future, it is necessary to set up a wave model for more accurate results.

Q2: How the relative sea level rise (SLR) and river flood influence the estuarine process?

The relative sea level rise (SLR) resulting from climate change and flood discharged from Tairua River mouth have been suggested as two of the factors contributing to the high sedimentation rates within the estuary (Healy et al. 1981).

The interaction between tidal flows entering from the open ocean to the estuary and the river discharge through the river mouth to estuaries will influence the tidal range. Further into the estuary, the increased variation in tidal waves due to SLR becomes more prominent. Tidal range will decrease with increased river discharge when sea level is same, and tidal range will increase with SLR when river discharge keeps same. The effects of SLR on the change of tidal range will be more than the effects of river discharge for Tairua Estuary. This also indicates that Tairua Estuary will likely be dominated more by tides and less by river discharge with SLR. As sea level rises, the estuary would become increasingly flood dominated. At present, sediment near the tidal inlet is generally transported seaward and tends to deposit at the outer side of the tidal inlet where it forms the ebb tidal delta. However, as sea level increases, the model results predict greater sediment transport into the estuary and subsequent deposition on the intertidal flats and flood tidal delta. This would result in a sediment loss from the ebb tidal delta, and possibly Pauanui Ocean Beach.

With increasing flood tidal dominance, the saltwater intrusion was more likely to occur with increased sea level. However, the influx of sediment would compensate for some of the sea level rise, and reduce the tendency for flood dominance.

Q3: What are the forcing mechanisms of seiche? And what impacts could seiche have on sediment transport within the estuary?

The phase difference between water elevations and current speed is about 0º in the

beginning and is about 90º afterwards. It indicated that this water fluctuation event is a forced oscillation (most progressive) with little resonance in the beginning and it resulted in the real seiche, a standing wave. The spectrum analysis results of the observed fluctuations coincides well with the calculated seiche period based on Marian's Equation and indicate these fluctuations are a seiche that happened on 4 August, 2010.

The vertical profile of water density recorded by the DOBIE and SCUFA suggested that pulses of turbid water migrated to the lower reach of Tairua Estuary in a salt wedge under the river flow and resulted in density stratification before the seiche event on 4 August, 2010. Such a phenomenon has been suggested in the literature, but no data have been published to support it. The data showed that an intense, meso-scale storm produced heavy precipitation, resulting in a sediment laden flood discharging from the Tairua River mouth to Tairua Estuary. A MIKE 3 FM ST model was also developed to compute the vertical profile of water density. The results present two density stratification events which occurred at 2.30pm and 4.00pm during the seiche event. The estuary turbidity maximum (ETM) was enhanced with increasing current velocities, and displaced downstream during periods of high river discharge. During the flood event, the ETM was expelled out of the estuary, and the SSC along the estuary was controlled by the sediment load from the drainage basin.

Considering all these related information, this water elevations and current speed oscillation with little resonance and finally a real seiche was forced by a heavy wind together with a sediment-laden flood discharged from the Tairua River mouth to the lower reach of Tairua Estuary, which resulted in flow instability with the pycnocline, forming the seiche event. The absence of seiche in the rest of the record floods suggested that flood, sediment stratification and heavy wind are the three forcing mechanics of the seiche occurred on 4 August, 2010.

Q4: Are there other factors influence the oil spill trajectory? What is the relationship between estuarine process and the oil spill spreading pathway?

The factors influencing oil movement and fate processes were analysed qualitatively based on the simulation results. This study found that not only air temperature, the locations of oil spill resource and oil properties influence the oil spill trajectory which had been found by other scientists, such as Doerffer (1992), Cohen al. (1980), Huang (1983), Yapa et al. (1994), but also the estuarine physical features such as tidal currents, wind direction, wave, wind speed, tidal range, will have effects on oil spill trajectory.

The larger the tidal range, the larger area the oil slicks spread out on water surface, and vice versa. Long axis of the oil slicks is elongated during with wind directions. The extent of the slick is proportional to the wind speed. The oil slicks are thicker at the oil resource and elongated with thin film trailing. Wind directions interact with tidal flow direction during oil spilling. Some oil particles could be flushed outside of the estuary during ebb tides on spring, and some will stayed at the water surface within the estuary until it is stranded on intertidal areas or after evaporation, emulsification and biodegradation. Air temperature does not obviously influence the oil slicks thickness and distribution area in this study, it maybe because of the short simulation period. Oil properties do not influence oil slicks thickness and area obviously, however, the diesel (carbon number is 12) has more oil particles on water surface than the petrol (carbon number is 6) because the oil with less carbon number is easier to be evaporated. There is not much difference between the diesel and the petrol in terms of shoreline affected.

Q5: What are the potential impacts on the sediment transport at around tidal inlet because of a marina construction and channel dredging?

The Paku Marina project including the construction of Paku Marina, dredging the access channel and channel realignment. Even though Reeve et al (2009) suggested that the moderate human interference in the form of dredging and structural construction does not have a significant impact on the overall geomorphology of estuaries in the long-term. The impacts of the dredging and structural construction within an estuary on the estuarine process are also important for the coastal management.

Under present conditions, without the marina, sediment accumulation is likely within Paku Bay, with finer sediments settling out in the more isolated eastern and south eastern margins of the bay. After the Grahams Stream Channel is re-aligned, the current speed at the south-eastern corner of Pahu Bay is increased. However, this is insufficient to prevent fine sediment from depositing close to the Paku Beach and the area between the 1941 Grahams Channel and the realigned channel. With the increased flood flow into Paku Bay associated with the marina, the sediment flushed through the Grahams Stream Channel will not be taken out of the bay, but will be carried back to the beach at the south-eastern corner of the bay or be deposited on the sides of the Grahams Stream Channel, and the causeway across the Grahams Channel. As a result, any realigned Grahams Stream Channel will probably migrate and adjust over time.

The marina access channel will be dredged deeper and wider between the Paku shoreline and the flood tidal delta, resulting in slower flood and ebb flow. Channel dredging also changes the topography of the flood tidal delta, affecting the

hydrodynamics and sedimentation of the flood tidal delta, and as a result the entire tidal inlet system. More sediment will be flushed from the flood tidal delta to the ocean outside and deposit on the ebb tidal shoal. A portion of sediment taken from Pauanui Beach will be taken back to the tidal inlet with the flood tides and deposited on the left side of the main estuary channel where the Pauanui Wharf is located. More sediment will be transported from the access channel to the intertidal flat. However, the potential changes to the tidal delta system will not be significant compared to the approximately 22,000 tons per year sediment yield from the Tairua Estuary catchment.

Inside the marina will be dominated by flood flow. This means that the marina will fill with sediment, most likely at the landward end of the marina. The increased current speed across the front of the marina entrance by the breakwater will generate a turbulent flow that obstructs the water exiting the marina during ebb tides. As a result, the water circulation will be reduced, causing lower water quality.

Q6: What are the factors influencing oil Spill trajectory within an Estuary?

The larger the tidal range, the larger area the oil slicks spread out on water surface, and vice versa. Long axis of the oil slicks is elongated during with wind directions. The extent of the slick is proportional to the wind speed. The oil slicks are thicker at the oil resource and elongated with thin film trailing. Wind directions interact with tidal flow direction during oil spilling. Some oil particles could be flushed outside of the estuary during ebb tides on spring, and some will stayed at the water surface within the estuary until it is stranded on intertidal areas or after evaporation, emulsification and biodegradation. Air temperature does not obviously influence the oil slicks thickness and distribution area in this study, it maybe because of the short simulation period. Oil properties do not influence oil slicks thickness and area obviously, however, the diesel has more oil particles on water surface than the petrol because the oil with less carbon number is easier to be evaporated. There is not much difference between the diesel and the petrol in terms of shoreline affected.

These conclusions are in preparation to be published. Though this study focused on Tairua Estuary, it will supply a method of forecasting oil spill trajectory within estuaries for better coastal management and environment protecting.

11.4 LIMITATIONS AND FUTURE WORK

The MIKE and 3DD models are suitable tools for the study of estuarine hydrodynamics, sediment transport and pollutant dispersal. They are feasible for forecasting the impacts of natural hazards, harbour development, and also coastal environmental protection.

11.4.1 Limitations

For studying the impacts of the relative sea level rise on estuarine hydrodynamic and sediment transport features, the same bathymetry were used for the different sea level rise scenarios. However, it is well known that the estuarine geography will change with years.

For the marina construction case study, the dredged material which were deposited around did not been considered in the modelling, which will make the less accuracy of sediment transport rate through tidal inlet.

The coarser grids of bathymetry reduced the accuracy of model results, especially for comparing the model results and the field data at the location of instrument. However, the finer the grids, the longer time the modelling process will take.

To reveal whether the sediment was eroded from Pauanui Beach and where it's gone, the wave from the open ocean should be an important factor influencing the direction of the sediment transport. However, waves did not be considered in the modelling because this research was more interested in the area inside the Tairua Estuary.

11.4.2 Future Issues

The recent estuarine process research has been this increased awareness of biological-physical interactions. The incorporation of biological processes into sediment transport and morphological models will be an important step in future attempts to forecast changes in sediment erosion, transport and deposition in response to climate change and sea level rise. Numerical and analytical models have been and will continue to be essential to the insights gained (Uncles, 2001).

How estuaries respond to projected estimates of sea-level rise, including associated changes to habitat assemblages such as sandy beaches, benthic areas, and marsh systems (Fitzgerald et al., 2008)? How the increases in storms, coastal flooding and water temperatures will change the form and function of estuaries in the future? How intertidal zones are modified or eliminated by human alterations

and whether the anticipated response of an estuarine transgression is prevented (Townend & Pethick, 2002)? And how the construction of hard protection structures along the shoreline in response to sea-level rise will prevent the migration of the marsh inland and also sequester sediment? All these questions are uncertain now and worthy to be done in the future.

References

ASCE Task Committee on Sea Level Rise and Its Effects on Bays and Estuaries,1992. Effects of sea level rise on bays and estuaries. Journal of Hydraul.Eng. ASCE 118(1), pp 1–10.

Acers, P., White, W.R., 1972. Study on hydraulic resistance and bedload transport rate in alluvial streams. Jssce, Tokyo, 206, pp 59-69.

Alvarez, O., Izquierdo, A., Tejedor, B., Mañanes, R., Tejedor, L. & Kagan, B. A., 1999. The influence of sediment load on tidal dynamics, a case study: Cadiz Bay. Estuarine, Coastal and Shelf Science 48, pp439–450.

ASCE, 1996. State-of-the-art review of modelling transport and fate of oil spills. ASCE Committee on modelling Oil Spills, Water Resources Engineering Division. Journal of Hydraulic Engineering, pp 594-609.

Anderson, F.E., 1972. Resuspension of estuarine sediments by small amplitude waves. Journal of sediment Petrol 42: pp602-607.

Aubrey, D.G., Speer, P.E., 1985. A study of non-linear tidal propagation in shallow inlet/estuarine systems, Part I: Observations. Estuarine, Coastal and Shelf Science, 21, pp 185-205.

Barnett Consultants Ltd. 1991. Pauanui Canal Housing Development: Hydrodynamic Study. Unpublished report to Hopper Brothers Developments Ltd.

Bell, R.G., 1994. Behaviour of dissolved silica, and estuarine/coastal mixing and exchange processes at Tairua Harbour, New Zealand. New Zealand Journal of Marine and Freshwater Research, 28: pp 55-68.

Bell, R., 2001. The modern ocean sea level on the move? Water & Atmosphere. 9(4).

Bernard Potter, 2001. What is an estuary? From: http://www.niwa.co.nz/education-and-training/schools/students/estuaries/

Black, K.P., 2006. Model POL3DD Description and User's Guide. The 3DD Computational Marine and Freshwater Laboratory.

Boicourt, W.C., 1992. Influences of circulation processes on dissolved oxygen in Chesapeake Bay. In Oxygen Dynamics in the Chesapeake Bay (Smith, D. E., Leffler, M. & Mackiernan, G., eds). Pub. Maryland Sea Grant College, Maryland, USA, pp7–59.

Boon, J.D., Byrne, R.J., 1981. On basin hypsometry and the morphodynamic response of coastal inlets. Marine Geology, 40, pp 27-48.

Boyd, R., Dalrymple, R., Zaitlin, B.A., 1992. Classification of clastic coastal depositional environments. Sedimentary Geology 80, pp139–150.

Bruun, P., 1962. Sea level rise as a cause of shore erosion. Journal of Waterways and Harbours Division, ASCE, 88, pp 117-130.

Carter, H.H., Pritchard. D.W., 1988. Oceanography of Chesapeake Bay. Hydrodynamics of Estuaries. Volume II. Esturine Case Studies. CRC Press, pp 1-15.

Cheng, R.T., Gartner, J.W., 1985. Harmonic analysis of tides and tidal currents in South San Francisco Bay, California. Estuarine, Coastal and Shelf Science 21 (1), pp 57-74.

Cheng, R. T., Ling, C.-H., Gartner, J. W. & Wang, P. F., 1999. Estimates of bottom roughness length and bottom shear stress in South San Francisco Bay, California. Journal of Geophysical Research 104 (C4), pp 7715–7728.

Chrystal, G., 1909. Investigation of the seiches of Loch Earn by the Scottish Loch Survey, Part III. Transactions of the Royal Society of Edinburgh 46(3): pp 455-517.

Church, J.A., White, N.J., 2006. A 20th century acceleration in global sea-level rise. Geophisical Research letters 33, L01602. Doi:10.1029/2005GL024826.

Cohen, Y., Mackay, D., Shiu, W.Y., 1980. Mass transfer rates between oil slicks and water. Canadian Journal of Chemical Engineering. 58 (5): pp 569-575.

Cooper, J.A.G., 1993. Sedimentation in a river-dominated estuary. Sedimentology 40, pp979–1017.

Cooper,M.J.P., Beevers,M.D., Oppenheimer,M., 2005. Future Sea Level Rise and the New Jersey Coast-Assessing Potential Impacts and Opportunities. Science, Technology and Environmental Policy Program. Woodrow Wilson School of Public and International Affairs, Princeton University, /http://www.princeton.edu/_cmi/news/Future%20of%2Sea%20Level%20Rise%20and%20the% 20New%20Jersey%20Coast.pdf

Christie, M. C., Dyer, K. R., Turner, P., 1999. Sediment flux and bed level measurements from a macro tidal mudflat. Estuarine, Coastal and Shelf Science 49, 667–688.

Csanady, G.T., 1972. Transverse internal seiches in Large Oblong Lakes and Marginal Seas. Journal of Physical Oceanography, 3(4): pp 439-447.

Cudaback, C. N., Jay, D. A., 2000. Tidal asymmetry in an estuarine pycnocline: depth and thickness. Journal of Geophysical Research 105 (C11), 26237–26251.

Dronkers, J., 1996. Morphodynamics of the Dutch Delta. Eighth International Biennial Conference on Physics of Estuaries and Coastal Seas, the Hague. Sep., pp 297-304.

Day, J.H., 1981. The nature, origin and classification of estuaries. Journal of Estuarine Ecology. A.A.Balkema, Rotterdam. pp 1-6.

Douglas, B.C., 1997. Global sea level acceleration. Journal of Geophys. Res. 97 (C8), pp 12699–12706.

Ding, Y., 2011. Handbook for Mitigating Climate Change. Sea-level rise and hazardous storms: impacts on coasts and estuaries. Springer, pp. 1523–1555.

D & A Instruments Co., 1991. OBS-3 Suspended Solids & Turbidity Monitor User Manual.

Dean et al., 1987. Committee on Engineering Implications of Changes in Relative Mean Sea-level. Responding to Changes in Sea-level: Engineering Implications. National Academy Press, Washington, D.C.

Delvigne, G.A.L., Sweeney, C.E., 1988. Natural dispersion of oil. Oil and Chemical Pollution 4, pp 281-310.

DHI water and environment (2005). Coastal hydraulics and oceanography hydrodynamic module reference manual.

Ding, Y, Kuiry, S.N., Elgohry, m., Jia, Y.F., Altinakar, M.S., Yeh, K.C., 2013. Impact assessment of sea-level rise and hazardous storms on coasts and estuaries using integrated processes model. Journal of Ocean Engineering. 71 (2013) pp 74–95.

Doerffer, J. W., 1992. Oil spill response in the marine environment. PERGAMON PRESS.

Dominic, E. R., Karunarathna, H., 2009. On the prediction of long-term morphodynamic response of estuarine systems to SLR and human interference. Journal of Continental Shelf Research.

Dronkers, J., 1986. Tidal Asymmetry and estuarine morphology. Netherlands Journal of Sea Research 20 (2/3): pp 17-131.

Dyer, K. R., 1986. Coastal and Estuarine Sediment Dynamics. A Wiley- Interscience publication, pp 246

Dyer, **K. R., 1979.** Estuaries and estuarine sedimentation. Estuarine and brackish-water sciences association handbook: Estuarine hydrograph and sedimentation, pp 3-7.

Earthtech Consulting Limited, 2007. Geotechnical and Engineering Report for an application for the redevelopment of the Existing Tairua Marina in Marina Zone 1.

Eldho, T.I., ISH, M., Chandramohan, P.V., 2005. Hydrodynamics and salinity transport modelling of Cochin Estuary. ISH Journal of Hydraulic Engineering. Vol. 11, No.3. pp. 163-177.

Elliot, A., J., Hurford, N., Penn, J., 1986. Shear diffusion and the spreading of oil slicks. Marine Pollution Bulletin 17, pp 308-313.

Falcão, A.P. et al, 2013. Influence of elevation modelling on hydrodynamic simulations of a tidally-dominated estuary. Journal of Hydrology. 497 (2013) pp 52‑164.

Fay, J.A., 1971. Physical processes in the spread of oil on a water surface. Proc. Conference of Prevention and Control of Oil Spills, American Petroleum Institute, Washington, DC, pp 463-467.

Festa, J.P., Hansen, D.V., 1978. Turbidity maxima in partially mixed estuaries: a two-dimensional numerical model, Estuarine and Coastal Marine Science 7: pp347-359.

FitzGerald, Duncan M., Fenster, Michael S., Argow, Britt A., and Buynevich, Ilya V., 2008. Coastal Impacts Due to Sea-Level Rise. Annual Review of Earth and Planetary Sciences. 36: pp 601-47

Fischer, H.B., List, J.E., Koh, R.C.Y., Imberger, J., Brooks, N.H., 1979. Mixing in Inland and Coastal Waters. Academic Press, New York.

Foreman, M.G., 1977. Manual for Tidal Heights Analysis and Prediction. Pacific Marine Science Report 77-10, Institute of Ocean Sciences, Canada.

Friedrichs, C. T., Hamrick, J. M., 1996. Effects of channel geometry on cross sectional variations in along channel velocity in partially stratified estuaries. In Buoyancy Effects on Coastal and Estuarine Dynamics (Aubrey, D. G. & Friedrichs, C. T., eds). American Geophysical Union 53, pp 83–300.

Garel, E., L. Pinto, A. Santos, and Ó. Ferreira.,2009. Tidal and River Discharge Forcing Upon Water and Sediment Circulation at a Rock-bound Estuary (Guadiana Estuary, Portugal). Estuarine, Coastal and Shelf Science 84 (2) Sep.: pp269–281.

Geyer, W. R., 1997. Influence of wind on dynamics and flushing of shallow estuaries. Estuarine, Coastal and Shelf Science 44, pp713–722.

Gibbs, R. J., Matthews, M.D., and Link, D.A., 1971. The relationship between sphere size and settling velocity. Journal of Sedimentary Petrology, 41(1), pp7-18.

Goring, D.G., 1995. Short-term variations in sea level (2–15 days) in the New Zealand region. NZ Journal of Marine and Freshwater Research *29*: 69–82

Green, M. O., Black, K. P., Amos, C. L., 1997. Control of estuarine sediment dynamics by interactions between currents and waves at several scales. Marine Geology 144, pp97–116.

Green, M. O., MacDonald, I. T., 2001. Processes driving estuary infilling by marine sands on an embayed coast. Marine Geology 178, pp11–37.

Guo, L., He, Q., Roelvink, D., Wang, Z., Van Der Wegen, M., 2013. Medium- to long-term morphodynamic modelling in estuaries and coasts: Principles and applications. Acta Geographica Sinica. Volume 68, Issue 9, September 2013, pp 1182-1196.

Habib, E., Nuttle, W.K., Rivera-Monroy, V.H., Gautam, S., Wang, J., Meselhe, e., and Twilley, R.R. 2007. Assessing effects of data limitations on salinity forecasting in Barataria Basin, Louisiana, with a Bayesian analysis. Journal of Coastal Research: Volume 23, Issue 3: pp. 749 – 763.

Hallermeier, R.J., 1981. Terminal settling velocity of commonly occurring sand grains. Sedimentology, 28, pp 869-865.

Hannah, J., Bell, R.G., 2012. Regional sea level trends in New Zealand. Journal of Geophysical Research: Oceans.

Hansen, D.V., Rattray, M., 1965. Gravitational circulation in straits and estuaries. Journal of Marine Research 23, pp 104-122.

Hardisty, J., 2007. Estuaries: monitoring and modelling the physical system. Blackwell Publishing.

Harrison et al., 1975. Crude oil spills: Disappearance of aromatic and aliphatic components from small sea-surface slicks. Environmental Science & Technology, v9, n3.

Hong, B., Shen.J., 2012. Responses of estuarine salinity and transport processes to potential future sea-level rise in the Chesapeake Bay. Estuarine, Coastal and Shelf Science 104-105, pp 33-45.

Huang, J.C., 1983. A review of the state-of-the art of oil spill fate/behaviour models. Proceedings of teh 1983 Oil Spill Conference. Washington, DC, pp 313-322.

Hume, T.M., Gibb, J.G., 1987. The "Wooden-Floor" Marker Bed-A New Method of Determining Historical Sedimentation Rates in Some New Zealand Estuaries. Journal of the Royal Society of New Zealand, Vol. 17, No.1, 1987, pp.1-7

Hume, T.M. Herdendorf C.E., 1988. A geomorphic classification of estuaries and its application to coastal resource management—a New Zealand example. Journal of Ocean and Shoreline Management. 11: pp 249–274.

Hume, T.M., Herdendorf, C.E., 1992. Factors controlling Tidal Inlet Stability on Low Drift Coasts. Journal of Coastal Research,8(2): pp 355-375.

Hume, T.M., Herdendorf, C.E., 1993. On the Use of Empirical Stability Relationships for Characterizing Estuaries Journal of Coastal Research. pp413-422.

Hume, T. M., et al., 2003. A new approach to classify New Zealand's estuaries. Coasts & Ports Australasian Conference 2003.

Intergovernmental Panel on Climate Change, 2007. IPCC Fourth Assessment Report: Climate Change 2007 (AR4).

Intergovernmental Panel on Climate Change, 2001. (Houghton, J.T., Ding, Y., Griggs, D.J., Noguer, M., van der Linden, P.J. & Xiaosu, D.). Contribution of working group to the third assessment report of the inter-governmental panel on climate change (IPCC). Cambridge University Press, UK, pp 944.

Jackson, N.L., 2013. 10.12 Estuaries. Treatise on Geomorphology. Volume 10. Pp308-326.

Johansen, Ø., 1984. The Halten Bank experiment – observations and model studies of drift and fate of oil in the marine environment. Proceedings of the 11th Arctic Marine Oil Spill Program (AMOP) Technology Seminar, Environment Canada, pp 18-36.

Jones, K.E., Preston, N.J., 2008. Connectivity of landslides in the Waipaoa catchment, New Zealand. Australian and New Zealand Geomorphology Group 13th Conference Queenstown Tasmania: program and abstracts: pp 122.

Joordens, J. C. A., Souza, A. J., Visser, A., 2001. The influence of tidal straining and wind on suspended matter and phytoplankton distribution in the Rhine outflow region. Continental Shelf Research 21, pp 301–325.

Kang, J.W., Jun, K.S., 2003. Flood and ebb dominance in estuaries in Korea. Esturine, Coastal and Shelf Science 56, pp 187-196.

Kettle, N.P., 2012. Exposing compounding uncertainties in sea level rise assessments. Journal of Coastal Research 28 (1), pp 161-173.

Kirk, R.M., 1991. River-beach interaction on mixed sand and gravel coasts: a geomorphic model for water resource planning. Applied Geography. Volume 11, issue 4. Oct. 1991, pp 267-287.

Korgen, B.J. 1995. Seiches. American Scientist. 83(4): pp 330-341.

Kraus, N. C., Lohrmann, A., Cabrera, R., 1994. New acoustic meter for measuring 3D laboratory flows. J. Hydraul. Eng., Vol. 120, pp. 406-412.

Lacy, J. R., Monismith, S. G., 2001. Secondary currents in a curved, stratified, estuarine channel. Journal of Geophysical Research 106 (C12), 31238–31302.

Liu, C., De Lange, W., Winter, C., Bryan, K., 2011. Forcing Mechanisms of a seiche Event at Tairua Estuary, New Zealand. Coasts & Ports 2011, September, Perth, Australia.

Lopes, J.F., Dias, J.M., 2007. Residual circulation and sediment distribution in the Ria de Aveiro lagoon, Portugal. Journal of Marine Systems. 68, pp 507-528.

Li, C., O'Donnell, J., 1997. Tidally driven residual circulation in shallow estuaries with lateral depth variation. Journal of Geophysical Research 102 (C13), pp 27915–27929.

Luettich, R. A., Carr, S. D., Reynolds-Flemming, J. V., Fulcher, C. W., 2000. Semi-diurnal seiche in a shallow, micro-tidal lagoonal estuary. Continental Shelf Research, 22(11-13): pp 1669-1681.

Manh, D, V., Yanagi, T., 2000. A study on residual flow in the gulf of Tongking. Journal of Oceanography, Vol. 56, pp 59-68

Masselink, G., Short, A. D., 1993. "The effect of tidal range on beach morphodynamics and morphology: a conceptual beach model". Journal of Coastal Research 9 (3): pp 785–800. ISSN 0749-0208

McAuliffe, C.D. 1987. Organism exposure to volatile/soluble hydrocarbons from crude oil spills–a field and laboratory comparison. Proceedings of the 1987 Oil Spill conference, April 6-9, 1987, Baltimore, Maryland, pp. 275-288.

McDowell, D.M., O'Connor, B.A., 1977. Control of Estuaries. Hydraulic Behaviour of Estuaries. M. Printed in Great Britain at the University Printing House, Cambridge.

McDowell, D.M. & O'Connor, B.a., 1977. Hydraulic behaviour of estuaries. Civil Engineering Hydraulics. Series, MacMillan, London: pp 1-292.

Mead, S., Black, K., 2005. Development of a multi-purpose reef at Orewa Beach, New Zealand. 17th Australiasian Coastal and Ocean Engineering Conference 2005 and the 10th Australasian Port and Harbour Conference, Coasts and Ports 2005, pp 679-684.

Ministry for the Environment, 2008. Coastal Hazards and Climate Change. A Guidance Manual for Local Government in New Zealand. 2nd edition. Revised by Ramsay, D, and Bell, R. (NIWA). Prepared for Ministry for the Environment. Viii. pp 127

Nelson, H, 1976. Late Pleistocene and Holocene depositional trends, processes, and history of Astoria deep-sea fan, Northeast Pacific. Marine Geology, Volume 20, Issue 2, February 1976, pp 129-173.

Nepf, H. M., Geyer, W. R., 1996. intertidal variations in stratification and mixing in the Hudson estuary. Journal of Geophysical Research 101 (C5), pp12079–12086.

New Zealand Land Information. From: www.linz.govt.nz

NIWA Coastal Xplore Webtool, 2013. Water resource explore NZ. From:http://wrenz.niwa.co.nz/webmodel/

Nicholls, R.J.,2003. Case study on sea-level rise impacts. OECD Workshop on the Benefits of Climate Policy: Improving Information for Policy Makers, http://www.oecd.org/dataoecd/7/15/2483213.pdf.

Nicholls, R.J. and Cazenave, A., 2010. Sea-level rise and its impact on coastal zones. Science, 328, pp 1517–1520.

Nicholls, R.J., Wong, P.P., Burkett, V.R., Codignotto, J.O., Hay, J.E., McLean, R.F., Ragoonaden, S., and Woodroffe, C.D., 2007. Coastal systems and low-lying areas. Climate Change 2007: Impacts, Adaptation and Vulnerability. Contribution of Working Group II to the Fourth Assessment Report of the Intergovernmental Panel on Climate Change. Cambridge, United Kingdom: Cambridge University Press, pp. 315–356.

O'Brien, M.P., 1969. Equilibrium Flow Areas of Inlets on Sandy Coasts, J. Waterways and Harbours. Div., ASCE,95, WW1, pp 43-52.

Pacific Tsunami Warning Centre, 2010. From: http://ptwc.weather.gov/?region=1.

Pattiaratchi, C., Hegge, B., Gould, J. & Eliot, I., 1997. Impact of sea-breeze activity on nearshore and foreshore processes in southwestern Australia. Continental Shelf Research 17, pp1539–1560.

Pattiaratchi, C., 2001. Oceanographic Engineering 447 Lecture Notes. Centre for Water Research, University of Western Australia, Perth.

Pethick, J., 2001. Coastal management and sea level rise. Catena 42, pp 307–322.

Perumal, M., T. Moramarco, B. Sahoo, and S. Barbetta, 2007. A methodology for discharge estimation and rating curve development at ungauged river sites, Water Resource. Res., 43, W02412, doi:10.1029/2005WR004609.

Postma, H, 1966. The cycle of nitrogen in the wadden sea and adjacent areas. Netherlands Journal of Sea Research, Volume 3, Issue 2, August 1966, pp 186-221.

Postma, H., 1967. Sediment transport and sedimentation in the estuarine environment, Estuaries, ed. Lauff, American Academy for the Advancement of Science. Washington: pp 158-179.

Power, W., 2013. Review of Tsunami Hazard in New Zealand (2013 Update). GNS Science Consultancy Report 2013/131.

Prandle, D., 2009. Estuaries: Dynamics, Mixing, Sedimentation and Morphology. Cambridge University Press.

Pritchard, D.W., 1967. What is an estuary: physical viewpoint. In: Estuaries. American Association for the Advancement Science Publication 83, Washington, DC. pp 3-5.

Pugh, D.T., 2004. Changing Sea Levels. Effects of Tides, Weather and Climate. Cambridge University Press, Cambridge, pp 265.

Quang Tri, D., Cao Don, N., Yi Ching, C., 2013. Trajectory modeling of marine oil spills: Case study of lach huyen port, Vietnam. Lowland Technology International. Volume 15, Issue 2, pp 41-55.

Raicich, F., 2003. Recent evolution of sea-level extremes at Trieste (Northern Adriatic). Continental Shelf Research. 23 (2003), pp 225–235.

Reed, M., Turner, C., Odulo, A., 1994a. The role of wind and emulsification in modelling oil spill and drifter trajectories. Spill Science and Technology Bulletin 1(2), pp 143-157.

Robertson, G., Peters, M., 2006. Turning the tide: an estuaries toolkit for New Zealand communities. Christchurch, Taieri Trust.

Ruhl, C. A., Schoellhamer, D. H., Stumpf, R. P. & Lindsay, C. L., 2001. Combined use of remote sensing and continuous monitoring to analyze the variability of suspended-sediment concentrations in San Francisco Bay, California. Estuarine, Coastal and Shelf Science 53, 801–812.

Rye, Henrik, 1995. A multicomponent oil spill model for dissolved aromatic concentrations. IOSC International Oil Spill Conference Proceedings. Volume 1995, Issue 1 (February 1995).

Scarfe, B.E., Healy, T.R., Rennie, H.G., and Brooks, S., 2009. An Approach to Hydrographic Data Management using Customised GIS and Geodatabases. Hydrographic Journal, No 128, pp 129, 23-34.

Schubel, J.R., Meade, R.H.,1977. Man's impact on estuarine sedimentation. Proc. Conf. est. poll. Control and Assess, Vol. 1. US Environment Protection Agency, Washington: pp193-209.

Shen, H.,T., Yapa, P., Petroski, M., 1987. A simulation model for oil spill transport in lakes. Water Resources Res. 23(10), pp 1949-1957.

Simpson, J. H., Souza, A. J., 1995. Semidiurnal switching of stratification in the region of freshwater influence of the Rhine. Journal of Geophysical Research 100 (C4), pp7037–7044.

Singsaas, I., Daling, P.S., 1992. Meso-scale flume test for laboratory weathering of oil. Proceedings of the 158th Arctic and Marine Oil Spill Program Technical Seminar, Environment Canada, pp 55-66.

Sinha, P.C., Rao, Y.R., Dube, S.K., 1997. Effect of sea-level rise on tidal circulation in the Hooghly Estuary, Bay of Bengal.

Smagorinsky, J., 1964. Implications of dynamical modelling of the general circulation on long-range forecasting. In, WMO-IUGG Symposium on Research and Development Aspects of Long-range Forecasting, Boulder, CO., WMO Technical Note 62, pp 131-137.

Soulsby, R., 1997. Dynamics of marine sands-a manual for practical applications. Thomas Telford Publishing, pp 45-52.

Soulsby, R.L. and Whitehouse, R.J.S.W., 1997. Threshold of wave-current interaction at the sea bed, in Water Wave Kinematics, eds A. Torum and O.T.Gudmestad, Kluwer Academic Publishers, Dordrecht, pp. 413-428.

Speer, P.E., Aubrey, D.G., 1985. A study of non-linear tidal propagation in shallow inlet/estuarine systems: Part II. Theory. Estuarine, Coastal and Shelf Science, 21, pp 207-224.

Spaulding, M.L., 1995. Oil spill trajectory and fate modelling : State-of-the art review. Proceeding of the 2nd International Oil Spill Research and Development Forum, IMO,London, UK.

Stacey, M. T., Burau, J. R., Monismith, S. G. 2001 Creation of residual flows in a partially stratified estuary. Journal of Geophysical Research 106 (C8), pp17013–17037.

Statistics New Zealand, 2007.
From:http://www.stats.govt.nz/browse_for_stats/businesses/business_growth_and_innovation/innovation-in-new-zealand-2007.aspx.**Surf-Forecast.com company, 2013.** TairuaBeach Water Temperature and Wetsuit Guide (New Zealand – Coromandel). From: http://www.surf-forecast.com/breaks/Tairua-Beach/seatemp/.

Tairua History Group, 2012.
From:http://www.tairua.info/uploads/61039/files/Tairua_History_A4_Final_LR1.pdf

The Encyclopedia of New Zealand. Sea Surface Temperatures. From: http://www.teara.govt.nz/en/interactive/8810/sea-surface-temperatures.

The national climate database, 2010-2013. From: http://cliflo.niwa.co.nz/.

Thompson, K.,R., 1982. The influence of local winds and the southern North Sea on the level of the River Thames. Estuarine, Coastal and Shelf Science 15(6), pp 605-610.

Tonkin & Taylor Ltd, 2008. Tairua Marina: Response to further information request – Physical coastal processes. Report for Tairua Marine Ltd., T& T Ref: 18298.400.

Toorman, E. A. 2002. Modelling of turbulent flow with suspended cohesive sediment. Proceedings in Marine Science, Volume 5, 2002, pp155-169.

Townend, I., Pethick, J., 2002. Estuarine flooding and managed retreat. Philosophical Transactions of the Royal Society London: Series A 360, pp 1477–1495.

USACE, 2011. Sea-level Change Considerations for Civil Works Programs, EC1165-2-212. U.S. Army Corps of Engineers, Washington, DC. Available at: /http://planning.usace.army.mil/toolbox/library/ECs/EC11652212Nov2011.pdf.

US-CCSP (U.S. Climate Change Science Program), 2008. Coastal Sensitivity to Sea Level Rise: A Focus on the Mid-Atlantic Region for Synthesis and Assessment Product 4.1. /http://www.climatescience.gov/Library/sap/sap4-1/public-re view-draft

Valentim, J.M., Vaz, L., Vaz, N., Caçador, I., Dias, J.M., 2013. Sea level rise impact in residual circulation in Tagus estuary and Ria de Aveiro lagoon. Journal of Coastal Research. Issue SPEC. ISSUE 65, 2013, pp 1981-1986.

Valle-Levinson, A., Wong, K.-C. & Lwiza, K. M. M., 2000a. Fortnightly variability in the transverse dynamics of a coastal plain estuary. Journal of Geophysical Research 105 (C2), pp3413–3424.

Valle-Levinson, A. & Atkinson, L. P., 1999. Spatial gradients in the flow over an estuarine channel. Estuaries 22, pp179–193.

Valle-Levinson, A. & Wi1son, R. E., 1998. Rotation and vertical mixing effects on volume exchange in eastern Long Island Sound. Estuarine, Coastal and Shelf Science 46, pp573–585.

Van Goor, M.A., Zitman, T.J., Wang, Z.B., Stive, M.J.F, 2003. Impact of sea-level rise on the morphological equilibrium state of tidal inlets. Journal of Marine Geology. 202(2003), pp 211-227.

Van Rijn, L.C., 1984. Sediment transport: part I: bed load transport; part II: suspended load transport; part III: bed forms and alluvial roughness. J. Hydraul. Div., Process of ASCE, 110 (HY10), pp1431-1456; (HY11), pp 1613-1641; (HY12), pp 1733-1754.

Van Rijn, L.C. 1985. Mathematical model for sedimentation of shipping channels. Proc. Int. Conf. Numerical and Hydraulic modelling of Ports and Harbours, Birmingham, UK, BHRA, Cranfield, UK, pp 181-186.

Van Rijn, L.C. *et al.*, 2003. The predictability of cross-shore bed evolution of sandy beaches at the time scale of storms and seasons using process-based Profile models. Coastal Engineering 47 (2003), pp 295-327.

Van Der Wegen, M., 2013. Numerical modeling of the impact of sea level rise on tidal basin morphodynamics. Journal of Geophysical Research F: Earth Surface. Volume 118, Issue 2, 2013, pp 447-460.

Vaz, N., Dias, J.M., 2013. Physical analysis of a tidal channel (Espinheiro channel, Portugal): a modelling study. Ocean modelling for Coastal Management-Case Studies with MOHID. Ist Press, pp 41-54.

von Kármán, Th., 1930. Mechanical similitude and turbulence, National Advisory Committee for Aeronautics. Tech. Mem. NACA, no. 611, pp 58-76.

Waikato Regional Council, 1998. Waikato State of the Environment Report. Note: numbers include all properties in settlement, including those in the estuary catchments and the adjacent open coast beach of the same name.

Walrond, Carl, 2013. 'Coastal fish- New Zealand's coastal fish', Te Ara-the Encyclopedia of New Zealand, updated 9-Jul-2013. URL: http://www.TeAra.govt.nz/en/interactive/8810/sea-surface-temperatures

Jeffress Williams, Matthew A. Arsenault, Brian J. Buczkowski, Jane A. Reid, James G. Flocks, Mark A. Kulp, Shea Penland, and Chris J. Jenkins, 2006. Wentworth grain size chart from Surficial sediment character of the Louisiana offshore continental shelf region. United States Geological Survey Open-File Report. pp 1195,

Weiss, J.L., Overpeck, J.T., and Strauss, B., 2011. Implications of recent sea-level rise science for low-elevation areas in coastal cities of the conterminous U.S.A. Climatic Change, 105, pp 635–645.

Whitehouse, R.J.S., 1997. Scour at marine structures. A manual for practical applications. Report SR 417. HR Wallingford.

Whitehouse, R.J.S., Bassoullet, P., Dyer, K.R., H.J. Mitchener, Roberts, W., 2000. The influence of bedforms on flow and sediment transport over intertidal mudflats. Continental Shelf Research, Volume 20, Issues 10–11, 1 July 2000, pp 1099-1124.

Wilson, B. W., 1972. Seiches. Advances in Hydroscience 8: pp 1-94.

Winter, C., 2007. On the evaluation of sediment transport models in tidal environments. Journal of Sedimentary Geology, pp 562-571.

Wises Maps, 2012. Wises New Zealand Guide. From: http://www.wises.co.nz.

Yapa, P.D., Shen, H.T., Angammana, K., 1994. modelling oil spills in a river-lake system. Journal of Marine System 4, pp 453-471.

Appendix I

The raw data were extracted from NIWA's model results every 12 grid points (600 m in whole_50m bathymetry) and interpolated along the N, E and S boundaries. The locations of the data extracted from NIWA's tidal model and the cells for the 'whole-50m' numerical model are listed as follows.

I.1 Northern Boundary

No	Lon.	Lat.	Depth (m)	Whole_50m
1	175°51'9.21" E	36°57'53.90" S	-4.97	131, 298
2	175°51'42.63" E	36°57'53.33" S	-7.16	148, 298
3	175°52'6.87" E	36°57'52.58" S	-12.84	160, 298
4	175°52'31.11" E	36°57'52.16" S	-19.81	172, 298
5	175°52'55.35" E	36°57'51.58" S	-27.34	184, 298
6	175°53'19.59" E	36°57'51.00" S	-33.89	196, 298
7	175°53'43.81" E	36°57'50.40" S	-39.16	208, 298
8	175°54'8.06" E	36°57'49.80" S	-44.17	220, 298
9	175°54'32.28" E	36°57'49.22" S	-48.54	232, 298
10	175°54'56.51" E	36°57'48.62" S	-51.19	244, 298
11	175°55'20.74" E	36°57'48.02" S	-53.47	256, 298
12	175°55'44.98" E	36°57'47.42" S	-55.77	268, 298
13	175°56'9.21" E	36°57'46.82" S	-57.60	280, 298
14	175°56'33.42" E	36°57'46.22" S	-58.87	292, 298
15	175°56'57.67" E	36°57'45.63" S	-59.65	304, 298
16	175°57'21.90" E	36°57'45.01" S	-60.05	316, 298
17	175°57'46.14" E	36°57'44.48" S	-60.17	328, 298
18	175°58'10.38" E	36°57'43.81" S	-60.05	340, 298
19	175°58'34.60" E	36°57'43.20" S	-59.71	352, 298
20	175°59'2.08" E	36°57'42.51" S	-59.11	365, 298

I.2 Eastern Boundary

No.	Lon.	Lat.	Depth (m)	Whole_50m
21	175°59'3.18" E	36°58'11.05" S	-57.4	365, 0
22	175°59'4.47" E	36°58'43.45" S	-55.94	365, 20
23	175°59'5.71" E	36°59'15.85" S	-55.01	365, 40
24	175°59'6.95" E	36°59'48.29" S	-54.84	365, 60
25	175°59'8.28" E	37°0'20.67" S	-55.48	365, 80
26	175°59'9.49" E	37°0'53.10" S	-56.85	365, 100
27	175°59'10.79" E	37°1'25.47" S	-58.74	365, 120
28	175°59'12.06" E	37°1'57.88" S	-60.98	365, 140
29	175°59'13.35" E	37°2'30.31" S	-63.28	365, 160
30	175°59'14.63" E	37°3'2.73" S	-60.58	365, 180
31	175°59'15.87" E	37°3'35.08" S	-66.83	365, 200
32	175°59'17.14" E	37°4'7.51" S	-66.74	365, 220
33	175°59'18.42" E	37°4'39.96" S	-66.79	365, 240
34	175°59'19.72" E	37°5'12.36" S	-67.06	365, 260
35	175°59'20.99" E	37°5'44.74" S	-66.55	365, 280

I.3 Southern Boundary

No.	Lon.	Lat.	Depth (m)	Whole_50m
36	175°53'29.77" E	37°5'53.46" S	-4.32	192, 0
37	175°53'54.06" E	37°5'52.86" S	-6.72	204, 0
38	175°54'18.32" E	37°5'52.26" S	-10.81	216, 0
39	175°54'42.61" E	37°5'51.67" S	-17.21	228, 0
40	175°55'6.89" E	37°5'51.07" S	-22.85	240, 0
41	175°55'31.17" E	37°5'50.48" S	-26.99	252, 0
42	175°55'55.44" E	37°5'49.88" S	-31.22	264, 0
43	175°56'19.72" E	37°5'49.27" S	-36.69	276, 0
44	175°56'43.99" E	37°5'48.67" S	-42.23	288, 0
45	175°57'8.26" E	37°5'48.07" S	-47.66	300, 0
46	175°57'32.54" E	37°5'47.46" S	-50.31	312, 0
47	175°57'56.82" E	37°5'46.85" S	-53.45	324, 0
48	175°58'21.09" E	37°5'46.25" S	-57.29	336, 0
49	175°58'45.36" E	37°5'45.64" S	-61.07	348, 0

Appendix II

Dataflows Calibration Results

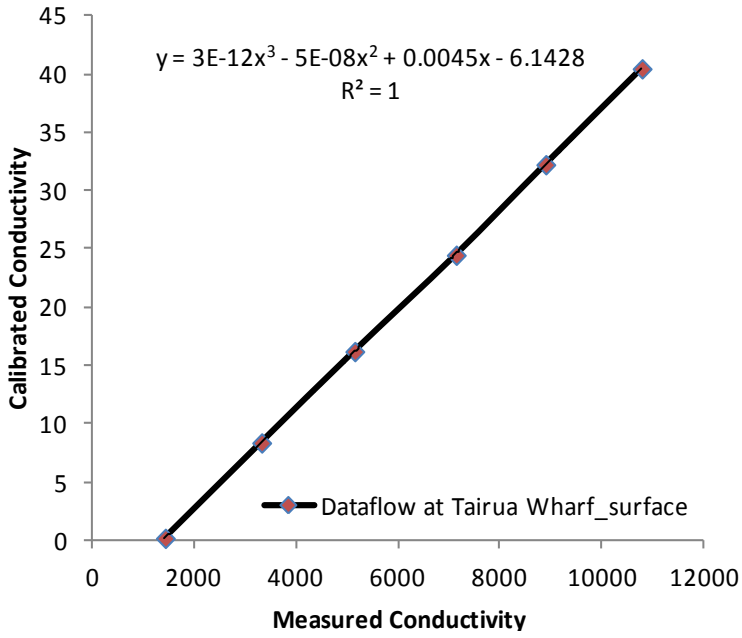

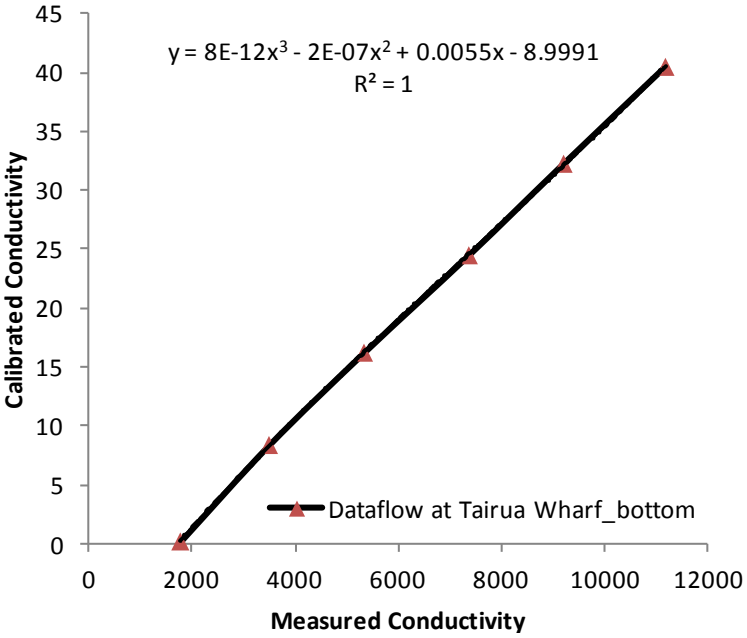

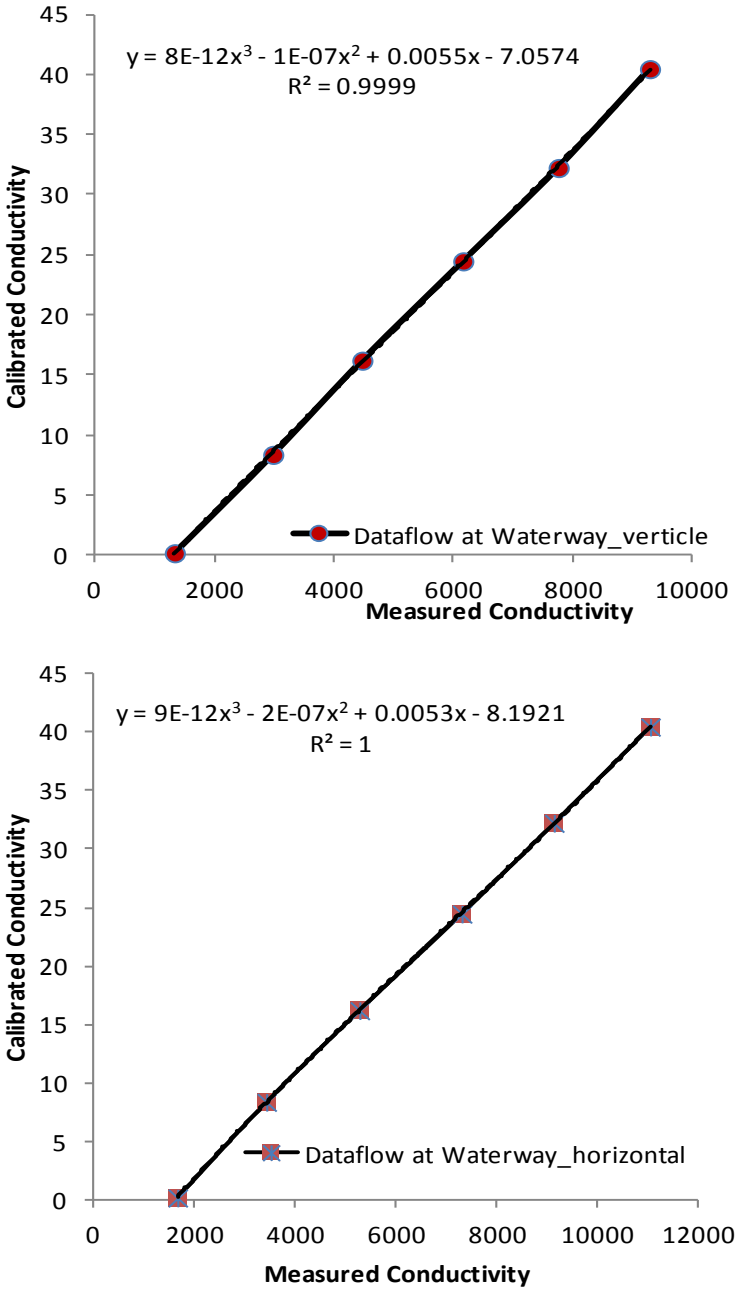

Figure II-1 Calibration results of the Dataflow conductivity (mS cm^{-1})

Table II-1 Calibration results of the Dataflow temperature

Dataflow Locations	Temperature °C
Dataflow 4053: Tairua Wharf_surface	$y = 93.29x + 54.22$
Dataflow 4054:Tairua Wharf_bottom	$y = 94.90x + 137.08$
Dataflow 4055: Pauanui Waterway_vertical	$y = 95.39x + 107.26$
Dataflow 4056: Pauanui Waterway_horizontal	$y = 92.19x + 129.54$

Appendix III

POL3DD Oil Spill Model Operation Files

D:\Tairua_3DD_Cathy_2012\Oil_spill_Tairua_Sep2012\estuary20m_new\OUT\oilspill_20m_O1.log
!
!
5 Model type options: 1=Conservative, 2=Chemical, 3=Nutrients, 4=Ecoli,5=Oil, 6=Tracer, 7=Sand, 8=Mud, 9=Settle, 10=Larvae, 11=Rapid
!
! General window
1 Vertical mixing options: 1=Well-mixed, 2=Layered
1 Layer orientation 1 = top down; -1 = bottom up
0.1 Constant layer thickness (m)
D:\Tairua_3DD_Cathy_2012\Oil_spill_Tairua_Sep2012\estuary20m_new\5layers.thk layer thickness filename
0 Initial seed
D:\Tairua_3DD_Cathy_2012\Oil_spill_Tairua_Sep2012\estuary20m_new\BND\wind_SW_5.wnd wind file
1 Include horizontal advection 0=No, 1=Yes
1 Vertical velocity included
35 Ambient background (magnitude)
1 Density inversion options: 1=Positive, 0=None, -1=Negative
0,0,0 Debug cell (Idbug, I, J)
!
! Input window
D:\Tairua_3DD_Cathy_2012\1estuary_20m_nested_done\HD_estuary_20m_nested_v9.out 3DD file
726 First block to use in 3DD file
751 Last block to use in 3DD file
1 At last block options: 0=Stop or 1=Loop
Wave file
1 First block to use in Wave file
1 Last block to use in Wave file
1 At last block options: 0=Stop or 1=Loop
0,0,0 free velocity cell (I,J,K)
!
! Output window
D:\Tairua_3DD_Cathy_2012\Oil_spill_Tairua_Sep2012\estuary20m_new\OUT\oilspill_20m_O1.pol Model output file
Model ID line
0,0,0,0 Output region (IS, IE, JS, JE)
1 Number of time steps between box writes (steps)

0,0,0,0,0 Box regions
!
! Time steps window
10 Model time step (seconds)
26 Model duration (hours)
1 Direction options: 1=Forward, -1=Backward
0,0 Integration period (hours)
0,0 Settlement period (hours)
0 Split steps (steps)
60 Time steps between disk output (steps)
0 First output time step (steps)
!
! Boundary window
D:\Tairua_3DD_Cathy_2012\Oil_spill_Tairua_Sep2012\estuary20m_new\BND\oilspill_
20m_petrol.bnd Boundary file
!
! Equations and Particles window
1 Bedload options: 0=None, 1=Yalin
2 Suspended load options: 0=None, 1=Einstein, 2=Nielsen, 3=Both
0.005 Nielsen multiplier
3 Nielsen power
0.2 Critical bedload velocity (m s^{-1})
0.4 Critical suspended load velocity (m s^{-1})
10 Number of bedload particles released along each wall
20 Number of suspended load particles released in each cell
10 Steps between releases (steps)
13 Release duration (hours)
!
! Diffusion window
2 Horizontal Diffusion Options: 0=None, 1=Constant, 2=Roughness,
3=File
0.001 Longitudinal diffusion coefficient (m2/s)
0.001 Lateral diffusion coefficient (m2/s)
75 Longitudinal Elder coefficient
0.5 Lateral Elder coefficient
Roughness length file
0.01 Uniform roughness length (m)
Horizontal eddy diffusivity file
0 Vertical Diffusion Options: 0=None, 1=Constant, 2=Mixing length,
3=Linear in z, 4=File
0.001 Vertical eddy diffusivity (m2/s)
0.001 Surfzone vertical eddy diffusivity (m2/s)
0.4 Mixing length gradient
0.05 Minimum mixing length (m)
2 Maximum mixing length (m)
Vertical eddy diffusivity file
!
!

! Decay window

	T90 Decay file
0	Constant T90 (hours)
0	Minimum die off age (hours)

!

! Oil Spills window

D:\Tairua_3DD_Cathy_2012\Oil_spill_Tairua_Sep2012\estuary20m_new\OUT\impacts_oilspill_20m_O1.out Impacts File name

0	X origin coordinate
0	Y origin coordinate
1	Oil conservation 1 = no decay 2 = oil evaporates and dissolves
10	Air/Water temperature
1	Solubility factor
3.5	Wind speed percentage (%)
1	Sticky coast 0 = no beachings 1 = sticky shoreline!

! Tracer window

0.2	Tracer D50 grain size (mm)
0.2	Mixing depth (m)

!

! Sand transport window

0.3	Median grain size (mm)
2650	Sediment density (kg/m3)
0.65	Sediment porosity
	Accumulation file
0.002	Uniform sediment thickness (m)
0	Uniform rock/shell cover (%)
10	Nikuradse roughness over rocks
10	Peak spectral period (seconds)
1	Significant orbital velocity ($m\ s^{-1}$)
0.00114	Fluid viscosity

!

! Mud transport window

0.0046	Mud cohesiveness factor

!

! Larvae window

	Fish behaviour file
0	Universal fish behaviour
0.5	Threshold current speed ($m\ s^{-1}$)
0	Threshold duration (hours)
0.5	Threshold wave height (m)
1	Day time surface layer thickness (m)
1	Night time surface layer thickness (m)
0	Start hour of simulation (hours)
0	Advection probability (0,1)
100	Seagrass release interval (steps)
0.02	Swimming speed towards shallow water ($m\ s^{-1}$)

1000 Wind boundary layer distance (m)
4 Depth where fish dive down to the seabed (m)
0 Fish swimming speed against current (m s^{-1}) v
!
! Screen window
10 Screen update interval (steps)
1 Update options: 1=Screen, 2=Log file
0,0,0,0 Screen plot region (IS, IE, JS, JE)
7 Plotted variable options: 1=Sums of parts in cells, 2=Concentration, 3=Integrated, 4=Settlers, 5=Bed, 6=Grain, 7=Positions
5 Vector density (cells)
1 Vector scale (m s^{-1})
32,3 Water level cell (I,J)
!
! Map factor Mapfactor file

Appendix IV

POL3DD Oil Spill Model Boundary File

! BOUNDARY FILE
! Any number of lines can be placed at the top, with ! in column 1
!
!
D:\Tairua_3DD_Cathy_2012\Oil_spill_Tairua_Sep2012\estuary20m_new\BND\oilspill_20m_petrol.bnd

1	Release indicator
4	1=Particle, 2=Concentration 3=Volume 4=Oil Spills
0	0=Constant, 1=Time series
318,353	Centre of region
1	1=Rectangular, 2=Circular
0.5	Radius
1,4	Rectangle side lengths
0	Rotation
0,1	Upper and lower Z from surface down
0.0001	Fall velocity
10	Iterations between releases
0,13	Timing of release, start and end times (hours)

!

! Oil spills.	Values are not used unless oil is being simulated.
6	Carbon number
9	Percent of this consituent
0.012	Mass transfer coefficient (evaporation)

!
! Release fluxes

20	Particles to release
35	Concentration
1	Volume flux

Appendix V
Harmonic Components of Tides at Tairua Estuary

V.1 Principal Harmonic Components of Tidal Elevations

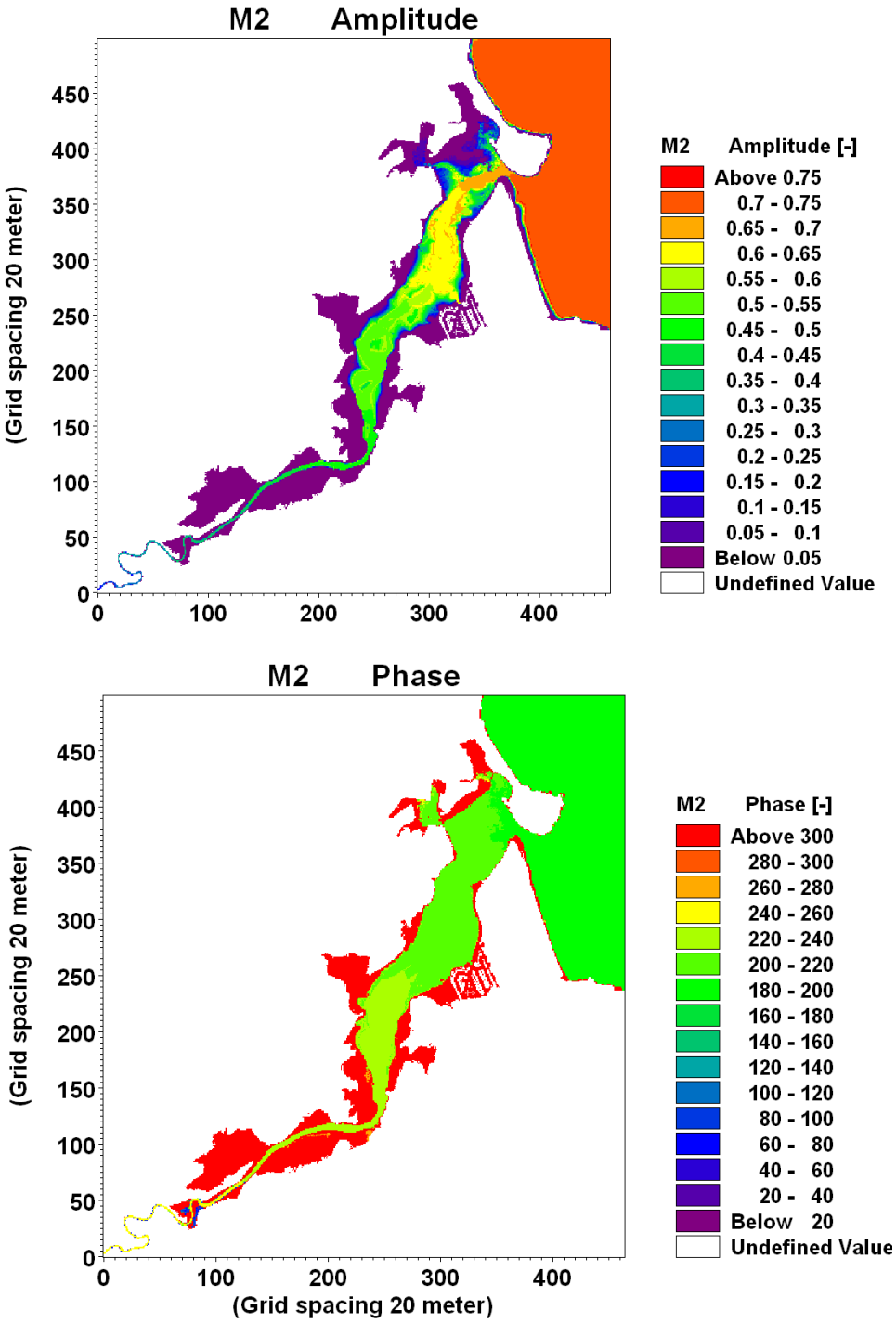

Figure V-1 Amplitude and the phase of the principal lunar component M_2 of the tidal elevation at Tairua Estuary

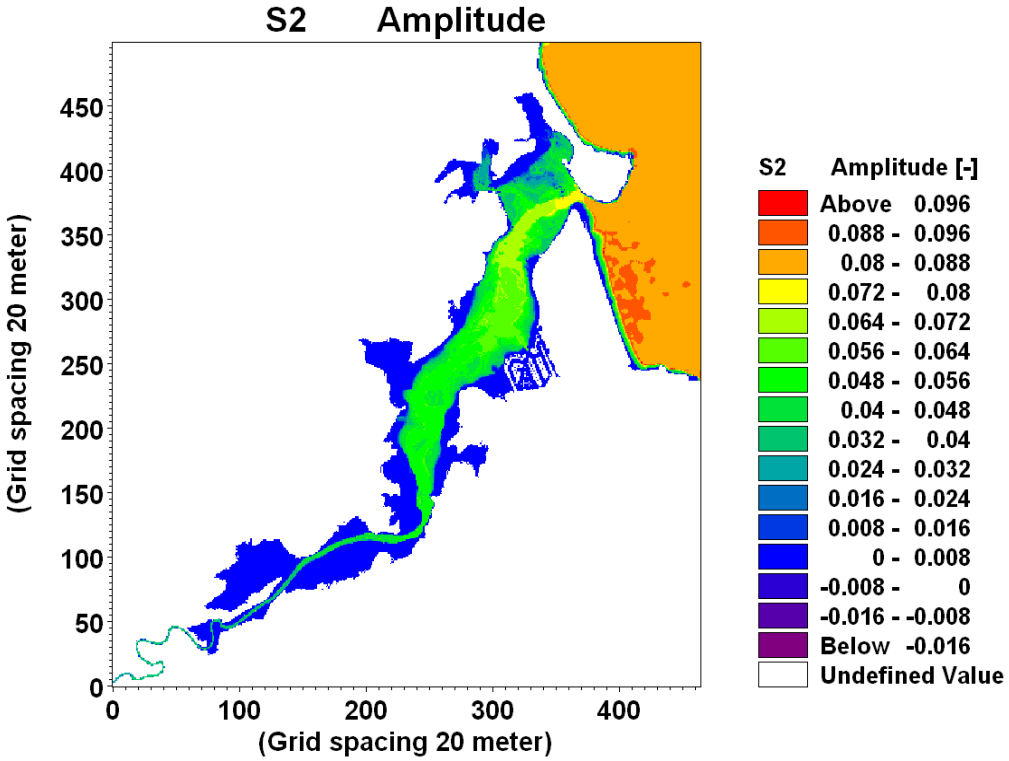

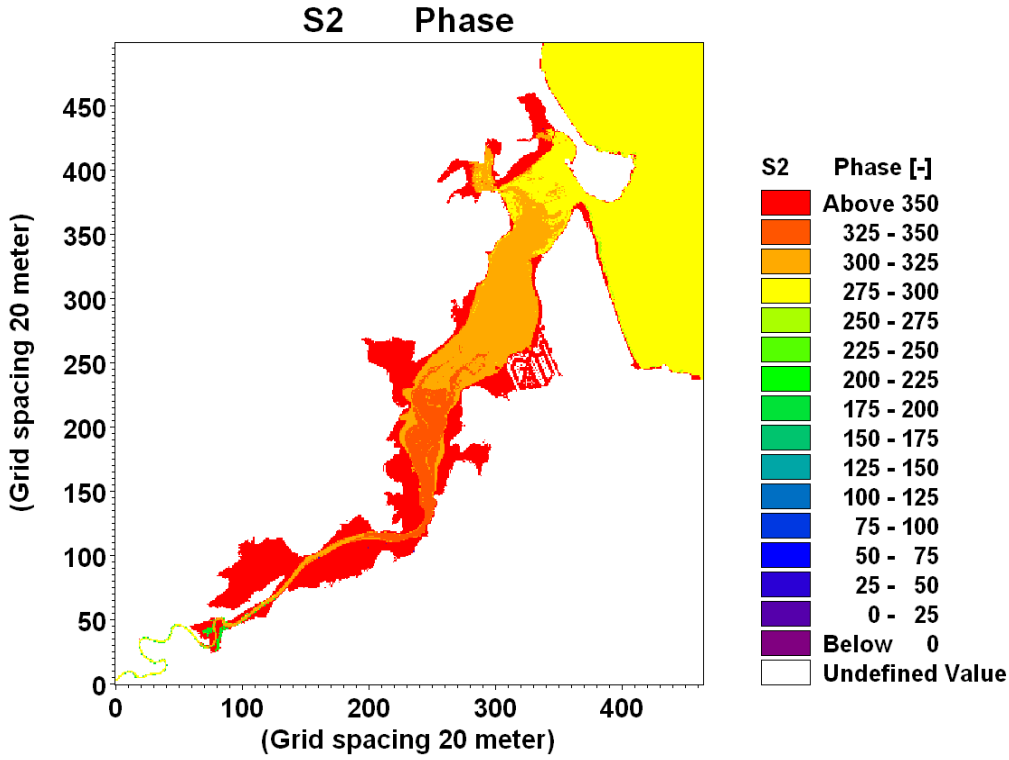

Figure V-2 Amplitude and the phase of the Principal Solar component S_2 of the tidal elevation at the Tairua Harbour

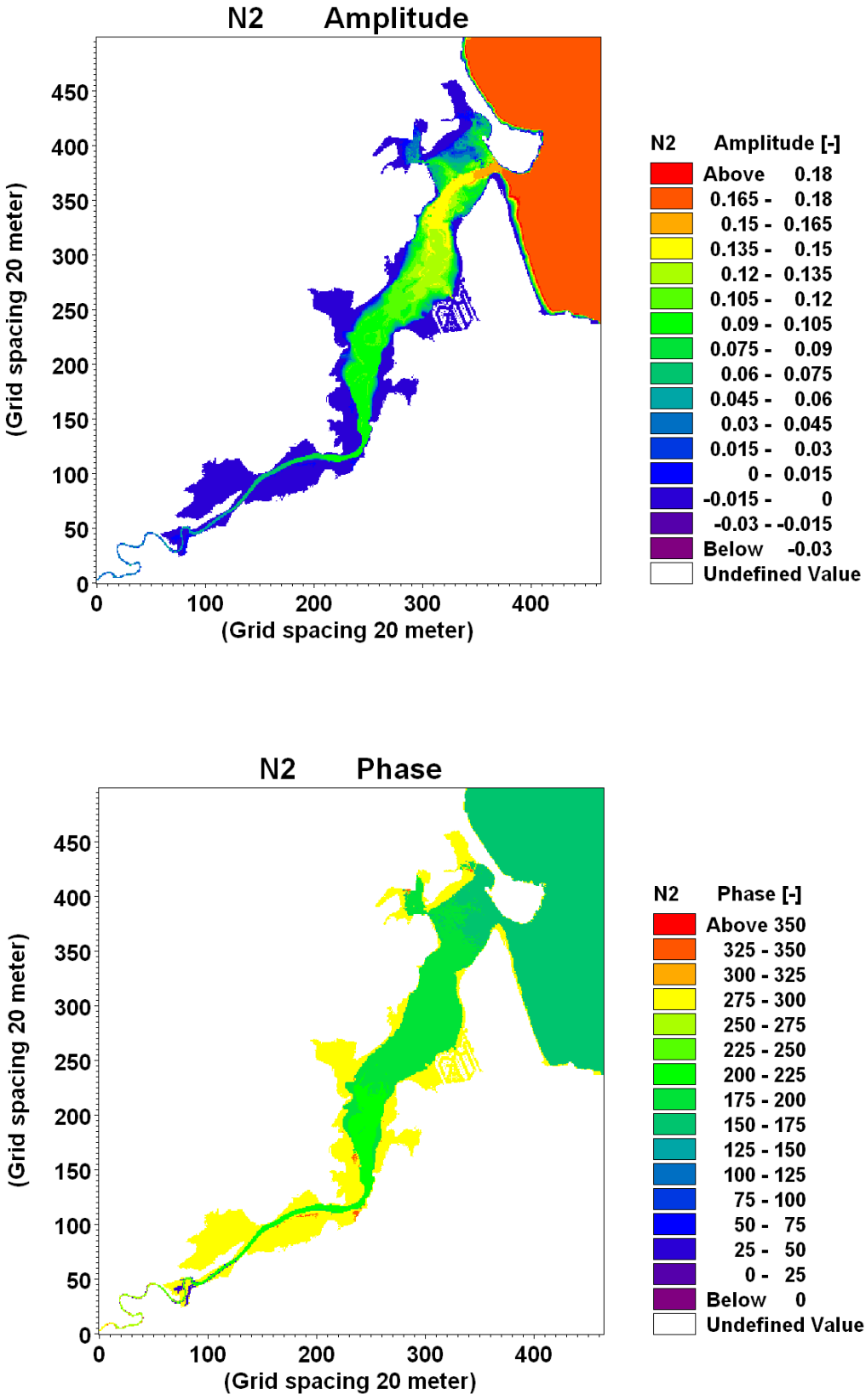

Figure V-3 Amplitude and the phase of the larger lunar elliptic component N_2 of the tidal elevation at Tairua Estuary

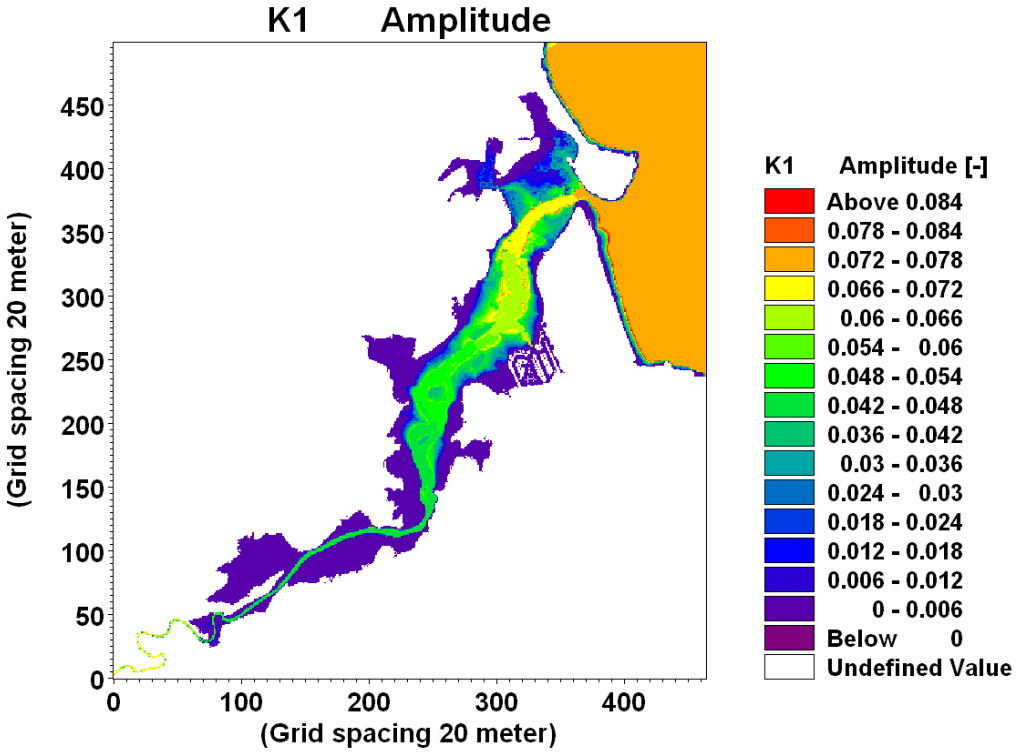

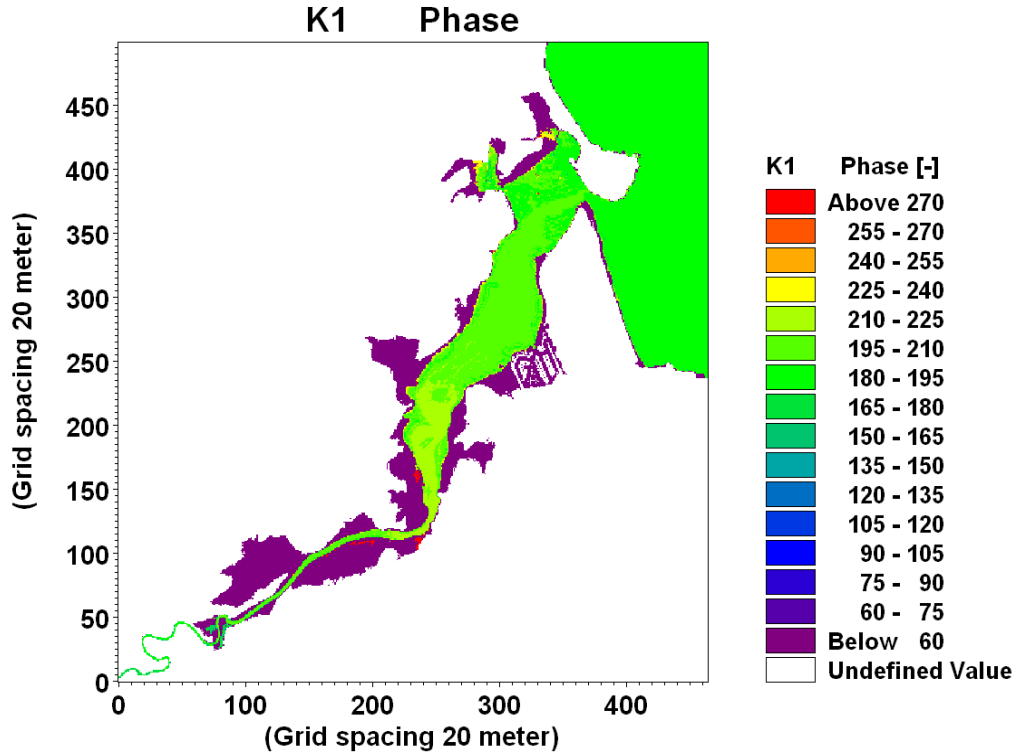

Figure V-4 Amplitude and the phase of the lunar-solar diurnal component K_1 of the tidal elevation at Tairua Estuary

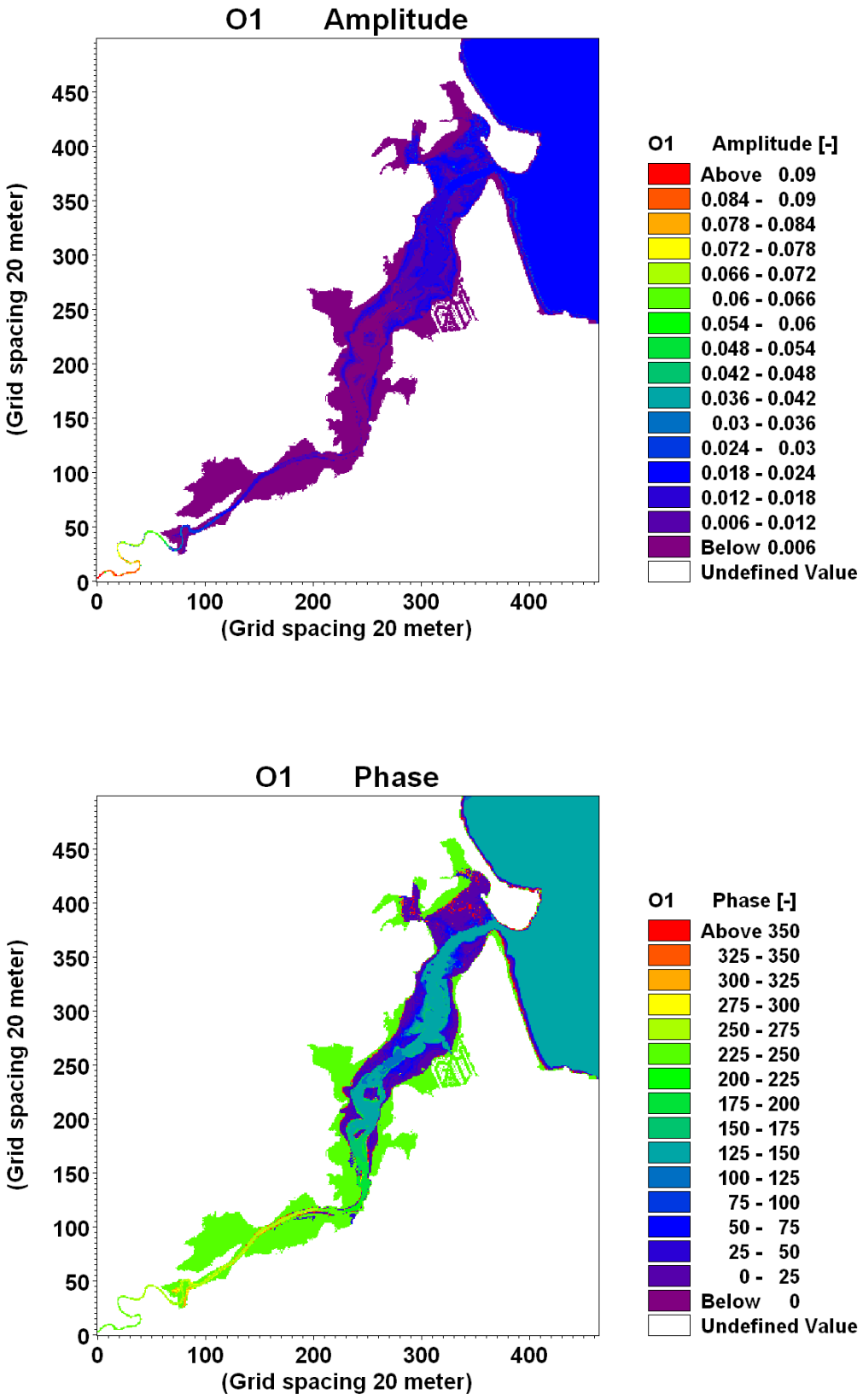

Figure V-5 Amplitude and the phase of the principal lunar diurnal component O_1 of the tidal elevation at Tairua Estuary

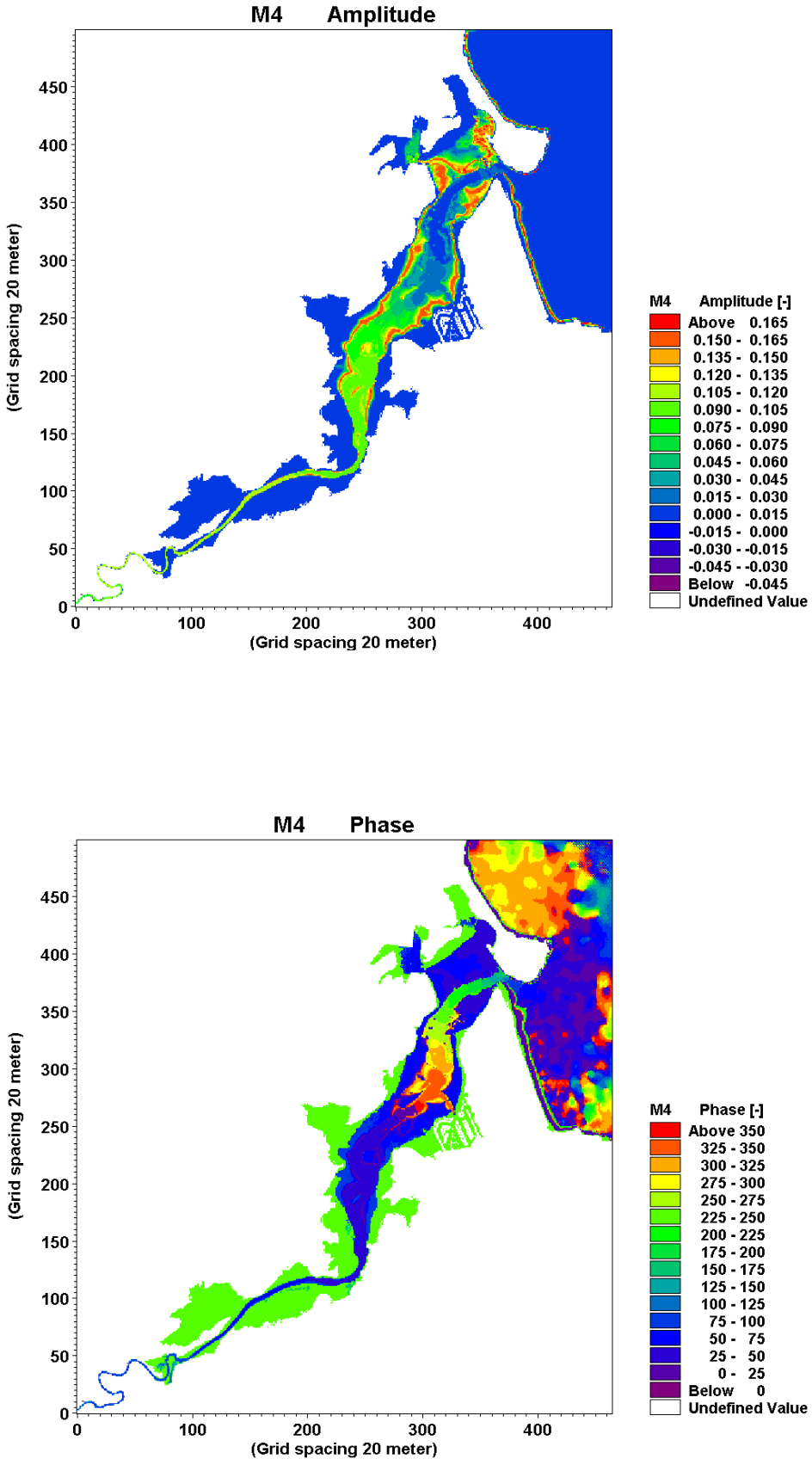

Figure V-6 Amplitude and the phase of the Shallow water overtides of principal lunar M_4 of the tidal elevation at Tairua Estuary

V.2 Principal Harmonic Components of Tidal Currents

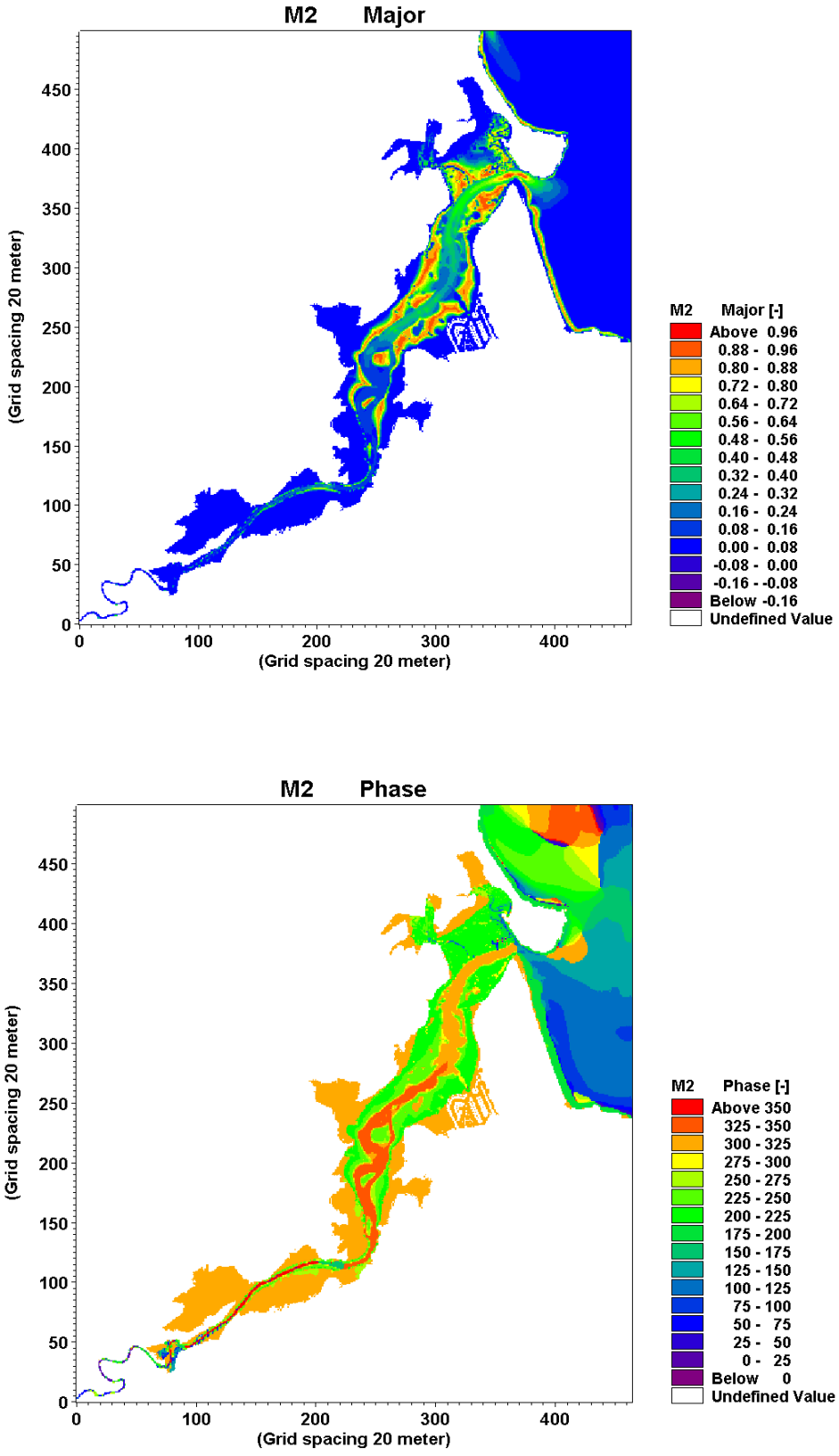

Figure V-7 M_2 major and the phase of the tidal current at Tairua Estuary

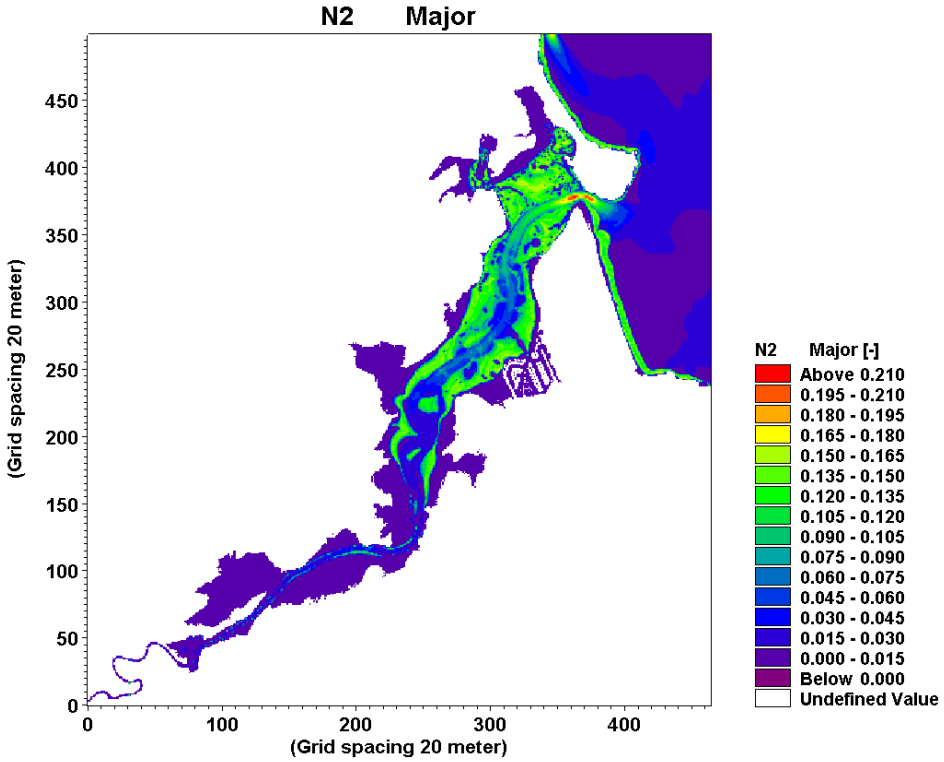

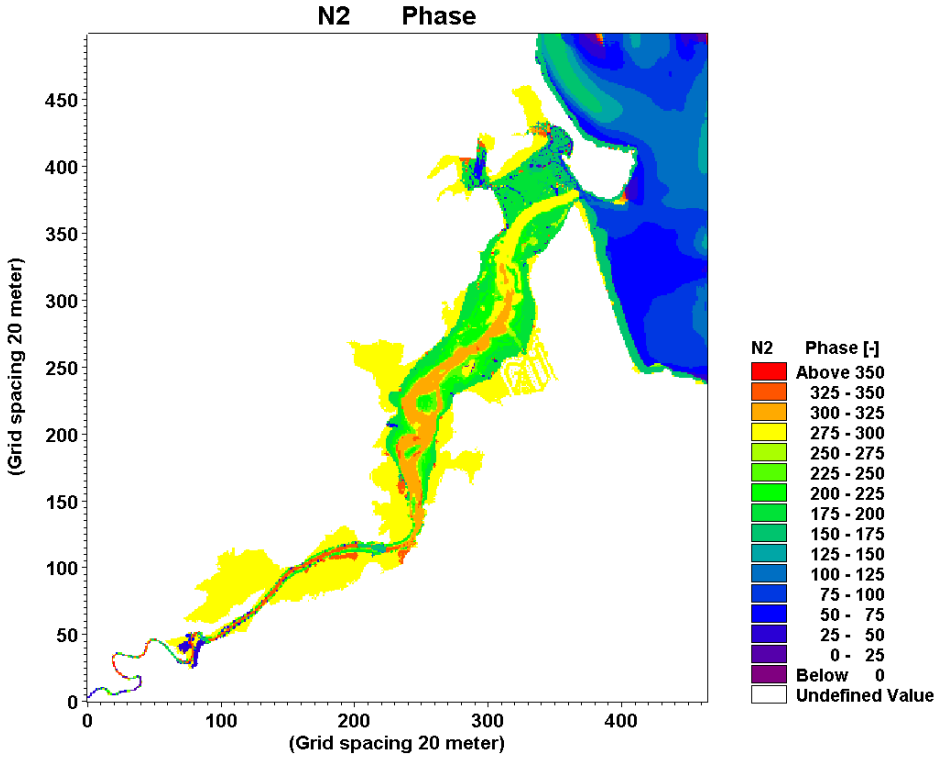

Figure V-8 N_2 major and the phase of the tidal current at Tairua Estuary

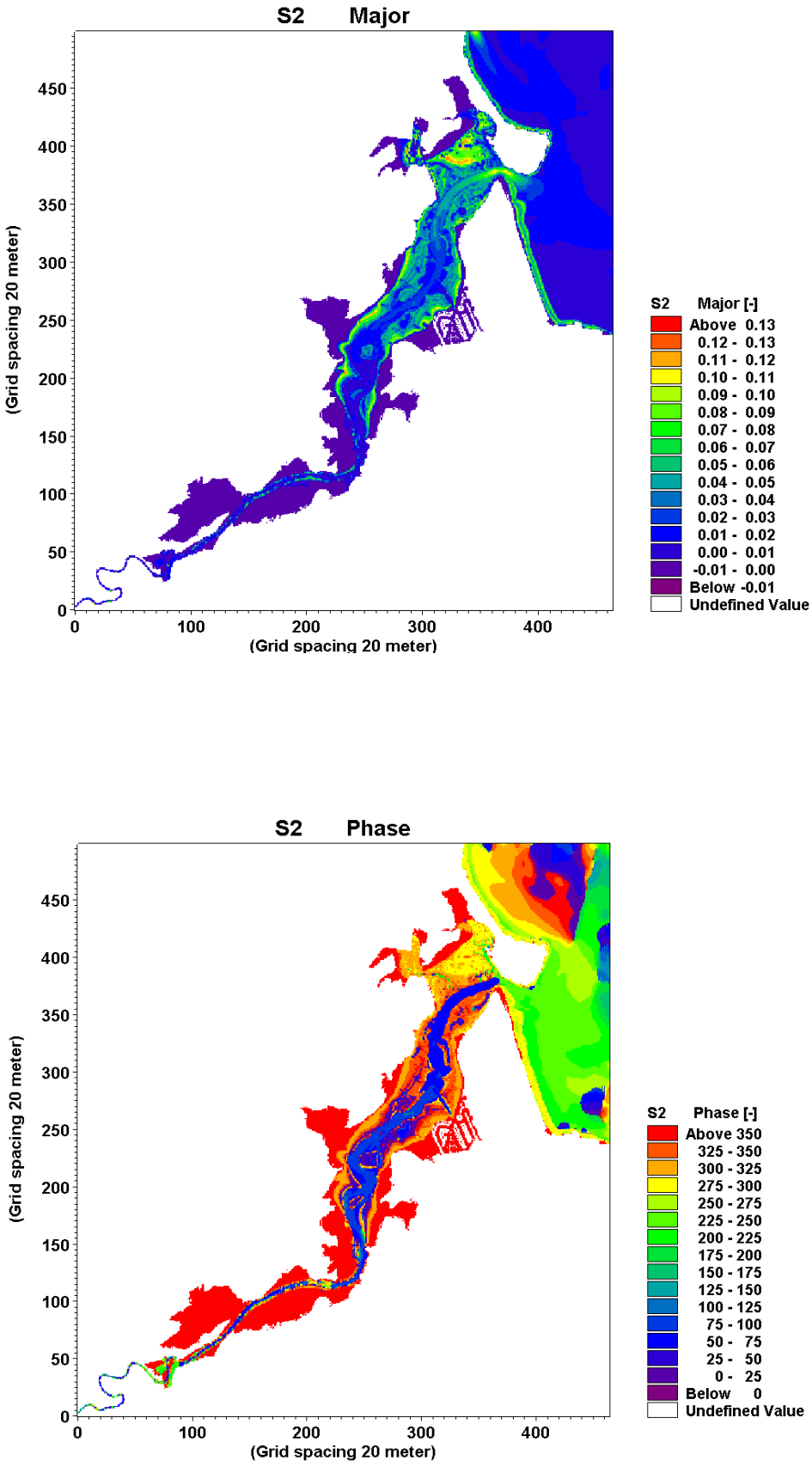

Figure V-9 S2 major and the phase of the tidal currents at Tairua Estuary

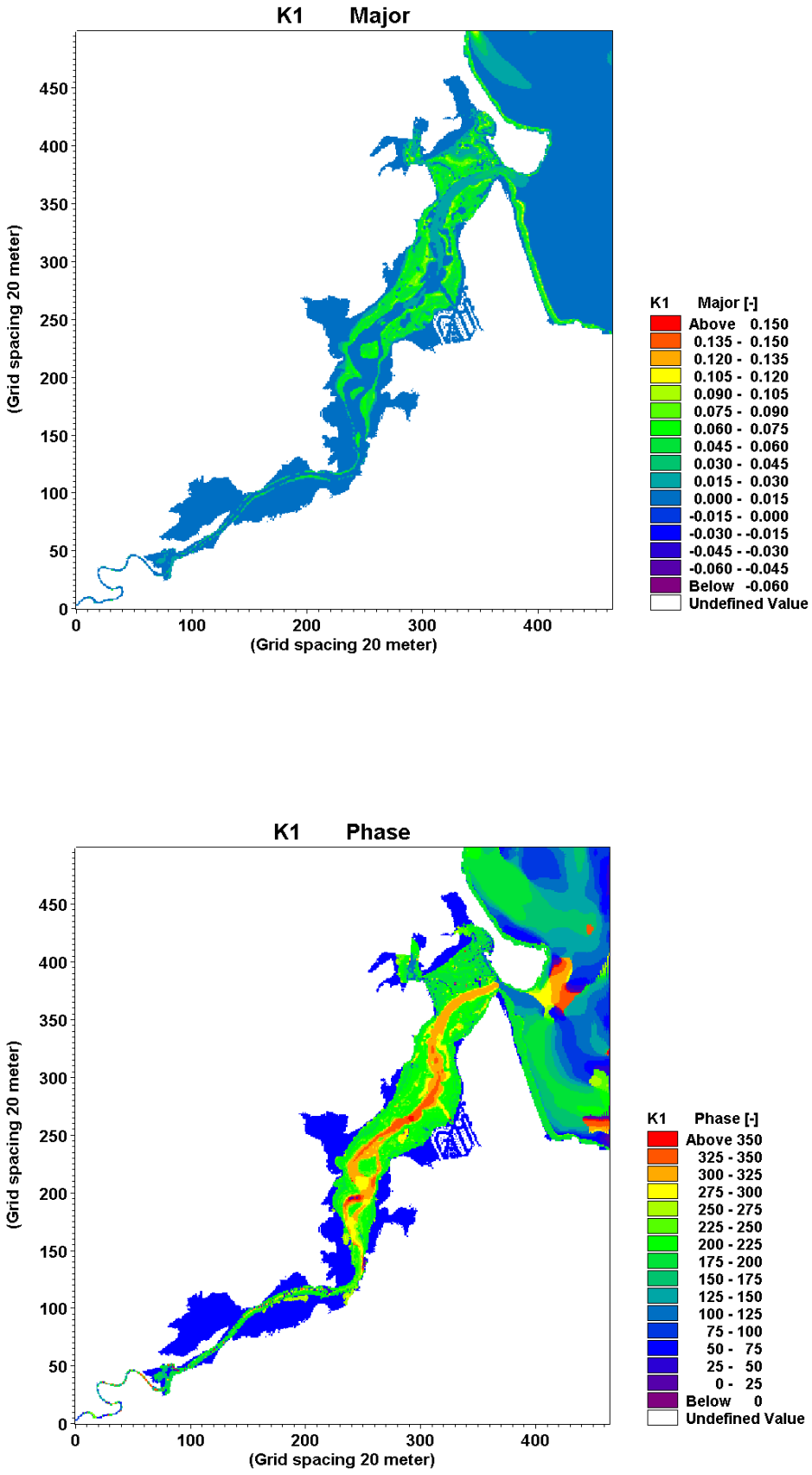

Figure V-10 K1 major and the phase of the tidal currents at Tairua Estuary

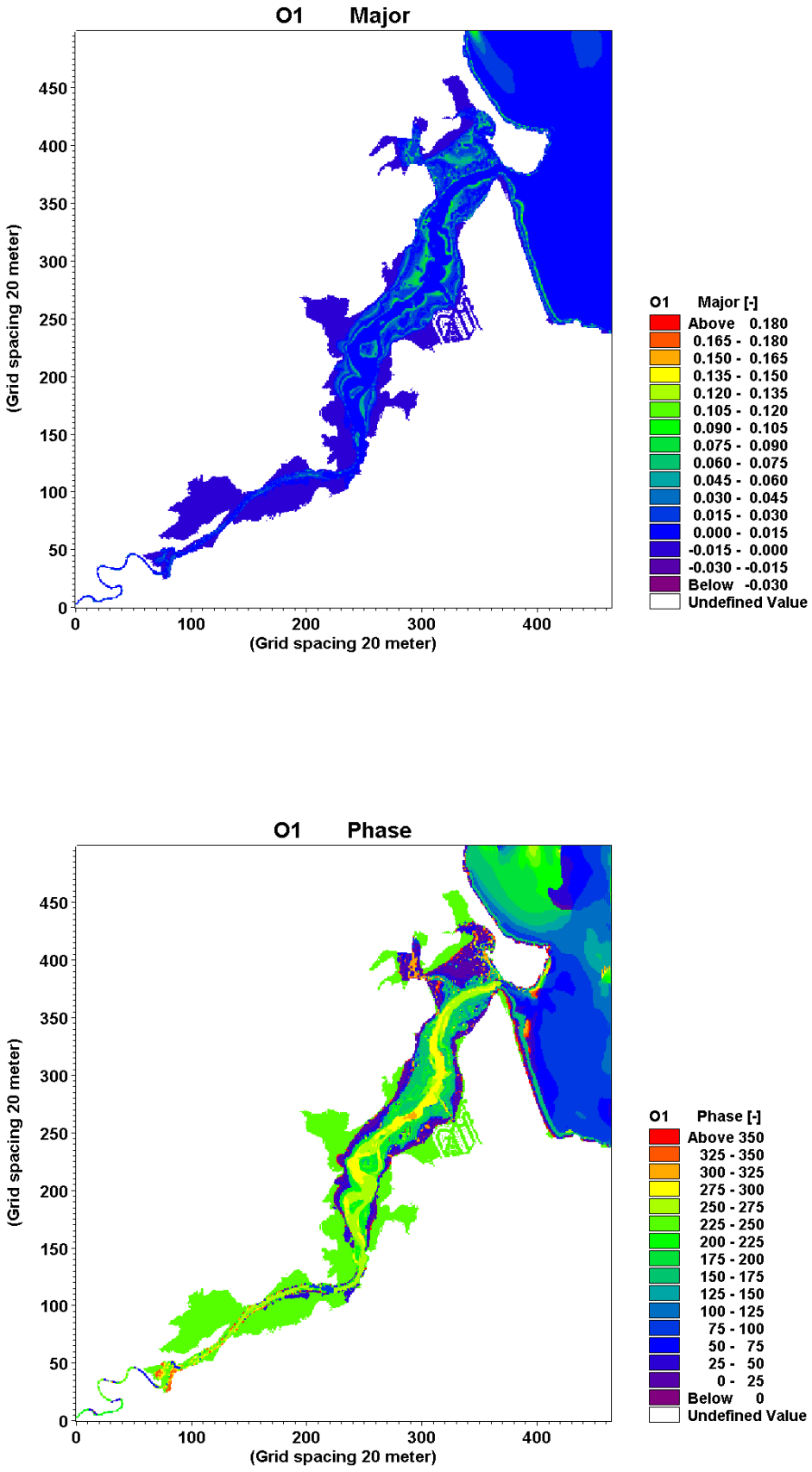

Figure V-11 O1 major and the phase of the tidal currents at Tairua Estuary

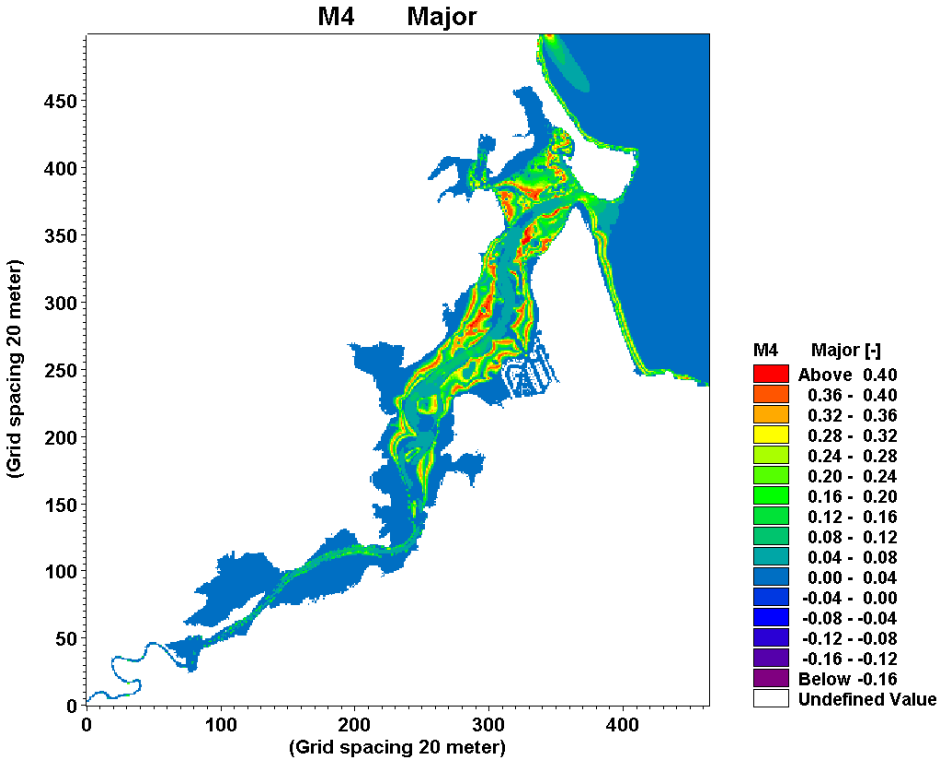

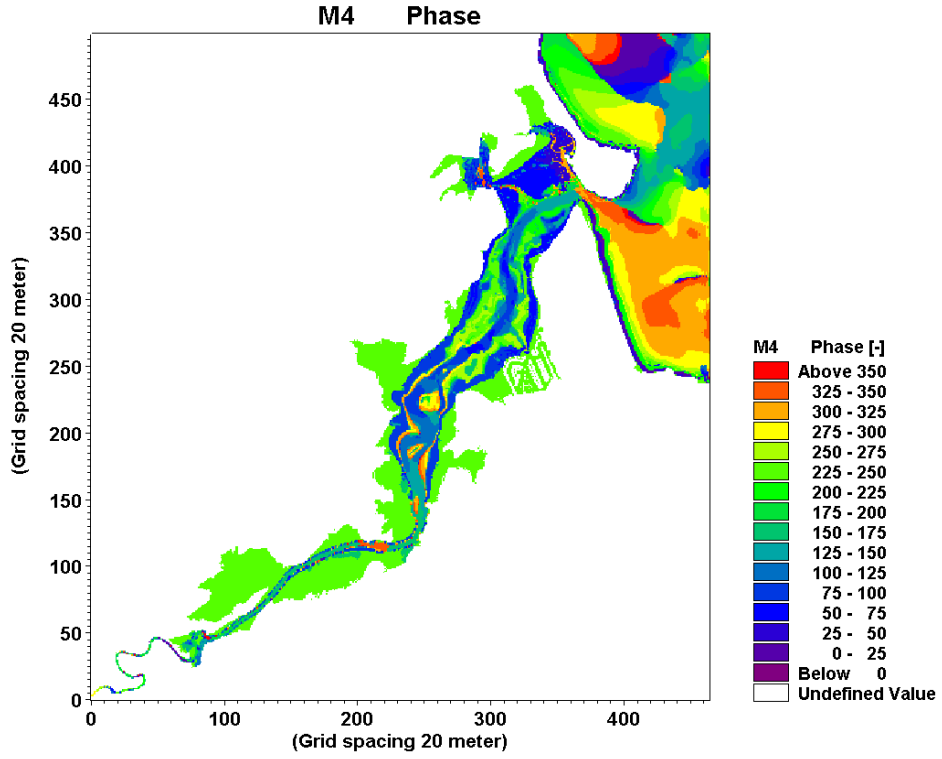

Figure V-12 M4 major and the phase of the tidal currents at Tairua Estuary